



Development of a reflexive control system for gait using human walking data

Catherine A. Macleod

This thesis is submitted in partial fulfilment of the requirements
for the degree of

DOCTOR OF ENGINEERING

Department of Biomedical Engineering
University of Strathclyde
Glasgow
2015

Declaration

This thesis is the result of the authors original research. It has been composed by the author and has not been previously submitted for examination which has led to the award of a degree.

The copyright of this thesis belongs to the author under the terms of the United Kingdom Copyright Acts as qualified by University of Strathclyde Regulation 3.50. Due acknowledgement must always be made of the use of any material contained in, or derived from, this thesis.

Signed:

Date:

Acknowledgements

First and foremost I offer my sincerest gratitude to my supervisors, Bernd Porr and Bernie Conway. Bernie quoted Douglas Adams in one of our first meetings, “I love deadlines. I like the whooshing sound they make as they fly by,” followed by the instruction that I should try to stick to deadlines. I tried and sometimes failed but I got the thesis finished in the end, thanks to the encouragement and support of those whom I have worked with over the course of my EngD. I must especially thank Bernd for his tireless scientific and personal support over the last five years. Sujay Galen of Wayne University in Detroit has also been a great mentor and I enjoyed our time working on the wi-GAT development. I must thank all my colleagues at the University of Strathclyde Neuro lab (Glial club), who kept me smiling, especially: Alejandra Aranceta-Garza, Pauline Axford, Niall McKenzie, Danial Kahni, Bilal Nasser, Ange Tano and Bahman Nasserolsami. I would like to acknowledge the work of Lin Meng of the University of Glasgow in our collaboration and the many valuable discussions we had during the endless hours watching RunBot face plant, stumble and finally walk using human walking data. I must express my gratitude to Sylvie Coupaud, for her guidance and encouragement during the writing of the thesis and for proof reading various parts. The advice of the electronics technicians, Tom O’Hara, University of Glasgow and John McLean, University of Strathclyde, was extremely valuable to my work. I also appreciate the advice of Claire Hastie, University of Glasgow on the statistical analysis. The research would not have been possible without the volunteers who gave up their time to take part in the study and their help is greatly appreciated. On a more personal note, I would like to thank my family for their love and patience. Apologies for all the moaning over the years... I would also like to express my deepest gratitude to Jamie for his support and encouragement of my aspirations.

This work was supported by the EPSRC and funding was received through the Doctoral training Centre in Medical Devices, University of Strathclyde.

Abstract

Control of human walking is not thoroughly understood, which has implications in developing suitable strategies for the retraining of a functional gait following neurological injuries such as spinal cord injury (SCI). Bipedal robots allow simple elements of the complex nervous system to be analysed to quantify their contribution to motor control. RunBot is a bipedal robot which has been developed to operate through reflexes without using central pattern generators or trajectory planning algorithms. Switches in the feet identify ground contact and are used to activate motors in the legs, generating a gait cycle visually similar to that of humans. If a causal relationship can be established between foot contact information and muscle activity in humans during walking, rather than developing a complicated biologically realistic neural system to control stepping, the model used in the control of the RunBot robot could instead be simplified using this relationship and the associated filter functions transferring the sensory data into motor actions.

By recording foot contact information and muscle activity (EMG) during human walking, both on a treadmill and overground, a relationship between heel contact and peaks in the muscle activity related to hip and knee joint actions was identified. Adaptive filtering was then used as a computational device to model the relationship between the recorded foot contact information and muscle activity data. Using these transfer functions, a minimal, linear, analogue control system for controlling walking could be created, based on the controller used in the RunBot robot. The human walking transfer functions were then applied to RunBot to analyse the produced gait. It was found that the gait cycle was stable and controlled, which is a positive indication that the control system has potential for use in controlling assistive devices for the retraining of an efficient and effective gait, with potential applications in SCI rehabilitation.

List of publications and conference presentations

Publications resulting from work carried out during the course of the EngD.

1. Macleod CA, Meng L, Conway BA and Porr B (2014) Reflex control of robotic gait using human walking data. PLoS ONE 9(10): e109959.
2. Macleod CA, Conway BA, Allan DB and Galen SS (2014) Development and validation of a low-cost, portable and wireless gait assessment tool. Med Eng Phys 36(4): 541-546.
3. Macleod CA, Porr B and Conway BA (2013) Reflexive control of functional electrical stimulation for spinal cord injury rehabilitation. 6th International IEEE EMBS Conference on Neural Engineering. San Diego, USA.
4. Macleod CA, Porr B and Conway BA (2013) Can heel strike information be used to control FES-assisted gait? Glasgow Neuroscience Day 2013. Glasgow, UK.
5. Macleod CA, Porr B and Conway BA (2011) Investigating ground contact information for use in neuro-prosthetic control of FES assisted gait in patients with spinal injuries. 6th IEEE EMBS UK & Republic of Ireland Postgraduate Conference on Biomedical Engineering and Medical Physics. Glasgow, UK.
6. Macleod CA, Porr B and Conway BA (2010) Investigating limit cycle walking in humans: analysing foot contact and EMG. 7th meeting of the Scottish Neuroscience Group. Glasgow, UK.

Contents

List of Figures	x
List of Tables	xiv
Abbreviations	xvi
1 Introduction	1
1.1 Background	1
1.2 Spinal Cord Injury (SCI)	3
1.2.1 Gait rehabilitation in SCI	8
1.3 Human gait	9
1.3.1 Receptors	12
1.4 Summary	14
1.5 Thesis overview	15
1.6 Research objectives	17
1.7 Thesis structure	17
2 Literature Review	19
2.1 Load dependent reflexes	19
2.2 Control of walking - animals	20
2.2.1 Interaction of reflexes with the locomotor rhythm generator	20
2.2.2 Sensory regulation of stepping	25
2.2.3 Relevance of animal models to human walking	30
2.3 Control of walking - humans	30
2.3.1 Central pattern generators (CPGs)	30
2.3.2 Reflex function during locomotion	33
2.3.3 Cutaneous reflexes (Feet)	38
2.3.4 Summary	41
2.4 How could knowledge of reflexes be used?	42
2.4.1 Functional electrical stimulation (FES)	42

2.4.2	Robotic bipedal walkers	46
2.5	Conclusion	49
2.6	Research hypothesis	51

I Preliminary Studies: Methods and materials development **52**

3	Preliminary investigation into the relationship between foot contact information and muscle activity during walking	54
3.1	Development of a causal control system	54
3.2	Participants and ethics	55
3.3	Materials and Methods	56
3.3.1	Data acquisition	56
3.3.2	EMG preamplifier	57
3.3.3	Ground contact information	60
3.3.4	Hip acceleration	66
3.3.5	Experimental setup	68
3.4	Data analysis	68
3.5	Results	73
3.5.1	Identifying correlation	76
3.5.2	Inter-subject variability	78
3.6	Discussion	82
3.7	Summary	85
3.7.1	Recommendations	86
4	Wireless gait analysis device (wi-GAT)	87
4.1	Introduction	88
4.2	Materials and methods	89
4.2.1	Materials	89
4.2.2	Experimental setup	93
4.2.3	Participants and ethics	93
4.2.4	Experimental protocol	94
4.2.5	Extraction of gait parameters	96
4.2.6	Statistical analysis	100
4.3	Results	102
4.4	Discussion	102
4.4.1	Limitations of Bluetooth technology	108
4.5	Summary	109

II Developing a control system for walking generation using human data 111

5 Treadmill and overground walking: EMG and foot contact data collection	114
5.1 Treadmill walking data collection	114
5.1.1 Ethics statement	115
5.1.2 EMG and foot contact recording	115
5.1.3 Treadmill control	119
5.2 Overground walking data collection	124
5.2.1 Ethics statement	126
5.2.2 Experimental setup	126
5.3 Event-related averaging of the walking data	128
5.3.1 Treadmill ERA	129
5.3.2 Overground ERA	130
5.3.3 Comparison of overground and treadmill walking EMG ERAs	130
5.4 Summary	132
6 Calculation of transfer functions and development of a control system for generating walking	134
6.1 Adaptive filtering	134
6.2 RunBot	138
6.3 Reflexive control system	139
6.3.1 Generating walking using human derived transfer functions	142
6.3.2 Optimisation	147
6.4 Summary	148
7 Applying human walking transfer functions to RunBot's reflexive control system	151
7.1 Results: Treadmill walking data	151
7.1.1 Transfer functions	151
7.1.2 RunBot performance	152
7.1.3 Conclusion	162
7.2 Results: Overground walking data	164
7.2.1 Transfer functions	164
7.2.2 RunBot performance	164
7.2.3 Conclusion	165
7.3 Summary	167

8	Comparison of treadmill and overground walking	168
8.1	Analysis	169
8.1.1	Temporal gait parameters	169
8.1.2	Muscle activity	170
8.2	Results	171
8.2.1	Temporal gait parameters	171
8.2.2	Muscle activity	175
8.3	Discussion	181
8.4	Summary	184
9	Ankle control	186
9.1	Calculating transfer functions	191
9.1.1	Tibialis Anterior (TA)	192
9.1.2	Lateral Gastrocnemius (LG)	193
9.2	Ankle transfer functions	194
9.3	RunBot ankle transfer functions	195
9.4	RunBot testing	195
9.5	Summary	196
10	Discussion	198
10.1	Interpretation of results	198
10.1.1	RunBot walking results	200
10.1.2	Limitations	202
10.2	Human walking	203
10.3	Control system	205
10.3.1	Comparison to human control	206
10.4	Implications	208
10.5	Significance and future work	210
11	Conclusions	213
11.1	Relevance to the research hypothesis	213
11.2	Summary of thesis conclusions	215
A	EMG preamplifier PCB layout and BOM	218
B	EMG/FSR preamplifier and BOM	220
C	USB-DUX Sigma pin diagram	222
D	Treadmill belt speed accuracy	223

E	Supplementary tables for RunBot	225
F	Adaptive filtering - MSE	226
G	Curve fitting - goodness-of-fit	230

List of Figures

1.1	RunBot's operation	2
1.2	ASIA score sheet	4
1.3	ASIA impairment scale (AIS) and muscle function grading	5
1.4	Spinal cord levels	6
1.5	The human gait cycle	10
1.6	Location of some of the major muscles recruited during walking	12
1.7	Black box approach to control.	15
1.8	Proposed system for FES	16
2.1	Control of human walking	21
2.2	Schematic demonstrating the hypothesis on reflex pathways involving load detecting afferents in cats.	24
2.3	Contribution of supraspinal control.	25
2.4	Block diagram of a muscle control system	28
2.5	Cutaneous stimulation in the cat and the effects on locomotion.	29
2.6	Possible mechanisms of sensorimotor interactions during human locomotion	34
2.7	Stretch reflex EMG responses after dorsiflexion using a mechanical actuator during stance phase of walking.	35
2.8	Phase-dependent modulation and reversal of cutaneous reflexes during locomotion	40
2.9	Demonstration of the functional effects of cutaneous reflexes from tibial nerve and SP nerve stimulation.	41
2.10	Example of some well known bipedal robots and their walking speed compared to humans.	48
2.11	The main functional roles of each group of reflexes during the human gait cycle.	50
3.1	USB-DUX D board	57
3.2	Position of EMG electrodes on the legs	58

3.3	Annotated schematic of the four channel EMG preamplifier	61
3.4	Force sensing resistor (FSR 402)	62
3.5	FSR response to applied force with different values of R_{FSR} . . .	64
3.6	FSR amplifier circuit	64
3.7	FSR amplifier circuit	65
3.8	Photograph of an FSR insole	66
3.9	Accelerometer circuit diagram	67
3.10	Photograph of the experimental setup	69
3.11	Graphs of the filtered and rectified EMG waveform, foot FSR data and acceleration (test subject PF)	70
3.12	Event-related averaging of EMG data	71
3.13	Event-related average (ERA) of the rectified EMG recordings - heel contact	74
3.14	Event-related average (ERA) of the rectified EMG recordings - hip acceleration	75
3.15	Hip movement during the gait cycle	77
3.16	Mean ERA from all subjects, for each of the four muscles (right heel trigger, ipsilateral (I))	79
3.17	Mean ERA from all subjects, for each of the four muscles (left heel trigger, contralateral (C))	80
4.1	Annotated schematic of the wi-GAT	91
4.2	Foot impressions	92
4.3	The process of making insoles for each study participant	92
4.4	Wi-GAT device and FSR insoles.	93
4.5	Plug-in-Gait marker placement guide	95
4.6	Schematic of the experimental setup	96
4.7	Screenshot of the Vicon Nexus software	97
4.8	Screenshot of the Wi-GAT software	101
4.9	Bland-Altman plots	104
5.1	Treadmill walking data collection protocol	116
5.2	Annotated schematic of the EMG/FSR preamplifier	117
5.3	Pin connections for the FSR insoles	118
5.4	EMG/FSR preamplifier	118
5.5	EMG/FSR preamplifier connected to the USB-DUX Sigma board	119
5.6	Set-up for the treadmill walking trials	120
5.7	Protocol for the treadmill walking study	121

5.8	Walking speed sequences for Subject H	124
5.9	User interface for controlling the treadmill	125
5.10	Figure-of-eight walkway used in the overground walking study . .	127
5.11	Maximum and minimum peak detection in the FSR voltage recordings from the right heel during treadmill walking (Subject H) . . .	129
5.12	EMG ERAs and FSR foot contact data over a range of treadmill walking speeds (Sequence 1)	131
5.13	EMG ERAs and FSR foot contact data over a range of treadmill walking speeds (Sequence 2)	133
5.14	EMG ERAs and FSR foot contact data (overground walking) . .	133
6.1	Example results of adaptive filtering of the Biceps Femoris (BF) .	136
6.2	Photograph series representing one stride duration during treadmill walking	137
6.3	Photograph of the RunBot II robot	140
6.4	RunBot II's gait cycle	140
6.5	Identifying features of the transfer function coefficients which correspond to muscle activity promoting knee and hip flexion/extension in human walking	144
6.6	Flow diagram of the signal processing procedure	149
7.1	Plots of the different transfer functions applied to RunBot's motors	153
7.2	Photographs of one RunBot stride duration	155
7.3	Box plots comparing RunBot's stride length (A), stride duration (B) and walking speed (C)	157
7.4	Comparison of knee flexion/extension angle of RunBot using transfer function sets which produced a stable gait	158
7.5	Knee flexion/extension angle of (A) subject C and (B) subject H .	159
7.6	Phase plots of knee angular velocity versus angular position . . .	161
7.7	Phase plots of knee angular velocity versus angular position during human walking	162
7.8	Angle-angle plot of hip angle against knee angle	163
7.9	Plots of the different transfer functions tested with RunBot	166
8.1	Temporal gait parameters - overground walking	172
8.2	Temporal gait parameters - treadmill walking (sequence 1)	173
8.3	Temporal gait parameters - treadmill walking (sequence 2)	174
8.4	Mean ERA - overground walking	176
8.5	Mean ERA - treadmill walking, sequence 1	177

8.6	Mean ERA - treadmill walking, sequence 2	178
8.7	Mean ERAs from the three different walking modalities	180
8.8	Further detail in the mean ERAs (RF and BF) from the three different walking modalities	183
9.1	Ankle joint dorsiflexion/plantar flexion during human walking . .	187
9.2	Ankle joint motion during walking	187
9.3	Relationship between foot contact information and muscle activity	189
9.4	Event-related averages of the TA muscle using the ipsilateral toe- off as the trigger	190
11.1	Control systems for walking	214
A1	PCB design of the four channel EMG preamplifier	218
B1	PCB design for the EMG/FSR preamplifier	220
C1	USB-DUX Sigma pin diagram	222

List of Tables

1.1	Action of muscles during the gait cycle	11
1.2	Sensory fibres	14
3.1	Table of subject information for the preliminary study	56
3.2	Muscles recorded during the study and their action during gait . .	58
3.3	Defining a control system for human walking compared to RunBot II	59
3.4	Electrode positioning for the muscles investigated	60
3.5	Average stride duration of each subject.	72
3.6	Mean time from peak in ERA of the heel FSR to peak (highest amplitude) in ERA	81
3.7	Variability measures of the event-related averages	82
4.1	Wi-GAT validation study participant information	94
4.2	The spatial and temporal gait parameter definitions	98
4.3	Repeatability coefficients	103
4.4	Table of the difference in gait parameter values between the two measurement systems.	105
5.1	Subject gait parameters	122
5.2	Treadmill belt speed sequence	123
5.3	Overground walking study participant information	126
6.1	Relating the muscle transfer function to RunBot's motor control .	143
7.1	Different sets of transfer functions applied to RunBot's control system	152
7.2	Results of the curve fitting for hip/knee, flexion/extension	154
7.3	Comparison of function characteristics	156
7.4	The different sets of transfer functions applied in RunBot's control system	164
7.5	Results of the curve fitting for hip/knee, flexion/extension	165

7.6	Function characteristics	166
8.1	Difference in gait parameter values between legs	175
8.2	Coefficient of variation (CV)	179
8.3	Time of peaks in muscle ERA	181
8.4	Results of the paired t-tests between the three walking modalities	181
9.1	Relating ankle joint motion with muscle transfer function	188
9.2	Results of the curve fitting for ankle dorsiflexion/plantar flexion - treadmill	196
9.3	Results of the curve fitting for ankle dorsiflexion/plantar flexion - overground	196
A1	Bill of materials (BOM) for the four channel EMG preamplifier	219
B1	Bill of materials (BOM) for the EMG/FSR preamplifier	221
D1	Treadmill belt speed error, without load	224
E1	Values for the extreme angle of each joint ($\theta_{L/R,H/K}$)	225
E2	The gain of the motor amplifier ($a_{L/R,H/K}$)	225
F1	The final mean square error result for each subject for each muscle transfer function from the adaptive filtering	226
F2	The final mean square error result for each subject for each muscle transfer function from the adaptive filtering (overground walking)	227
F3	The final mean square error result for each subject for each muscle transfer function from the adaptive filtering for use in ankle control (treadmill walking)	228
F4	The final mean square error result for each subject for each muscle transfer function from the adaptive filtering for use in ankle control (overground walking)	229
G1	Goodness-of-fit statistics - hip/knee (treadmill)	231
G2	Goodness-of-fit statistics - hip/knee (overground)	232
G3	Goodness-of-fit statistics - ankle (treadmill)	232
G4	Goodness-of-fit statistics - ankle (overground)	233

Abbreviations

AEA	Anterior extreme angle
AIS	ASIA impairment scale
ASIA	American Spinal Injury Association
ASIS	Anterior superior iliac spine
BF	Biceps Femoris
BOM	Bill of materials
BWS	Body-weight support
CH	Contralateral heel
CNS	Central nervous system
CPG	Central pattern generator
cSCI	Complete spinal cord injury
CV	Coefficient of variation
EMG	Electromyography
ERA	Event-related average
FES	Functional electrical stimulation
FIR	Finite impulse response
FSR	Force sensing resistors
GTO	Golgi tendon organ
ICC	Intra-class correlation coefficient
IH	Ipsilateral heel
IIR	Infinite impulse response
iSCI	Incomplete spinal cord injury
LG	Lateral Gastrocnemius
LMS	Least mean squares
MSE	Mean square error
PCB	Printed circuit board
PEA	Posterior extreme angle
PNS	Peripheral nervous system
RF	Rectus Femoris

RMSE Root mean square error
SCI Spinal cord injury
sEMG Surface electromyography
SSE Sum of squares due to error
TA Tibialis Anterior
wi-GAT Wireless gait analysis device

Chapter 1

Introduction

1.1 Background

Human walking can be viewed as a complex programme of central commands and reflexes which through the use of feedback and feed-forward processes allows stepping to adapt to changing terrain or walking environments. Loading of the limbs and foot contact provide important sensory components which enable the production of a walking pattern which is flexible and efficient. Sensory information can be measured directly or indirectly by a variety of specific and non-specific receptors in the skin and muscles of the body, to produce feedback control of the stepping. Gait is a cyclical sequence of movements with intrinsic muscle properties providing many constraints, which can influence individual muscle function and the coordination between the different muscles to perform the locomotion [1].

Bipedal robots have often tried to mimic human walking either by using intensive feedback control signalling the position of all of the limbs, or by using various model-based controllers, or central pattern generators (CPGs). Although there is mixed success, the majority tend to be slow, unstable and particularly vulnerable to falling when a change of terrain or an obstacle is encountered [2]. Conversely, RunBot is a bipedal robot walker which is driven by simple local reflexes without any use of position or trajectory-tracking control algorithms, and without using CPGs [3–5]. Phase switching of the legs is triggered by ground contact signals [4]. Concisely, when one foot contacts the ground this signal triggers motors driving hip flexion/extension and knee flexion/extension of the swing and stance legs, driving the walking forward, Fig. 1.1. The reflexive locomotion controller design implemented in RunBot is based on simple reflexive mechanisms observed in human gait [6].

Knowledge of RunBots operation could have an impact on the understanding

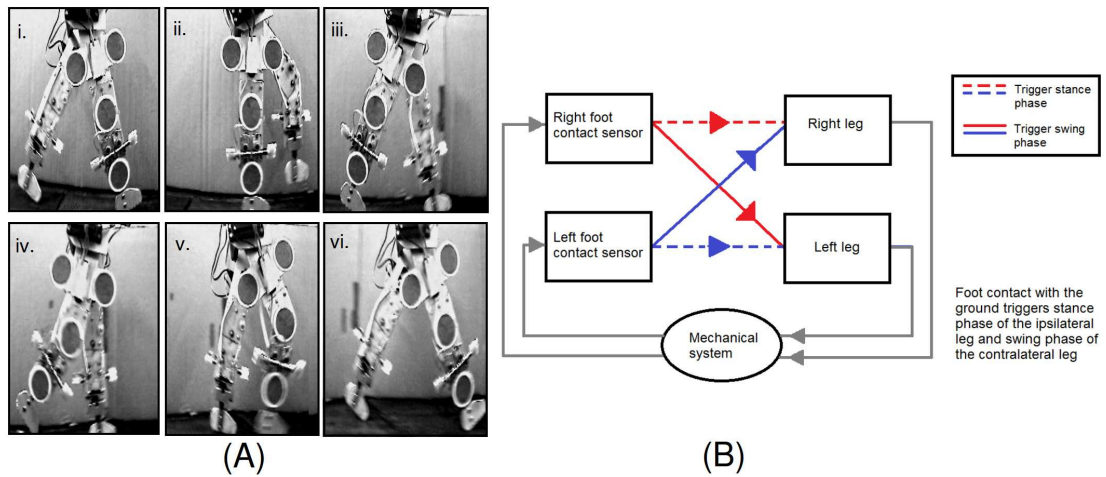


Figure 1.1: **RunBot’s basic operation involves phase switching of the legs triggered by contact signals from the feet.** Foot contact with the ground triggers the stance phase of the ipsilateral leg and the swing phase of the contralateral leg. RunBot’s controller minimally imposes this sequence on the walker, the natural dynamics of the robot determines its gait pattern. (A) Photographs of RunBot’s gait cycle and (B) the system used by RunBot to generate stepping.

of human locomotion. This thesis research aims to investigate the role of sensory feedback, specifically related to contact and proprioceptive information, in the control of human walking and determine whether it could be possible to generate locomotion using simple reflexes and without CPGs. This has potential use in the development of spinal cord injury (SCI) rehabilitation strategies for the re-training of functional gait. The idea is not to attempt any complex mapping or reconstruction of the brain and spinal cord but to follow a minimalistic approach to the problem and create a closed loop system based on the concept of a black box control mechanism. Here, the input is ground contact information from the feet and the output is motor control signals to generate flexion and extension of the leg joints. It is a minimal approach for a real-time system where decisions on the movement are made by the patient and are not enforced by the machine.

To understand the context of the research it is important to first discuss the basic concepts and terminology related to the loss of gait control following SCI, and the problems related to gait rehabilitation. In addition, an introduction to the mechanisms involved in controlling human walking and how this knowledge could be used in the development of new rehabilitation technology will be discussed.

1.2 Spinal Cord Injury (SCI)


Spinal cord injury (SCI) is the result of a lesion to the spinal cord and nerve roots following a traumatic event, which can result in sensory, motor and autonomic dysfunction [7]. The extent of neural damage and subsequent disability resulting from the lesion depends on the severity and level of injury in the spinal cord. SCI is defined as either complete or incomplete and the resulting sensory and motor deficits or dysfunctions, as either temporary or permanent. Typically, functional recovery is usually seen within the first few months of rehabilitation [8,9].

The American Spinal Injury Association's (ASIA) International Classification of SCI is typically used as guideline for defining the neurological level of the damage and completeness of injury as well as a measure of recovery. [10,11]. Motor function is graded within the different myotomes, and sensory function in the dermatomes. This is outlined in the ASIA classification of SCI form, provided in Fig. 1.2 and 1.3. Most patients are able to progress one grade on the ASIA impairment scale (AIS) in the first few months following injury, most often it is those who are diagnosed initially as grade B or C [7]. SCI can be additionally sub categorised with a classification of either Quadriplegia or Paraplegia. Quadriplegia is a high level spinal cord injury within the cervical region and results in muscle strength loss in all four of the body's extremities. Paraplegia is an injury in the thoracic, lumbar or sacral segments [10,12], see Fig. 1.4. Using the ASIA scale for neurological impairment, complete SCI (cSCI) is defined as the total loss of sensory and motor function in the sacral segments S4-S5 [10]. Incomplete SCI (iSCI) is identified when there is some sensory or motor function that has been preserved below the level of injury, including the S4 and S5 segments. Sacral-sparing is used as a diagnosis of potential for some motor recovery as it is evidence of physiologic continuity of spinal cord long tract fibres.

Three phases of response follow a spinal injury: the acute, subacute, and chronic injury processes [14,15]. Initially during the acute phase of injury there is the immediate mechanical damage to neural tissue and endothelial cells of the vasculature. Micro Haemorrhage occurs within the central grey matter and there is localised oedema and loss of micro-circulation by thrombosis and vasospasm, which leads to ischemia and tissue death [14,16]. All of these results of trauma act to exacerbate the neural injury. Initially following SCI, most patients experience spinal shock where the reflexes, which are controlled by the spinal cord, are suppressed or absent. This is a temporary condition but may persist for a short period until the reflexes gradually re-emerge. It is only when the reflexes return that any form of rehabilitation therapy can begin [14,15]. During the secondary


Patient Name _____ Date/Time of Exam _____

Examiner Name _____



ASIA
AMERICAN SPINAL INJURY ASSOCIATION

INTERNATIONAL STANDARDS FOR NEUROLOGICAL CLASSIFICATION OF SPINAL CORD INJURY



ISCO

MOTOR

KEY MUSCLES
(scoring on reverse side)

C5	R	<input type="checkbox"/>	L	<input type="checkbox"/>	Elbow flexors
C6	R	<input type="checkbox"/>	L	<input type="checkbox"/>	Wrist extensors
C7	R	<input type="checkbox"/>	L	<input type="checkbox"/>	Elbow extensors
C8	R	<input type="checkbox"/>	L	<input type="checkbox"/>	Finger flexors (distal phalanx of middle finger)
T1	R	<input type="checkbox"/>	L	<input type="checkbox"/>	Finger abductors (little finger)

UPPER LIMB TOTAL (MAXIMUM) (25) (25) + = (50)

SENSORY

KEY SENSORY POINTS

C2	R	<input type="checkbox"/>	L	<input type="checkbox"/>	Pin Prick
C3	R	<input type="checkbox"/>	L	<input type="checkbox"/>	Light Touch
C4	R	<input type="checkbox"/>	L	<input type="checkbox"/>	Pin Prick
C5	R	<input type="checkbox"/>	L	<input type="checkbox"/>	Light Touch
C6	R	<input type="checkbox"/>	L	<input type="checkbox"/>	Pin Prick
C7	R	<input type="checkbox"/>	L	<input type="checkbox"/>	Light Touch
C8	R	<input type="checkbox"/>	L	<input type="checkbox"/>	Pin Prick
T1	R	<input type="checkbox"/>	L	<input type="checkbox"/>	Light Touch
T2	R	<input type="checkbox"/>	L	<input type="checkbox"/>	Pin Prick
T3	R	<input type="checkbox"/>	L	<input type="checkbox"/>	Light Touch
T4	R	<input type="checkbox"/>	L	<input type="checkbox"/>	Pin Prick
T5	R	<input type="checkbox"/>	L	<input type="checkbox"/>	Light Touch
T6	R	<input type="checkbox"/>	L	<input type="checkbox"/>	Pin Prick
T7	R	<input type="checkbox"/>	L	<input type="checkbox"/>	Light Touch
T8	R	<input type="checkbox"/>	L	<input type="checkbox"/>	Pin Prick
T9	R	<input type="checkbox"/>	L	<input type="checkbox"/>	Light Touch
T10	R	<input type="checkbox"/>	L	<input type="checkbox"/>	Pin Prick
T11	R	<input type="checkbox"/>	L	<input type="checkbox"/>	Light Touch
T12	R	<input type="checkbox"/>	L	<input type="checkbox"/>	Pin Prick
L1	R	<input type="checkbox"/>	L	<input type="checkbox"/>	Light Touch
L2	R	<input type="checkbox"/>	L	<input type="checkbox"/>	Pin Prick
L3	R	<input type="checkbox"/>	L	<input type="checkbox"/>	Light Touch
L4	R	<input type="checkbox"/>	L	<input type="checkbox"/>	Pin Prick
L5	R	<input type="checkbox"/>	L	<input type="checkbox"/>	Light Touch
S1	R	<input type="checkbox"/>	L	<input type="checkbox"/>	Pin Prick
S2	R	<input type="checkbox"/>	L	<input type="checkbox"/>	Light Touch
S3	R	<input type="checkbox"/>	L	<input type="checkbox"/>	Pin Prick
S4-5	R	<input type="checkbox"/>	L	<input type="checkbox"/>	Light Touch

LOWER LIMB TOTAL (MAXIMUM) (25) (25) + = (50)

NEUROLOGICAL LEVEL
The most caudal segment with normal function

NEUROLOGICAL LEVEL: R L

COMPLETE OR INCOMPLETE?
Incomplete = Any sensory or motor function in S4-S5

ASIA IMPAIRMENT SCALE (AIS):

ZONE OF PARTIAL PRESERVATION
If not caudal level with any preservation

R L

SENSORY MOTOR

Comments:

UPPER LIMB TOTAL (MAXIMUM) (25) (25) + = (50)

LOWER LIMB TOTAL (MAXIMUM) (25) (25) + = (50)

TOTALS (MAXIMUM) (50) (50) + = (50) (50)

(DAP) Deep anal pressure (yes/no)

PIN PRICK SCORE (max: 112)

LIGHT TOUCH SCORE (max: 112)

NEUROLOGICAL LEVEL: R L

COMPLETE OR INCOMPLETE?

ASIA IMPAIRMENT SCALE (AIS)

ZONE OF PARTIAL PRESERVATION

SENSORY MOTOR

REVISION 06/11

This form may be copied freely but should not be altered without permission from the American Spinal Injury Association.

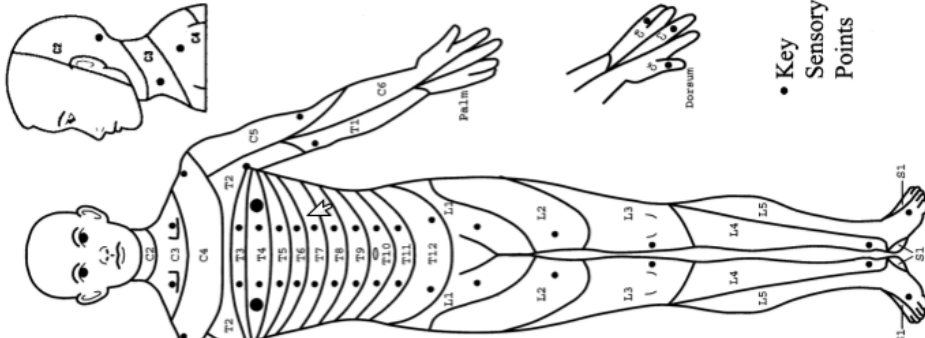


Figure 1.2: ASIA score sheet. Taken from [10].

Muscle Function Grading

- 0** = total paralysis
 - 1** = palpable or visible contraction
 - 2** = active movement, full range of motion (ROM) with gravity eliminated
 - 3** = active movement, full ROM against gravity
 - 4** = active movement, full ROM against gravity and moderate resistance in a muscle specific position.
 - 5** = (normal) active movement, full ROM against gravity and full resistance in a muscle specific position expected from an otherwise unimpaired person.
 - 5*** = (normal) active movement, full ROM against gravity and sufficient resistance to be considered normal if identified inhibiting factors (i.e. pain, disuse) were not present.
- NT = not testable (i.e. due to immobilization, severe pain such that the patient cannot be graded, amputation of limb, or contracture of >50% of the range of motion).

ASIA Impairment (AIS) Scale

- A = Complete.** No sensory or motor function is preserved in the sacral segments S4-S5.
- B = Sensory incomplete.** Sensory but not motor function is preserved below the neurological level and includes the sacral segments S4-S5 (light touch, pin prick at S4-S5; or deep anal pressure (DAP)). AND no motor function is preserved more than three levels below the motor level on either side of the body.
- C = Motor incomplete.** Motor function is preserved below the neurological level** and more than half of key muscle functions below the single neurological level of injury (NLI) have a muscle grade less than 3 (Grades 0-2).
- D = Motor incomplete.** Motor function is preserved below the neurological level** and at least half (half or more) of key muscle functions below the NLI have a muscle grade ≥ 3 .
- E = Normal.** If sensation and motor function as tested with the ISNCSCI are graded as normal in all segments, and the patient had prior deficits, then the AIS grade is E. Someone without an initial SCI does not receive an AIS grade.

**For an individual to receive a grade of C or D, i.e. motor incomplete status, they must have either (1) voluntary anal sphincter contraction or (2) sacral sensory sparing with sparing of motor function more than three levels below the motor level for that side of the body. The Standards at this time allows even non-key muscle function more than 3 levels below the motor level to be used in determining motor incomplete status (AIS B versus C).

NOTE: When assessing the extent of motor sparing below the level for distinguishing between AIS B and C, the *main level* on each side is used; whereas to differentiate between AIS C and D (based on proportion of key muscle functions with strength grade 3 or greater) the *single neurological level* is used.

Steps in Classification

The following order is recommended in determining the classification of individuals with SCI.

1. Determine sensory levels for right and left sides.
2. Determine motor levels for right and left sides.
Note: in regions where there is no myotome to test, the motor level is presumed to be the same as the sensory level, if testable motor function above that level is also normal.
3. Determine the single neurological level.
This is the lowest segment where motor and sensory function is normal on both sides, and is the most cephalad of the sensory and motor levels determined in steps 1 and 2.
4. Determine whether the injury is Complete or Incomplete. (i.e. absence or presence of sacral sparing)
If voluntary anal contraction = No AND all S4-5 sensory scores = 0 AND deep anal pressure = No, then injury is COMPLETE. Otherwise, injury is incomplete.

5. Determine ASIA Impairment Scale (AIS) Grade:
Is injury Complete?
If YES, AIS=A and can record ZPP (lowest dermatome or myotome on each side with some preservation)

Is injury motor incomplete?
If NO, AIS=B (Yes=voluntary anal contraction OR motor function more than three levels below the motor level on a given side, if the patient has sensory incomplete classification)

Are at least half of the key muscles below the single neurological level graded 3 or better?

NO → AIS=C
YES → AIS=D

If sensation and motor function is normal in all segments, AIS=E
Note: AIS E is used in follow-up testing when an individual with a documented SCI has recovered normal function. If at initial testing no deficits are found, the individual is neurologically intact; the ASIA Impairment Scale does not apply.

Figure 1.3: ASIA impairment scale (AIS) and muscle function grading. Taken from [10].

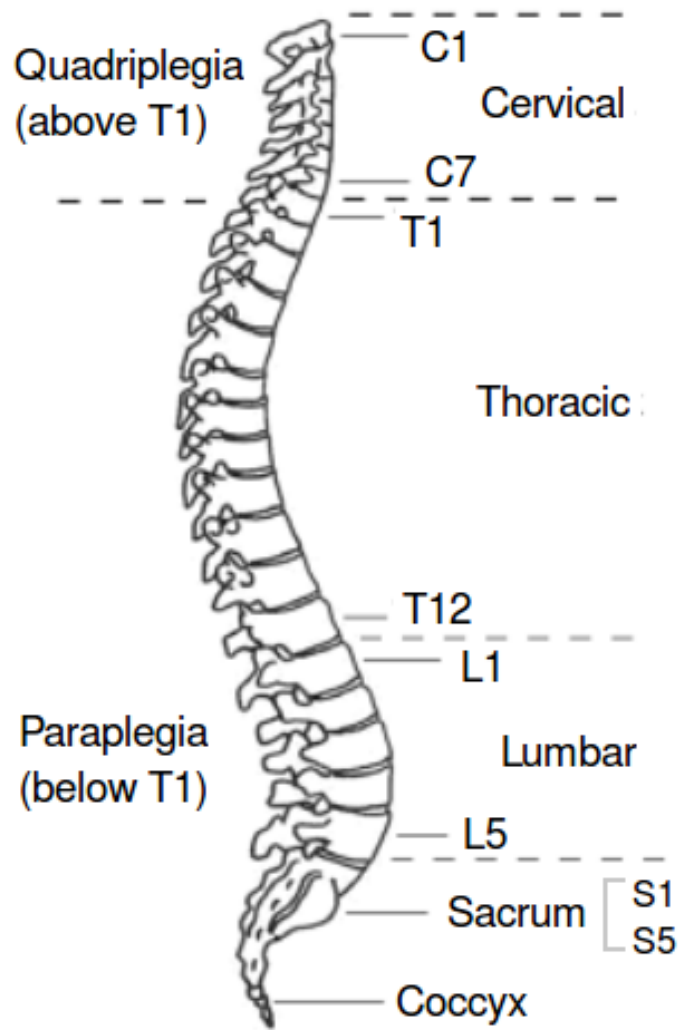


Figure 1.4: Levels of the spinal cord. Adapted from [13].

cascade, cells, axons and blood vessels damaged in the acute phase release toxic chemicals, leading to further ischemia, apoptosis of neighbouring cells and continuation of oedema [16]. The chronic phase can last from days to years and is a continuation of secondary phase processes including cell death or apoptosis.

The outcome of the primary injury is a change to the spinal cord's normal function, causing motor, sensory and autonomic impairment or loss, which can be either temporary or permanent. Intervention in SCI can result in an improvement in function and is focused on targeting the actions of the three stages of SCI response following injury. This includes reducing oedema and free radical damage, prevention of the cell death of neural tissue, control of inflammation and promotion of neurite growth [14].

There is a consensus in the literature that locomotion has potential to improve after SCI due to mechanisms within the spinal cord that are either compensatory or result in neuroplasticity [17,18]. Neuroplasticity demonstrates the adaptability of neural circuits (that have survived the injury (iSCI)) to reorganise and produce recovery of sensorimotor function [19]. These mechanisms are generally thought to be influenced by sensorimotor training, through techniques such as physiotherapy, which aim to re-establish motor control [20]. The process and mechanisms underlying successful rehabilitation include, primary sensory neurones sprouting in the spinal cord, modification of grey matter within the cord and conduction through demyelinated axons which have remained intact following the injury [21]. However, it should be noted that recovery of motor function is, most likely, not only due to neuroplasticity but in addition to compensatory strategies of the body to enable movement, such as the opening of new pathways in the spinal cord and changes in posture and gait in reaction to muscle spasticity or to reduce weight applied to weakened or paralysed limbs.

Although it is generally accepted that rehabilitation should begin as soon as possible following SCI, how significant the timing of training post injury is in the recovery of function is not thoroughly established. And although locomotor training is seen as an important therapy, approximately 25% of people initially classified with iSCI on the ASIA impairment scale, do not progress to being able to walk independently [8,9]. This demonstrates that although there is potential for recovery of walking ability with iSCI, the quantity and location of surviving neural tissue is a significant factor in determining the long-term outcome following rehabilitation [19]. It is therefore vital for the development of new neurorehabilitation technologies with the aim of improving limb function and promoting mechanisms of neuroplasticity to produce a recovery of independent ambulatory

ability.

1.2.1 Gait rehabilitation in SCI

Limitations of overground walking ability in patients with SCI are: (i) reduced co-ordination, (ii) leg paresis, and (iii) impaired balance [22]. For this reason, rehabilitation involves a plan combining different therapeutic approaches. Physiotherapy strategies involve repetitive and intensive exercises and training of gait, with or without a treadmill, to regain muscle strength in the legs [7]. Restorative treatment and rehabilitation strategies should aim to improve the quality of life for the patient by restoring useful function. The retraining of walking should maximise the patient's potential to regain functional stepping and promote the mechanisms of neuroplasticity to allow a 're-learning' of gait ability. Current rehabilitation strategies include using physiotherapy exercises, braces and walkers, body-weight assisted treadmill training (BWSTT), robotic assisted devices (such as the Lokomat (Hocoma, Switzerland) [23]) and functional electrical stimulation (FES). Key to these methods involves supporting the body-weight of the individual to allow stepping to be made easier to improve functionality, for a further review on these methods see [7, 24].

FES is commonly recruited as a rehabilitation strategy for SCI to exercise and strengthen weakened muscles as well as artificially replace muscle activation that is missing or lacking (for review see [25]). FES uses small electrical currents to directly stimulate peripheral nerves, alpha motor neurones, to cause muscle contraction. For this reason, FES is only effective when peripheral nerves and lower motor neurones remain intact as the high currents required to contract denervated muscle may cause further injury [16]. For gait rehabilitation, FES is applied to nerves which innervate leg muscles with particular motor functions during the swing and stance gait phases, activating them (artificially) with timing consistent with a normal walking gait cycle [26–31]. Research within the last decade has suggested walking function is vastly improved in individuals with incomplete SCI undergoing functional electrical stimulation (FES) therapy [32]. However, high human energy requirements and a current complexity of FES systems for assisting walking mean these devices are not routinely used [16]. It is thus of fundamental importance to find a successful mechanism to control FES, one which is real-time, simple and does not override or counteract voluntary control originating from the patient.

1.3 Human gait

Spinal cord injuries demonstrate that walking ability in humans requires pathways within the spinal cord and between the brain and spinal cord to be intact. However, the exact processes responsible for controlling stepping are not thoroughly understood. What is evident, is that a functional gait is dependent on mechanisms which involve the interaction of muscles and limbs, reflexes, spinal neuronal networks and supraspinal commands [33, 34].

A reflex can be defined as an unconscious action in response to a sensory stimulus [35]. A load-dependent reflex in the context of walking would thus be described as a motor response due to the influence of body loading or contact with a surface. Sherrington (1906) was among the first to recognise the importance of reflexes in controlling stepping in the locomotion of mammals [36]. The definition of a reflex response during something as complex as walking is not simple and other mechanisms need to be considered when attempting to understand the pathways in operation. Sherrington (1906) described the problem indicating that there is no such thing as a stereotypical reflex response.

“A simple reflex is probably a purely abstract conception, because all parts of the nervous system are connected together and no part of it is probably ever capable of reaction without affecting and being affected by various other parts, and it is a system certainly never absolutely at rest.” [36]

To walk, mammals require a complex series of reflexes involving the muscles of the trunk, legs and feet to produce co-ordinated responses ensuring balance and stability. These mechanisms depend on an integration of somatosensory information which is fed back from the muscles and limb segments (including the feet, knees and hips); visual information from the eyes as well as balance from the inner ear. Only by combining the information from the afferent inputs can the body maintain an equilibrium to enable an efficient gait while remaining flexible to changes in terrain and the environment.

Humans are bipedal walkers, ambulating only on two legs with the sole of the foot making contact with the floor during the gait cycle (plantigrade). The majority of other mammals are quadrupeds, walking on four limbs, usually on the toes (digitigrade). The human gait cycle has been well documented alongside the relative sequence of action of the major muscle groups in the legs, Fig. 1.5 and Table 1.1. To produce a functional and energy efficient gait, the main locomotor muscle groups of the trunk and legs act to produce moments of force

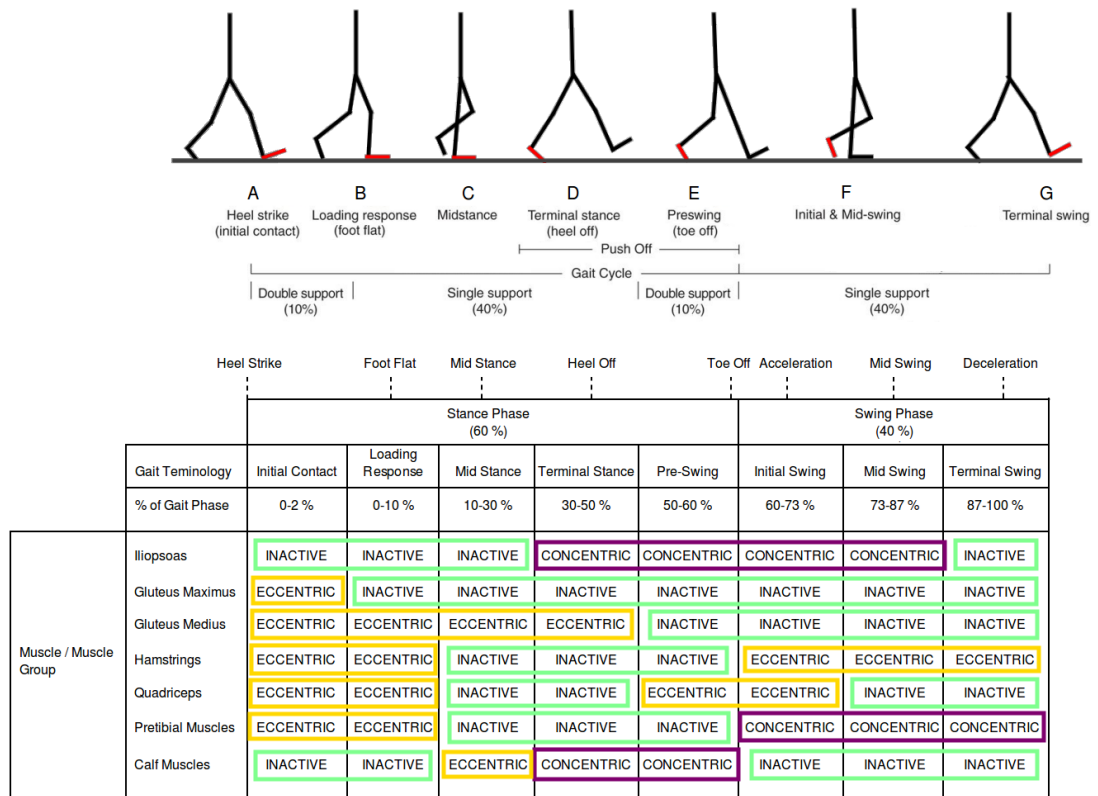


Figure 1.5: **The human gait cycle and muscle activation generalised pattern.** During the different phases of the gait cycle, the muscle groups in the legs are either at rest or contracting eccentrically or concentrically. Table of muscle action adapted from [38].

across the hip, knee and ankle joints [37]. These main groups include: the gluteal muscles, hamstrings and quadriceps in the thigh, pretibial and calf muscles in the lower leg and the iliopsoas in the trunk, Fig. 1.6. During the gait cycle these muscles go through three states: (i) inactive, (ii) concentric contraction and, (iii) eccentric contraction. Where a contraction which allows the muscle to shorten ($force > load$) is described as a concentric contraction and eccentric contraction is one where the muscle lengthens ($force < load$). The specific role of the muscle groups can be subdivided into either flexor or extensors of the joint they control. Furthermore, the flexor and extensor muscles are often in antagonistic pairs and work against each other to control the stepping motion of the leg. The actions of the different muscle groups during the different phases of the gait cycle are to propel the body forward, produce stability of the trunk and provide shock absorption for the leg to prevent damage to the joints. To study individual muscle contractions and their contribution to movement during the gait cycle, a measure of the electrical activity in the muscle can be taken using electromyography (EMG). This can either be recorded intramuscularly using needle electrodes inserted into

Table 1.1: Action of muscles during the gait cycle. Adapted from [13]

Gait Phase	Action	Active Muscle Groups & Specific Muscles	
Stance	Heel Strike (A)	Tibialis Anterior	
		Hip extensors; Gluteus Maximus	
		Intrinsic muscles of foot; Flexor Digitorum Brevis; long tendons of foot	
	Loading Response (B)	Accept weight	Knee extensors; Quadriceps
		Decelerate mass (slow dorsiflexion)	Ankle plantar flexors, Triceps Surae (Soleus and Gastrocnemius)
		Stabilise pelvis	Hip abductors; Gluteus Medius and Minimus; Tensor of Fascia Lata
		Preserve longitudinal arch of the foot	Intrinsic muscles of the foot; long tendons of the foot; Tibialis Posterior; long flexors of digits
	Midstance (C)	Stabilise knee	Knee extensors; Quadriceps
		Control dorsiflexion (preserve momentum)	Ankle plantar flexors (eccentric and Gastrocnemius); Triceps Surae (Soleus contraction)
		Stabilise pelvis	Hip abductors; Gluteus Medius and Minimus; Tensor of Fascia Lata
Terminal Stance (D)	Stabilise pelvis	Hip abductors; Gluteus Medius and Minimus; Tensor of Fascia Lata	
	Preserve arches of foot and fix forefoot	Intrinsic muscles of the foot; Long tendons of the foot; Adductor Hallucis Tibialis Posterior; Long flexors of digits	
Preswing (E)	Accelerate mass	Long flexors of digits; Flexor Hallucis Longus; Flexor Digitorum Longus	
	Preserve arches of foot and fix forefoot	Intrinsic muscles of foot; Long tendons of foot; Adductor Hallucis; Tibialis Posterior; long flexors of digits	
	Decelerate thigh and prepare for swing	Flexor of hip (eccentric contraction); Iliopsoas; Rectus Femoris	
Initial Swing (F)	Accelerate thigh and vary cadence	Flexor of hip (concentric contraction); Iliopsoas; Rectus Femoris	
	Clear foot	Ankle dorsiflexors; Tibialis Anterior	
Midswing (G)	Clear foot	Ankle dorsiflexors; Tibialis Anterior	
	Decelerate thigh	Hip extensors (eccentric contraction); Gluteus Maximus; Hamstrings	
Terminal Swing (H)	Decelerate leg	Knee flexors (eccentric contraction); Hamstrings	
	Position foot	Ankle dorsiflexors; Tibialis Anterior	
	Extend knee to control stride and prepare for ground contact		Knee extensors; Quadriceps

Swing

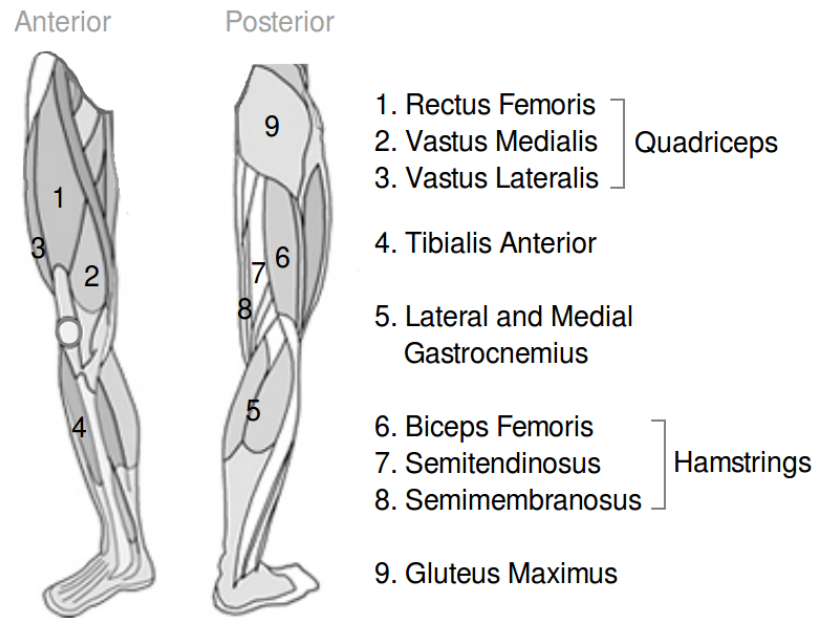


Figure 1.6: **Location of some of the major muscles recruited during walking.**

the muscle or by using surface electrodes placed over the muscle belly on the skin surface (sEMG). The resulting recordings demonstrate the timing and durations of activity in the muscle during ambulation, which can be associated with the muscle's function.

There is a good understanding in the literature on the biomechanics of human gait that allows walking to be modelled on a purely mechanical level. However, this does not explain the processes involved in the control of gait. To understand the neural control of walking a thorough examination of the role of the peripheral (PNS) and central nervous systems (CNS) in both humans and animals is needed.

1.3.1 Receptors

Control of gait requires a vast quantity of information to be fed back from the PNS to the CNS. Receptors located in the muscles and skin are able to sense loading of the body during the gait cycle and transmit this information back to the spinal cord to adapt the stepping to suit changes in the terrain. Duysens et al. (2000) lists the main load receptors for mammals as being the Golgi tendon organ (GTO) and cutaneous receptors in the soles of the feet. The accessory receptors are the muscle spindle (neuromuscular receptor) and other joint receptors (Ruffini endings and Pacinian corpuscles) [39]. Cutaneous, muscle, joint and deep fascial receptors project via the dorsal roots to the dorsal column, spinocerebellar and spinothalamic sensory pathways as well as branching directly to spinal cord

interneurones and motor neurones to provide reflex control. Different groups of afferent fibres carry these nerve impulses from the corresponding receptors or sense organs, these different groups are described in Table 1.2.

1. **Muscle spindles**

Muscle spindles are located within the muscle belly. These sensory receptors detect changes in the muscle length and feed this information back to the CNS. The responses of these sensors to changes in muscle length are important in regulating muscle contraction by activating motor neurones via the stretch reflex to resist the stretch and prevent damage. Information fed back to the CNS is also involved in determining the position of the limbs.

2. **Cutaneous mechanoreceptors**

Cutaneous mechanoreceptors are located in the dermis or epidermis of the skin and are a part of the somatosensory system. Unlike other cutaneous receptors such as nociceptors (pain receptors) and thermoreceptors (temperature receptors), mechanoreceptors respond to mechanical stimuli such as pressure, distortion and vibration.

3. **Golgi tendon organs**

The Golgi tendon organ (GTO) is a stretch receptor which senses changes in muscle tension and signals the force developed in the muscle back to the spinal cord. The GTO is located at the origin and insertion of muscle fibres to the tendons of muscle.

4. **Joint receptors**

Joint receptors are proprioceptors. They relay information to the CNS about the position of a joint. Ruffini endings are mainly found in the joint capsule and are stimulated by a stretching in the tissue and other tactile stimulation methods. Ruffini endings are able to signal joint position under static conditions and during periods of movement, when they can also feed back the direction and speed of the displacement, as a muscle flexing produces joint movement, which causes stretching of the receptor. Pacinian corpuscles (also known as Lamellar corpuscles or acceleration receptors) are the largest cutaneous receptor and adapt rapidly, becoming active at the onset and termination of movement, signalling quick mechanical deformation or vibrations. These receptors can be classed as cutaneous, proprioceptive or visceral receptors, depending on their location as they are found in subcutaneous tissue, connective tissue and internal organs. As a joint receptor

Table 1.2: **Sensory fibres**

Group		Response
I	Ia	Primary afferent fibre. Component of the muscle spindle and the largest and fastest fibre which responds to the change in length and velocity of a muscle. Adapts rapidly to changes in muscle length.
	Ib	Present in the Golgi tendon organ. Controls muscle contraction by generating spinal reflexes and supraspinal responses.
II		Secondary fibre. Second component of the muscle spindle. Provides information on the position of the muscle and in turn, the position of the limb.
III/IV		Type III responds mainly to mechanical stimuli. Type IV are primarily nociceptors but include mechanoreceptors. Both afferent groups have an inhibitory influence on motor neurones innervating the muscle and its synergists. Slow and long-lasting response.

they can only measure joint movement, not static position, so they are involved in signalling the movement velocity of the joint.

1.4 Summary

It can be seen that the whole nervous system in the human is still, to a large extent, poorly understood in terms of how gait is controlled. However, the system can be treated as a black box. Instead of trying to thoroughly understand the exact mechanisms in place, a control strategy for generating stepping can be derived by examining the simple concept of feedback from sensory information, relating to the walking environment, as a means of generating motor output, Fig. 1.7. Knowledge of how sensory information from the PNS relates to motor actions of the muscles and limbs throughout the gait cycle has potential use in SCI rehabilitation. Specifically if foot contact information is related to muscle activity, then contact information from the feet could be used as a feedback control mechanism for use with functional electrical stimulation (FES) of leg muscles to generate walking. In theory, transfer functions can be found to translate information from the feet during the gait cycle into muscle activation signals with correct timing to promote flexion and extension of the hip, knee and ankle joints (analogous to the function of RunBot's motors). A simplified flow diagram of the proposed system can be seen in Fig. 1.8. The long-term aim would be the development of a device

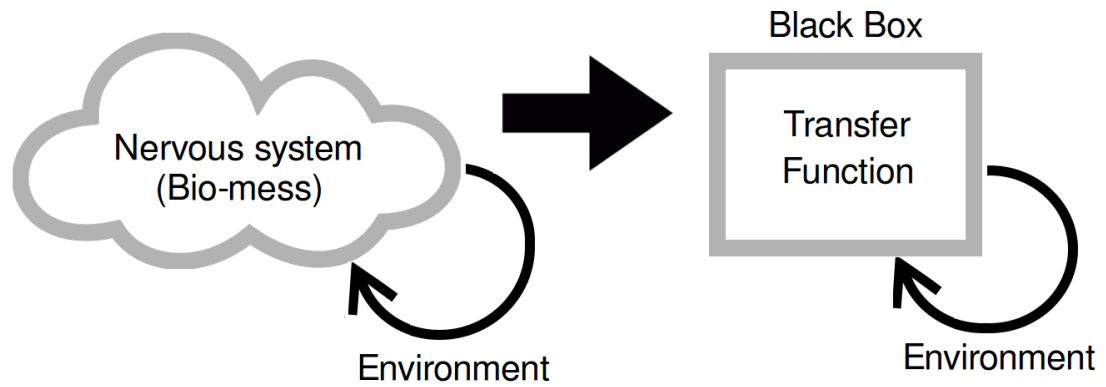


Figure 1.7: **Black box approach to control.** Instead of trying to create a biologically realistic control system, the idea is to generate transfer functions which will translate information fed back about the walking environment into a suitable motor output.

which will promote limit cycle walking, allowing the walker to adapt their gait to suit changing loading conditions dependent on terrain or the environment.

1.5 Thesis overview

Further understanding is needed on the control of human walking and the underlying physiological adaptations that occur after rehabilitative training in patients with incomplete spinal cord injuries. This could lead to an improved functional ability. A deeper understanding of neural control mechanisms may help identify the rehabilitation strategies which will be most beneficial for the patient, but does not necessarily allow technological advancement due to the over complexity and difficulty of trying to mimic a biological system. Instead, a simplistic black box approach in the development of an FES control system based on feedback from the walking environment should assist in the retraining of a functional and adaptive walking behaviour and promote neural repair and/or neural plasticity.

The aim of this research is to investigate sensory feedback in the control of human walking. By taking inspiration from the mechanism of walking used by RunBot, the project focuses specifically on studying ground contact information and the relationship with muscle activity during human walking to determine whether foot contact could be used in a causal system to control muscles and whether this has potential to be used to drive non-invasive FES for use with iSCI patients to assist in their gait capability.

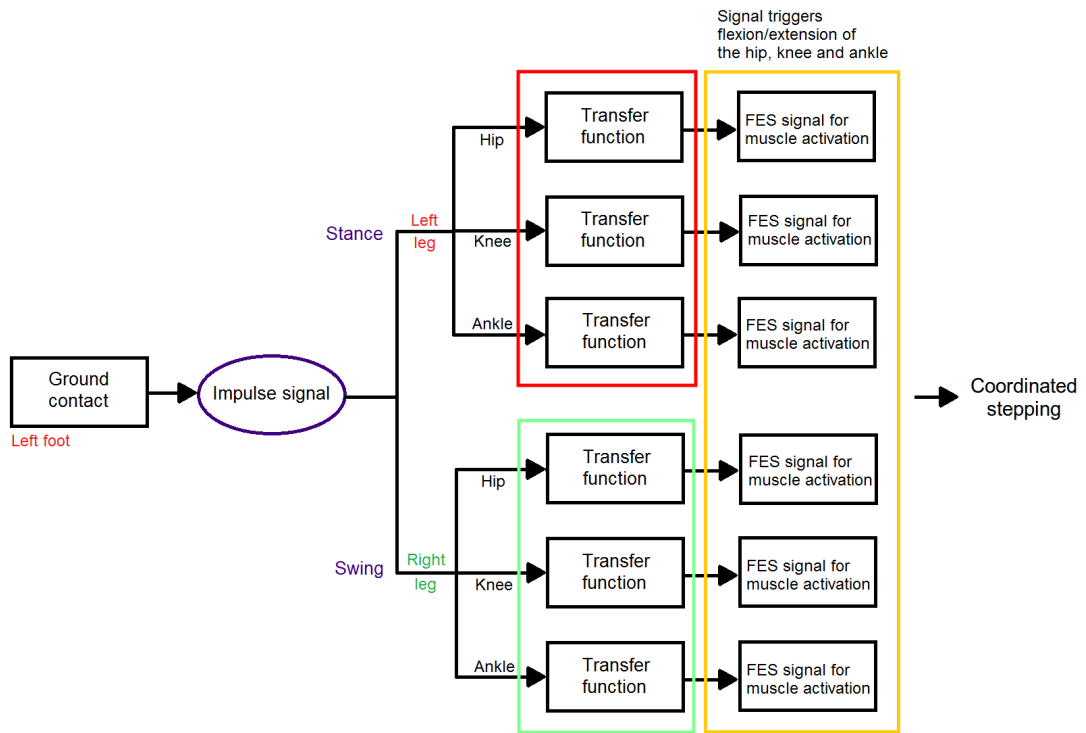


Figure 1.8: **Proposed system for FES.** The calculated transfer functions will translate the ground contact information from the feet into FES muscle activation signals (yellow box). A different transfer function is used to promote flexion/extension of the hip, knee and ankle joints (red box = right leg, green box = left leg). Like the system used with RunBot (see Fig. 1.1) the proposed system will use foot contact to trigger the stance phase of the ipsilateral leg and swing phase of the contralateral leg to produce a coordinated stepping response.

1.6 Research objectives

The objectives of this EngD project were to:

1. Determine which physical quantities, which could be measured on a patient, have a correlation with muscle activity.
2. Determine the transfer functions which translate the physical quantities found to have a correlation with muscle activity into muscle activation signals.
3. Develop feedback control by closing the loop between sensory input and the motor output.
4. Develop an adaptive control system based on physiological principles which could be applied to an extrinsic device in order to develop gait cycle modifications to suit the loading conditions.

1.7 Thesis structure

The thesis is structured in the following way: Initially a thorough background and context to the thesis will be given in Chapter 2 with a literature review on load dependent reflexes and motor control in human walking. Subsequently, how SCI affects walking ability will be discussed alongside an overview of the current therapeutic research using FES as an assistive technology for gait rehabilitation.

The experimental research described in this thesis is divided into two parts:

Part I: Preliminary studies: methods and materials development

Chapter 3 introduces the devices used for recording muscle activity, foot contact information and hip acceleration during treadmill walking and a preliminary study designed to establish the feasibility of the project. The initial walking study resulted in recommendations for developing the methodology for designing definitive studies for recording and processing the walking data. Based on insight from the preliminary study, Chapter 4 discusses a wireless device which was developed and validated for recording gait parameters using healthy participants during overground walking.

Part II: Developing a control system for walking generation using human data

Following the preliminary studies, Chapter 5 focuses on the methodology used to record muscle activity and foot contact data during varying speed treadmill walking and overground walking.

Chapter 6 introduces the techniques used in the analysis and calculation of the transfer functions which translate the foot contact data and muscle activation signals. A minimal, linear, reflexive control system for walking is outlined which is based on the controller used in the RunBot robot.

To analyse the potential of the transfer functions calculated from both the treadmill and overground walking data in producing a functional and stable gait, the derived transfer functions were applied to the second generation of the RunBot bipedal robot (RunBot II) to study how it walked using human data. The results are discussed in Chapter 7.

The outcome of applying the transfer functions to RunBot II suggested that there was a difference between the transfer functions calculated from treadmill and overground walking data. Chapter 8 is a comparison of the data recorded from the treadmill and overground walking modalities.

The RunBot II robot only features actuated hip and knee joints with a fixed ankle so it was not possible to study the transfer functions related to ankle motion on this model. However as the aim of the project is to study a means of controlling FES for use in SCI rehabilitation, the calculation of transfer functions related to ankle joint movement during walking is important in the creation of a complete control system for generating a functional gait. This is discussed in addition to the outline of a suitable control system, to be integrated with that proposed for the hip and knee, in Chapter 9.

Chapter 10 is a discussion of the main outcomes of the research and the thesis conclusions are provided in Chapter 11. Here, the main aspects and contributions of the suggested control method for use in SCI gait rehabilitation are summarised and an outlook on possible future research is provided.

Chapter 2

Literature Review

The literature review describes the current understanding of the neural control mechanisms involved in human walking with particular emphasis on load dependent reflexes as a motivation for the research hypothesis. How this knowledge can be applied in the development of new rehabilitation procedures and assistive technology is subsequently discussed, specifically focusing on functional electrical stimulation (FES), to improve the ambulatory ability of patients with incomplete spinal cord injuries (iSCI).

A comprehensive review of the evidence is necessary to analyse the effects and suitability of gait training using FES for rehabilitation following iSCI. From this information, how robotic walkers have tackled the problem of control in bipedal walking can be addressed and how RunBot's minimal reflexive control system can be related to the mechanisms involved in human walking. Furthermore, whether the strategy could be adapted for use in FES can be established, with the aim of providing maximum control to the paralysed patient over the output of the system to improve in functional walking.

2.1 Load dependent reflexes

There has been substantial progress in the understanding of the role of reflexes in the regulation of locomotor movements since the work of Sherrington at the start of the 20th century. The neuronal mechanisms generating locomotor patterns for animal walking have been well documented [40–42] and there has been a substantial progression in establishing these mechanisms in humans [43,44] which has provided an understanding of the neuronal processes that are associated with function [24]. Insight into the control of locomotion has been established by studying quadrupedal walking in mammals (particularly in cats), stick insect and

crayfish walking, lamprey swimming and bird flight [45, 46]. And more recently in the rat [47]. Although this has produced a significant amount of information on locomotion in animals, there are obvious difficulties in forming comparisons with the bipedal locomotion of humans. As the control of locomotion is closely related to the control of gravitational load, the bipedal human has to compensate for changes in load with postural reactions with different requirements to a quadrupedal mammal supported by four limbs [39, 48, 49]. For this reason, the control of human gait is still poorly described and the degree of similarity in the motor processing to other species requires further investigation. This includes debate regarding the significance of reflex responses produced by sensory input from sensory receptors, spinal networks and also higher centre involvement in the generation of human walking.

Specifically the main focus of the literature review is on how the human body senses and regulates loading information and how this information is used in the control of a walking behaviour. Fig. 2.1 outlines a brief overview in the progression of thinking on the control of walking in humans, which will be discussed in this review. This evolution has shifted from the idea of an open-loop control system to a closed-loop one.

The various publications on the subject can be split into different topics for discussion: centrally generated locomotor patterns (CPGs) (open-loop control); transmission modification in reflex pathways during locomotion (adaptive control); and the role of afferent signals from load receptors in regulating the locomotor movements (closed-loop control).

As the neural control of locomotion in non-primate vertebrates is more thoroughly understood in comparison to human walking, it is appropriate to also consider this research in the review.

2.2 Control of walking - animals

2.2.1 Interaction of reflexes with the locomotor rhythm generator

Common to the locomotor pattern for walking in all mammals, is rhythmic alternating activity in flexor and extensor muscles of the legs [24]. CPGs can be described as a functional neural network of neurones located in different parts of the CNS, which generate periodic motor commands for producing rhythmic actions such as breathing, mastication and locomotion, including flying and swim-

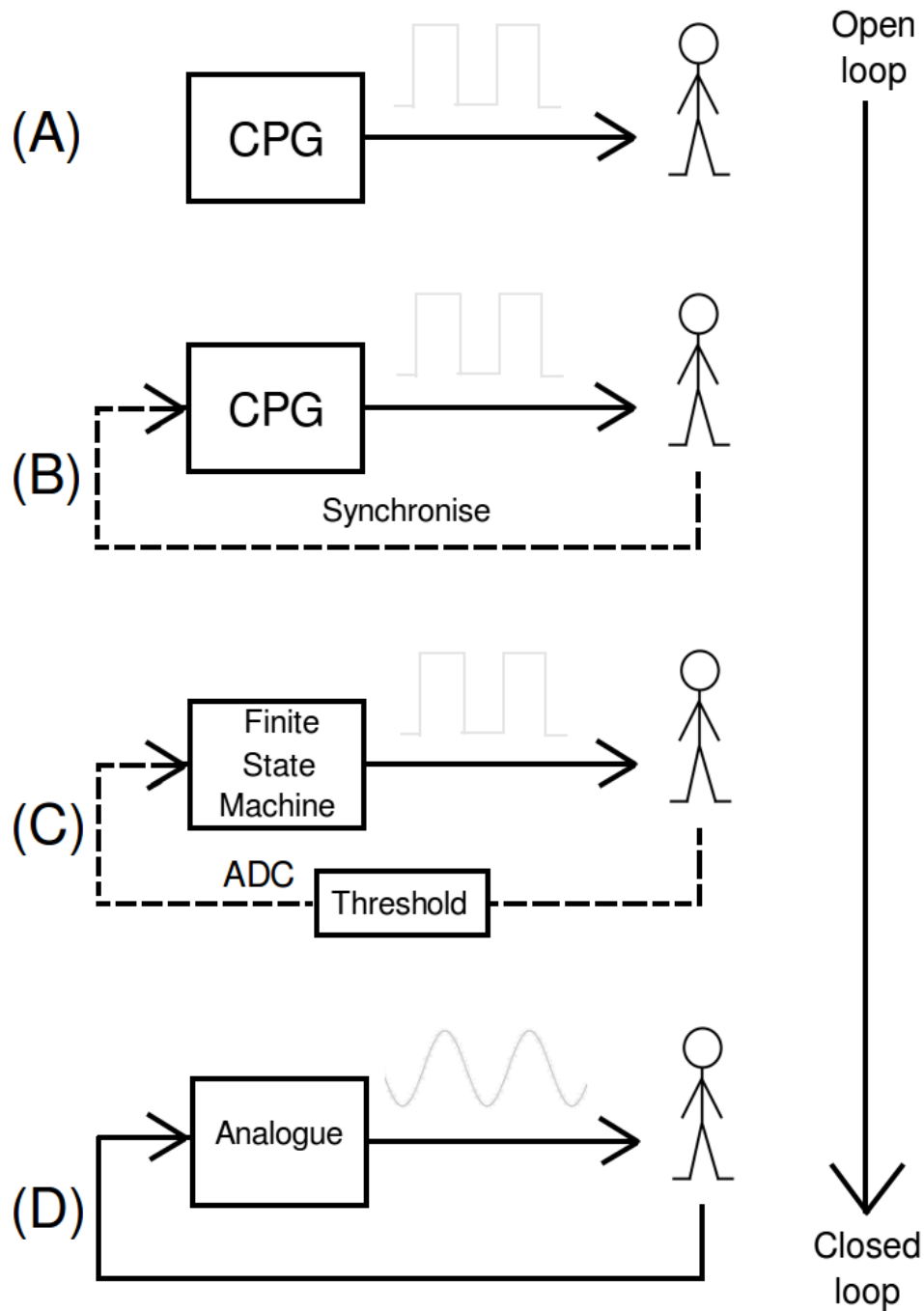


Figure 2.1: **Control of human walking.** There has been a progression in the thinking on how human walking is controlled which has its origins in animal and human based studies. This evolution is moving from the idea of a open-loop control system to a closed-loop one. (A) Central pattern generator (CPG) controls the stepping completely independent of feedback information. (B) CPG operates with the integration of feedback information to synchronise the walking to the environment. (C) Finite state controller, feedback controls the output state of the system. Thresholding acts like an ADC to determine the input state, converting the feedback signals from analogue to digital. (D) A completely analogue system is the hypothesis of this thesis. Feedback controls the output of the system.

ming [40, 50, 51].

The half-centre model was initially proposed by Brown (1914) to address the neuronal control of walking [52]. In this model, two linked neural networks (the half-centres) that produce swing and stance by generating bursts of activity in either flexor or extensor motor neurones. These two networks mutually inhibit each other by being connected through reciprocal inhibition. The coupling between these two systems of neurones results in reciprocity in the motor output, and produces a rhythmical movement of two basic phases.

The half-centre model is based on experiments demonstrating that cats with a transected spinal cord and cut dorsal roots can still show a rhythmic alternating contraction of the flexors and extensors in the ankle [44]. However, it should be noted that not all afferent input is removed by dorsal root transection as it can be communicated to the spinal cord via the ventral (motor) roots, but this is very limited. Nevertheless, this activity is powerful evidence that, in quadrupeds, neuronal networks within the spinal cord have the ability to generate rhythmic motor patterns in the flexor and extensor motor neurones without sensory feedback from the limbs or descending input from the brain [40, 52–55]. This suggests CPGs can provide open-loop control of locomotion, this relates to the control system shown in Fig. 2.1A and can be labelled a Class A system. Stepping could be produced in four limbs by a central interaction of coupled generators from each leg. The ability of the spinal cord to produce a rhythmic motor output resembling a normal motor pattern, even when motor and sensory feedback is removed, suggests that the patterning of the motor neuronal activity, which underlies stepping movements, is largely dependent on the properties and organisation of the interneurones within the spinal cord of vertebrates. To understand the function of reflex pathways requires knowledge of these central elements.

For quadrupeds, it is now understood that the CPG for each of the hind legs of the animal are located in the lumbar section of the spinal cord where the primary components of the network are distributed in spinal segments L2 to L4 [24]. The function of CPGs has been found to be very flexible with the majority able to generate a variety of patterns to adapt to changing conditions. This is dependent on how they are activated, the amount of neuronal tissue isolation and the chemical environment [56]. Neuromodulators have the ability to effect the timing and amplitude of activity as well as initiate the rhythmic activity. Similarly, state-dependent modulation of afferent pathways can effect the function of CPGs, allowing the function to be adapted by input from afferent signals [56], Class B system, Fig. 2.1B.

To enable walking over an uneven surface with a smooth, efficient and stable gait, the motor control system must have the ability to compensate for the changing terrain, from step to step, so the locomotor output is adapted to the walking environment. Behaviours in mammals, including walking, most particularly in the quadrupedal cat have been documented to make use of peripheral inputs in eliciting reflex responses together with CPGs (for review see [46]). However, there is evidence which suggests that some of the muscle activity seen during stance may be produced through reflex pathways some of which do not involve CPGs [39].

In cat models, CPGs can be activated by a variety of different afferent signals conveying sensory information. ‘A-specific’ sensory stimulation (such as tail pinches) has been found to induce or facilitate spinal locomotion [43]. In general it can be seen that if sensory input has a direct connection to the CPG, stimulation of a group of afferents produces rhythm entrainment and/or resetting, with the potential to either block or induce the switching between the alternating flexor and extensor muscle activity [43]. In addition, the mesencephalic or spinal cat has been found to have the ability to match the rate of stepping to the speed of the treadmill [57, 58]. This again reinforces the suggestion that, as the swing phase is relatively constant across different walking speeds, the rate of stepping must have some dependency on sensory input causing the switching from stance to swing [59]. Thus, peripheral feedback signals have function to shape the rhythmic locomotor pattern by controlling phase transitions, delaying or promoting the beginning of the swing phase, and additionally can reinforce the ongoing activity, thus determining the appropriate co-ordinated locomotor pattern [40, 60, 61]. This is a significant mechanism which defines the CPG [62]. Fig. 2.2 demonstrates the hypothesis on CPG activity in the cat. Although this mechanism integrates feedback to modulate the motor output to suit the walking environment, it can still be seen as a predominantly open-loop system as it will continue to function even when all the feedback is absent, Fig. 2.1B.

Observed similarities between fictive and normal locomotor patterns has provided significant and extensive evidence for the existence of locomotor CPGs in various species. Fictive preparations use neuromuscular blockers such as curare to block the neuromuscular junction, causing paralysis, instead of cutting the sensory afferents. This method prevents movement and so eradicates any related sensory feedback. Hence motor output from the spinal cord needs to be recorded directly from the motor nerve (using neurograms) rather than from the muscle. These experiments have shown that locomotor activity, in these animals,

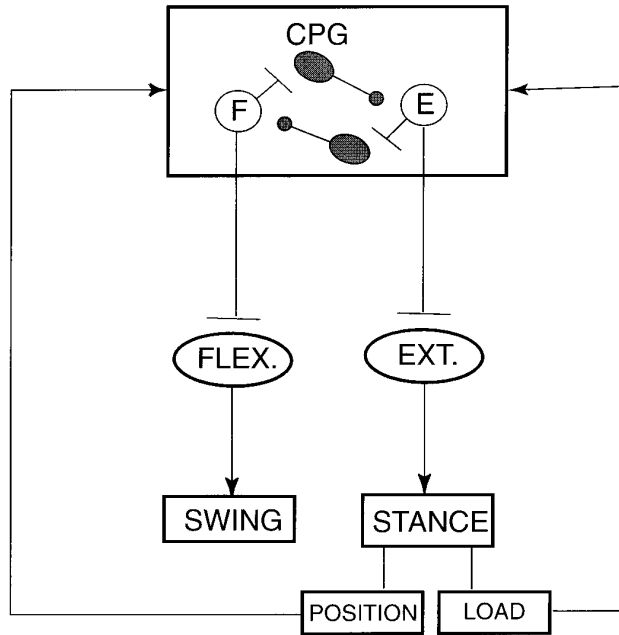


Figure 2.2: **Schematic demonstrating the hypothesis on reflex pathways involving load detecting afferents in cats.** A central pattern generator (CPG) contains flexor (F) and extensor (E) half-centres, controlling flexors (Flex.) and extensors (Ext.), respectively. Group II cutaneous afferents are from the sole of the foot, and group I muscle afferents are from extensor muscles in the leg and act to shape the locomotor pattern. Taken from [39].

is produced by interneurons located in the spinal cord [51]. However, the stability of the pattern and activation may require intact afferent input to be present and it is possible that in intact animals, some of the locomotor output is derived through reflexes and not from CPGs [44].

In summary, it is theorised that sensory regulation of stepping can function through reflex pathways to motor neurones, bypassing locomotor CPGs, or by directly influencing locomotor spinal networks. Sensory feedback can control the timing of the different phases in the step cycle, having action to modify the pattern of muscle activity and contributing to excitation of motor neurones [63], this will be examined further in Section 2.2.2. It is well understood that transmission in many of the reflex pathways alters significantly during walking. In the cat, sensory feedback from the skin and muscles play a substantial role in the regulation of the spinal network which generates the basic walking pattern. This network is controlled by supraspinal structures [40, 64]. Supraspinal drive, together with spinal drive from CPGs and a contribution from the feedback-mediated reinforcement of activity in flexor muscles, work to propel the body

forward [65], see Fig. 2.3.

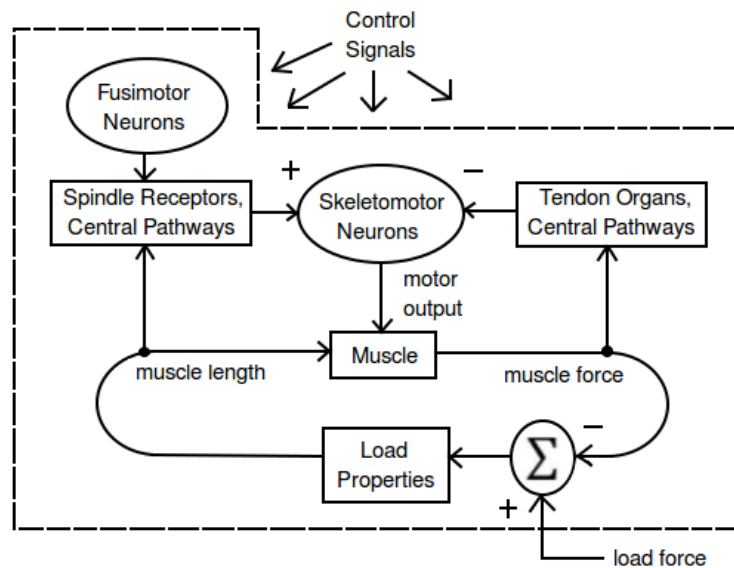


Figure 2.3: **Figure showing the basic organisation of the output stage of the spinal cord (encapsulated within the dashed lines).** The arrows at the top of the diagram indicate the central control (supraspinal) signals to the fusimotor (gamma) and skeletomotor (alpha) motor neurones as well as to interneurons (not shown in diagram). Excitation and inhibition are denoted by + and - symbols. Adapted from [66]

2.2.2 Sensory regulation of stepping

As it has been established that load can be communicated by afferent feedback from different receptors, how can this load information be used in the control of reflexes during walking? This section will examine the effect of stimulation on cutaneous and muscle afferents in mammals (animal) and how this has provided evidence for the role of load dependent reflexes during walking.

Muscle afferents

Muscle afferents have various different roles including, most importantly, in the setting of the phase timings within the step cycle and facilitating the changes between the phases. The feedback has also been found to be important in providing regulation to muscle output amplitude during the different phases of walking [67].

Contraction of a muscle produces sensory input which can directly or indirectly function to either reinforce or inhibit the activity in the motor neurones which are contracting the muscle. This is known as reinforcing and inhibiting

reflexes [59]. Locomotor systems in which sudden unexpected changes in load can occur have a need for these reinforcing reflexes, although the need for reflexes for all types of load compensation is not necessary [68]. When an additional load is presented and the speed of contraction in shortening muscle is to be maintained, reinforcing reflexes can act to recruit inactive motor neurones or increase the discharge rate of the active motor neurones [59].

In the stance phase of gait, Ia afferents are considered to cause reflex effects analogous to negative feedback and Ib afferents, positive feedback. However, as they both only provide facilitation of extensor activity, they can both be seen as assisting reflexes in extensor muscle contraction and load compensation [39]. It should be noted that although group Ia afferents have the potential to contribute to ongoing activity during gait, the magnitude of their contribution remains uncertain [69]. It can however be seen how both these assisting (reinforcing) and resisting (inhibitory) influences could be useful in locomotion to prevent damage to muscles and ligaments during loading. Negative feedback is required when loading is fast (resistive) and positive feedback is needed during gradual loading as is seen during stance (assistive) [39].

Stimulus of extensor group I fibres can be seen as exciting the extensor half-centre of Brown's half-centre model. A close relationship has been found to exist between ground reaction force and ankle extensor activity [69]. Pearson et al. (1976) found that, in the cat, the swing phase (flexor activity) is inhibited and extensor activity reinforced when the ankle extensors are loaded (Ib activity) which suggests that a necessary condition for swing phase initiation is that the leg extensors are unloaded [45,59,70]. Afferent feedback, during the stance phase, from receptors in the extensor muscles enhance force production in ankle extensors by approximately 30% [71]. This reinforcing signal comes from receptors in the muscle, providing reflex excitation for that particular muscle. However, they may also supply reflex inhibition. The main source of this feedback is believed to come from the Golgi tendon organs, which are the main force sensors in vertebrates [39,72]. The action of the Golgi tendon reflex is thus opposite to the myotatic (stretch) reflex pattern and so it is also called the inverse myotatic reflex.

What is important to understand is that there is a task-dependency to reflexes and a reflex reversal is seen during a progression from one task (i.e standing) to another (i.e walking). Inhibitory reflexes can be observed like reinforcing reflexes, in rhythmic functions including walking, flight and swimming. Muscle spindles have pathways which act to inhibit antagonist motor neurones. The inhibitory

reflexes function to limit the amplitude of the movement when it is not subjected to variation in load [59]. For example, generally when there is an activation of flexor muscles, the antagonist extensors are inhibited and in turn, when the extensors are activated, the flexors are then inhibited.

During locomotion the reflex reversal can be seen when there is a suppression of Ib inhibition of motor neurones and an Ib excitation develops, this demonstrates the flexibility of the spinal reflexes and demonstrates their state-dependence [73]. Different locomotor movements in cats can be ‘reset’ by stimulation of various afferents, including flexor reflex afferents (FRA) [74] as well as Ib afferents, which act on interneurons of the extensor generator [75]. Electrical stimulation of joint afferents, cutaneous afferents and group II and III muscle afferents (from both flexor and extensor muscles), in spinal cats, elicit polysynaptic actions matching the pattern of the flexion reflex and crossed extension reflex (withdrawal reflex). For this reason, these afferents have been named the flexor reflex afferents (FRA) (for review, see [73]). These studies highlight that sensory feedback is of significant importance in control of the generated movement and in driving protective reflexes such as the withdrawal reflex. The information being sent from these afferents requires assimilation into the ongoing spinal network activity which is producing the stepping, to allow adaptations to the movement.

The timing and amplitude of locomotor bursts in the spinalised cat have been found to be significantly affected by changes in hip position by Grillner et al. (1978) [76]. This implies that sensory input from receptors detecting the load carried by the leg and the leg position must have an influence on the swing generation. Regulation of stance duration is provided by afferent feedback from stretch-sensitive receptors in hip flexor muscles [76–78] and load-sensitive receptors in ankle extensor muscles [70, 79]. Muscle spindles measure the muscle length and the rate of this change, signals taken from the opposing muscles are combined and give information on the position of the joint and the speed of movement, this demonstrates a control system operating on negative feedback, Fig. 2.4.

As has been discussed, afferent regulation of stance duration and swing initiation ensures that the leg is unloaded (reduced force in leg extensor muscles signalled by load receptors) and extended beyond a certain position (stretching of leg flexor muscles signalled by hip afferents) [45, 59]. This process suggests that Ib extensor input has a direct pathway to the centres involved in generating the pattern of flexor and extensor activity seen during walking cycle. What is clear, is that sensory receptor input has a major influence over the extensor motor neu-

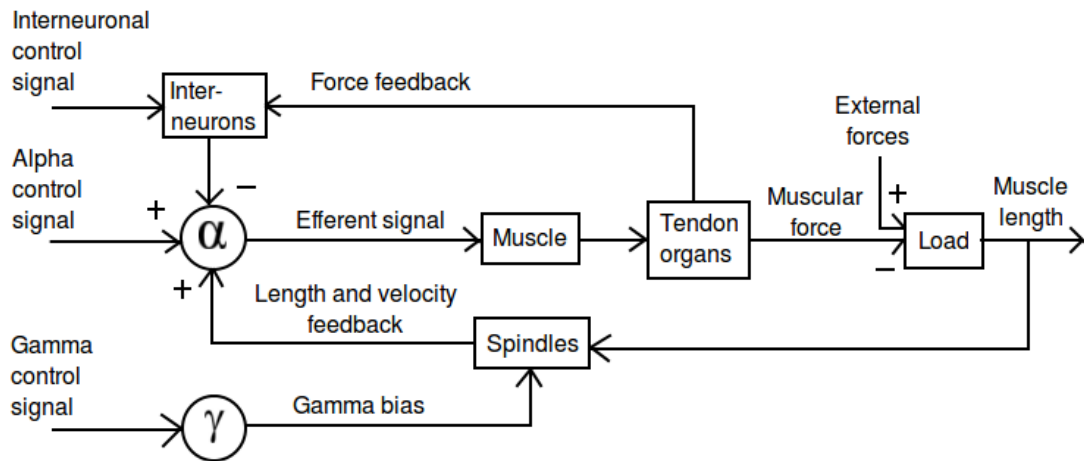


Figure 2.4: **Block diagram of a muscle control system.** In this diagram, the muscle and loading are regulated by feedback from tendon organs and spindles which project to the spinal neurones (they also project centrally to the brain, but this is not shown). Descending feed-forward central controls reach all the spinal interneurons, only some are included in the diagram. The symbols + and - indicate excitation and inhibition. Adapted from [66].

rones during the stance phase of walking, and thus have the ability to regulate the magnitude of activity in response to the sensory feedback.

Cutaneous afferents (Feet)

A co-ordinated reflex with a function as a “stumbling corrective response” was first documented by Forssberg (1979) [80]. This reflex response allows the stability of the ongoing locomotion to be maintained when an obstacle is encountered, leading first to a knee flexion to provide clearance of the obstacle, followed by an exaggerated swing to compensate. The response can be seen in the cat when an electrical or mechanical stimulus is applied to the dorsum of the paw, which evokes a significant flexor response during every phase of the step cycle [80]. If the stimulus is applied during the swing phase, the flexor muscles are activated with a short-latency, which enables the limb to lift the paw clear over the obstacle. If the stimulus is given during the support period, an inhibition followed by an excitation of the extensor muscles occurs. Consequently, the extension is not affected, but there is an increased flexor activity in the following swing phase as the limb is withdrawn from the stimulus. The results demonstrate how intact cats are able to compensate quickly for sudden or unpredicted perturbations; furthermore, the reflex pattern and the induced gait corrections are adapted to the ambulatory activity so that functional movements are produced during every phase of the gait cycle [80]. The origin of this corrective response was found to

be the cutaneous afferents in the paw dorsum of the cat (for review see [46]), Fig. 2.5. It follows that cutaneous afferents can produce reflex responses which can functionally modify the ongoing quadrupedal locomotion.

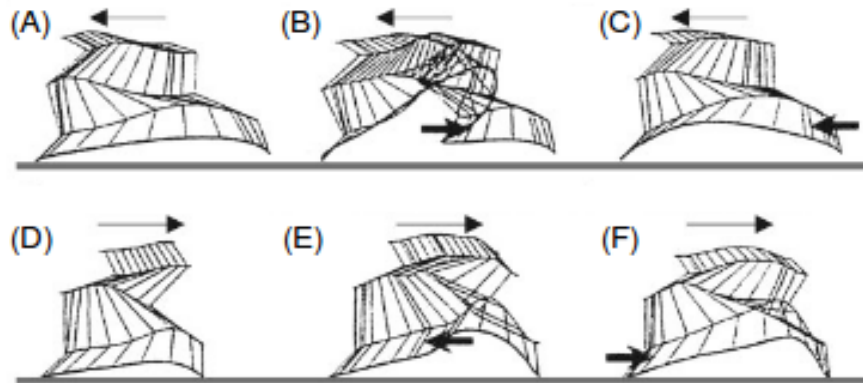


Figure 2.5: **Cutaneous stimulation in the cat and the effect on locomotion.** This figure shows the trajectories of the hind limb before and after mechanical stimulation was applied during the swing phase in forward and backward walking. (A) and (D) show normal, unperturbed swing phase trajectories. (B) and (E) show the response to obstructing stimuli and (C) and (F) show reposes to non obstructing stimuli. Direction of walking is indicated by arrows. Adapted from [67].

Sherrington (1910) demonstrated the extensor thrust reflex, which is a reinforcing reflex [81]. Stimulation of foot pad cutaneous receptors excites extensor motor neurones that results in a strong thrust of the foot downward and backward. It is now understood that, during stance, reflexes produced from sensory input from cutaneous receptors in the foot function to reinforce activity in the discharge of motor neurones during the leg movement [82]. Removal of cutaneous receptor input from the hind leg paws of normal intact cats has been shown to have little influence on the gait pattern produced while stepping on a smooth horizontal surface [83, 84]. However, a substantial effect is seen when the animals walk on sloped ground. In chronic spinal cats, removal of cutaneous receptor input from the paws produces inadequate weight support of the lower body while stepping on a moving treadmill [84]. Cutaneous receptors within the sole of the foot register the deformation of the foot and ankle due to the application of load, seen during the stance phase [39]. Just after the foot contacts the ground, there is a step increase in nerve activity supplying the foot in normal intact cats [85]. Recordings from single afferents in cats, during the stance phase, demonstrate that activity is produced during stance even from skin areas that do not directly contact the ground [86, 87]. This is potentially due to skin stretch, activating mechanoreceptors with low thresholds, and could thus have a proprioceptive function [39]. From these studies, it can be concluded that cutaneous

signals are vital for producing skilled locomotor actions, and in spinal subjects, appropriate signals from cutaneous receptors of the paws are required for load feedback to control stepping.

2.2.3 Relevance of animal models to human walking

The upright position of the body during bipedal gait means that the specific neuronal mechanisms are different to those used in the regulation of quadrupedal locomotion. Fundamentally, load-compensating reflexes in humans need to act to regulate the centre of gravity of the body over the feet. However, in quadrupeds, control of body geometry, rather than centre of gravity, has been found to be the action of these reflexes [88]. A combination of afferent input is required to provide all the information necessary to precisely control the body's equilibrium [43, 89]. It is known that similarly to cats, loading of limb by gravity is registered in the human by several types of afferents which indirectly and directly signal the load. Proprioceptive reflexes, which are involved in controlling body equilibrium, are dependent on contact forces being present, opposing gravity [39].

2.3 Control of walking - humans

2.3.1 Central pattern generators (CPGs)

Although CPGs have been identified and documented in vertebrates and invertebrates, they have yet to be conclusively described in humans. This is mainly due to the inability to replicate in humans the experimental procedures used in other species of mammal. The vast quantity of evidence for locomotor CPGs and a Class B control system (Fig. 2.1B) in various different species suggests it would be unusual if humans were completely without some kind of pattern generating structure. However, the lack of evidence could be due to other mechanisms of control being of greater importance than CPGs in bipedal gait, and could include reflex and supraspinal processes [44]. There are also uncertainties about whether mammal (non-primate) models are suitable analogues for human walking [90, 91]. For example, in humans, plantar flexor muscles are dominant for propulsion during stance but they are of less importance in cats [44]. One of the main observations which identifies the potential differences between human CPGs and those found in other species, is that following complete spinal cord lesions (cSCI), humans become completely paralysed below the site of injury and evidence of locomotor activity is usually not seen for many years [63]. This indicates

that humans do not follow a Class A control system, Fig. 2.1A.

There is limited evidence which does promote the existence of a spinal locomotor CPG in humans, with some properties being defined as being similar to that of the cat. For example, pathways which produce disynaptic reciprocal Ia inhibition, autogenic Ib inhibition, recurrent inhibition and the flexion reflex have been identified in the human spinal cord and have a similar function as is found in cats [92]. In addition, these processes modulate in a phase dependent way again demonstrating similarities with cat data. The method for establishing these similarities has been through the use of non-invasive electrophysiological experiments to study the neuronal pathways and mechanisms for motor control in the human spinal cord [63].

There remains a significant lack of information identifying the role of feedback from load receptors on CPGs in humans but there has been suggestion of some significant similarities with the interactions documented in the control of walking in cats. The most convincingly has been studies conducted on stepping in young children. Yang et al. (1998) conducted a study where additional load was applied during the stance phase of infant stepping and concluded that the loading acted to prolong the stance phase and delay the onset of swing phase, which is similar to what has been observed in cats [93]. Although this observation does not apply directly to adult walking, there is indirect evidence in adult humans, that extensor unloading may be important in the initiation of the the swing phase, as seen in cats (and also in invertebrates [62]). When humans progress from standing to walking, this begins by suppression of activity in extensor muscles (like the Soleus) and then, following a short delay, flexors including the Tibialis Anterior contract [94]. This agrees with the concept that input from the Soleus Ib system of afferents needs to fall below a certain threshold value before there can be activation of the Tibialis Anterior [39].

Researchers studying Macaque monkeys with spinal cord transections did not manage to produce stepping motions using methodology equivalent to that used in cat studies, which is evidence against the existence of CPGs in primate mammals [24, 95]. However, rhythmic alternating activity could be produced if the spinal cord remained partially intact (incomplete transection) and more successfully when locomotor centres within the brain stem were stimulated in decerebrate¹ animals with an intact spinal cord. Similarly, a study of spinal cord injury (SCI) patients by Dietz et al. (2002) describes the limited coordination between the two

¹Decerebrate is defined as a lesion made at the level of the mammillary bodies, leaving the brainstem intact.

legs of the patients, demonstrating the idea that there is limited coupling between CPGs (if they are indeed present) when the input from supraspinal structures is reduced [96]. The conclusion from these studies is that, if a CPG is present in primates, then it has a more significant dependence on intact supraspinal control pathways than in the cat [63].

Direct evidence for the presence of locomotor CPGs in primates is limited. One instance is that fictive locomotion can be produced in Marmoset monkeys after administration of Clonidine (an alpha-2 receptor agonist) or NMDA (a glutamate receptor agonist) [97]. This study suggests that in each species, the pharmacology of the spinal CPG varies significantly and activation with the correct method would require substantial further research [24].

Calancie et al. (1994) documented evidence of a human CPG based on observations of a patient with chronic spinal cord injury [98]. The individual had suffered an injury to the cervical spinal cord and had little voluntary motor function below the neck for the past 17 years. However when lying supine with extended hips, the patient experienced step-like movements of the legs involving alternating flexion and extension of the hips, knees, and ankles, which were smooth and rhythmic and could not be ceased by voluntary effort. The investigators suggested that afferent input to the spinal cord due to ongoing osteoarthritis at the hip was a prime factor in promoting the CPG movement in the particular individual [98]. A hypothesis reinforced by observation of reduced movement following Lidocaine being injected into the hip joint capsule. Sensory input facilitating CPG driven movement is consistent with research involving spinalised animals where the application of afferent input such as tail pinches and stimulation of the perianal area causes the strength and rate of locomotion to be increased [43].

Although the observation of locomotor movement in a chronic SCI patient appears significant as evidence of CPGs in humans, the fact that the individual's injury was an incomplete lesion of the spinal cord indicates that it is impossible to conclude that the observed movements were only generated by the spinal cord. It also highlights the difficulties in comparing motor function following spinal injuries in humans with research animals which have had clean, precise transections to the spinal cord. As crush injuries caused by a compressive force of the vertebrae on the spinal cord is the most common form of spinal injury found in humans [15], evidence for CPGs through observation of recovery of function may be unreliable due to incomplete transection of the cord and spinal pathways remaining intact.

Again, what appears evident is that even if a CPG is in operation in the

human spinal cord, supraspinal control centres may have a greater contribution to locomotion generation than has been observed in other mammals. This may explain why it has been difficult to activate a CPG in primates independent of the normal supraspinal control.

2.3.2 Reflex function during locomotion

Continuous neuronal regulation is required to maintain the body's centre of mass over the support base of the feet, which is indicated by gravity-dependent receptors, or load receptors [99]. As has already been described in non-primate mammals in this chapter, specific and non-specific load receptors also exist in humans. Cutaneous receptors in the foot sole are activated upon loading, in addition to receptors that can sense joint angle changes of the hip, knee or ankle which results on applying load to the limb [48]. Specific load receptors are located in the muscles and give a measure of muscle force. And, non-specific load receptors perceive load, indirectly, along with their direct functions such as signalling length, position or movement. Fig. 2.6 highlights the possible mechanisms involved in generating walking in humans.

Stretch (myotatic) reflex

The stretch (myotatic) reflex operates to keep muscles at a constant length and to regulate this by resisting any change in length. Reciprocal inhibition can be observed where stretching of one muscle also causes the synergist muscle to contract and the antagonist muscles to be inhibited. It is known that the spinal cord is involved in the stretch reflex because of observation that if the dorsal roots are cut then it disappears [100].

It has been suggested that the function of the stretch reflex is to adapt the motor patterns of the leg muscles in reaction to, and to compensate for, any unexpected changes in ground level or terrain [101, 102]. However, depending on the stance conditions, signals from receptors in the leg signalling muscle stretch do not always result in a compensatory stretch reflex but instead result in activation of antagonistic muscles. This supports results from investigations which have found leg muscle EMG adjustments related to control of the bodies equilibrium, keeping the centre of mass over the feet [103, 104]. Neuronal mechanisms could explain rapid unilateral patterns of reflex activity in leg extensor muscles but a more complex bilateral coordination of leg muscle activation is required in order to try to maintain the body's equilibrium when gait has to adapt to sudden

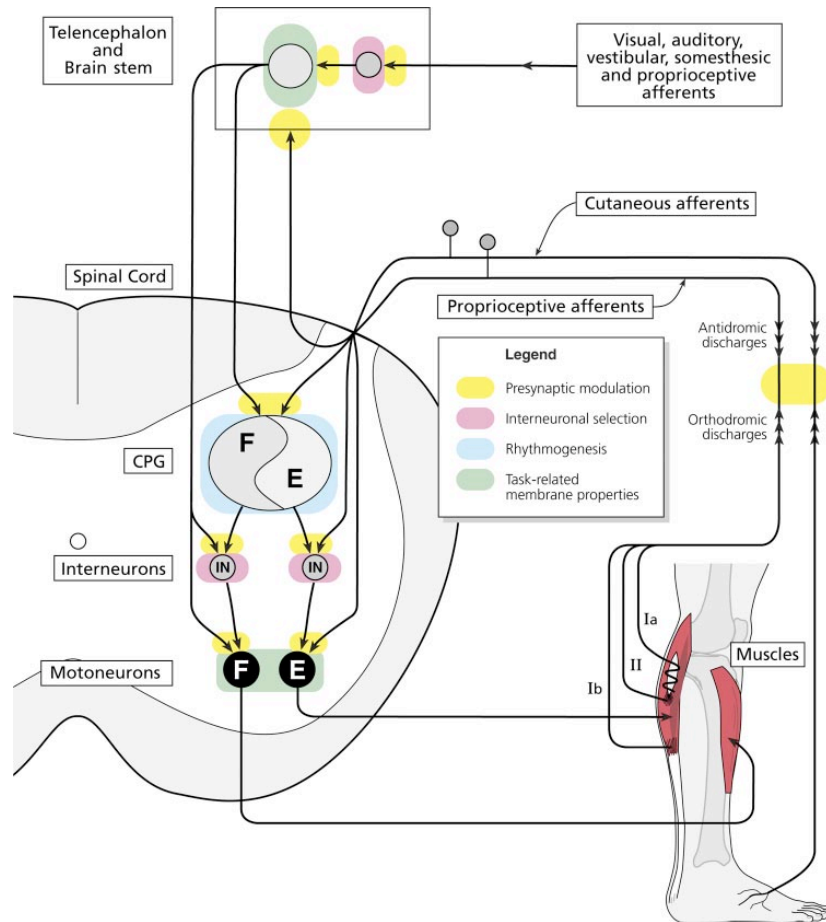


Figure 2.6: **Possible mechanisms of sensorimotor interactions during human locomotion** This diagram demonstrates how afferent inputs project to motor neurones directly or via interneurons or via a CPG itself. The sensory inputs are under phase-dependent inhibitory control (highlighted in yellow) generally as they enter the spinal cord or brain stem. Pre-synaptic inhibition allows the transmission efficiency to be regulated during different tasks. The inputs then make contact with second-order neurones which are modulated rhythmically, so excitatory or inhibitory responses can be produced during the different phases of the gait cycle. Similarly, transmission pathways may be opened or closed depending on the required task (task-dependency) (interneuronal selection is highlighted in pink). Figure is taken from [67].

obstacles [43, 105].

Researchers have used pneumatic devices to dorsiflex the foot and thus stretch the Soleus muscle during the stance phase of walking and have estimated that the stretch reflex could contribute up to 30-60% of the activation of Soleus muscle during walking, particularly during the early part of stance [48, 106]. A study by Sinkjaer et al. (1996) verified the conclusion of the study by Yang et al. (1991) by constructing and using an actuator which was capable of stretching the ankle joint during all of the phases of the step cycle [107, 108]. Both studies concluded that activation of ankle extensors during stance is significantly contributed to by muscle afferent input, see Fig. 2.7.

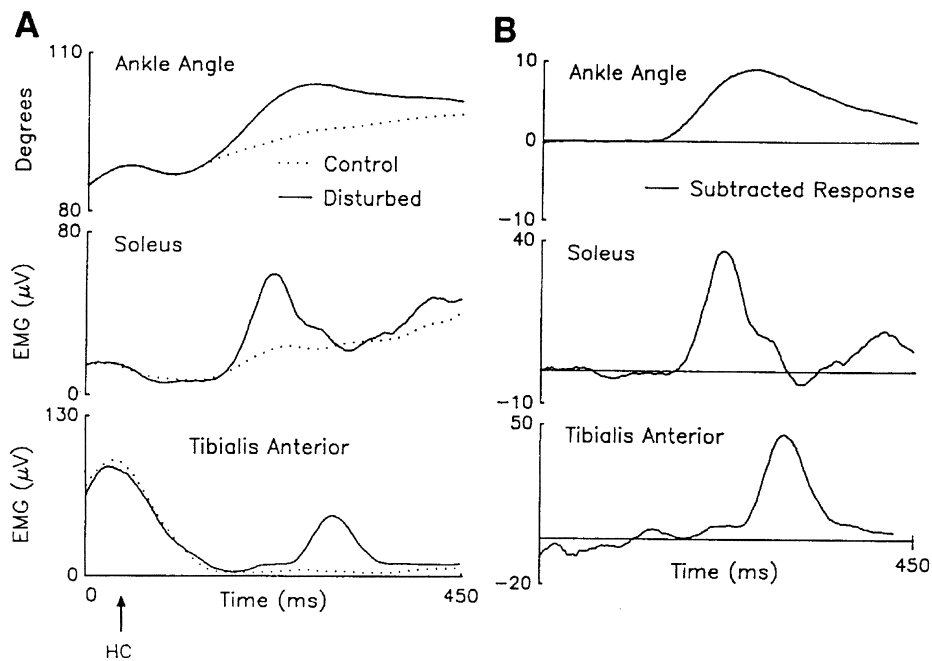


Figure 2.7: **Stretch reflex EMG responses after dorsiflexion using a mechanical actuator during stance phase of walking on a treadmill.** This diagram shows a sample of data demonstrating the stretch reflex response in the Soleus and Tibialis Anterior muscle when a perturbation was introduced during early stance. (A) shows the control and disturbed gait cycle data, whereas, (B) shows the subtracted results. A large EMG peak in the Soleus muscle can be seen at short latency following ankle stretch (B (middle graph)), from [46, 106].

These studies used perturbation to evoke sensory activity in order to measure the change in EMG activity following a stretch reflex, however this method cannot be used to evaluate the role of sensory information during normal unperturbed walking. Sinkjaer et al. (2000) used a portable accentuator to provide a sudden blockage to plantar flexor muscles lengthening during mid stance in order to study the result of removing sensory feedback from the active muscles (sudden

unloading) [109]. The investigation found that removal of sensory feedback caused a drop in Soleus muscle activity with a short latency of 60 ms, which implied that the spinal pathway was primarily involved as the supraspinal pathway requires a longer latency period. As blockage of Ia afferents with ischemia provided little change to the reduction in EMG activity, it is believed that group Ib and group II afferents are responsible [109]. This verifies previous suggestion by Dietz et al. (1987) that Ia afferents do not have such an important role in Soleus EMG activity, in comparison to feedback from other afferents [102].

Studies on the stretch reflex have suggested that the reflex may have a function in stabilisation and in load-bearing in early stance but may not provide much contribution to propulsion in late stance [46]. Although more research is required to fully characterise the stretch reflex and its role in walking, it does appear to be of functional importance in force production during locomotion in humans.

Load receptor reflexes

Investigation of stepping in infants has found that, from birth, infants will step continuously when their feet are put on a moving treadmill [110,111]. The stepping rate adapts to changes in treadmill belt speed, an observation which echoes the stepping seen in spinalised cats. This suggests that the regulation of infant stepping is by afferents signalling the position of the hip in addition to input from load-sensitive receptors [111]. As immature descending pathways from the spinal cord are not believed to be fully functional in young infants it is thought that stepping is regulated predominantly by neuronal circuits in the spinal cord [24]. The rule governing afferent regulation of stance duration, which is identified in the walking mechanism of cats, has also been found to correspond to the walking system of human infants [112] but does not clearly compare to walking in adult humans.

Water immersion experiments have been used to investigate the effect of reduced body weight on the receptors involved in signalling changes in the body's centre of mass compared to the support base [113]. This technique enables the manipulation of body mass without affecting vestibular function. If there is a gravity dependence of compensatory EMG responses, a manipulation of the force between the feet and the support surface should affect the responses to destabilisation due to movement of the platform beneath the feet. Dietz et al. (1989a) found a close relationship between actual body weight and the amplitude of EMG responses following forward and backward displacements [113]. However, no correlation was found between loading of the subjects and muscle activity on ground.

When the body is immersed in water, the body weight is reduced and in turn muscle activity amplitude and postural reflex responses are observed to be reduced in the ankle extensors [114]. Interestingly, a similar gravity-dependence is missing in the ankle flexor muscles, which suggests that proprioceptive input has a more significant role in extensor muscles, than in the flexors.

Body weight is dependent on the surrounding environment so load is of different importance depending on the motor activity. In overground walking, gravitational load is crucial but in underwater locomotion, frictional load is the crucial element. Similar differences can be observed between walking and swimming in mammals where similar locomotor programs are used but the relative phase timing is dependent on the load [39].

Immersion experiments identify that there is some evidence that reflexes which function to stabilise human posture, muscle proprioceptive and vestibulospinal reflexes, depend on activity of receptors which indicate changes of the body's centre of mass from a neutral position. Extensor load receptor input could provide this information [105]. These receptors are believed to be important for producing leg extensor activation during locomotion in cats [115] and man [99] and are thought to signal changes in the projection of the body's centre of mass compared to the position of the feet. Unloading of one leg results in compensatory reflexes which produces bilateral responses, as long as the contralateral leg is acting to support the body [116]. Split-belt treadmill studies conducted by Dietz et al. (1989b) investigated applying perturbations to walking during the stance phase [117]. These bilateral displacements resulted in responses that were most significant when both of the two treadmill belts moved in the same direction. Displacement of the belt in the opposite direction caused the body's centre of mass to be between the legs, causing less of a compensatory response. This was shown to be due to an automatic co-contraction of the homologous muscles of the legs. The result is a reduced level of leg muscle activity when both legs are displaced in the same direction and a linear subtraction when they are displaced in opposite directions [117]. It can thus be argued that ankle extensor load receptors must be vital in the maintenance of body posture. Observations in cats suggested that this afferent input probably comes from the Golgi tendon organs, demonstrating these receptors have a function in the regulation of stance during the gait cycle [43]. The conclusion from these experiments implies that, during locomotion, there is a switching between extensor Ib inhibitory pathways closing and Ib facilitatory paths opening.

Swing bursts have a similar duration and timing in swimming and walking

(assuming the muscles are contracted to their maximum rate during the activities), whereas extensor bursts differ due to presence or absence of ground reaction forces [39, 118]. Load receptors in the leg extensors could be responsible for the different EMG patterns, explaining their anti-gravity function. This is a potentially excitatory function of load receptors which, for extensor muscles of the cat has already been described [70, 75, 115]. The findings suggest that these receptor signals may arise from Golgi tendon organs and are mediated by Ib afferents to the control system.

Jensen et al. (1998) used a split-belt treadmill to study gait adaptation to different walking speeds in each leg, in human subjects [119]. Unloading or loading of the body during the training duration of the split-belt walking produced an improvement in the ability to adjust the stepping to the belt speeds. This was suggested as being due to an associated change in kinaesthetic feedback with change in load, increasing awareness or sensory sensitivity which could promote better matching of limb speeds [119].

2.3.3 Cutaneous reflexes (Feet)

It has been documented that ground reaction forces influence the locomotor activity of the leg during human treadmill walking [120–122]. The action of plantar pressure signals from the foot sole have been implicated in the reflex regulation of locomotion [123–125]. As is documented in spinalised and decerebrated animals, sensory afferents from the foot sole signal spinal interneuronal circuits which can delay or suppress the initiation of swing, promoting stance and effecting the correct placement of the foot during stepping [82, 84, 124, 126]. Load receptors can act to signal unloading and contribute to the termination of stance [39].

Cutaneous reflexes, in particular those with responses to stimulation of the sural and tibial nerves (nerves innervating the lateral border of the foot and the ventral foot surface), have shown phase-dependent modulation of discrete reflex responses occurring with restricted latencies [127]. There is a significant amount of afferent activity originating from the cutaneous receptors of the foot following heel strike with the ground [128]. Research studying electrical stimulation of nerves that supply the skin of the foot suggests that strong reflex activations in various leg muscles can be generated during human gait [127]. This information could have great potential for use in spinal cord injury rehabilitation strategies. Where reflexes can be triggered using sensory input to the foot and used to reinforce training and provide feedback to undamaged pathways.

Humans can carry loads of up to 70% of their own body mass during walking

[86]. When bearing loads or walking uphill there is an increase in extensor muscle activation [129]. In patients with incomplete or complete spinal cord injury, the level of activity in leg extensor muscles is found to be dependent on the amount of body weight support. Normal human walking requires anti-gravity leg muscles to be scaled with the load provided by body weight to provide effective gait. This is produced by cutaneous receptors in the foot signalling loading while Golgi tendon organs in extensor muscles measure the force which is exerted by these muscles (see Section on load receptor reflexes) [39].

Task-dependent changes in the effect of cutaneous afferent input on certain muscles of the lower limb was investigated by Burke et al. (1991) [130]. In human subjects during standing on stable, tilted and unstable bases, the sural nerves were electrically-stimulated with stimuli trains designed to activate afferents from cutaneous mechanoreceptors. Clear reflex responses were observed in the ipsilateral Tibialis Anterior, Soleus, Biceps Femoris and Vastus Lateralis, but only when the muscles were contracting and there was no reflex effect found when the muscles were inactive. The researchers found that cutaneous mechanoreceptors in the foot produce reflexes which are widespread across muscles in both limbs, but most significantly in the ipsilateral limb. They indicated that the reflex pattern in muscles and between the muscles is task-dependent and that these task-dependent changes demonstrate a plasticity of the expression of cutaneous reflex activity to ensure stability [130].

Muscle and cutaneous reflexes thus appear to have a task-dependency, with the amplitude of cutaneous reflexes varying throughout the step cycle. Task-dependent and phase-dependent changes in the modulation of group I (muscular afferents) and cutaneous inputs have also been identified in human locomotor activity. Like the cat [80], a complete reversal in the sign of a cutaneous reflex has been found during human walking [127,131]. Excitation during swing changes to inhibition during the swing-to-stance transition in the Tibialis Anterior muscle. DeSerres et al. (1995) studied post-stimulus time histograms (PSTHs) of single motor units during walking and found that the reflex reversal is probably due to parallel inhibitory and excitatory pathways to Tibialis Anterior motor units [131], Fig. 2.8B. The reflex reversal is usually seen in muscles with a two-burst pattern during the step cycle, like the Tibialis Anterior, and only subsequent to stimulation of cutaneous nerves [46,132].

Yang and Stein (1990) studied tibial and sural nerve reflexes and reflex reversals and concluded that cutaneous reflexes are important in withdrawal response to stimuli as well as preserving balance during the step cycle [127], Fig. 2.8A.

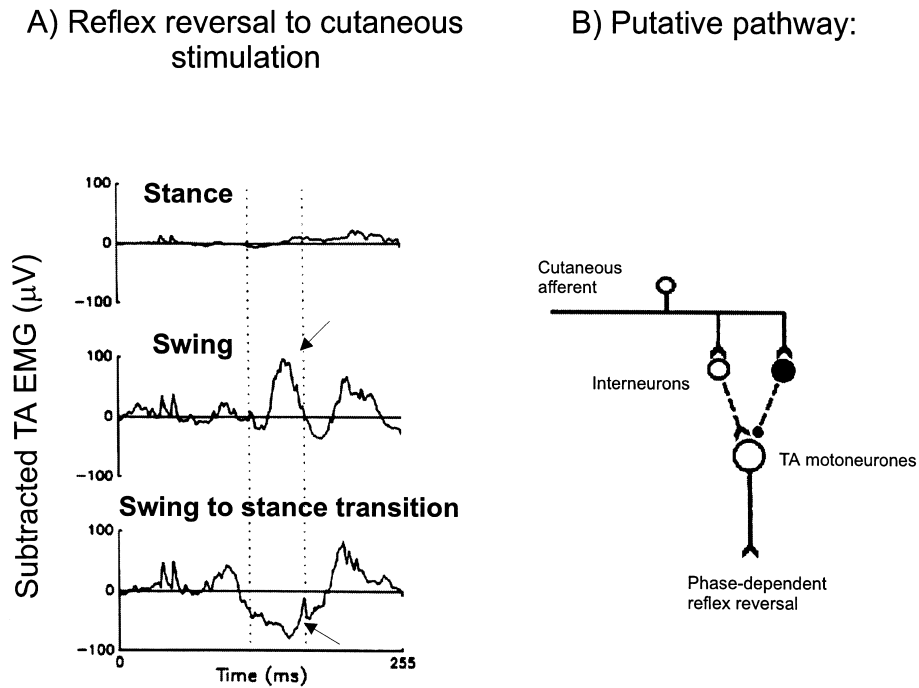


Figure 2.8: **Phase-dependent modulation and reversal of cutaneous reflexes during locomotion.** (A) EMG traces from Tibialis Anterior muscle showing the reflex response to tibial nerve stimulation (background EMG has been subtracted). The arrows point to the excitatory reflex observed during swing which is reversed to an inhibitory reflex during the swing to stance transition. Taken from [46] but original unadjusted figure is from [127]. (B) This schematic shows the pathway which might account for the reflex reversal to cutaneous stimulation observed in (A), from [131].

The net reflex response of stimulation of the tibial and superficial peroneal (SP) nerves were described by Zehr et al. (1997) [133]. Reflexes to stimulation of these nerves have functional effects during swing or during the swing-to-stance transition. During the early part of the swing phase, stimulation of the SP nerve elicits a stumble corrective response which involves ankle plantar flexion and knee flexion. Stimulation of the tibial nerve generates a withdrawal response at the stance-to-swing transition and a placing response at late swing. In addition, phase-dependent reversal of the reflex is identified when the tibial nerve is stimulated so that dorsiflexion of the foot can be seen during one phase and plantar flexion in another [133]. Fig. 2.9 illustrates the functional effects of cutaneous reflexes from stimulation of the tibial and SP nerves.

Zehr et al. (1998) demonstrated that sural nerve stimulation during swing produced responses which resulted in the withdrawal of the foot from the point of stimulus [134]. The reflex acts at different phases of the step cycle for an

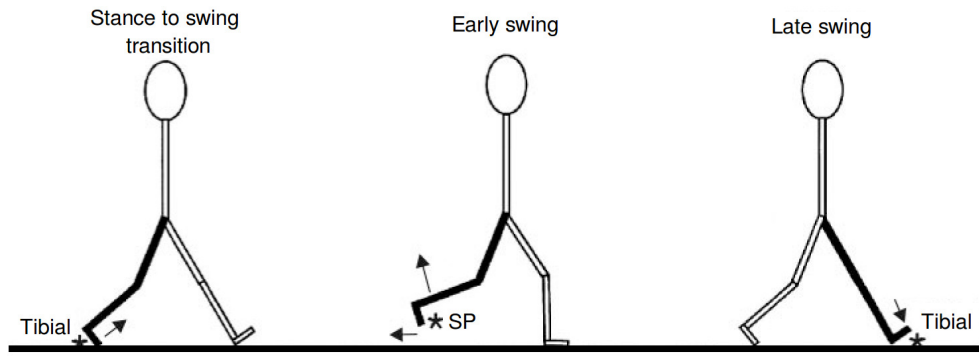


Figure 2.9: **Demonstration of the functional effects of cutaneous reflexes from tibial nerve and superficial peroneal (SP) nerve stimulation.** Following SP nerve stimulation there is a stumbling corrective response which involves a linking action between knee and ankle joint mechanics. A phase-dependent reflex reversal in the response of the ankle is seen when the stance to swing transition is compared to the late swing reflex following tibial nerve stimulation. The * indicates the general cutaneous field activated by the electrical stimulation for each nerve. Figure is adapted from [46, 134].

obstacle to be cleared by the foot, or to allow the stance limb to accommodate to uneven terrain. For example, if uneven terrain causes pressure activation of cutaneous receptors on the lateral foot border during early stance, the foot would be stabilised by Tibialis Anterior and Medial Gastrocnemius muscle activation causing mechanical aversion and dorsiflexion of the foot. Potentially, this could help to prevent damage to the ankle joint, such as sprain, caused by excessive foot inversion [46, 134].

It can be reasoned that the flexion reflex excitability of the isolated human spinal cord could potentially be modulated by activation of plantar mechanoreceptors. This could have use in the rehabilitation of standing and stepping in patients with spinal cord injuries [125].

2.3.4 Summary

In summary, load during gait appears to have two distinct types of effect. From animal studies it is known that sensory input from proprioceptive and cutaneous afferents related to loading can induce reflexes which can influence the output of the CPG [45, 70, 75, 135–138]. These reflexes have a phase- and task-dependency. Task-dependency refers to the change in reflexive activity that can be observed during different motor tasks. The task-dependency of cutaneous reflexes in leg muscles has been shown in standing compared to walking [139] and standing compared to running [140]. Most significantly, from these experiments it can be

seen that reflexes which arise from cutaneous afferents are specific to the motor task that is being performed. Where, rhythmic contractions of muscles occurring during movements such as walking producing distinctly different reflex patterns compared to under static conditions. Similarly, in relation to locomotion there is a phase-dependent modulation of these reflex responses related to the gait timing being either during stance or swing [134, 141] (for full review, see [39]). This modulation is believed to be involved in the adaptation of the pattern of gait to suit the terrain and underfoot conditions [142].

The second main influence of load during gait is the generation of transmission in different afferent pathways which act to modulate the reflex responses [143]. For example, postural reflexes in humans have been found to depend on body load [48, 105, 144].

2.4 How could knowledge of reflexes be used?

The main research question is: how can knowledge of reflexes in human locomotion be exploited effectively and applied to gait rehabilitation for recovery of function following iSCI? As has been discussed, evidence of CPGs is limited in humans and so a Class A and B system is not indicated as a suitable control mechanism for generating stepping, Fig. 2.1. Knowledge of reflexes suggests a progression from CPGs being the dominant control mechanism to a reactive control system, one which is dependent on feedback in order to operate. Producing an improvement in stepping with training depends on evoking a suitable pattern of sensory input in order to effectively modify neuronal systems in the spinal cord [24]. It is valuable then to consider how the sensory input produces these valuable modifications to adapt stepping to compensate for changes in terrain or environment. Bouyer and Rossignol (2003) demonstrated that cutaneous input from the feet is essential in evoking stepping movements in the spinal cat [84] but the exact effect in humans is unknown, as is the mechanism for using this information to aid recovery from SCI. Similarly, the reloading of the body during rehabilitation training sessions appears to act as a stimulus for extensor load receptors. This has been documented as being of fundamental importance for leg extensor activation during walking in cats [115] and in humans [48, 145].

2.4.1 Functional electrical stimulation (FES)

The underlying mechanisms which result in the therapeutic benefits of FES combined with voluntary motor drive remain unknown but it has been suggested that

plasticity of the CNS within the spinal cord and/or cerebrum is producing these results [146]. A 2014 study in SCI rats found that hind limb rehabilitation with FES improved locomotion, indicating that through the application of FES in the acute phase of SCI, the CNS preserves or acquires a capacity to respond to peripheral electrical stimulation which can replace the lack of descending neuronal drive [146]. This implies a need for FES to be administered as soon as possible after a spinal injury. However the similarities between a rat and human model are not exactly known and more studies are required to further understand the neurological outcomes of FES in SCI. It has been suggested that increased afferent feedback directly from the stimulation of muscle afferents and/ or indirectly by feedback pathways from the joints, tendons, and proprioceptors during motion of the limb may produce the CNS plasticity. Therefore, the addition of simultaneous afferent stimulation from voluntary motion is likely to be important in the recovery of a natural locomotion pattern over time, compared to only using direct stimulation of efferent fibres [147].

Sophisticated FES devices have been designed to enable patients with SCI to stand, walk and sit but the most common form of commercial stimulator systems available are primarily for correcting drop-foot and for standing in individuals with paraplegia (for review see [148]). The most simple method of control used by stimulator systems, including the Parastep I (Sigmedics, Inc., Fairborn, OH) [149, 150], is open-loop control to provide stimulation pulses to assist in standing or walking by coordinating the activation of muscles. A simple heel switch inside the shoe or push button controlled by the therapist or patient on a walker frame or crutches, triggers the stimulation; electrical current is applied to the neural tissue with constant intensity during the different gait phases. The user can trigger different stimulation sequences for standing, stepping, or sitting down and to control the intensity of the stimulation [151–154]. For these systems, the level of stimulation can require frequent manual adjustment of high currents, causing fast fatigue of the muscles. Most commonly, progressive fatigue of the quadriceps muscles receiving the stimulation is seen [155]. It can be observed that open-loop FES systems will generally always over-stimulate the muscles in order to produce a sufficient level of stimulation to perform the desired action. This is a significant downside in clinical applications and, in part, explains why limited long-term kinematic gains have been described in the literature [156].

Automatic control was examined by Popovic et al. (2005) as an alternative for push button control, using a pre-programmed multi-channel electrical stimulation system for stroke patients [157]. Stimulation of the Quadriceps, Gastrocnemius,

and Tibialis Anterior was applied for support during stance, push-off at terminal stance, and to provide stability at foot contact, as well as during the swing phase. The timing used for stimulation was pre-set to mimic the onset and switching off of muscle activity found in healthy individuals during slow pace walking. Issues with the system involved the timing, which was based on data from healthy individuals, and hence did not match the timing of voluntary activity in stroke patients. It was also found that patients with stroke, modified their muscle activation when their muscles were stimulated, especially if the stimulation applied to the muscles was not in phase with any voluntary contraction.

Open-loop involves no direct feedback to the controller about the actual state of the system and so there are complications in producing accurate control of movement generation using these systems. These complications relate to difficulty in predicting the correct timing of stimulus, non-linearity of the neuromuscular-skeletal system and an inability for modulation during deviations from an ideal gait cycle [25]. Automatic control, analogous to an open-loop central pattern generator (Class A system, Fig. 2.1A), does not allow for any control of the individual over the stepping and instead overrides any remaining function rather than being a supportive. In addition the control system would only be able to produce stepping at one set speed without any capability for adjusting the stimulation output to improve stability. Providing sensory feedback from the patient to the FES device should allow improvement in control of the generated movement and produce walking which is more normal than seen with open-loop systems, improving speed and efficiency [158]. Feedback allows a modulation of the stepping by the walking, adapting the gait in compensation for changes within the terrain or environment.

Although push-button control is still the most common method for controlling FES within a clinical environment, there has been innovation within the last decade for improving FES control using closed-loop methodology applied to either surface, percutaneous or implanted electrodes. Closed-loop control has been studied using two different forms of feedback; biological signals generated by the individual (measured using electromyography (EMG) (from muscles), electroneurography (ENG) (nerves), electroencephalography (EEG) (brain)) [159] and signals derived from artificial sensors (including electrogoniometers, potentiometers, Hall effect sensors, accelerometers, piezoelectric transducers, capacitive sensors and force sensing resistors (FSRs) (for review of FES control see [160])).

Biological signals are theoretically the most logical choice for feedback control as the signals originate from residual function of the sensory-motor system

remaining post-injury. In individuals with brain and spinal injuries, there is often a significant amount of the peripheral sensory system surviving intact. This has been suggested as an ideal means of controlling FES as these sensors are transmitting usable feedback signals through the peripheral nervous system [159]. However, to date, the technology still requires further development to improve in the speed and reliability. A significant challenge for researchers has been to successfully extract accurate, reliable and relevant information from the nerves, muscles and neurons over long time periods and successfully integrate the signals into a real time control system. The complexity of the human CNS means it is difficult to accurately interpret biosignals into motor control. Any error or misinterpretation in processing could produce unpredictable responses of the FES system, which is not suitable for clinical use. In addition, electrodes are required in order to record the signals and can either be implanted, which could be highly invasive, or positioned on the skin surface but this has issues with practicality and accuracy in placement.

An alternative to using natural biosignals in the control of FES, which may prove to be more reliable and simple, is using artificial sensors. The advantage of these sensors is that they are non-invasive and can easily be applied to the body as an external measurement system with a predictable response to electrical or mechanical signals. For this reason they should also theoretically provide consistent measurements and be suitable of use with the majority of individuals. A study by Kojovic et al. (2009) compared the automatic FES control system, proposed by Popovic et al. (2005) [157], with an FES control system using rule based IF-THEN type finite state control and incorporating artificial feedback from force sensing resistors and accelerometers [161]. They found that this alternative provided timing for muscle activation which was in synch with required voluntary movements. Pappas et al. (2001) combined a gyroscope, measuring the angular velocity of the foot, with force sensing resistors (FSRs), to determine toe-off and heel strike which enabled them to detect the swing phase of gait [162]. Their system success rate was above 96% for subjects with impaired walking.

It is clear that the choice of control system is significant in establishing the adaptability and suitability of an FES system for SCI rehabilitation. Many strategies for producing closed-loop control of FES have been proposed and described in the literature. FES closed-loop control involving gait event detection has traditionally been based on a single type or an integration of different body-worn sensors typically positioned on the thigh, shank or foot to measure ambulation and have included accelerometers [163, 164], gyroscopes and FSRs [162], and ac-

celerometers and FSRs [161] These fall into categories which include dynamic controllers, finite state controllers and artificial neural networks [160].

Artificial neural networks are computational models that have been modelled on the CNS and are capable of machine learning and pattern recognition. However, the requirement for an adaptive FES control system for walking to be real-time dismisses the concept of a artificial neural networks as being suitable for this purpose. Finite state controllers incorporate feedback to control the output state of the system and can be labelled a Class C system (Fig. 2.1C). Thus finite state machines are closed-loop systems. Thresholding acts like an analogue to digital controller (ADC) to determine the input state, converting the analogue feedback signals from the body into a digital input to the system (1 or 0). Although a Class C system appears to be suitable for replicating human motor control in stepping compared to the Class A and B systems, there are still some problems with using this strategy to control FES. The issue of having to set thresholds for the feedback in order to define when the input is in an ON or OFF state can produce errors in wrong estimation of the state by over estimation (setting the threshold too low) or under estimation (setting the threshold too high). The devices discussed previously [161, 162] which use this method in their controller may require recalibration for each person they are used with, complicating setup and potentially reducing functional outcome. This may explain why, although the control strategies prove successful in the study, the research was not taken further.

To summarise, using feedback information from the individual to the stimulation device is preferential to using open-loop or predefined and preprogrammed timing information as a control mechanism. It is also clear that the incorporation of artificial sensors such as accelerometers and FSRs provide a simple and reliable substitution for biological sensory feedback which is missing or lacking due to injury.

It is clear that further research is still required to integrate artificial sensors and feedback signals into an FES system to produce a functional and efficient gait for rehabilitation. It is thus relevant to examine how robotic bipedal walkers have attempted to solve the problem and whether their operation could be functionally relevant in the development of an FES control system for human walking.

2.4.2 Robotic bipedal walkers


Many different control strategies have been used within robotics not only to produce bipeds with a stable and efficient gait pattern, but also to learn more about

motor control in human walking. From this information, development can be made in the area of rehabilitation engineering with the aim of improving functional gait in individuals with spinal cord injuries (SCI) and other neurological injuries. Rehabilitation technologies for restoring ambulatory function and re-training of a functional gait include devices such as the exoskeleton, ReWalk (Argo Medical Technologies Inc., Marlborough, MA, USA) [165] and the robotic gait orthosis, Lokomat (Hocoma, Switzerland) [23].

Passive dynamic walkers with a biomechanic inspired design are simple and can remain stable while walking down slopes [166]. Robots featuring this design have demonstrated gait which appears visually human-like [167], however they cannot adapt and/or change their speed or walk on a level or inclined surface without the addition of actuators and controllers. Other robotic walkers use precise joint-angle control and trajectory-based methods, such as the well publicised bipedal walker ASIMO [168]. However the need for precise actuators and frequency response in the operation of these systems cannot be easily related to the human model which uses the less precise musculoskeletal system integrating muscles, tendons and joints under neuronal control [169]. Machine learning and CPG methodology have also been investigated, producing robot walkers, which can be partially autonomous using local oscillators to generate limb motion patterns and limited sensory information as feedback (Class A and B systems, Fig. 2.1). These devices however can be complex and have difficulty adapting and correcting during deviations from an ideal gait cycle. And although based on the control systems identified in animal models, these mechanisms may be of less importance in human walking control.

Within a human model, feedback on the current status of the walking process is fed back from different sensory organs located in muscles and tendons and from the peripheral vestibular and visual systems. At high walking speeds, coordination between the sensory input and motor output needs to act efficiently and quickly, which are high dynamic walking demands very difficult to replicate using existing biologically-inspired robotic control systems [5, 167, 170]. The gait cycle of bipedal walkers has only one foot in contact with the ground for the majority of the time, which is a major issue in the development of dynamic control avoiding tripping or falling.

RunBot is a bipedal robot which, compared to these other robots, uses a closed-loop system based on the idea of a causal relationship between foot contact and the leg motor output [3–5]. Simply, when switches in the foot are pressed when the leg makes contact with the ground, there is a triggering of knee flexion



	Human (World record)	Spring Flamingo	RABBIT	ASIMO	MABEL	RunBot I
Mass (kg)	~70	14.2	32	54	65	0.53
Leg length (m)	0.9~1.15	0.9	0.8	0.64	1	0.23
Max. speed (m/s)	4.6	1.25	1.2	0.75	1.5	0.8
Relative speed (leg length/s)	4~5	1.39	1.5	1.17	1.5	3.48

Figure 2.10: **Example of some well known bipedal robots and their walking speed compared to humans.** Figure shows the walkers: Spring Flamingo [173], RABBIT [174], ASIMO [168], MABEL [175] and RunBot I [5]. RunBot I only practices flat-footed walking, while RABBIT and MABEL feature no flat feet, and walk on a point, like stilts. Spring Flamingo and Honda’s ASIMO both feature an actuated ankle. The figure is inspired by, and adapted from [5, 175].

and hip flexion of the contralateral leg and hip and knee extension of the ipsilateral leg. This process switches between legs as the stepping continues. The result is so-called limit cycle walking, which is defined by Hobbelen and Wisse (2007) as a “nominally periodic sequence of steps that is stable as a whole but not locally stable at every instant in time” [171]. Using this definition, a walker is able to adapt its gait to the changes in the natural dynamics, producing a convergence to the desired motion following any deviation from the desired trajectory. As can be expected, this is more energy efficient than using high feedback gain to force the walker to remain on an intended path, which is a constant fight against natural deviations [171]. RunBot’s motion is able to return naturally to the desired trajectory following a perturbation, after only a short time and without using CPGs or trajectory control [5]. The development of RunBot I was able to demonstrate that minimal adaptive neuronal control, based on a reflexive mechanism [172] integrated with a biomechanic inspired design, can produce a fast walking and adaptive robot with a maximum walking speed comparable to that of humans (corrected walking speed (leg length/s)) [5], see Fig. 2.10.

Examples of some biped robots which have achieved a bipedal gait are provided in Fig. 2.10. RunBot I uses only a fully-actuated ankle (only practices flat-footed walking), while RABBIT and MABEL use only the underactuated phase (feature no flat feet, and walk on a point, like stilts). ASIMO and the spring Flamingo robots feature a more human inspired ankle joint allowing both a fully-actuated and underactuated foot during the gait cycle.

Similar to controllers developed for bipedal robotic walkers, the different controllers applied to FES have issues with computational power. These issues include: (i) high gain requirements for error correction, (ii) complicated algorithms for trajectory control, and (iii) difficulties in implementing the control strategy on a human model (with complications such as latency, muscle spasticity, voluntary control and fatigue). None of these control methods has managed to produce an adaptive gait pattern based on self-stabilising dynamic processes as observed in natural walking, which may explain why open-loop controllers remain the most common in commercial FES systems. Although there has been a significant progression in the design of FES control to improve in the rehabilitation of functional stepping in SCI patients reported in the literature, to date the majority of these gait assistive devices have not been FDA approved in the USA, or been made available commercially, or used extensively outside of clinical trials.

It can be argued that RunBot's control strategy may provide a suitable system for generating stepping in humans. An ideal system would be one which is entirely analogue and, like RunBot, does not depend on CPGs or trajectory control. This closed-loop system would use sensory feedback to determine the output but unlike a finite state machine, which has been common to previous FES control design and uses thresholding on the input to determine the state of the output (Fig. 2.1C), would have a causal output response to any input fed back from the body. This strategy can be termed a minimalistic controller where the overall control is returned to the individual and will not override any residual function that may be present, Fig. 2.1D.

2.5 Conclusion

Sensory feedback influences the progression between the swing and stance phases of walking, promotes corrective reflexive responses to recover from any externally sensed perturbations and also has action to reinforce the muscle activity during the locomotor activity. It can be concluded that load information is important for the regulation of different types of motor behaviour. The main functional roles for each group of reflexes during walking is summarised in Fig. 2.11.

What can be seen is that load compensating reflexes are very flexible and have an adaptability to suit the task or the phase of the gait cycle. Cutaneous reflexes have a strong task-dependency, a characteristic which allows the generation of different functional behaviours. It would be logical to theorise that the pathways used to feed back load information during standing may not be the same as

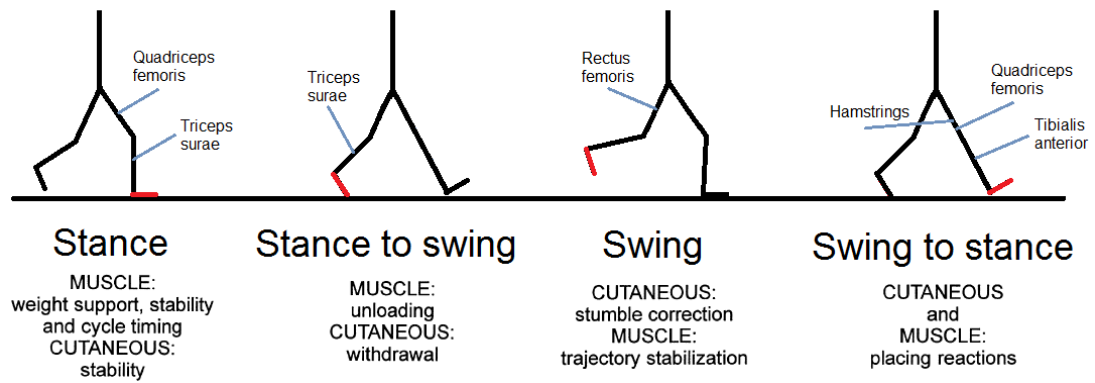


Figure 2.11: **The main functional roles of each group of reflexes during the human gait cycle.** Also highlighted are some of the main muscles which have action during each phase. Adapted from [46].

those recruited during walking [39, 139]. The reinforcement of force feedback is not a constant and appears only when appropriate, such as during ambulation. During other behaviours, such as during rest, these pathways are closed and other reflexes become of more importance. These findings are of significant importance in rehabilitation strategies for patients with SCI. For example, Dietz et al. (1994) demonstrated that manipulation of load feedback is essential for gait recovery in SCI patients [176].

In order to design a rehabilitation strategy for patients with iSCI requires a simple design incorporating processes to reinforce and promote existing gait potential while providing assistance to compensate for loss of function. FES has already proved to be a successful and effective technology for improving gait and strengthening muscles. What is still required is to integrate this rehabilitation method with functional feedback from the patient to produce a control over the generated movements, which is based on the natural mechanisms in the human. This has potential to produce a functional rehabilitation of walking, allowing gait cycle modifications to suit the loading conditions and the development of the idea of limit cycle walking, something which the bipedal human walker is proficient at. Previous studies which have looked at 'closing the loop' between body worn sensor and FES have had good results but have failed to get their devices passed the initial patient trial stages due to complexity of the system, mechanical problems and inefficiency. These are issues which are shared with developers of robotic bipedal walkers in their various controller designs. Bipedal robotic walkers teach us that complexity in computational processes involving CPGs, constant monitoring of trajectory and calculation and pre-planning of the execution of the next movement, all together can cause the robots to be slow.

Furthermore, this requires precise and complicated engineering. By focusing the design on simple mechanical concepts, as seen in RunBot, fast walking speeds with low energy requirements with a stable limit cycle could be achieved. What is required in terms of controlling an FES gait rehabilitation system is the same, a simple approach, which can maximise in the existing potential of the patient and be supportive rather than providing constant monitoring and fixed control.

2.6 Research hypothesis

The hypothesis of this thesis is that a causal control system for generating gait can be defined using the relationship between foot contact information and muscle activity found during normal human gait. This strategy will be tested muscle by muscle, using data recorded from healthy individuals during walking. Calculated transfer functions will then be applied to the RunBot II bipedal robot to identify whether a coordinated stepping response can be generated using this causal control system.

The approach can be categorised as a closed-loop analogue Class D control system (Fig. 2.1D) and has potential to provide a minimalistic control system for FES, where the cyclic sequence of joint movements is minimally imposed on the walker, which has an application for producing functional gait in individuals with iSCI.

Part I

Preliminary Studies: Methods and materials development

Introduction

In the preliminary study, the protocol and equipment necessary for collecting data to examine the relationship between foot contact information and leg muscle activity were devised and developed. Healthy test subjects without any neurological injury or deficit were recruited to determine the feasibility. Here, subjects walked on a treadmill at a constant speed of 4 km/h while muscle activity (EMG) was recorded from four muscles in their right leg together with foot contact information from under their heel and first metatarsal, and acceleration of the right hip.

Analysis of the subject data showed a correlation between foot contact information from the heel and peaks in the muscle activity. Several recommendations were made following the preliminary study for advancing the protocol before transfer functions relating the two parameters could be calculated.

As a treadmill creates an unnatural walking environment, further data collection was required to remove any correspondence which may exist between walking speed and the identified correlations. By varying the speed of the treadmill, the subject's gait will be more closely related to that found in natural over-ground walking where changes in pace are commonly encountered.

Wi-GAT [177] was designed as a simple gait analysis system for calculating common gait parameters used in quantifying movement in various neurological conditions including spinal cord injury. This device was validated against the large-scale and commonly used Vicon system. The validation study demonstrated good concurrent validity of the wi-GAT system. The device was subsequently used to measure gait parameters including cadence and average walking speed from ten healthy subjects. This allowed a varying speed program for the treadmill to be created, which was suited to each individual's leg length and comfortable walking speed range.

Chapter 3

Preliminary investigation into the relationship between foot contact information and muscle activity during walking

In this chapter, the preliminary study designed to investigate the relationship between foot contact information and muscle activity during walking will be described. Taking inspiration from the mechanism of walking used by RunBot bipedal robot, the aim of the study was to determine whether foot contact could be used in a minimalistic control system for FES for use with iSCI patients to assist in their gait capability. Healthy volunteers were recruited to walk on a constant speed treadmill while muscle activity (EMG) from four leg muscles (right leg), foot contact information from under their heel and first metatarsal (both feet), and acceleration of the right hip were recorded. Correlations between foot contact (from the heel), accelerometer data and the EMG contact were identified using event-related averaging. A relationship between heel contact and peaks in muscle activity was observed in all ten participants but was less evident in the accelerometer data. Several recommendations for further work were highlighted from the study which were used in the development of the data collection protocol.

3.1 Development of a causal control system

The RunBot II robot uses causal finite impulse response (FIR) filters in its control system to generate a coordinated walking behaviour. Ground contact information is the main sensory input producing impulse responses which promote joint move-

ments and stepping. Causal FIR filters are linear and time-invariant with the output only dependent on past and present inputs, i.e. the output $y(n)$ is a weighted sum of the present input, $x(n)$, and previous inputs, $x(n-1), x(n-2), \dots, x(n-M)$. To generate a functional stepping behaviour that is adaptable to changes in the terrain or environment, the walking control system needs to be realisable, i.e. work in real-time, thus it needs to be causal as it cannot act on future input, i.e. $x(n+1), x(n+2), \dots, x(n+M)$. The control system for walking is based on there being a relationship between sensory input and motor output, where the input drives the progression of the stepping. The initial treadmill based data collection study was designed to examine, if, like RunBot, a causal relationship between ground contact information from the feet and muscle activity during human walking could be established, which could be used in the development of a control system for FES for use in gait rehabilitation in SCI. To study this, healthy subjects were recruited to walk at a constant speed on a motorised treadmill while muscle activity (EMG) was recorded from four leg muscles in the right leg. Foot contact was measured simultaneously with EMG from sensors placed under the heel and first metatarsal. To further determine what physical quantities might be valid to record from an individual with SCI and be used in the control of FES, an accelerometer was also used to measure acceleration of the hip during walking.

The specific tasks of the preliminary research study included:

- Design and development of an insole with embedded sensors and a suitable amplifier for measuring and recording foot contact.
- Development of an accelerometer circuit which could be attached to the test subject to record kinematic data during treadmill walking.
- Integration of an EMG preamplifier with the accelerometer and foot contact circuitry to allow synchronisation during data recording.
- Comparison of the subject data to establish whether a relationship between muscle activity and foot contact can be quantified.

3.2 Participants and ethics

Ethical approval was obtained from the departmental ethics committee at the Department of Bioengineering, University of Strathclyde and also from the ethics committee at the Faculty of Biomedical & Life Sciences at the University of Glasgow. All volunteers were fully informed of the procedure and provided written

consent. Ten healthy, active subjects without any gait abnormalities volunteered and completed the study; seven males and three females with a mean age of 25 years (range 23 - 30 years), average height of 1.74 m (1.55 - 1.88 m range) and an average weight of 75 kg (56 - 94 kg range). Table 3.1 outlines the demographic of subjects.

Subject ID	Gender	Handedness	Age	Height (m)	Weight (kg)	Shoe size (UK)
PA	M	R	24	1.85	83	9
PB	M	R	23	1.83	87	10
PC	M	R	25	1.81	83	10
PD	F	R	24	1.55	56	4
PE	M	R	30	1.88	94	11
PF	M	R	23	1.71	70	8
PG	F	R	23	1.71	87	6
PH	F	L	23	1.65	61	6
PI	M	R	28	1.67	70	8
PJ	M	R	25	1.70	62	9
Mean (STD):			25 (2)	1.74 (0.10)	75 (13)	8 (2)

Table 3.1: **Preliminary study subject information.** The subject ID was randomly assigned to the subject after they were recruited to the study.

3.3 Materials and Methods

3.3.1 Data acquisition

The USB-DUX D data acquisition device (Incite Technology Ltd., UK) was used to record the EMG, accelerometer and foot contact information. The A/D converter has 12-bit resolution, eight channels and a sampling frequency of $f_s = 1$ kHz. The board is powered by a USB connection and provides a ± 5 V supply for any additional circuitry while providing electrical isolation on the analogue input and output stages. This isolates any connected circuitry from the mains supply, ensuring safety of the subjects during the study. The device has the advantage of being small with dimensions of 144 x 90 x 30 mm allowing it to be easily attached to the side of the treadmill during data acquisition. USB-DUX D pin diagram and images provided in Fig. 3.1.

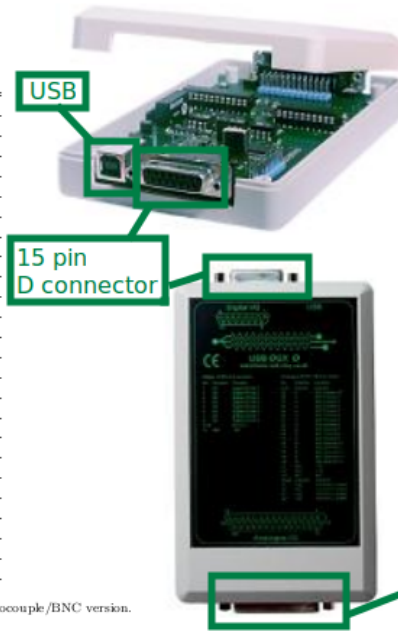
The USB-DUX D connects via USB to a computer for data acquisition. The device uses a Linux driver which is part of the COMEDI framework. Comedi-record (open source software available from <http://www.linux-usb-daq.co.uk/soft>

USB-DUX Pinouts

25 pin D connector (f)

Pin	Direction	Function
1	I	A/D channel 7
2	I	A/D channel 6
3	I	A/D channel 5
4	I	A/D channel 4
5	I	A/D channel 3*
6	I	A/D channel 2
7	I	A/D channel 1
8	I	A/D channel 0*
9	O	D/A channel 0, bipolar
10	O	D/A channel 1, bipolar
11	O	D/A channel 2, bipolar
12	O	D/A channel 3, bipolar
13	O	$V_{ref} = 4.096V$
14	Supply	+5V
15	Supply	-5V
16	GND	
17	GND	
18	GND	
19	GND	
20	GND	
21	GND	
22	O	D/A channel 0, unipol
23	O	D/A channel 1, unipol
24	O	D/A channel 2, unipol
25	O	D/A channel 3, unipol

*: Please leave disconnected if you have the thermocouple/BNC version.



15 pin D connector (f)

Pin	Direction	Function	Counter
1	I/O	digital I/O bit 7	
2	I/O	digital I/O bit 6	reset1
3	I/O	digital I/O bit 5	up/down1
4	I/O	digital I/O bit 4	/CLK1
5	I/O	digital I/O bit 3	
6	I/O	digital I/O bit 2	reset0
7	I/O	digital I/O bit 1	up/down0
8	I/O	digital I/O bit 0	/CLK0
9-14	GND		
15	NC/5V		

Figure 3.1: **USB-DUX D board.** Pin diagram and images taken from <http://www.linux-usb-daq.co.uk/dev2/>.

ware2/comedi-record) is an oscilloscope program which displays and records data from COMEDI devices and was used to record the walking data and save the output in an ASCII file for further analysis.

3.3.2 EMG preamplifier

EMG data were collected from four leg muscles located in the subject's right leg. Using the example of RunBot, a requirement for generating a functional gait is muscle activations with suitable timing for producing coordinated hip, knee and ankle joint motions. For this reason, the muscles chosen for analysis were selected for their different roles in the gait cycle; two muscles located in the lower leg (Tibialis Anterior (TA), Lateral Gastrocnemius (LG)) and two in the thigh (Biceps Femoris (BF) and Rectus Femoris (RF)), Table 3.2 and Fig. 3.2. These muscles have potential be activated in the same way RunBot uses motors at the hip and knee joints to control flexion and extension of the joint to generate a functional gait cycle, Table 3.3.

The aim was for EMG to be measured from the participant as they walked on a treadmill. Thus it was necessary for the EMG preamplifier to be of small size and light weight in order to facilitate attachment to the participant and therefore avoiding the need for long cables between the subject and preamplifier. Introducing a preamp circuit close to the recording site also minimises movement

Muscle	Action during gait
Tibialis Anterior (TA)	Dorsiflex and inverts the foot. Stabilises the ankle as the foot hits the ground during foot contact, controlling the tibia during stance. Pulls the foot clear of the ground during swing.
Lateral Gastrocnemius (LG)	Plantar flexor of the foot at the ankle joint and knee flexor. Helps support the knee during the stance phase.
Rectus Femoris (RF)	Knee extensor and hip flexor.
Biceps Femoris (BF)	Knee flexor and hip extensor. Helps slow hip flexion and knee extension at terminal swing.

Table 3.2: Muscles recorded during the study and their action during gait. Definitions taken from Rose and Gamble (2006) [37].

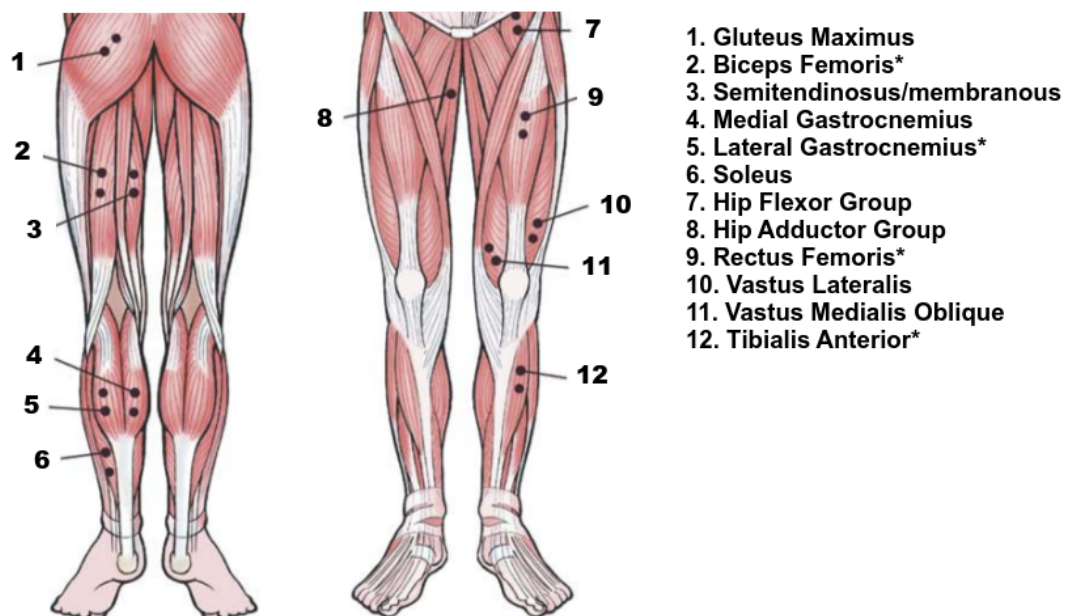


Figure 3.2: Position of EMG electrodes on the legs. * The muscles measured during the preliminary study. Adapted from [178].

Joint	RunBot II	Human	
	Flexion/Extension	Flexion	Extension
Hip	Motor at hip joint	RF	BF
Knee	Motor actuated by springs	BF and LG	RF
Ankle	N/A	TA	LG

Table 3.3: **Defining a control system for human walking compared to RunBot II.** RunBot II uses motors at the hip joint to control flexion/extension and motors and springs to control knee flexion/extension. In humans, different leg muscles can be activated to control flexion/extension of the joints during the gait cycle. For further details on RunBot’s control system see Chapter 6, Section 6.3.

artefacts normally associated with cable motion. The EMG preamplifier was designed using an adapted 3-lead ECG amplifier, available from <http://www.linux-usb-daq.co.uk/howto2/ecg/>. When the amplifier is used to measure ECG, three inputs are connected to electrodes on the right arm (RA), left arm (LA) and left leg (LL) following Einthoven’s triangle configuration. An instrumentation amplifier is used for differential amplification of the signals, calculating the potential difference between the input channels in three pairs (lead) LA-RA (I), LL-RA (II) and LL-LA (III) creating the triangle. In addition to the instrumentation amplifier, a second stage amplifier provides each channel with a gain of 1000 and a simple high-pass filter at $f_c = 0.1 \text{ Hz}$ to remove electrode drift and DC potentials. The bandwidth of the preamp is 0.1 to 1000 Hz. A fourth connection to the amplifier is connected to the right leg (RL) and is used as the ground.

To adapt the preamp to amplify four channels of EMG signals, the connections between the three input channels were removed so each channel has two independent inputs to the instrumentation amplifier stage. This creates a bipolar configuration for measuring EMG. The instrumentation amplifier provides differential amplification of the two signals from a muscle to calculate the potential difference between the electrodes and remove external interferences, which are common to both electrodes. The ECG amplifier features an extra ‘unused’ channel for recording additional signals such as pressure, which is ideal for recruiting as an extra channel for EMG meaning the preamplifier is suitable for amplifying signals from four muscles rather than three.

The EMG preamplifier was constructed on PCB (Beta LAYOUT, Ireland). In total the preamp has eight channels for recording the EMG signals of the four selected leg muscles, two channels per muscle using a bipolar electrode configuration, and a ground electrode. The PCB design uses surface mount (SMD) components to keep the device as small and lightweight as possible so it can be

Name	Position
TA	Lateral to the anterior border of the tibia at approximately the junction of the upper and middle thirds of the lower leg, on the ventral side of lower leg.
LG	Lateral aspect of the leg, at approximately the upper third of the muscle bulge.
RF	Middle of the thigh, at approximately the junction of the lower and middle thirds of the thigh.
BF	Lateral to the lateral edge of the Semitendinosus muscle, at approximately the junction of the upper and middle thirds of the thigh.

Table 3.4: **Electrode positioning for the muscles investigated.** Instruction of EMG electrode placement which was followed, taken from [180].

attached to a belt worn around the subject’s waist during the treadmill walking.

The annotated schematic design (Eagle, CADSoft, USA) for the EMG preamplifier is shown in Fig. 3.3 and the full PCB design and BOM are included in Appendix A. Shielded audio cable was used for the cables connecting the preamplifier to the electrodes on the leg muscles.

Standard skin preparation of the electrode sites was followed [179]. The skin over the area of the muscle was shaved if necessary, thoroughly cleaned with an alcohol wipe and then abraded using NuPrep gel (Weaver and Company, Colorado, USA), lowering skin impedance to improve conductivity. Pre-gelled, one use, surface electrodes (Blue Sensor N-10-A, Ambu, St. Ives, Cambridgeshire) were positioned in the centre of the muscle belly (in accordance to the recommendations of SENIAM [179]) and a ground reference electrode was attached to the ankle over the lateral malleoli, Table 3.4. Elastic straps and bandage sleeves were used to reduce electrode and electrode lead movement, in order to minimise movement artefact in the EMG recording. The EMG preamplifier was connected to a USB-DUX D device to power the circuit and log the EMG data. The test subjects were instructed to wear shorts during the experiment so the electrodes could easily be attached to the leg muscles.

3.3.3 Ground contact information

The requirements for finding a suitable sensor for in-shoe measurement of foot contact with the ground were: durability, consistency in measurement over repeated trials and timing accuracy. As the component needed to be fitted within a shoe it also had to be flexible, light, low in power consumption, thin in depth

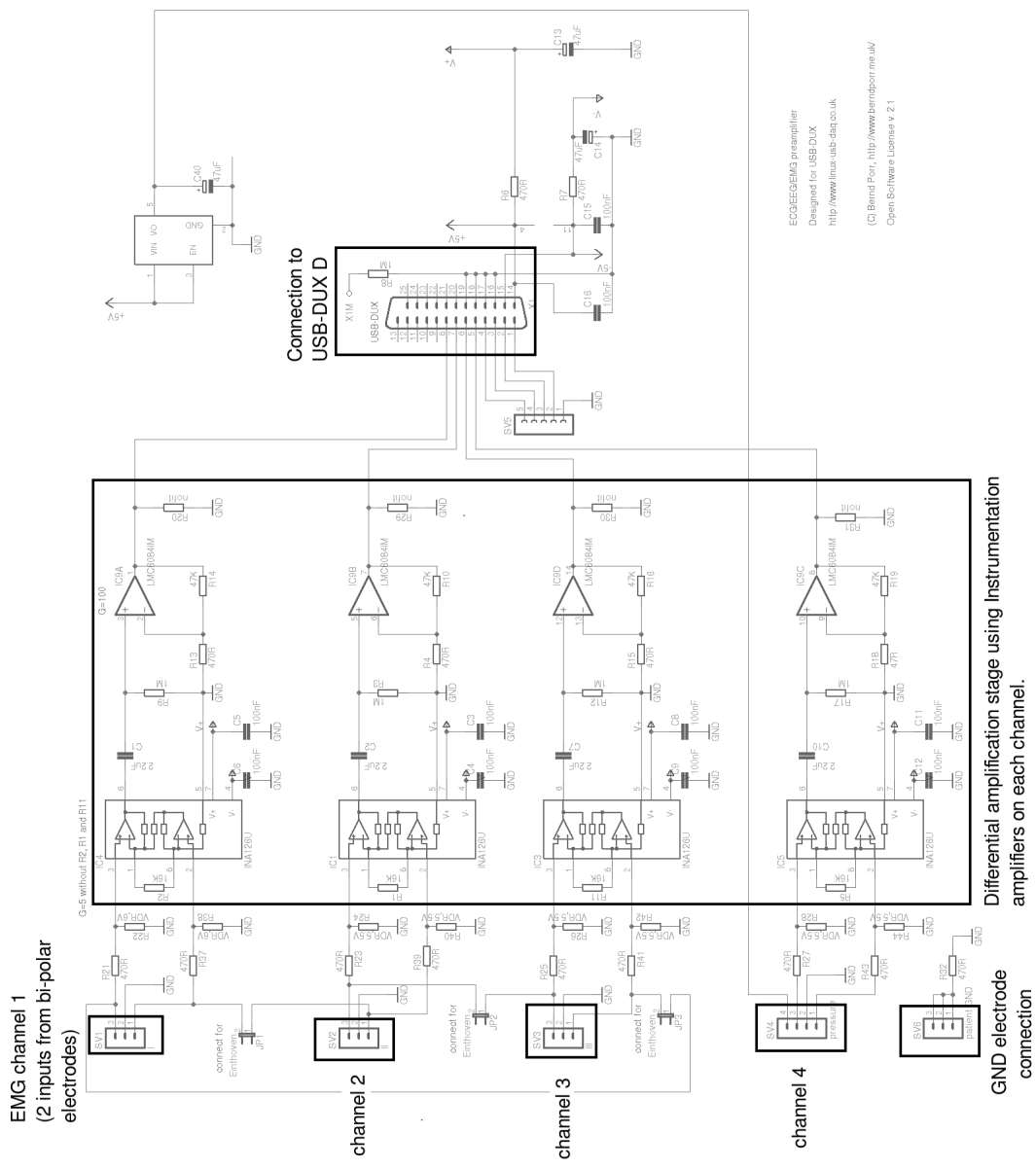


Figure 3.3: Annotated schematic of the four channel EMG preamplifier.

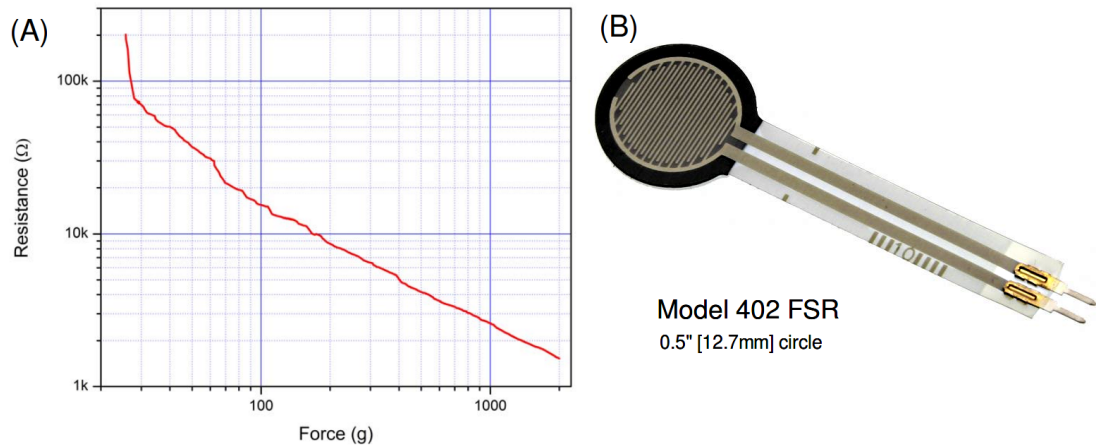


Figure 3.4: **Force sensing resistor (FSR 402)** (A) Typical response of an FSR 402 to applied force (plotted on logarithmic scales). Resistance decreases rapidly at low forces until the resistance reaches below $100\text{ k}\Omega$, then resistance follows an inverse power law. At high forces the response of the FSR reaches a saturation point where any increase in applied force produces little or no decrease in resistance. Graph taken from [181]. (B) Photograph of the FSR 402. The active area is 12.7 mm in diameter.

and able to withstand pressure and heat within a shoe. Force plates or mats are typically used in research to measure ground reaction forces during gait, however they have major limitations in the area they can measure and are restricted to overground walking. Various small sensors have been used in foot contact measurement systems for walking and include capacitive sensors, resistive sensors, piezoelectric sensors and piezoresistive sensors. Many commercial systems are also available including the Tekscan F-Scan pressure sensor system (Tekscan, Inc., South Boston, MA) which uses matrix film resistive sensors and the Pedar in-shoe system (Novel, Germany) which uses capacitive sensors for measurement. However, as the sensors require integration with other hardware, be adapted for the requirements of the study and able to be fitted in shoe insoles for treadmill walking, the majority of these sensors and devices were considered unsuitable, over engineered and failed to produce a suitable real-time linear response to applied force.

Force sensing resistors (FSRs) are constructed from a conductive polymer film which produces a decrease in resistance with increasing applied force to its surface. The typical response of an FSR to applied force is provided in Fig. 3.4. The advantage of their simple construction are their small size and a thickness of typically less than 0.5 mm as well as having a low cost of approximately £3.40 per FSR (FSR 402, Interlink Electronics, CA, USA). FSRs can be damaged if constant prolonged pressure is applied and they have been noted for their low precision in terms of force measurement and repeatability, with hysteresis producing +10%

or more error in readings [181]. However, for measurement of foot contact timing, the FSR is reliable and has been used in a number of studies involving foot contact measurement [182,183], and integration of the device with additional circuitry can reduce the error and improve in the linearity of the response to applied force.

To use FSRs as a suitable means of accurately measuring foot contact information during walking, a relationship of $V_{OUT} \propto Force$ is desirable. This implies,

$$R_{FSR} \propto \frac{1}{Force} \quad (3.1)$$

To improve in the linear relationship between voltage output and force, integration circuitry for the FSRs was based on a simple inverting amplifier configuration, Fig. 3.6. A negative reference voltage gives a positive output swing from 0 V to $+V_{REF}$, Fig. 3.5. As the power supply for the circuit is taken from the USB-DUX D, which can provide ± 5 V, the output has a maximum swing of 0 to 5 V. The FSRs were calibrated to give a maximum voltage output of 1 V corresponding to the maximum ground reaction force of a subject during gait. This is realised by changing the value of R_G , where decreasing the value of R_G means more force is required to increase the voltage output.

$$V_{OUT} = \frac{-R_G \cdot V_{REF}}{R_{FSR}} \quad (3.2)$$

Where R_{FSR} is the resistance of the FSR which varies with applied force.

Using this configuration, $V_{OUT} \propto \frac{1}{R_{FSR}}$. To produce a zero force intercept value of 0 V and resolution at low forces a second resistor (R_P) is placed in parallel to the FSR. The gain of the amplifier (G) is calculated as:

$$G = \frac{V_{OUT}}{V_{IN}} = \frac{-R_G}{(R_{FSR} \cdot R_P)/(R_{FSR} + R_P)} \quad (3.3)$$

The circuit digram is provided in Fig. 3.6.

As defined in Eqn. 3.1, the ideal relationship of R_{FSR} with force (F) is $R_{FSR} \propto \frac{1}{F}$, which can be written as $R_{FSR} = \frac{k}{F}$ and substituted into Eqn. 3.3,

$$\frac{V_{OUT}}{V_{IN}} = -\frac{R_G \cdot (F \cdot R_P + k)}{k \cdot R_P} \quad (3.4)$$

Solving for force,

$$F = -\frac{k \cdot (R_P \cdot V_{OUT} + R_G \cdot V_{IN})}{R_G \cdot R_P \cdot V_{IN}} \quad (3.5)$$

Where k is defined as the constant of proportionality between force and R_{FSR} .

It should be noted that although the FSRs were optimised to give an indication

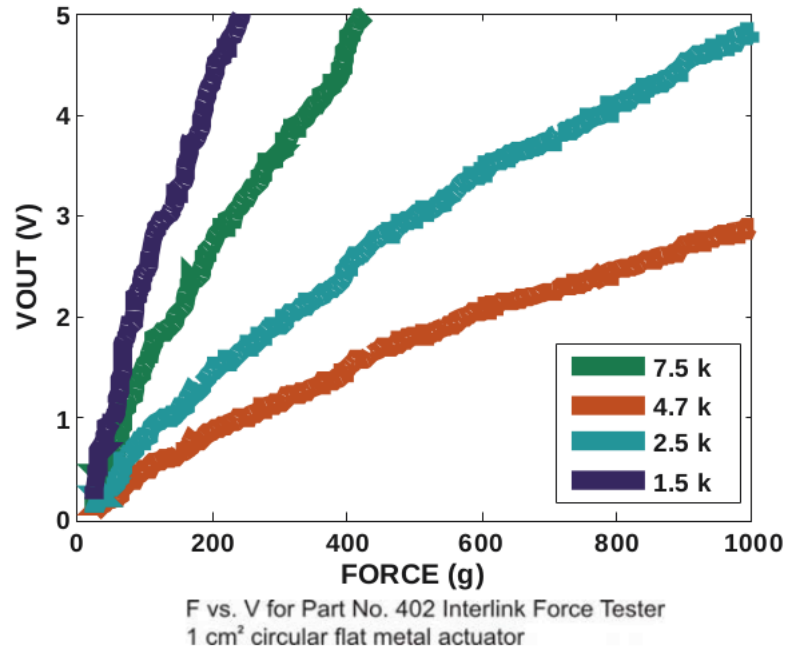


Figure 3.5: **FSR response to applied force with different values of R_{FSR} .** Using integration circuitry improves in the linearity of the relationship between resistance and force (compare with Fig. 3.4). V_{OUT} is inversely proportional to R_{FSR} . Graph is taken from [181].

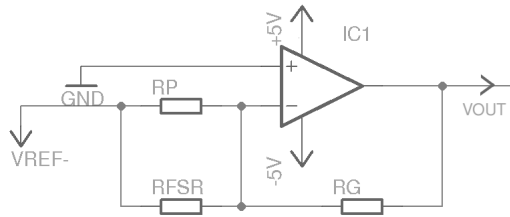


Figure 3.6: **FSR amplifier circuit.** Using $-V_{REF}$ as the input to the inverting amplifier produces a positive voltage swing when force is applied to the FSR.

of foot loading during walking, a measurement of force was not taken from the sensors but rather a change in voltage over time. Thus the phrase ‘foot contact information’ is used within this thesis to mean a measure of this quantity.

The amplifier circuit for the FSR insoles was soldered on matrix board and fitted in a box to be worn on the belt around the subject’s waist alongside the EMG pre-amplifier, Fig. 3.7.

As the USB-DUX D data acquisition device only has eight channels, data were collected from the FSR insoles using a second USB-DUX D board. These two devices were both connected to the same laptop so the EMG, accelerometer and FSR data could all be recorded simultaneously. Four channels were recorded from the feet during the walking experiment, right heel, right first metatarsal head, left

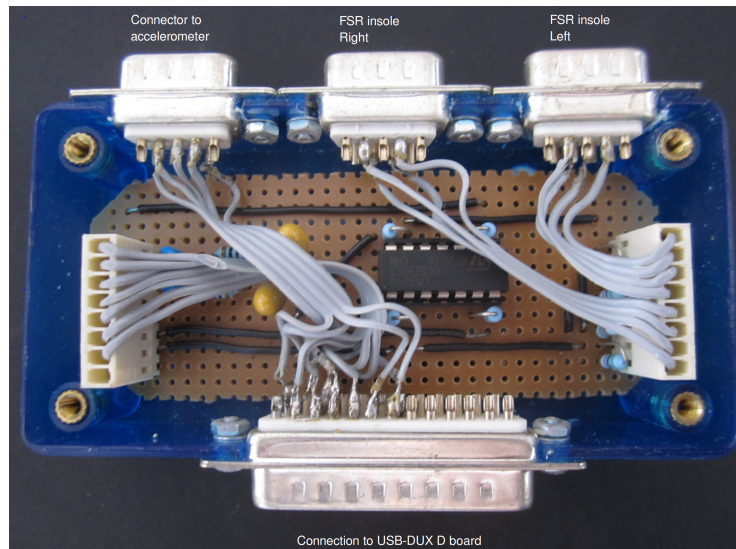


Figure 3.7: **FSR amplifier circuit.** This was soldered onto matrix board and built into a small enclosure for attachment to the waist belt worn by the subject. The device connects to the FSR insoles, accelerometer and USB-DUX D data acquisition device via a D-connector.

heel and left first metatarsal head. Synchronisation was achieved using two open Comedirecord windows (one corresponding to each USB-DUX D device) and a push-button connected to one channel on each device so a spike is recorded in the two data files which can be used as a time stamp for the start of data collection.

Ground contact information was required to be recorded from both the left and right feet as the subjects walked on the treadmill to establish whether muscle activity correlates with foot contact from either the ipsilateral (I) or contralateral (C) leg. Custom designed insoles containing embedded FSRs were made for the study. FSRs were positioned under the foot at two areas of peak pressure distribution during walking (main weight bearing areas), beneath the heel to record foot strike information and under the first metatarsal head in order to record foot off data, as described by Granat et al. [182]. Six different sizes of full insoles were made to accommodate the different shoe sizes of the test subjects, Table 3.1. The insoles were made of linoleum which is durable and provides a flat, solid surface for the FSRs which was recommended by the manufacturer. A leatherette fabric cover was glued on top of the lino and FSRs to protect the components from the feet, provide comfort for the wearer and to prevent interference with a normal walking behaviour. A photograph of an insole (without the leatherette cover) is shown in Fig. 3.8. The insoles were connected via ribbon cable to the amplifier circuit worn on the waist belt alongside the EMG preamplifier. This configuration produces an increase in voltage output with applied force to the FSRs and

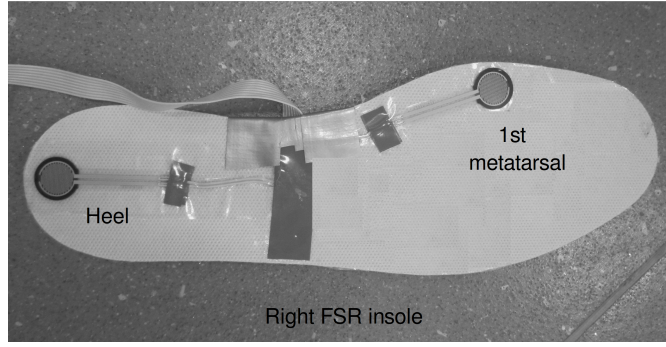


Figure 3.8: **Photograph of an FSR insole.** The FSRs were positioned under the heel and first metatarsal head.

calibrates the output to a typical subject applying their full body weight to the insole, to prevent saturation of the signal.

Each subject was instructed to wear sports shoes during the data collection so footwear was as similar as possible to allow comparison of the results and minimise any potential confounding affects of different shoe types.

3.3.4 Hip acceleration

Acceleration of the hip was measured using a 2-axis linear accelerometer (LIS2L02 AS4, STMicroelectronics, Switzerland). Acceleration of the hip changes with every step as the joint flexes and extends during the stance and swing phases of gait. Acceleration of the hip was measured to investigate how kinematic data are involved in normal motor control. The accelerometer was built into a circuit on matrix board in accordance to the recommendations of the manufacturer [184]. The circuit was designed to measure ± 6 g with a bandwidth of 12 Hz to remove high frequency noise, following recommendations by Verplaetse (1996) for foot/leg acceleration measurement applications [185], Fig. 3.9.

The accelerometer chip requires only a single supply between 2.4 and 5.25 V, with the output voltage, offset and sensitivity ratiometric to the supply voltage. This means that the accelerometer circuit can be powered by the 5 V power supply from the USB-DUX D board which has the advantage of electrically isolating the circuit from the mains supply. The voltage output of the accelerometer is proportional to acceleration which means the output can be recorded via the USB-DUX D and Comedirecord and then converted to an acceleration measure (g) during post processing using Eqn. 3.6.

$$A_{X/Y}(t) = \frac{V_{X/Y}(t) - V_{X/Y_i}}{0.36} \quad (3.6)$$

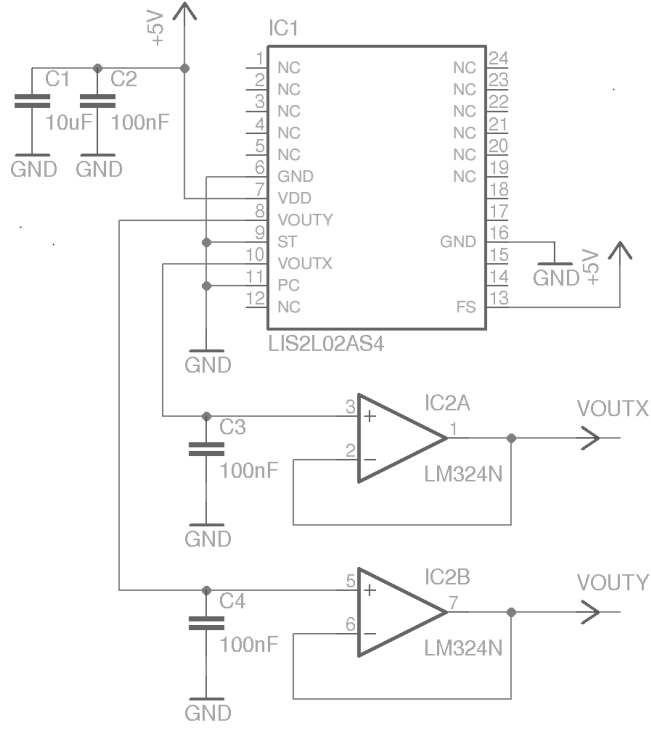


Figure 3.9: **Accelerometer circuit diagram.** The sensor was calibrated following the manufacturers instructions [184].

Where $V_{X/Y}(t)$ is the voltage output of the accelerometer measured in the x or y (horizontal and vertical) directions and V_{X/Y_i} is the initial voltage measurement taken during stance for calibration (zero g value). The constant of 0.36 is the sensitivity (V/g) reading for the accelerometer, calculated using Eqn. 3.7.

$$S_{X/Y} = \frac{\pm 1g \text{ value (largest)} - \pm 1g \text{ value (smallest)}}{2} \quad (3.7)$$

The value of 3.6 V/g is in agreement with the data sheet sensitivity estimate (Eqn.3.8), accounting for a zero-g offset due to mounting the sensor on the matrix board.

$$\frac{V_{dd}}{15} + 10\% \quad (3.8)$$

Where V_{dd} is the 5 V supply from the USB-DUX D.

The accelerometer was attached to the test subject's right hip using an elastic strap worn around the hips to hold it in place and restrict movement of the enclosure. The x-axis measured acceleration in the horizontal direction of walking, in the sagittal plane, and the y-axis measured the vertical acceleration experienced by the hip. The accelerometer was statically calibrated using a horizontal reference surface, following the manufacturers instructions. Readings were taken

of the output values of the x- and y-axis during stationary stance for each subject before the treadmill experiment began to enable individual calibration. The device was connected to the same USB-DUX board as the FSR insoles and a separate channel was used to record the x- and y-axis data in Comedirecord.

3.3.5 Experimental setup

The study involved each subject walking on a slatted treadmill (WOODWAY, Waukesha, WI, USA) located at the Centre for Spinal Rehabilitation, University of Glasgow set to a comfortable walking speed of 4 km/h (1.11 m/s) for a duration of 3 minutes. Two walks were recorded for each subject.

Before any measurements were taken, the subjects had time to acclimatise to the treadmill speed and practice walking wearing the apparatus so they could become familiar with the experimental conditions. Recording did not begin until the subject verified they were comfortable at the speed and with the experimental setup, Fig. 3.10.

In total ten channels of data from the treadmill walking needed to be recorded via two USB-DUX D devices with an additional channel used on each device for the manual push-button synchronisation.

3.4 Data analysis

The recorded data were synchronised and analysed using the GNU Octave program (John W. Eaton, University of Wisconsin, Madison, WI) and MATLAB (MathWorks, Inc., Natick MA). The EMG recordings were recorded using a digital 50 Hz notch filter in Comedirecord to remove mains supply noise. Noise content was identified using a Fourier transform of the EMG data of the EMG data for each muscle in the right leg emg_{mus} (where $mus = TA, LG, RF$ or BF) and a band pass filter (h_{BP}) (FIR filter, 15-500 Hz) used to remove these frequencies above and below the EMG frequency spectrum (following recommendations of SENIAM [179]). A Full-wave rectification of the filtered EMG waveform gives the absolute value of the raw signal.

$$EMG_{mus}(t) = |(emg_{mus}(t) * h_{BP}(t))| \quad (3.9)$$

Further artefact removal and smoothing of EMG_{mus} was conducted using a 5-point median filter, \hat{EMG}_{mus} is the completely filtered and rectified EMG. Graphs of the filtered and rectified EMG waveform, foot FSR data and acceleration can

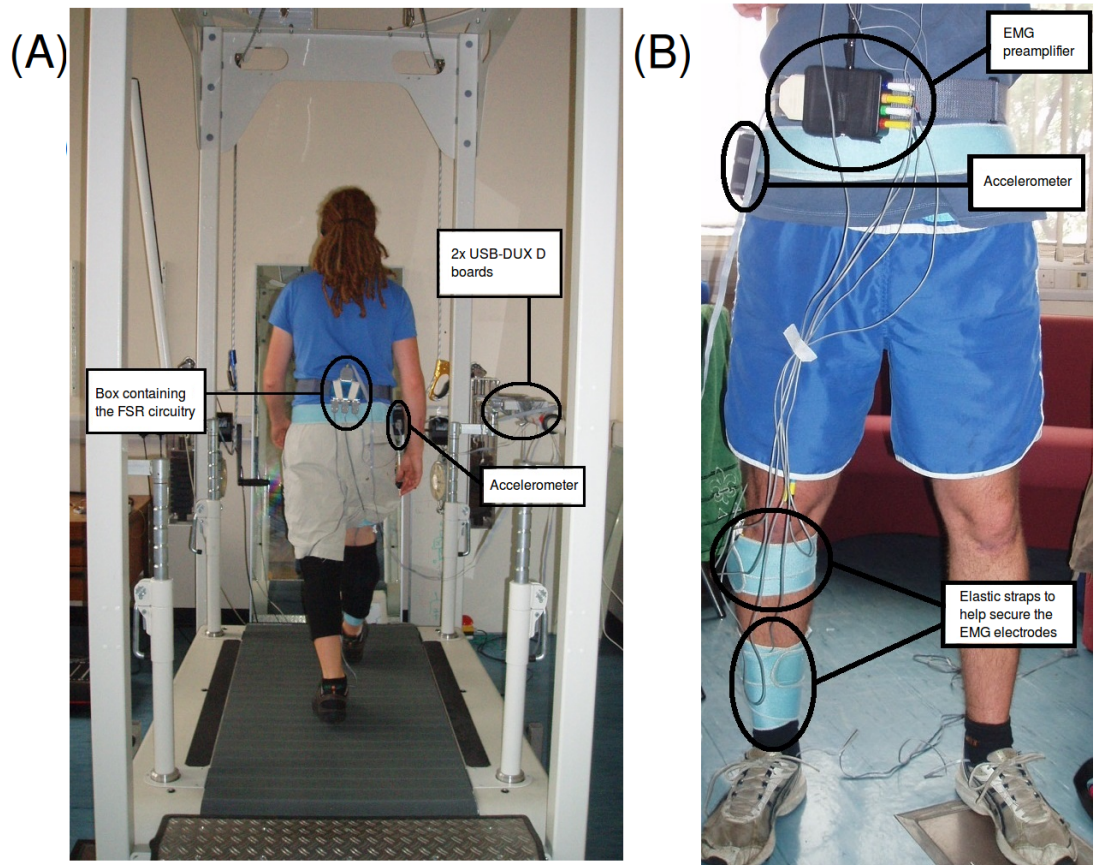


Figure 3.10: **Photographs of the experimental setup** (A) The EMG preamplifier was attached to a strap worn around the subject's waist and connected to electrodes on the leg muscles. The accelerometer was held in position on the right hip using a tight elastic strap. (B) The circuitry for the FSR insoles was attached to a waist strap and connected to the insoles via ribbon cable. Both devices on the strap were connected to the USB-DUX boards which were secured to the side of the treadmill so long cables were not necessary.

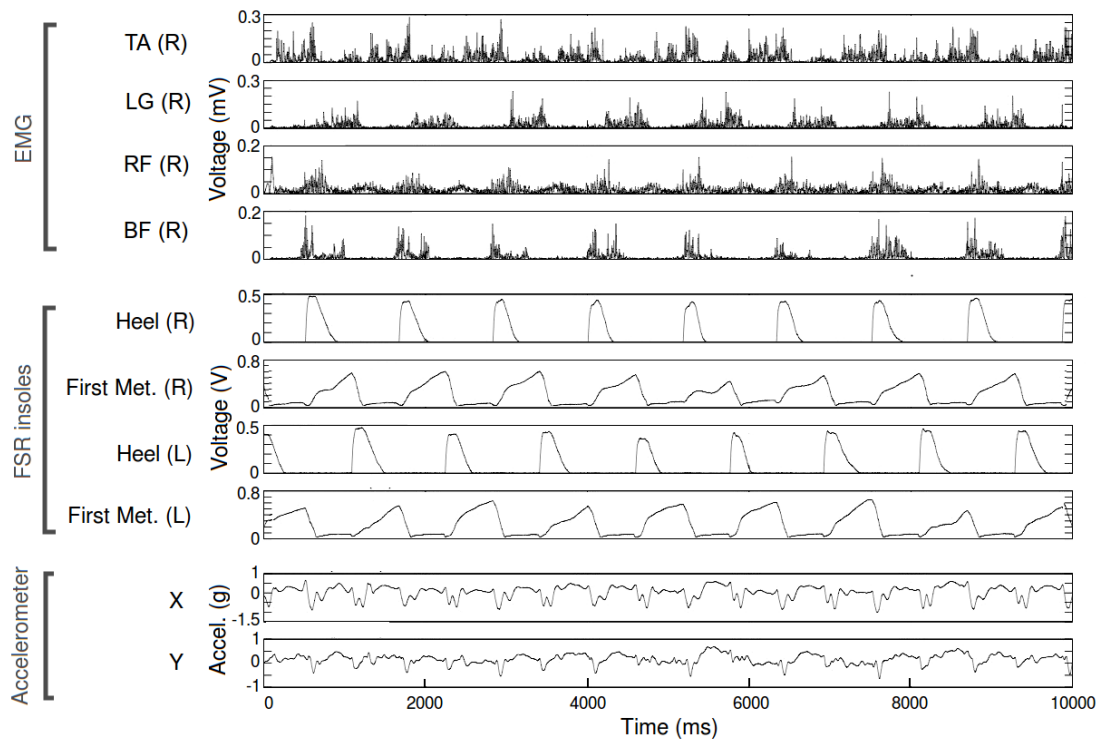


Figure 3.11: **Recordings from test subject PF over a ten second time interval.** The EMG recordings have been filtered to remove noise using a digital FIR bandpass filter and 5-point median filter. Full-wave rectification of the filtered EMG waveform gives the absolute value of the raw signal. The FSR shoe insoles exhibit an increase in voltage output with an increase in applied force.

be seen in Fig. 3.11.

Event-related averaging

Modulation curves of a rectified and averaged EMG recording are a measure of neural motor drive [46]. This can be visualised by using the signal processing technique of event-related averaging, where the event is a discrete time point indicative of an event, for example, an electrical stimulus to a nerve. This average represents the net EMG response to the given stimulus, and is often used to measure reflexes or other triggered muscle actions. Peaks or troughs observed in the average, indicate that the active motor neuron pool, which innervates the muscle in question, has received facilitatory or suppressive synaptic drive, time-locked to the trigger [186]. Using this technique, the voltage waveform related to peak heel contact with the ground was taken as the trigger and the rectified EMG signal was averaged in a time period of 1 s before and after the trigger, see Fig. 3.12. The concept was to analyse the phase relations of the EMG activity with respect to heel strike.

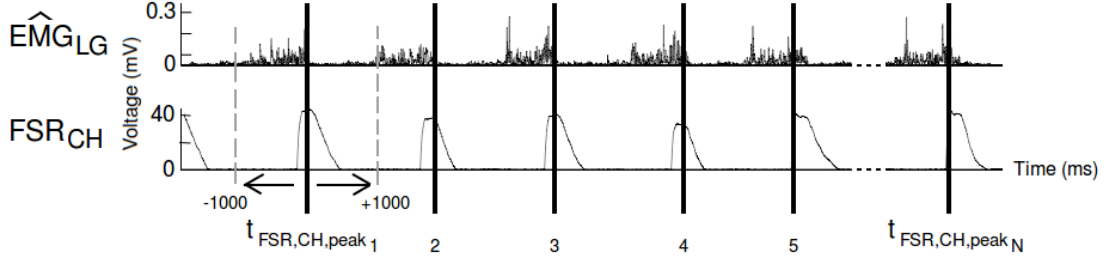


Figure 3.12: **Event-related averaging EMG data.** Using this technique, the maximum peak in the heel FSR data (corresponding to heel contact with the ground) ($t_{FSR,CH/IH,peak}$ is taken as the ‘event’ and \hat{EMG} is averaged in a time period of 1000 ms before and after the event. This example demonstrates the process of calculating $ERA_{LG,CH}$ of \hat{EMG}_{LG} using FSR_{CH} .

The general equation describing the event-related average (ERA) of the EMG (\hat{EMG}) for each muscle (mus) can be described as:

$$ERA_{mus,CH/IH}(i) = \frac{1}{N} \sum_{k=1}^N \hat{EMG}_{mus_k}(i + t_{FSR,CH/IH,peak}) ; -1000 \leq i \leq 1000 \quad (3.10)$$

Where N is the total number of events (peaks measured in the heel FSR ($t_{FSR,CH/IH,peak}$) recorded during the treadmill walk and CH/IH describes whether the FSR contact data are taken from the contralateral (CH) or ipsilateral (IH) heel to the muscle. And \hat{EMG}_{mus_k} is the k th sequence of EMG muscle activity for which an event occurred, in the range of 1000 ms before and after the trigger.

In addition, the ERA was also taken in a range of one stride duration (D) before and after the event to allow comparison between all of the subjects, with range $-D \leq i \leq D$. Stride duration was calculated as the average time between subsequent peaks recorded from $FSR_{CH/IH}$. A table of the mean and standard deviation of stride duration for each subject is given in Table 3.5.

$$D = \frac{1}{N} \sum_{k=1}^N t_{FSR,CH/IH,peak_{k+1}} - t_{FSR,CH/IH,peak_k} \quad (3.11)$$

Where $t_{FSR,CH/IH,peak}$ is the time of the peak in the heel FSR in seconds.

Following averaging, the baseline offset was amended using a 1-point baseline correction. A constant, which was taken to be the minimum averaged EMG value in the array, was subtracted from all the spectral data points so the baseline was reset to 0 V.

For clarity, the time-base was normalised so it could be expressed as a proportion of the actual stride time (from 0 to 100%). Where the k th normalised

Subject	No. of recorded strides		Average stride time (STD)	
	R	L	R (s)	L (s)
PA	142	143	1.25 (0.04)	1.25 (0.03)
PB	150	149	1.20 (0.04)	1.20 (0.03)
PC	141	140	1.27 (0.04)	1.27 (0.03)
PD	154	155	1.16 (0.03)	1.16 (0.04)
PE	157	157	1.14 (0.03)	1.14 (0.07)
PF	153	152	1.17 (0.04)	1.17 (0.04)
PG	159	158	1.13 (0.04)	1.13 (0.06)
PH	161	162	1.11 (0.02)	1.11 (0.02)
PI	162	163	1.10 (0.04)	1.10 (0.05)
PJ	158	158	1.13 (0.02)	1.13 (0.03)

Table 3.5: **Average stride duration of each subject.** Stride duration was measured from a peak in $FSR_{CH/IH}$ to subsequent peak in both the right and left legs during walking at constant speed of 4 km/h.

value ($\hat{t}_{ERA,mus,CH/IH_k}$) is calculated using the standard method.

$$\hat{t}_{ERA,mus,CH/IH_k} = \frac{t_{ERA,mus,CH/IH_k} - t_{ERA,mus,CH/IH_{MIN}}}{t_{ERA,mus,CH/IH_{MAX}} - t_{ERA,mus,CH/IH_{MIN}}} \cdot 100 \quad (3.12)$$

As a maximum voluntary contraction (MVC) calibration of the amplitude of the EMG has been observed to increase variability between subjects [187], instead, the amplitude of the within-subject ERA was scaled between 0 and 1 by normalising to the maximum value ($ERA_{mus,CH/IH_{MAX}}$).

$$E\hat{R}A_{mus,CH/IH_k} = \frac{ERA_{mus,CH/IH_k} - ERA_{mus,CH/IH_{MIN}}}{ERA_{mus,CH/IH_{MAX}} - ERA_{mus,CH/IH_{MIN}}} \quad (3.13)$$

Where $E\hat{R}A_{mus,CH/IH_i}$ is the i th normalised value.

Finding the mean ERA of the EMG across-subjects required averaging over the entire subject population. A time-base interpolation method transformed the ERA for each subject into a 3000 sample representation, as described in [188,189]. From this, simply, the population mean ($M_{E\hat{R}A,mus,CH/IH}$) and standard deviation ($STD_{E\hat{R}A,mus,CH/IH}$) of the ERA for each measured muscle could be found.

Temporal values

Measuring the time of the maximum peak ($t_{mus,CH/IH,peak}$) in muscle activity following a peak in the $t_{FSR,CH/IH,peak}$ provides a strategy for analysing the relationship between heel contact and muscle activity and to identify correlation. To compare this information across subjects, the stride time information needs to be normalised using a scaling equation to account for the various different heights (and leg lengths) of the subjects, as described by Hof (1996) [190].

$$\hat{t}_{mus,CH/IH,peak} = \frac{t_{mus,CH/IH,peak}}{\sqrt{\frac{l_{sub}}{g}}} \quad (3.14)$$

Where $\hat{t}_{mus,CH/IH,peak}$ is the normalised time parameter for the peak in the EMG, l_{sub} is the subject's leg length measured from the anterior superior iliac spine (ASIS) to the medial malleolus (true leg length) and g is acceleration due to gravity (9.81 ms^{-2}).

Measure of variability

The coefficient of variation ($CV_{E\hat{R}A,mus,CH/IH}$) was used as a statistical method to measure the overall variability between subjects of the averaged ERAs. Where $CV_{E\hat{R}A,mus,CH/IH}$ is described as the ratio of the standard deviation to the mean.

$$CV_{E\hat{R}A,mus,CH/IH} = \frac{\sum_{k=1}^N STD_{E\hat{R}A,mus,CH/IH_k}(i)}{N \sum_{k=1}^N M_{E\hat{R}A,mus,CH/IH_k}(i)} ; 1 \leq i \leq 3000 \quad (3.15)$$

Where N is the number of subjects ($N = 10$).

3.5 Results

The graphs of the ERAs were analysed for each of the ten test subjects to identify a correlation between EMG and foot contact information from the heel, and EMG and vertical acceleration of the hip. Example plots of the ERAs triggered from the right heel (FSR_{IH} , ipsilateral to the leg muscles), left heel (FSR_{CH} , contralateral to the leg muscles) and y-axis (vertical) acceleration for subject PF demonstrate the EMG pattern and phase relationships between muscle activity and heel contact/hip acceleration, Fig. 3.13 and 3.14 respectively.

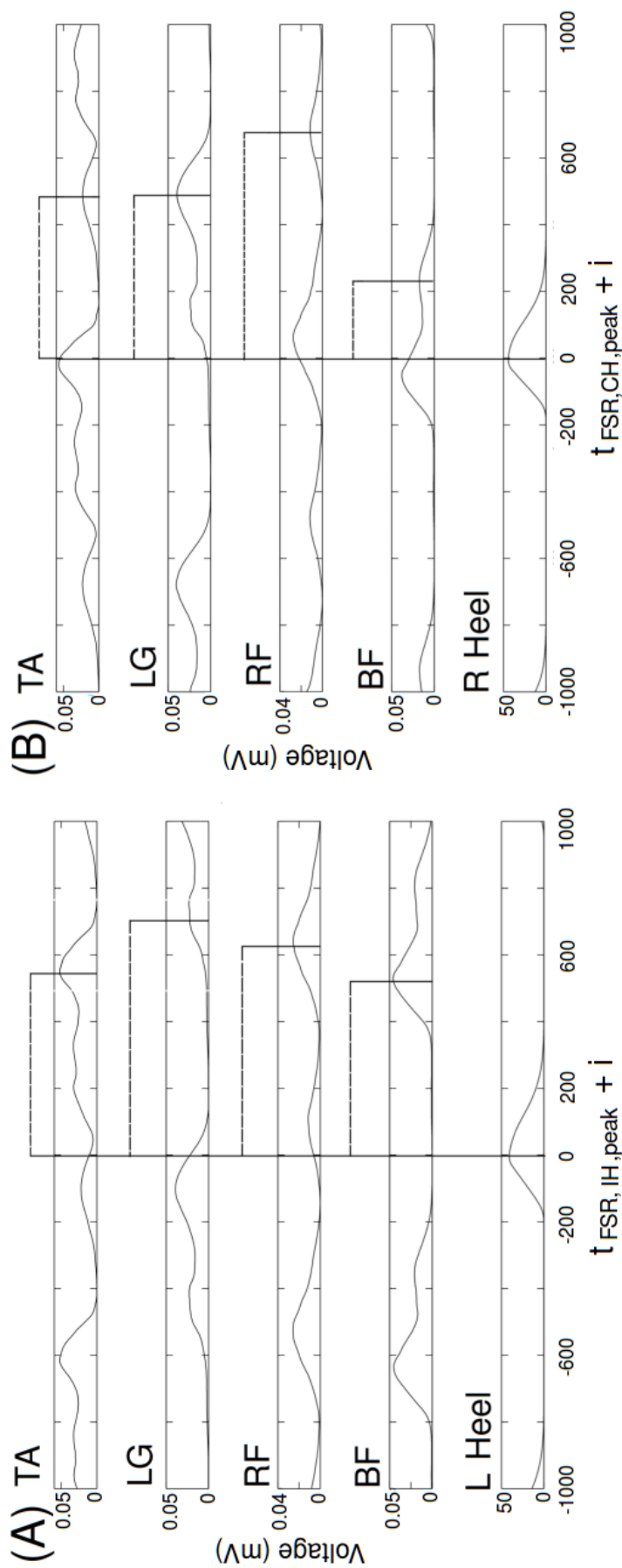


Figure 3.13: **Event-related average (ERA) of the rectified EMG recordings - heel contact.** (A) Event trigger = Peak FSR output measured during left heel contact. (B) Right heel contact. Relationship between peaks in the data are identified by black dashed lines. $t_{FSR, CH/IH, peak}$ is the time of occurrence of the event A and B (FSR), and i is the time period of 1000 ms before and after the event (subject PF).

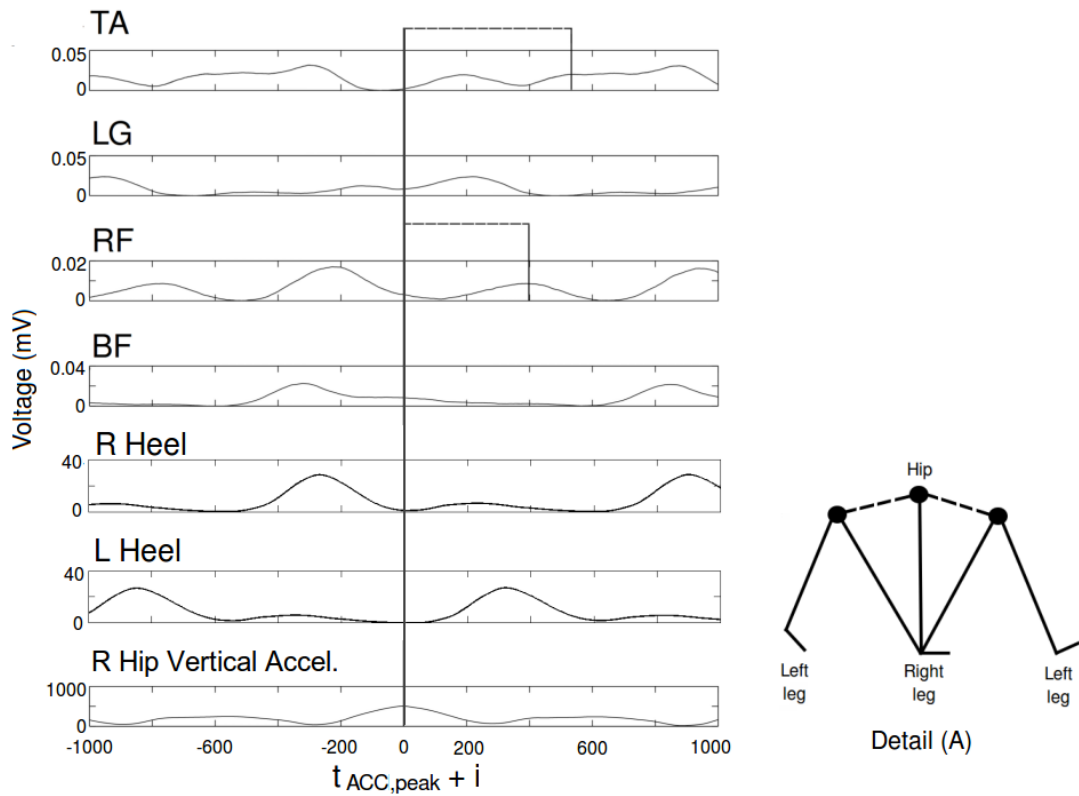


Figure 3.14: **Event-related average (ERA) of the rectified EMG recordings - hip acceleration.** Event trigger = Acceleration of the right hip in the y vertical direction. Relationship between peaks in the data are identified by black dashed lines. Peak acceleration of the hip occurs during mid-stance of the leg, Detail (A). $t_{ACC,peak}$ is the time of occurrence of the event (ACC) and i is the time period of 1000 ms before and after the event (subject PF).

To identify correlations, peaks and troughs in the EMG signal were analysed to determine whether they corresponded to the ground contact information from the feet and/or hip acceleration in the vertical direction. Since the event to cue the averaging process is taken as the maximum peak value in the heel contact/accelerometer waveform, this can be seen as analogous to taking a binary spike input signal and thus is the same as the cross-correlation between an event and the EMG response waveform [191]. The results were found to be consistent among the majority of subjects with similar patterns in the event-related average EMGs emerging. Correlations can be identified by quantitative analysis of the data.

3.5.1 Identifying correlation

An aim of the research study was to identify a relationship between physical quantities, which can be measured on the participant, and muscle activity. This would imply that the physical quantity could be used in a causal control system to generate muscle activation signals to drive steady state walking. For this reason only muscle activity which follows peaks in the hip acceleration and foot contact data can be seen as useful, as a linear, causal system operating in real-time can only depend on past and present inputs.

In muscle activity measurement, peak activity and burst duration are both important factors to consider as the envelope of activity differs from muscle to muscle during the gait cycle. This information is thus important in the development of a control system for generating a functional gait in patients with SCI. However, to initially establish the relationship between foot contact and the muscle activity it is simplest to examine the relationship between peak activity in the signals which will determine the feasibility of using foot contact and hip acceleration as input signals to trigger the muscle activation.

Right hip acceleration (vertical y-direction)

The 2-axis accelerometer measured acceleration of the hip in the direction of walking (x-axis) and vertical acceleration in the longitudinal axis (y-axis). From studying the accelerometer recordings there are distinct negative and positive accelerations which are due to the device detecting the impact of heel strike of the contralateral and ipsilateral leg. The x-axis provides limited useful information during treadmill walking as the bodies forward momentum is minimal. In the y-axis recordings, the hip decelerates immediately at heel contact of the ipsilateral foot and then accelerates to a peak during stance before deceleration at toe-off and

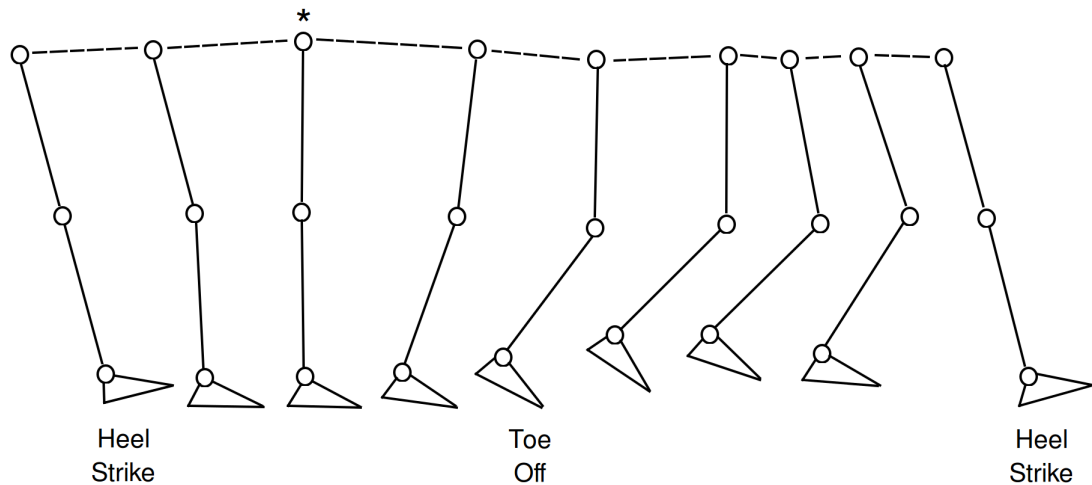


Figure 3.15: **Hip movement during the gait cycle.** Peak vertical acceleration of the hip was observed to occur at mid-stance (denoted by *), compare with Fig. 3.14.

the beginning of swing. This observation fits with the sinusoidal curve motion of the hip in the sagittal plane seen during normal walking [37], illustrated in Fig. 3.15.

Although the peak vertical acceleration of the hip occurs at mid-stance, a second peak with lower amplitude can also be observed during swing, as the hip flexes to move the limb forwards. This second lower amplitude peak can be observed in Fig. 3.14 as occurring approximately 600 ms after the peak acceleration of the right hip.

A relationship between peak activity in the ERA of the EMG and peak acceleration of the right hip in the vertical direction was not obvious and peak acceleration was more closely related to troughs rather than peaks in the signals, Fig. 3.14. This finding relates to the muscle groups the EMG data were sampled from and their known actions throughout the gait cycle (see Table 3.2. However there was a relationship with a small peak from the RF muscle and a less distinct peak in TA activity which corresponds to the dorsiflexion of the foot preventing it from contacting the floor during swing (identified by dashed lines in Fig. 3.14). This suggests that peak vertical acceleration of the right hip has limited use as a parameter for triggering muscle activations for production of coordinated joint actions for generating walking.

Heel contact

The FSR insole exhibited an increase in voltage output with an increase in applied force. Correlations of muscle activity with the heel FSR data were identified by observing patterns and peaks of muscle activity (where a peak is defined as being

between two troughs), which followed the maximum FSR output on foot contact, Fig. 3.13A and B. In all of the muscles measured there are identifiable phase relations between peaks in activity and foot contact, either from the contralateral or ipsilateral leg. This suggests, as was expected, that heel contact information recorded using the FSR insoles is phase locked to the patterns of muscle activity generation, during steady state walking, Fig. 3.13A and B.

3.5.2 Inter-subject variability

To further study the relationship between foot contact and muscle activity, and compare the inter-subject variability in the ERA, the average waveform for each muscle during two strides (before and after a heel FSR event) was found. Fig. 3.16 and 3.17 show the population mean (solid line) and standard deviation (dashed line) of the ERAs. It can be observed that the standard deviation is not uniform across the stride and fluctuates according to the level of muscle activity during the different phases of the gait cycle.

The distinct peaks in the subject average EMG activity which followed the specific 'event' (ERA) will be discussed separately.

The heel contact from both feet related to peaks of activity in all four of the muscles, The Tibialis Anterior (TA), Rectus Femoris (RF) and Biceps Femoris (BF) Fig. 3.16 and 3.17. Where the duration of activity encompassing a peak is defined as being between two distinct troughs. Each of the observed peaks in muscle activity are discussed separately due to functionality of muscles during different phases of the gait cycle.

Tibialis Anterior (TA)

Following the maximum peak in heel contact of the contralateral foot (FSR) (Fig. 3.17A, the TA becomes active and assists in the dorsiflexion of the foot during swing (seen at 23.4% of stride), there follows a peak in the activity which relates to stabilisation of the ankle at heel contact with the ground at 51.1%. Following the peak in heel contact of the ipsilateral foot (Fig. 3.16A), there is a peak in the muscle activity at 45.4% due to the muscle controlling progression of the tibia during stance.

Lateral Gastrocnemius (LG)

The LG muscle is involved in knee flexion, support of the knee during stance and in plantar flexion during the foot-off transition from stance to swing phase. In the subject average of the ERA there is a distinct peak at 42.6% (Fig. 3.16B)

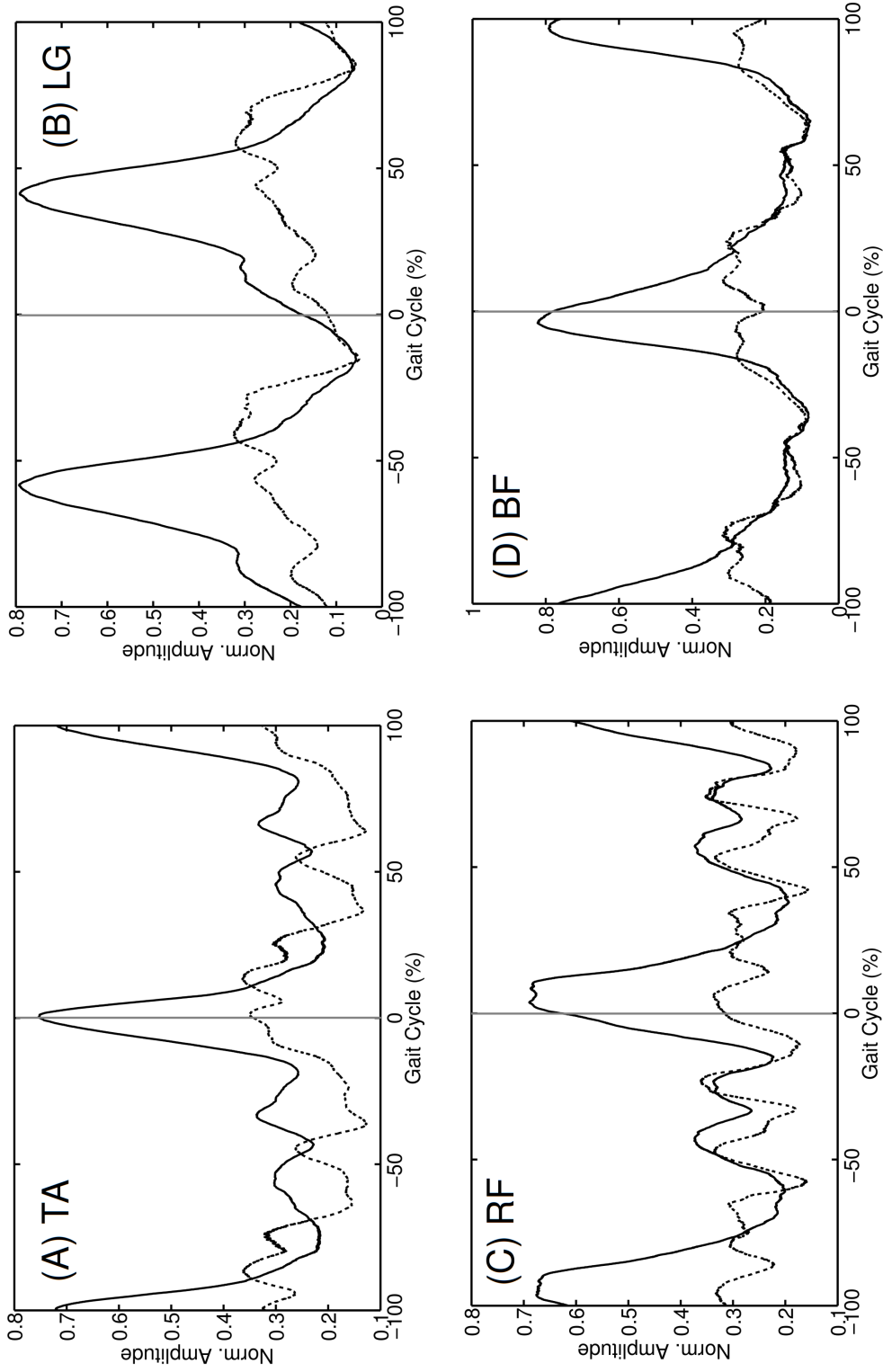


Figure 3.16: Mean ERA from all subjects, for each of the four muscles (right heel trigger). $(-)$ = $M_{ERAmus,IH}$, $(- -)$ = $STD_{ERAmus,IH}$ and $(-)$ = time of peak from $F SR_{IH}$.

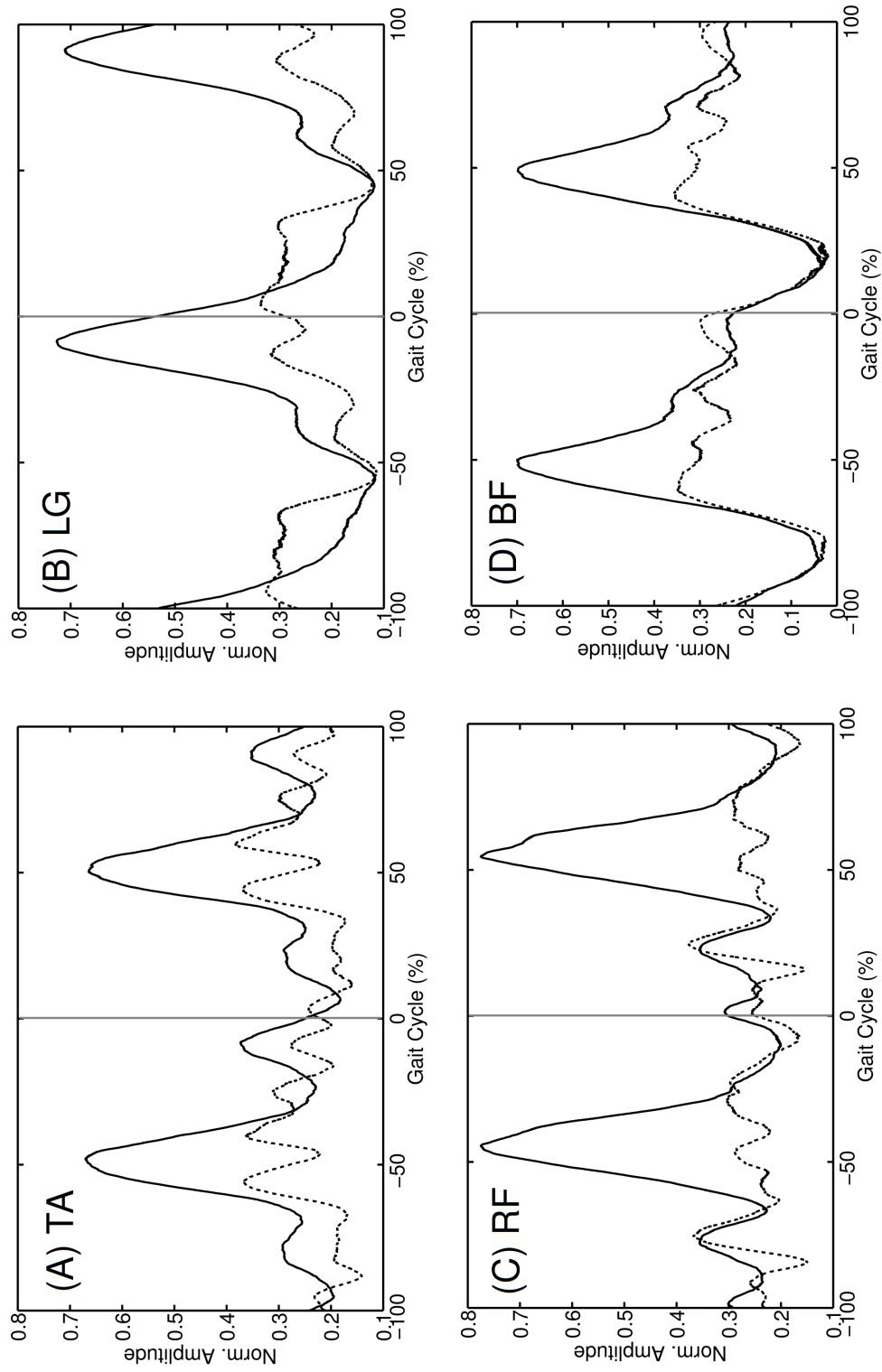


Figure 3.17: Mean ERA from all subjects, for each of the four muscles (left heel trigger). $(-)$ = $M_{ERAmus,CH}$, $(- -)$ = $STD_{ERAmus,CH}$ and $(-)$ = time of peak from FSR_{CH} .

Muscle	CH/IH	Dimensionless time	% of stride
		Mean (STD)	Mean (STD)
TA	CH	1.91 (0.30)	51.1 (7.1)
LG	IH	1.60 (0.30)	42.6 (7.2)
RF	CH	2.10 (0.19)	56.0 (5.2)
BF	CH	1.79 (0.23)	47.7 (5.6)

Table 3.6: **Mean time from peak in ERA of the heel FSR to peak (highest amplitude) in ERA.** This value was recorded for each subject in dimensionless time to accommodate for different leg lengths and as a % of the subject’s stride time.

occurring towards the end of the stance phase of the gait cycle. The timing of this activity in the gait cycle relates to plantar flexion of the ankle during push off of the foot off the ground to begin the swing phase of the gait cycle.

Rectus Femoris (RF)

The RF muscle is involved in hip flexion and knee extension. Hip flexion occurs following heel strike of the contralateral leg and acts to bring the limb forwards during swing, so this coincides to the small peak in muscle activity seen following the peak in heel contact of the contralateral FSR insole (Fig. 3.17C at 23.2%). The large peak in EMG activity at 59% relates to action of the muscle at knee extension as there is an increase in activity prior to the TA peak related to ankle stabilisation on heel strike (during leg extension at terminal swing).

Biceps Femoris (BF)

The BF is part of the hamstring group of muscles which are involved in knee flexion during swing and work to slow hip flexion and leg extension at terminal swing. A peak in activity can be seen at 47.7% (Fig. 3.17D), as this occurs just prior to the RF activity (related to knee extension) suggests this can be viewed as antagonist action to the quadriceps.

Heel contact is indicated as having a correlation to peaks in the muscle activity following a delay in time. The mean time between the peak in the ERA of the heel FSR to the peak (with largest amplitude) in the ERA of the EMG is summarised in Table 3.6. The contralateral heel (CH) was found to correlate with a peak in activity with the TA, RF and BF muscles, whereas the ipsilateral heel (IH) had a correlation to the peak in LG muscle activity. The timing information is given in both dimensionless time to account for subject leg length, and thus cadence variability and as a percentage of the total stride time.

Muscle	CV	
	IH	CH
TA	0.70	0.70
LG	0.61	0.64
RF	0.73	0.71
BF	0.67	0.67

Table 3.7: **Variability measures of the inter-subject event-related averages (ERAs).** Coefficient of variation (CV) of the muscle ERA related to FSR_{IH} (IH) or FSR_{CH} (CH).

The inter-subject variability was further studied using measures of the CV, Table 3.7.

3.6 Discussion

EMG activity during gait is well known to follow a cyclic pattern but establishing the underlying relationship between ground contact information and leg muscle activity during normal human walking will determine whether it is possible to use foot contact information in the same manner as RunBot, where foot contact is used as a trigger for driving motors in the legs to generate stepping.

The timing pattern of EMG is of interest, as it is directly related to the neural control of the muscle [192]. Whereas amplitude is of less importance for this study as it is known to be influenced by a number of factors such as, electrode position, muscle fibre orientation and quantity of subcutaneous fat [193] and is not easily correlated to force. For heel contact information to be the predictor of peaks and patterns in muscle activity, the foot contact (stimulus to the system) should occur before the muscle activity (reaction). Using this analogy, observation of the recorded data suggest that the TA, RF and BF muscles are activated and have their peak activity following heel contact from the contralateral leg during treadmill walking, Fig. 3.13A and Fig. 3.17A,C and D. This relates well to knowledge of the muscle's action during walking. Peak activity in the LG was found to be activated with peak activity following heel contact from the ipsilateral right foot along with a smaller peaks in the other muscles activity, Fig. 3.16B and Fig. 3.13B. These findings suggest foot contact information from the feet could determine which muscles need to be stimulated and when, to assist in the gait capability of patients with spinal cord injuries. The ERA waveforms (Fig. 3.16 and 3.17) agree with ensemble averaged muscle activity reported widely in the literature, for review and examples see [194, 195]. However it is of interest to

note that EMG averages reported as a % of stride are typically only reported in relation to the heel contact from the ipsilateral foot and not the contralateral foot as has been studied in this chapter.

A general relationship was also evident between vertical acceleration of the hip and troughs in muscle activity. This could suggest a relationship with suppression of synaptic input to the motor neuron pools of the recorded muscles at peak vertical acceleration of the ipsilateral hip, or could simply be due to removal of the excitation. Attaching an accelerometer on the posterior side of the body at the lumbar position of the spine could give an estimate for the locomotion of the body at the theoretical centre of mass. As motor output requires adjustment to maintain stability of the upper body during walking, studying the relationship between the centre of mass and muscle activity may be useful in the development of a control system for generating a stable gait cycle in patients with SCI.

An observation in the correlation of the RF muscle with contralateral foot contact is that the maximum peak of activity, which is associated with knee extension at terminal swing, occurs 59% of the stride after the maximum peak in heel contact. This is a significant duration of time after the event suggesting that heel contact may not be a suitable input for use in defining the timing for knee extension in terminal swing in gait control. As this event occurs prior to a heel contact of the ipsilateral foot and does not directly follow any other foot contact gait events, such as toe contact or toe-off, it is prudent to consider that, for this particular joint motion during walking, foot contact is not an ideal sensory trigger. Afferent feedback is well understood to be important in controlling the transition from stance to swing (including in cats [45,76,79] and in human infants [111]), so it is predictable that the transition from swing to stance has a similar dependence. utilising the afferent regulation of this transition is vital in finding an effective way to ensure correct placement of the foot during stance to adapt to the different movements required by the variable walking conditions. A stable transition to stance is dependent on the leg being sufficiently protracted in front of the body, which implies that the position of the hip is important for generating an afferent signal regulating the swing-to-stance transition [196]. In the RunBot robot, knee extension at terminal swing is initiated when the ipsilateral hip reaches a pre-determined anterior extreme angle (AEA). This process has a basis in spinal reflexes observed in different animals [196,197] and also in humans [6], where a direct connection has been found between joint angle and motor output. It can be considered that AEA could be a suitable alternative as an indicator for knee extension in a human gait control system.

Only measuring muscle activity in one leg meant that a relationship between the hip acceleration and contralateral leg muscle activity could not be examined. This was a limitation of the study and may be of interest in further research. However, as heel strike from both legs was picked up by the accelerometer due to shock travelling up the leg from ground impact, there was some loss of hip acceleration measurement during the gait cycle and may suggest accelerometers are less suitable in the development of a control strategy for FES in comparison to the FSR foot contact sensors.

A relationship is implied from the results from the treadmill walking, with an identifiable pattern of muscle activation following heel contact in the intra- and the inter-subject ERAs, Fig. 3.13, 3.16 and 3.17. However, the delay in time of peaks in the muscle activity subsequent to heel contact differed across subjects by 5.2-7.2% which is quite a large discrepancy when compared to the typical durations of the gait phase divisions of stride. This could be due to the range of subject height and leg lengths recruited for the study. A difference in stride length which is a factor of leg length results in a variance in stride duration. Table 3.5 demonstrates the variation in subject stride duration although they were all walking with the same treadmill belt speed. The coefficient of variation (CV) found in the calculation of the inter-subject ERA was highest in the RF muscle, in the ERA using FSR_{IH} as the event, with a standard deviation of 73% of the mean value. The lowest CV was in the LG, with a standard deviation of 61% of the mean. These values show that there is large inter-subject variability in the ERAs demonstrating that no-one walks identically. However, it should be noted that the ERAs calculated from the two different events (FSR_{CH} and FSR_{IH}) had a very similar CV. Being the same in the TA and BF, and only differing by 2-3% in the LG and RF muscles. Studying the standard deviation plots in Fig. 3.16 and Fig. 3.17, it is clear that the standard deviation is affected by the different phases of the gait cycle. The peaks in muscle activity demonstrate variability in magnitude and duration across subjects, which can be seen clearly in the standard deviation. The LG muscle demonstrates the greatest variability in the duration of its major phase of activity, which agrees with the findings of Shiavi et al. (1987) [189].

What can be established is that a significant amount of variability exists between the subject ERA of the muscle activity during a constant speed walking of 4 km/h. Although EMG patterns have been well documented as having high CV values ($> 50\%$) [198] and are not an unusual finding, for the context of this research, it will not be valid to average the ERA across the subject population

as the EMG profile, at this speed, appears specific to the individual. However, key features in the ERA related to muscle function during the gait cycle can be identified and are consistently seen across the subjects. This includes peaks in muscle activity following foot contact information in the contralateral leg (TA, RF and BF) and ipsilateral leg (LG). Another observation is that although the peak in heel contact correlates with peaks in muscle activity, the onset of foot contact (rising edge of the peak) would perhaps be better suited to being used as the trigger point for averaging the EMG recordings. This would have the effect of shifting all of the ERA plots to the left by approximately 10% and would mean the onset of foot contact would more closely relate to an onset of muscle activity in the correlated muscle to foot contact combinations already discussed. This would also more closely resemble the control system of RunBot which uses a digital ON/OFF switch in the foot to indicate foot contact as well as corresponding to typical methodology used in gait research using foot switches as a means of averaging EMG data by stride duration (ensemble averaging) [189, 195, 199].

Although a correlation between foot contact information and muscle activity is implicated by the data, it should be considered that using one constant belt-speed of 4 km/h for all subjects may have an influence on the relationship between the muscle activity and heel contact information. This can be defined as a correspondence problem due to the periodic gait cycle. To remove this influence and reduce the variability between subjects, the data collection should be repeated but using a varying walking speed, which as well as more closely relating to overground walking, where speed can change from step to step, will produce an average which should remove the correspondence of walking speed with the correlations. It should also allow the influence of speed on the EMG and foot contact patterns to be analysed which could be valuable in the development of a control system for generating stepping.

3.7 Summary

The preliminary study demonstrated an observable relationship between foot contact and muscle activity which has potential to be used in the development of a control system for generating gait. There were however some limitations to the study which require adaptation to the data collection methods before further development of a gait control system can be made.

3.7.1 Recommendations

- Measure EMG from muscles in both the right and left legs to ensure symmetry assumption.
- Develop a device incorporating an eight channel EMG preamplifier (for measuring EMG in both legs) and the amplifier for the FSR insoles to improve setup and remove need for push-button synchronisation of two USB-DUX D devices.
- Vary the speed of the treadmill in a pseudo-random manner to average out and remove potential correspondence of the relationship between foot contact information and muscle activity with walking speed.
- Use a range of walking speeds which relate to a subject's natural range during normal overground walking.
- The EMG should be averaged (ERA) using onset of foot contact activity rather than peak to coincide with heel strike at the start of the gait cycle.
- Compare measurements of EMG and foot contact taken during treadmill walking and overground walking to analyse if the data are affected by the walking modality.

Chapter 4

Wireless gait analysis device (wi-GAT)

One finding from the preliminary study was that an irregular walking pattern should be encouraged to remove correspondence between walking speed and the relationship between EMG and foot contact. This can be achieved by recording the data during overground walking, where the participant is unconstrained to a set walking pace, or by recording during treadmill walking using a belt speed control program to automatically vary the treadmill belt speed. To use these two walking modalities it is necessary to study suitable methods of data collection. For recording during overground walking it is desirable to develop a wireless system for recording EMG/FSR data so the device is portable and does not require long cables which limit the walking distance and introduce a potential tripping hazard. In addition, for developing a treadmill control program for varying belt-speed, knowledge of a subject's gait parameters is required to create a suitable belt-speed sequence catered to the individual participant, based on their walking speed and cadence during normal overground walking.

In this chapter the development and validation of a wireless gait analysis device (wi-GAT) will be discussed. This device was developed with the aim of being a low-cost and portable alternative to large scale, expensive and primarily lab based equipment for the measurement of gait parameters. The wi-GAT was developed based on an original 'wired' version constructed by Galen et al. (2011) [200]. This device was selected for measuring gait parameters for the creation of a treadmill speed control program as it has been previously used to collect gait parameters with individuals with Spinal cord injuries (SCI) [200] and children with cerebral palsy [183], it is a simple and portable system, and provided an opportunity for investigating wireless communication and analysis of the potential

for adapting the EMG/FSR preamplifier, described in Chapter 3, Section 3.3.2, for recording during overground walking.

In addition, the development of a wireless gait analysis device has implications in quantifying movement in various neurological conditions such as stroke [201, 202], cerebral palsy [183,203], spinal cord injury [204], and also among the elderly population to assess the risk of falls [205], making it a valuable research tool.

To ensure the wi-GAT provided accurate measurement of gait parameters, a validation study was undertaken which is described in detail within this chapter along with details of the design of the device. A technical note based on the wi-GAT validation study was published in the journal of Medical Engineering and Physics [177].

Following the validation study, the wi-GAT device was used to collect measurements of gait parameters from ten healthy subjects prior to them taking part in a treadmill data collection study. These gait parameter values were used to develop a treadmill belt speed sequence which was catered to the subjects individual walking speed range and cadence, the control program is discussed further in Chapter 5, Section 5.1.3.

4.1 Introduction

Three dimensional (3D) gait analysis has been developed over the years as a method of producing accurate measures of human movement, however access to these sophisticated systems is often limited to gait laboratories within academic institutions or large hospitals with embedded research facilities [206]. In addition to limited access, the costs associated with gait assessments also make it difficult for clinicians to perform them routinely to monitor their patient's progress. It has been estimated that a gait study can cost anything up to \$2000 and the cost to set up a movement laboratory can be on average about \$300,000 [207].

In a recent review reporting on gait deficits in patients with traumatic brain injury, it was found that out of 15 studies that had used 3D gait analysis as an outcome measure only 2 of the studies reported on the kinematics and kinetics of gait [208]. The majority of the studies that were reviewed reported the temporal-spatial gait parameters, such as walking speed, cadence, stride duration, stride length and step length. A 3D gait analysis is often difficult to perform in a clinical setting, due to the reasons stated previously, however recording spatio-temporal gait parameters is less time consuming and feasible. The advantage of a 3D gait analysis is that provides extensive data that includes kinematics and kinetics,

which often gait assessment tools that record spatio-temporal parameters alone, do not provide. There are commercially available gait assessment tools that can record spatio-temporal gait parameters such as instrumented mats with pressure sensors [209] and body worn sensors that incorporate accelerometers [210]. The limitations of these systems include difficulties in setup within a clinical environment, where space is often limited, and although they may not be as expensive as the 3D gait analysis system, they are still costly for individual departments or independent rehabilitation clinics to utilise in providing a cost effective clinical assessment.

Therefore there is a need for a low-cost, low-tech alternative that provides accurate measures that can be easily used by rehabilitation professionals without specialist motion capture/analysis training and most importantly within a clinical environment. The wireless gait analysis tool (wi-GAT) described in this chapter, meets these goals. The aim of the validation study was to establish the concurrent validity of spatio-temporal gait parameters recorded by this newly developed and novel, wireless system among adult able bodied subjects.

4.2 Materials and methods

The wi-GAT was recently upgraded as a standalone data acquisition device which required adaptations to its circuitry and data acquisition software, this justifies the need for a validation study. The spatio-temporal gait parameters which were validated include stride length, stride duration, cadence, stance duration, swing duration, stance%, swing%, double support duration and walking speed. These parameters were calculated using the definitions provided in Table 4.2. The Vicon (Vicon MX, Oxford Metrics, Oxford, UK) is a three dimensional motion analysis system which is commonly used for recording spatial and temporal gait parameters with high accuracy [211]. It was thus deemed an appropriate standard on which to validate the gait parameters recorded using the wi-GAT.

4.2.1 Materials

A custom designed printed circuit board (PCB) (Beta LAYOUT, Ireland) was used in the development of the wi-GAT. The PCB was designed using the Eagle PCB Design Software (CadSoft, USA). The schematic is provided in Fig. 4.1 and incorporates a Bluetooth module (BlueGiga model: WT11, Espoo, Finland) and microcontroller chip (Microchip model: pic18f4520, Chandler, AZ, USA) powered by a 9 V battery. Bluetooth was chosen as the wireless transmission

interface as it is low-cost and has low power radio frequency transmission. There is also the advantage that most computers have built-in Bluetooth receivers or if not, Bluetooth USB dongles are readily available. For these reasons, Bluetooth has been widely used in the development of biomedical devices used in healthcare including pulse oximeters, heart rate monitors, asthma inhalers and stethoscopes.

The PCB is housed in a plastic enclosure with dimensions of 12x10x4.5 cm and a total weight (including battery) of 225 g. The small size and weight enables the device to be attached to a belt on the participant's waist during data collection. The device amplifies and transmits data from two instrumented insoles each comprising of four 13 mm diameter force sensing resistors (FSRs) (FSR 402, Interlink Electronics, Camarillo, CA, USA) which are used to capture temporal information during gait. These are positioned under the heel, 1st metatarsal head, 5th metatarsal head and the big toe as described by Granat et al. [182]. Insoles were custom-made for each subject using FootDoc foot impression sheets (Visual Footcare Technologies, LLC, NY, USA) to position the FSRs as accurately as possible under the location of each anatomical landmark previously described. By stepping on and off the pressure sensitive paper an imprint of the foot is left with more ink deposited on the film in the areas of peak pressure under the foot, Fig. 4.2.

A grid reference system was used with the foot impression sheets to make insoles for each participant. Standard shoe insoles were trimmed to the correct size and FSRs were attached under a clear plastic film in the correct positions for collecting the foot contact data, Fig. 4.3.

The insoles are connected via ribbon cable to the waist worn device, Fig. 4.4. The wi-GAT uses a Bluetooth connection to computer for data collection by an interface program implemented in LabVIEW (National Instruments Inc., Texas, USA), an adaptation of the program discussed in [200]. The signals were sampled at 30 Hz and logged directly to a spreadsheet file.

The spatio-temporal gait parameters were also recorded simultaneously using a twelve camera Vicon MX system operating at 100 Hz. The Vicon Plug-in-Gait lower limb marker set and model was used. Plug-in-Gait uses methodology which has been described by Davis et al. [212] and Kadaba et al. [213] and requires sixteen 15 mm reflective markers to be attached to anatomical landmarks of the lower extremity.

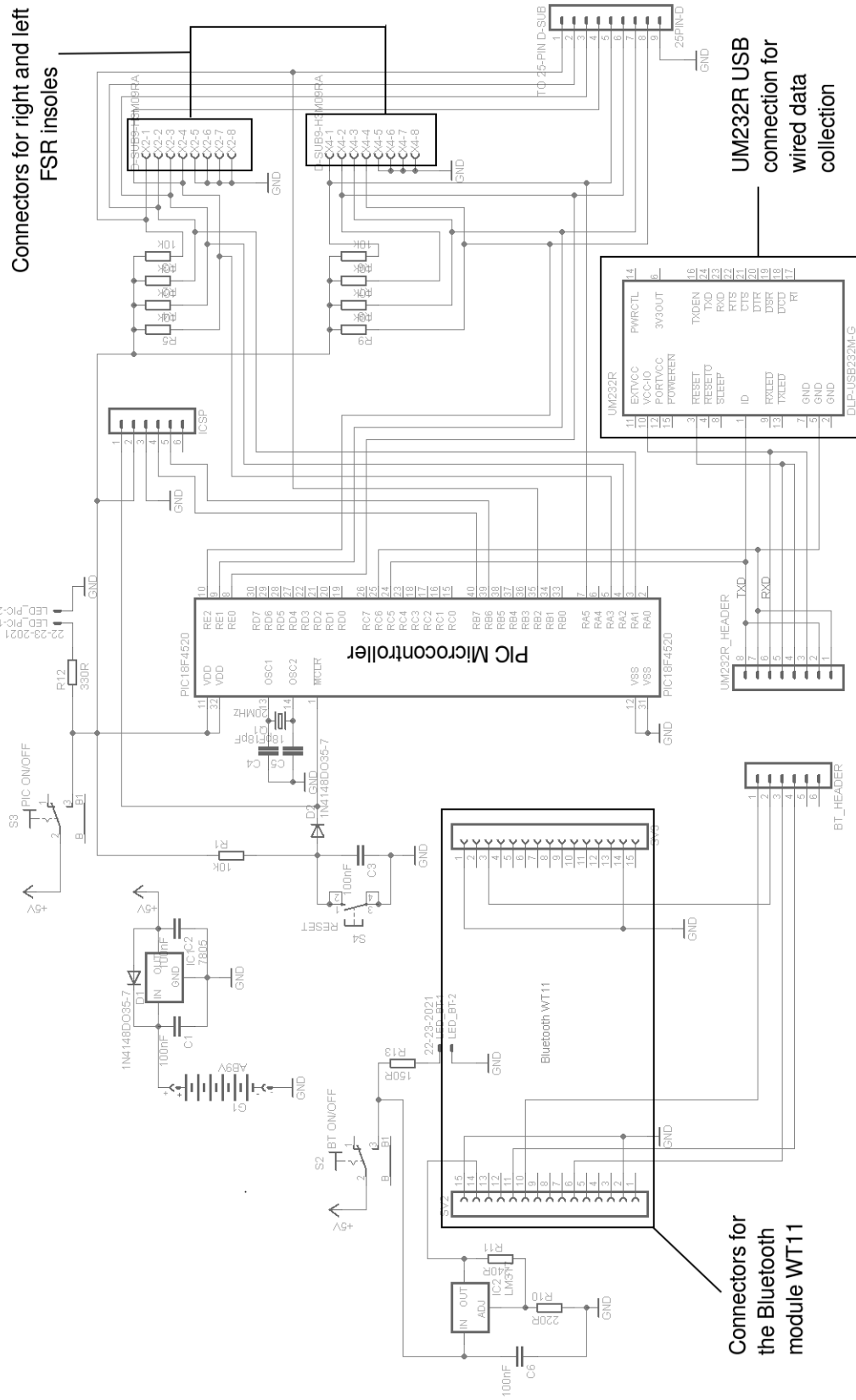


Figure 4.1: Annotated schematic of the wi-GAT device.



Figure 4.2: **Foot impression sheets were used to make insoles for each study participant.** The ink is deposited on the film in the areas of highest pressure under the feet. This allows accurate measurement of where the FSRs should be positioned on the insole for recording foot contact data. Each photo (i-iv) is a foot impression from a different subject.

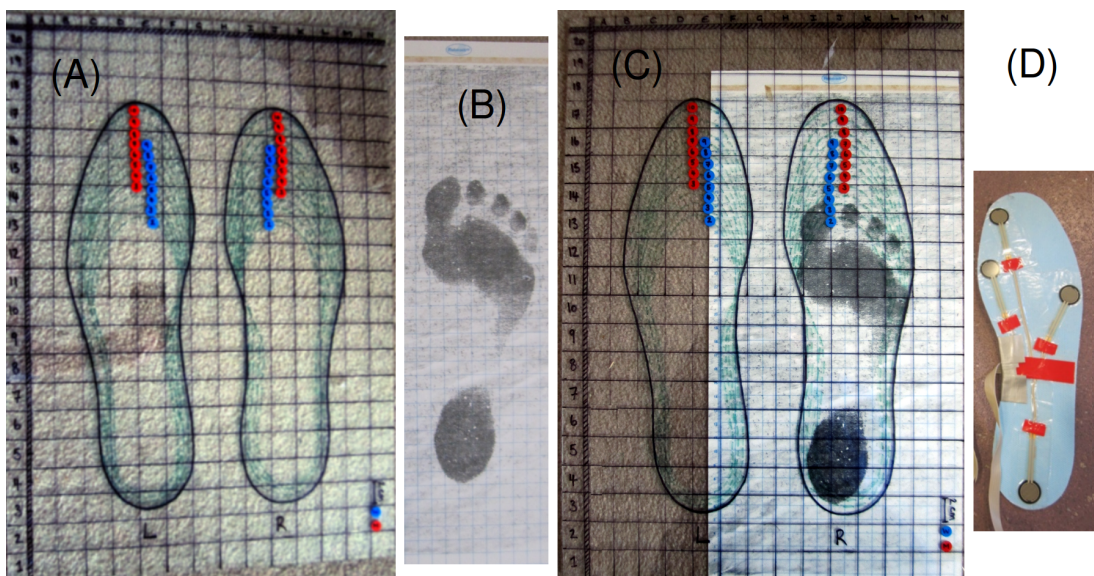


Figure 4.3: **The process of making insoles for each study participant.** (A) A grid reference was made on clear acrylic to size the foot imprint to the required insole shoe size and help position the FSRs on the insole. (B) Foot impressions are taken from each participant. (C) The foot imprint is sized using the grip reference. (D) The insoles can be cut to the correct size and the FSRs accurately positioned under the feet.

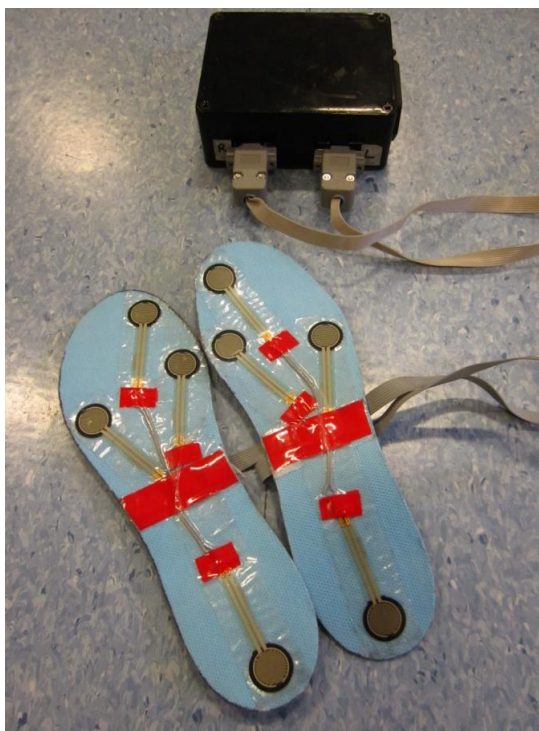


Figure 4.4: **Wi-GAT device and FSR insoles.**

4.2.2 Experimental setup

The spatio-temporal gait parameters were recorded over a 10 m walkway located within a gait lab at the Department of Biomedical Engineering, University of Strathclyde. The capture volume of the Vicon system was set to approximately 6x6x2 m and was calibrated to the distance of the walkway using standardised protocols recommended by the manufacturer (Vicon MX, Oxford Metrics, Oxford, UK) at the beginning of each testing session.

4.2.3 Participants and ethics

Ten healthy participants with no known gait abnormalities volunteered to take part in the study. These included four males and six females with a mean age of 27 years (range 23-30 years). The average height of the subjects was 1.72 m (1.6-1.87 m range) with an average weight of 73 kg (54-86 kg range). Ethical approval for the study was provided by the Biomedical Engineering ethics committee at the University of Strathclyde and the volunteers were fully informed of the procedure and provided written consent.

Table 4.1 outlines the demographic of subjects who participated in the study.

Table 4.1: **Wi-GAT validation study participant information.** The subject ID was randomly assigned to the subject after they were recruited to the study.

Subject ID	Gender	Handedness	Age	Height (m)	Weight (kg)	Shoe size (UK)
A	M	R	26	1.85	83	9
B	F	R	26	1.60	59	4
C	M	R	30	1.84	75	11
D	F	R	25	1.64	63	6
E	F	L	23	1.61	71	7
F	M	R	30	1.87	86	9
G	M	R	27	1.83	86	9
H	F	R	26	1.66	62	7
I	F	R	25	1.69	91	6
J	F	R	27	1.63	54	4
Mean (STD):			27 (2)	1.72 (0.11)	73 (13)	7 (2)

4.2.4 Experimental protocol

Subjects were required to wear flat-soled training shoes and shorts. Anthropometric data were recorded for each subject on arrival and reflective markers were then attached to their lower extremities as defined by the lower limb Plug-in-Gait model, Fig. 4.5.

The instrumented insoles were placed in the subjects shoes and the wi-GAT box was positioned on a belt around their waist. Each subject was given the opportunity to perform practice walks to allow familiarisation with the equipment and the experimental procedure. During data capture each subject was instructed to walk at a self-selected comfortable speed [210]. The first 2 m of a 10 m level surface walkway allows the subject to accelerate to a self selected comfortable walking speed, and the last 2 m to decelerate to a stop at the end of the walkway [200,211]. The middle 6 m of the walkway was used for data capture. Coloured cones marked the start and finish of the middle 6 m pathway, ‘data collection zone’, for easy identification by the investigator for starting and stopping the data capture, a diagram of the experimental setup is given in Fig. 4.6. Subjects performed a total of ten walks each.

Plug-in-Gait Marker Placement

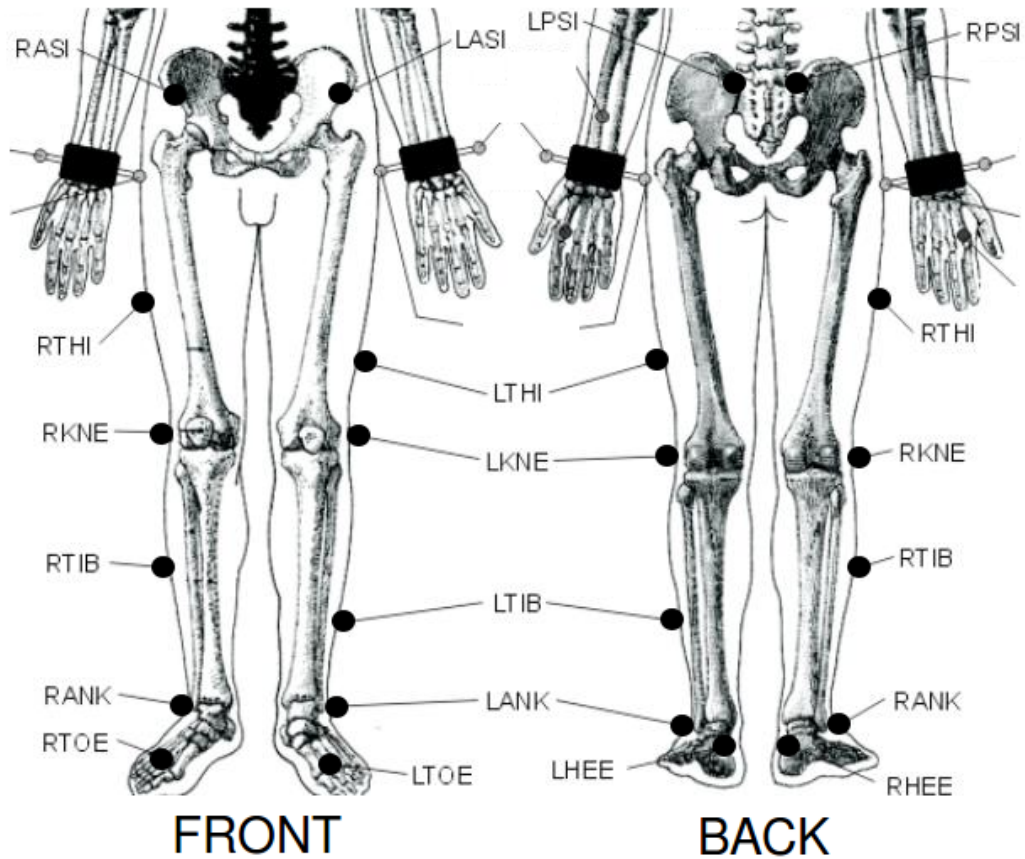


Figure 4.5: **Plug-in-Gait lower limb marker placement guide.** Vicon lower limb placement figure adapted from full body guide provided by Vicon, Oxford Metrics, UK.

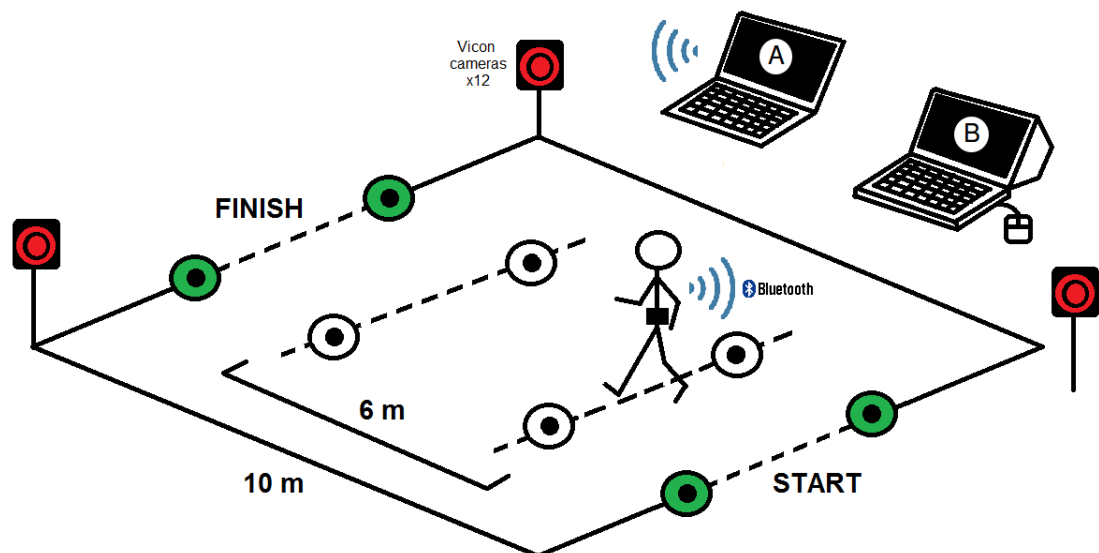


Figure 4.6: **Schematic diagram of the experimental setup for data capture.** Subjects wore the wi-GAT device around their waist with the FSR insoles placed in their shoes and Vicon markers attached to their lower body. Coloured cones identified the 6 m and 10 m distances. A laptop (A) was used to record from the wi-GAT device over a Bluetooth connection and a second desktop computer (B) operated and recorded from the Vicon camera system.

4.2.5 Extraction of gait parameters

Vicon

Gait parameters were extracted from both the wi-GAT and the Vicon system for comparison. Vicon Nexus 1.7.1 software (Oxford Metrics, UK) was used to analyse the data recorded from the Vicon system. Although force plates were present at the centre of the 10 m walkway, they were not used for detecting the heel strike and toe off events of the stride cycle because the size and position of the force plates limited data capture to a distance of 1.2 m or approximately a single stride cycle, compared to data recorded over 6 m and multiple strides by the wi-GAT. Instead, the Vicon Nexus software was used to manually identify the heel strike and foot-off time points during each trial using the position of the xyz coordinates of the heel and toe marker as a point of reference, Fig. 4.7.

The 3D coordinates and time frame that corresponded to each event were then exported as an ASCII file. Although the Vicon Nexus software can compute gait parameters from gait event information using the “Generate gait cycle parameters pipeline process, these values are only calculated from the first identified stride cycle and not averaged over every recorded stride. As the wi-GAT averages over a series of strides, to preserve as many similar calculation methods

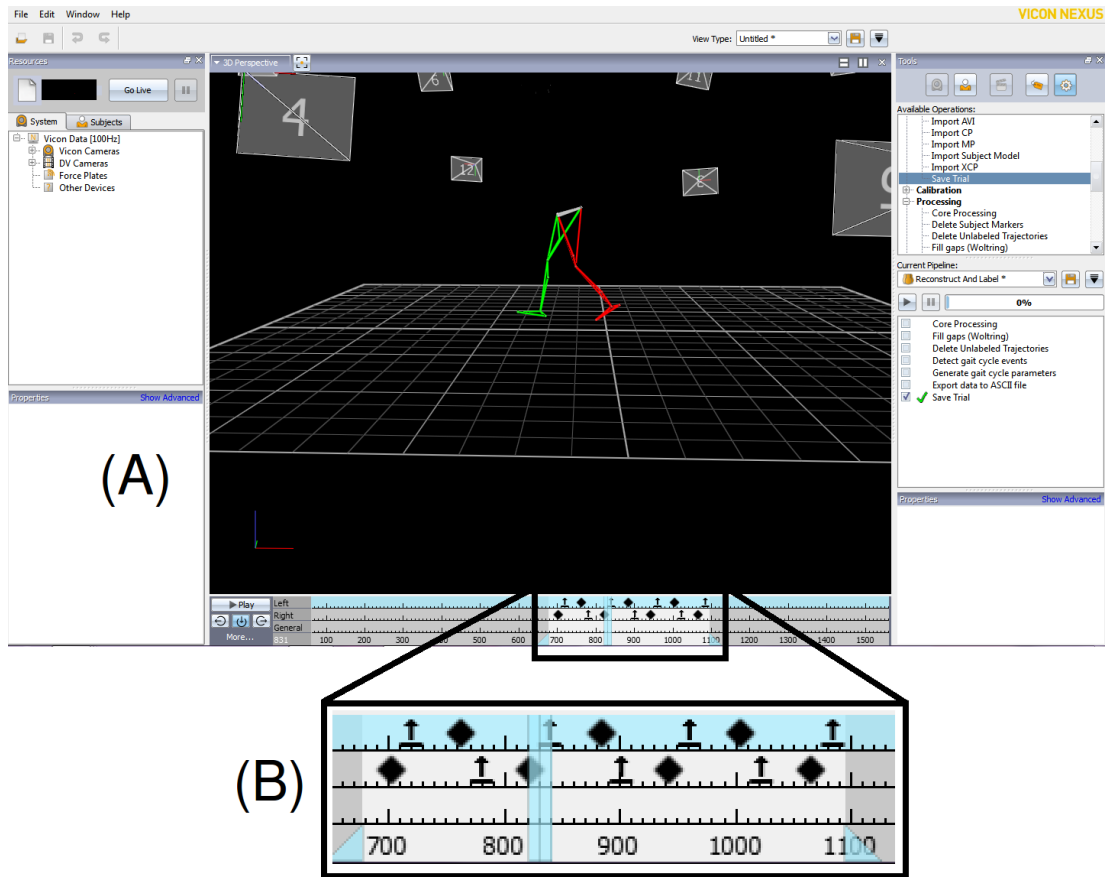


Figure 4.7: **Screenshot of the Vicon Nexus program.** (A) The heel strike and toe off timing was identified by visual analysis of the heel and toe marker positions during each of the recorded gait cycles. (B) The time line of the recorded walk features diamond symbols signifying heel strike and a vertical arrow for toe off. The left and right sides are shown on separate lines. The timing corresponding to these events can be saved to a spreadsheet file for calculation of the desired gait parameters.

Table 4.2: **The spatial and temporal gait parameter definitions used by the gait analysis device for the calculations.** Foot strike was taken as the instance of a heel FSR switching over a given threshold and foot off as a time when no signal from the FSRs was measured for that particular foot. Definitions taken from Rose and Gamble (2006) [37].

Gait parameters	Definition
Stride length (m)	Distance covered between two subsequent foot strikes of the same foot.
Stride duration (s)	Time taken to complete a single stride.
Cadence (strides/min)	The number of strides taken in 1 minute.
Stance duration (s)	Time taken from foot strike to the foot off of the same leg.
Swing duration (s)	Time taken from foot off until the next foot strike of the same leg.
Stance (%)	Percentage of the gait cycle when the foot is in contact with the ground (period between foot strike and ipsilateral foot off).
Swing (%)	Percentage of the gait cycle when the foot is in the air (starting with foot off and ending with the second ipsilateral foot strike).
Double support duration (s)	Time taken from foot strike to opposite foot off.
Walking speed (m/min)	Total distance travelled divided by the time taken to cover that distance.

as possible between the two systems, the Vicon trajectory and gait event timing data were used to manually calculate the gait parameters using the same gait parameter definitions used by the wi-GAT. The definitions used to determine the parameters from the Vicon data are outlined in Table 4.2 and the corresponding equations in Eqn. 4.1-4.9. In this study the wi-GAT measured a mean of 2.54 strides (STD of 0.58) and the Vicon a mean of 2.43 strides (STD of 0.54) across subjects.

Stride length (m)

$$Sl_{L/R} = \frac{1}{N} \sum_{k=1}^N x_{L/R,heel_{k+1}} - x_{L/R,heel_k} \quad (4.1)$$

Where $x_{L/R,heel}$ is the x-coordinate of the left or right (L/R) heel marker at heel strike (the x axis is in the direction of walking) and N is the number of recorded strides.

Stride duration (s)

$$D_{L/R} = \frac{1}{N} \sum_{k=1}^N t_{L/R,heel_{k+1}} - t_{L/R,heel_k} \quad (4.2)$$

Where $t_{L/R,heel}$ is the time of heel strike in seconds.

Cadence (strides/min)

$$C_{L/R} = \frac{60}{D_{L/R}} \quad (4.3)$$

Stance duration (s)

$$St_{L/R} = \frac{1}{N} \sum_{k=1}^N t_{L/R,toe_k} - t_{L/R,heel_k} \quad (4.4)$$

Where $t_{L/R,toe}$ is the time when the toe marker leaves the ground, indicating a toe off gait event, in seconds.

Swing duration (s)

$$Sw_{L/R} = \frac{1}{N} \sum_{k=1}^N t_{L/R,heel_k} - t_{L/R,toe_k} \quad (4.5)$$

Stance%

$$St\%_{L/R} = \frac{100St_{L/R}}{D_{L/R}} \quad (4.6)$$

Swing%

$$Sw\%_{L/R} = \frac{100Sw_{L/R}}{D_{L/R}} \quad (4.7)$$

Double support duration (s)

$$Ds = \frac{1}{N} \sum_{k=1}^N t_{L/R, toe_k} - t_{R/L, heel_k} \quad (4.8)$$

Where the toe off timing is taken from the contralateral foot to the heel contact on each recorded step.

Walking speed (m/min)

$$W_{S_{L/R}} = \frac{60S_{L/R}}{D_{L/R}} \quad (4.9)$$

Wi-GAT

In order to extract the gait parameters from the wi-GAT, software implemented in LabVIEW was used (Refer to screenshot Fig. 4.8). This software up samples the recorded data file from 30 Hz to 100 Hz to match the sampling frequency of the Vicon system. The gait parameters: stride length, stride duration, cadence, stance duration, swing duration, stance%, swing%, double support duration and walking speed are calculated by averaging the FSR temporal data from the entire trial. The values were then saved to an excel file for subsequent analysis.

4.2.6 Statistical analysis

Statistical analyses of all the gait parameter data were performed using SPSS (version 20.0) software (IBM Corp., Armonk, N.Y). A preliminary descriptive analysis and the Shapiro Wilk test were used to ascertain that the data were distributed normally. In order to compare the gait parameters generated by both devices, the mean values were taken over the ten trials for each subject. Intra-class correlation coefficients (ICCs) of the type (2, k) with absolute agreement [214], and repeatability coefficients were used to evaluate the level of agreement between the wi-GAT and Vicon systems for averaged stride data, as performed and recommended by previous investigations [210]. The repeatability coefficient was calculated according to Bland and Altman as 1.96 times the standard deviation of the differences between the wi-GAT and Vicon measurements [215]. The difference between the two measurement systems is expected to be less than this coefficient with a probability of 95%. The repeatability coefficient was also calculated as a percentage of the mean value of the two measurement systems.

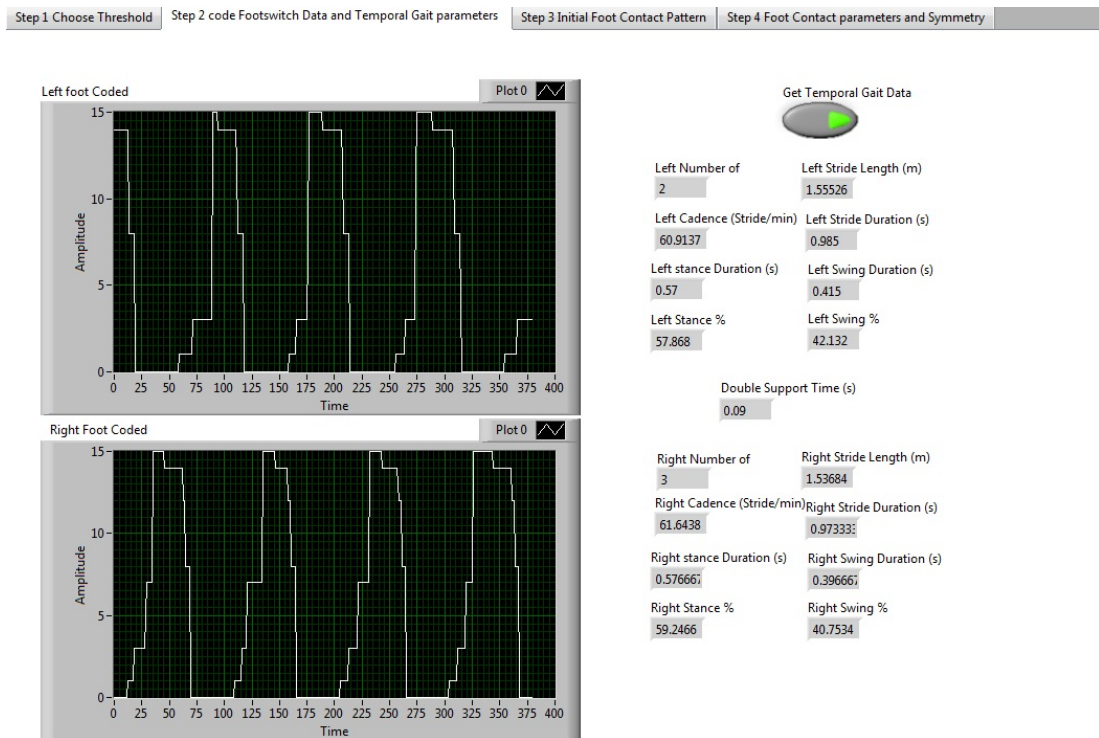


Figure 4.8: Screenshot of the wi-GAT analysis software. The software automatically calculates the spatio-temporal gait parameters when a gait recording is selected. The values can then be saved to a spreadsheet for further analysis.

4.3 Results

Comparative data for the Vicon and wi-GAT systems are presented in Table 4.3. The mean value and standard deviation of each parameter from the ten subjects has been included to demonstrate the overall difference in measurement between the two systems. The majority of the ICCs (Table 4.3) demonstrate an excellent level of absolute agreement between the wi-GAT and Vicon systems. These range from 0.94 to 0.996. The ICCs which showed less agreement ranged from 0.299 to 0.847, these were observed in four of the parameters: swing duration, stance%, swing% and double support duration. It should be noted that the actual stance (left = 0.94, right = 0.94) and swing (left = 0.847, right = 0.782) duration had moderate to good agreement but due to the short duration of each stride, when normalised, the stance% and swing% showed less agreement. However, these differences were consistent across all the subjects and the repeatability coefficients (Table 4.3) were small in magnitude which may indicate that a close agreement still exists between the wi-GAT and Vicon. Small repeatability coefficients were observed for all of the gait parameters. For example, the absolute coefficient of 0.05 m for left stride length in Table 4.3 indicates that the largest difference which can be expected between the two systems of data capture would be approximately 5 cm in 95% of the measurements.

Bland and Altman plots were produced for stride length, stride duration, cadence and walking speed for the left and right legs combined, Fig. 4.9. This is to verify that the assumptions of the limits of agreement are correct [215,216].

The mean value of the true error was calculated as the mean difference between the ten averaged subject walks to identify how much the parameter values differ between the two systems (as reported by [210]), Table 4.4. The mean percentage error was then calculated between the wi-GAT and the Vicon mean values. The mean percentage error was defined as the difference in the measurement between the two systems divided by the Vicon measurement and recorded as a percentage.

The parameters with the largest discrepancies are the parameters which use toe-off timing in their calculations (see Table 4.2). The largest difference in measurement was a 16% error in double support duration, which equates to a 0.024 s or 24 ms time difference.

4.4 Discussion

The validation results show good concurrent validity for most of the spatio-temporal gait parameters that were recorded using the wi-GAT. The two main

Table 4.3: **Repeatability coefficients.** Mean (STD) values of each gait parameter averaged across all ten subjects for both the gait analysis and Vicon systems. Intra-class correlation coefficients (ICCs) and repeatability coefficients are also provided.

Gait parameters	Average (STD)		ICC	Repeatability coefficients	
	wi-GAT	Vicon		Absolute	Mean (%)
Stride Length, L (m)	1.45 (0.12)	1.48 (0.12)	0.973	0.05	3.5
Stride Length, R (m)	1.46 (0.12)	1.49 (0.12)	0.975	0.04	2.8
Stride Duration, L (s)	1.08 (0.08)	1.08 (0.08)	0.996	0.01	1.0
Stride Duration, R (s)	1.07 (0.07)	1.08 (0.08)	0.981	0.03	2.8
Cadence, L (strides/min)	55.65 (3.82)	55.79 (3.89)	0.996	0.53	1.0
Cadence, R (strides/min)	55.53 (3.62)	55.84 (3.82)	0.985	1.27	2.3
Stance Duration, L (s)	0.67 (0.05)	0.69 (0.05)	0.940	0.02	3.6
Stance Duration, R (s)	0.67 (0.05)	0.69 (0.05)	0.940	0.02	3.5
Swing Duration, L (s)	0.42 (0.03)	0.39 (0.03)	0.847	0.03	6.6
Swing Duration, R (s)	0.42 (0.03)	0.39 (0.03)	0.782	0.03	6.5
Stance, L (%)	61.50 (1.12)	63.60 (1.16)	0.299	2.30	3.7
Stance, R (%)	61.78 (0.95)	64.13 (1.15)	0.343	1.56	2.5
Swing, L (%)	38.50 (1.12)	36.46 (1.26)	0.338	2.36	6.3
Swing, R (%)	38.22 (0.95)	35.92 (1.21)	0.344	1.76	4.7
Double Support (s)	0.13 (0.01)	0.15 (0.02)	0.494	0.02	12.1
Walking Speed (m/min)	80.83 (7.90)	82.65 (7.15)	0.977	2.59	3.2

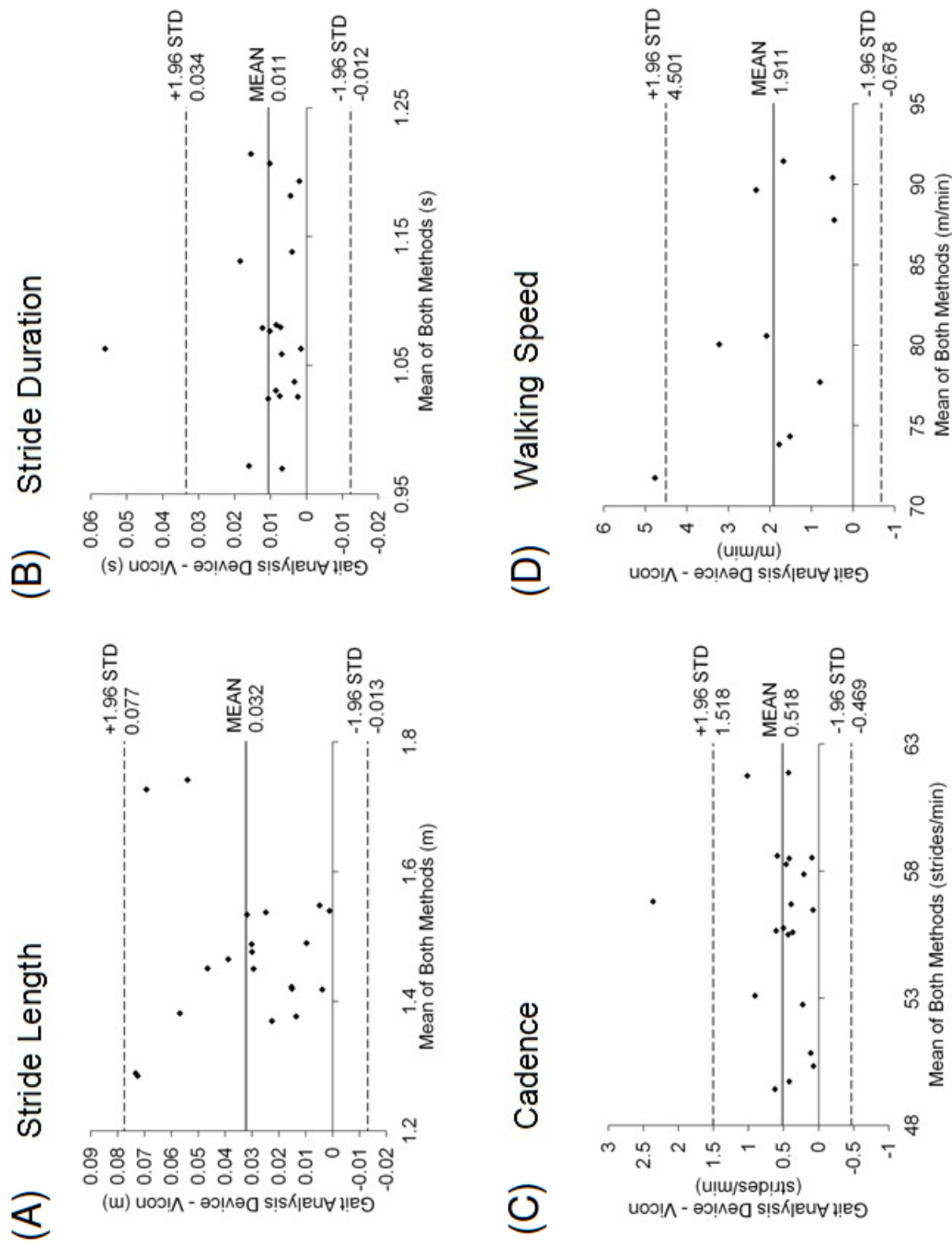


Figure 4.9: **Bland and Altman plots of stride length, stride duration, cadence and walking speed for the left and right legs combined.** The difference between the two systems (gait analysis device Vicon) is plotted against the mean value of both devices for each subject. Limits of agreement are included as the mean value \pm 1.96 standard deviations (STD).

Table 4.4: **The difference in measurement value of the studied gait parameters between the wi-GAT and Vicon systems.** Provided as both a value and % error.

Gait parameters	Difference Between Systems (wi-GAT - Vicon)	% Error
Stride Length, L (m)	-0.03	-2.0
Stride Length, R (m)	-0.03	-1.8
Stride Duration, L (s)	0	0.3
Stride Duration, R (s)	0.01	0.6
Cadence, L (strides/min)	-0.14	-0.25
Cadence, R (strides/min)	-0.31	-0.6
Stance Duration, L (s)	-0.02	-3.0
Stance Duration, R (s)	-0.02	-3.1
Swing Duration, L (s)	0.02	5.8
Swing Duration, R (s)	0.03	7.1
Stance, L (%)	-2.1	-3.3
Stance, R (%)	-2.4	-3.7
Swing, L (%)	2.0	5.6
Swing, R (%)	2.3	6.4
Double Support (s)	-0.02	-16.2
Walking Speed (m/min)	-1.81	-2.2

advantages of the wi-GAT are its low-cost and ease of use in a clinical environment. There has been a lot of interest over the last decade on the development of low-cost gait assessment tools that can measure spatio-temporal gait parameters. The low-cost devices that have been developed so far include the use of two electric switches placed under the feet [217], ultrasonic sensors [218], photoelectric cells [219] and body worn gyroscopes [220]. Although most of these systems have used the term ‘low-cost’ in their description, the actual costs of these devices are not easy to estimate. The wi-GAT system uses low cost components and a standard communication protocol. This provides the basis of what could be a low cost commercial product capable of operating in conjunction with any Bluetooth enabled device with the ability to run compact software applications.

The second most important advantage of the portable wireless device is its ease of use in a clinical environment. Although the wi-GAT is yet to be used in a clinical setting, the wired version of this device was successfully used to evaluate gait in a study on gait recovery in incomplete spinal cord injured subjects [200] and in an investigation of the combined effects of functional electrical stimulation and Botulinum toxin on walking in children with cerebral palsy [183]. The total duration to setup the portable wireless device and record the spatio-temporal gait parameters during a single trial is under 10 minutes, provided that insoles of various sizes are already instrumented and available. The analysis of the data using the graphical user interface (Fig. 4.8) is simple with only two buttons for activation, meaning analysis can be completed in less than 2 minutes. This should encourage clinical use, as the test is simple to perform, provides rapid reporting and can be completed within a single consultation.

The concurrent validity of the wi-GAT is comparable to other devices that have been developed to record spatio-temporal gait parameters such as body worn gyroscopes [210], and photoelectric cell walkways [219]. The spatio-temporal gait parameters: walking speed, stride length, stride duration, stance duration and cadence showed excellent agreement with the values estimated by the Vicon 3D motion analysis system (ICC values between 0.99 and 0.94), Table 4.3. The % errors for the above mentioned spatio-temporal parameters were also low and ranged between 0.25% and 2.2%. Given the low-cost and low-technology attributes of the portable wireless device, these are excellent agreements between a sophisticated 3D motion analysis system and the wi-GAT.

The other spatio-temporal parameters calculated, swing duration and double support time, showed lesser levels of agreement between the wi-GAT and the Vicon 3D motion analysis system (ICC values between 0.84 and 0.49), Table 4.3.

The reasons for this lesser agreement are thought to be due to anatomical reasons combined with the differences in the methods of estimation used by the wi-GAT and the Vicon 3D motion analysis systems. The gait analysis device uses an FSR positioned under the big toe to estimate toe-off as the time instance when this footswitch switches off. Whereas toe-off is identified by Vicon by manually entering a gait event in the software when the toe marker located over the 2nd metatarsal head has just left the ground. Due to the discrepancy in the timing of these toe-off events due to the anatomical difference in the placement of the FSR and marker, the stance% values for the wi-GAT are slightly larger and thus the swing% values are slightly smaller than the values estimated by the Vicon 3D motion analysis systems. Another source of error could be the low sampling frequency used which could also account for the timing discrepancy. These differences were typically in the range of a few milliseconds. However when they were normalised in respect to the duration of a single gait cycle, the percentage errors were in the region of 3-6.5%, Table 4.4. Similar differences in gait cycle durations have also been reported in a system that uses optoelectric cells to record spatio-temporal gait parameters [219]. Because these errors are consistent, the wi-GAT is a valid tool to assess the spatio-temporal gait parameters.

There are some limitations in the present study. The wi-GAT has been validated only among young healthy adults (23-30 years, see Table 4.1). Also in the current study subjects were asked to walk using a self-selected speed. Future study is necessary to evaluate the validity of the recorded spatio-temporal gait parameters using the wi-GAT during slow, regular and fast walking speeds and also establish the test-retest repeatability, which the current study has not investigated. The wi-GAT has also yet to be used in a clinical population. In order to address this, it would be of great interest to use the wi-GAT to investigate the recovery of gait among incomplete spinal cord injured subjects in a clinical setup.

There are also other gait parameters that the wi-GAT has a capability to record such as the mode of initial contact, heel contact time, inversion/eversion of the foot and the asymmetry index. These are often important clinical indicators that provide the clinician with a wealth of information. For example data on the mode of initial contact provides the clinician with an insight on the patients motor control of the foot during walking. Any muscle tightness or spasticity can also strongly influence the mode of initial contact. Therefore besides estimating the spatio-temporal gait parameters, the wi-GAT can also provide other clinically relevant data on the patients gait.

There is also potential to integrate further sensors into the Wi-GAT which

may provide further information on the gait cycle of the individual. These could include accelerometers and goniometers for measuring hip and knee joint hip motion during ambulation and in gait event timing calculation.

4.4.1 Limitations of Bluetooth technology

Bluetooth has the advantage of being low-cost and has low power frequency transmission, allowing the creation of a portable and mobile device. However, it has well documented constraints due to its limited bandwidth (v2.1+EDR ≈ 2.1 Mbit/s using the WT11 Bluetooth module), which may be significantly reduced in practice due to interference or data transmission issues. The development of the wi-GAT demonstrated that this wireless transmission interface was suitable for recording gait parameters. However the low sampling frequency of 30 Hz used to accommodate Bluetooth transmission may have resulted in some loss of data, which may have produced some of the variation in the gait parameters values observed between the Vicon and wi-GAT systems. An EMG signal is in the range of approximately 5 to 500 Hz [221]. Due to the high frequency components wireless transmission is not easy to accomplish with the limiting factor being the capacity of the wireless transmission. In addition, Bluetooth was found to be limited to a range of approximately 10 m during the wi-GAT validation study. During the data collection there was occasional loss of connection between the recording laptop and the wi-GAT device positioned on the subject's waist. This was prevented by ensuring the subject always walked towards the recording laptop during the data recording. Although this was acceptable for recording gait cycle parameters the limited range may present an issue during an overground walking study for recording EMG and foot contact information as the subject will need to walk for longer durations than necessary with the wi-GAT (approximately 15 minutes) and so will need to be able to walk away from the recording laptop rather than always towards it.

Due to these aforementioned issues, there is considerable advantage to maintaining a wired EMG/FSR preamplifier for recording during overground walking. USB 2.0 provides a much higher bandwidth than Bluetooth (480 Mbit/s compared to ~ 2.1 Mbit/s (maximum theoretical throughput rate)) and therefore allows higher sampling frequencies on more channels. It also does not encounter the issues of interference or dropped connection which would be detrimental during the long duration EMG/FSR data collection.

However, the developed wi-GAT system does provide a simple and portable method for analysis of gait parameters and is valuable in recording this data

for the creation of a treadmill speed control program which is suited to each individual participant.

4.5 Summary

The validation study of the wi-GAT demonstrated good concurrent validity when compared with the Vicon 3D gait analysis system, as shown by the excellent ICC values and low measurement errors. The low-cost, low-technology and simple user interface makes it suitable for use in a clinical setting. The time taken to setup and record the spatio-temporal gait parameters are also minimal. The wi-GAT also provides additional data on initial contact pattern, heel contact time and other clinically relevant data, as shown in previous studies that have used this device.

Part I conclusions

The preliminary studies discussed in Part I provided insight into how a control system for gait based on human walking transfer functions could be developed. In Chapter 3, a preliminary data collection study was conducted with ten healthy participants. Muscle activity (EMG), foot contact information (FSR insoles) and hip acceleration were recorded during constant speed treadmill walking. Event-related averages (ERAs) were used to analyse the relationship between the muscle activation signals and other recorded parameters, and to establish whether these parameters had potential to be used to control FES for walking rehabilitation in SCI. Heel contact information was found to exhibit a relationship with muscle activity related to hip and knee joint actions, which could be used in the development of a control system for walking. However, a correspondence problem was highlighted in these relationships with walking speed. Thus recommendations for repetition of the data collection were made to include varying the treadmill speed to remove the influence of walking speed on the relationship between foot contact information and muscle activity.

In Chapter 4 the development and validation of a wireless gait analysis device (wi-GAT) was described. This device was important in the generation of a treadmill speed control program, which was designed to remove the correspondence of foot contact information with muscle activity in the data average. The program was required to be catered to each individual participant's walking speed range and gait parameters during normal overground walking. The wi-GAT recorded

foot contact information during overground walking and used this information to calculate gait parameters including: walking speed, cadence, swing duration and stance duration. This data could then be used to develop a treadmill speed control program which will automatically change speed following a predefined sequence.

In Part II, the data collection studies and processes used in the calculation and testing of human walking transfer functions for development of a minimal, linear, reflexive control system for walking will be discussed.

Part II

Developing a control system for walking generation using human data

Introduction

In this part of the thesis, the development of the control system for generating a walking behaviour using transfer functions derived from human data will be presented.

The aim was to calculate transfer functions which relate sensory information and muscle activation signals. Following the recommendations of the preliminary study (Chapter 3, Section 3.7.1), the first stage involved a strategy of data collection, recording foot contact data and leg muscle activity (EMG) in healthy subjects as they walked on a speed controlled treadmill. To average out the periodicity in the recorded data, irregular walking patterns needed to be generated. As a treadmill can be viewed as a foreign environment for walking, which may also have an effect on the subjects walking, varying the walking speed in a random fashion should also create an environment which more closely captures the range of natural walking variability.

Another recommendation of the preliminary study, was to collect the foot contact and muscle activity data during overground walking to compare these transfer functions with those calculated from the treadmill walking. For this, participants walked around a large gait lab in a figure-of-eight pathway with varying self-selected walking speeds, as EMG and foot contact information was recorded.

Central to the thesis hypothesis is investigating the control between the sensor inputs of the RunBot bipedal robot and its motors. With this knowledge a control system based on human data can be designed. The original RunBot I attempted a biologically inspired approach where the sensor signals were translated into motor signals with the help of a neural network incorporating biologically inspired neuronal functions (see [3–5]). However the human nervous system is highly complex and has many unknown variables, in addition to controversy of how and even where the control of walking actually originates, means creating a robot with function comprised of neural networks, is highly speculative. Moving away from classical control theory, the strategy was to essentially create an abstract and purely analogue closed-loop system. To do this, all that was necessary was to identify a causal relationship between the foot contact information and the muscle activation (EMG). Studying how input signals can be translated into a functional motor output, produced a simple mechanism for generating stepping that can be described as a black box approach to modelling the complex neural control system in humans.

The transfer functions associated with knee and hip flexion/extension in hu-

mans were distinguished and then applied to the RunBot robot II (developed by Lin Meng (University of Glasgow)) as a proof of concept to identify whether the control system could be used to generate stepping. The application of the human transfer functions to the RunBot II robot's control system and analysis of the resultant gait was conducted in collaboration with Lin Meng and the University of Glasgow. A paper discussing the strategy for calculating the transfer functions from the treadmill walking data and the results of applying the functions to RunBot II was published in the PLOS ONE journal [222].

The findings were that a stable gait was exhibited (using the transfer functions calculated from the treadmill walking data) when hip extension and hip flexion were suitably coordinated. However, RunBot could not walk with a stable gait pattern using any of the transfer functions calculated from the overground walking data.

Supplementary videos are available for viewing at <https://www.youtube.com/user/reflexwalking> which demonstrate the set-up of the human walking data recording and RunBot's gait using the human walking transfer functions. Readers are encouraged to view these while reading this part of the thesis.

Following the findings of applying the human transfer functions to RunBot, the next stage was to compare the treadmill and overground walking data to analyse the difference between the two walking environments and establish why the transfer functions calculated from the treadmill walking produced a stable gait pattern in RunBot while the overground walking functions did not.

Finally in a prospective chapter, it was important to consider the effect of the addition of an ankle joint to the control system for walking, as the aim of the research was to establish an adaptive control system to generate a functional gait with future application in gait rehabilitation of individuals with spinal cord injuries (SCI). The transfer functions relating foot contact information to muscle activity controlling the actions of the joint were calculated and a control system designed in keeping with the control mechanism used with the hip and knee joints. Although this cannot be tested on the RunBot II robot as it does not feature an actuated ankle joint, this information is valuable in the development of the controller and in future designs of the robot.

Chapter 5

Treadmill and overground walking: EMG and foot contact data collection

The preliminary study (Chapter 3) provided evidence of the relationship between foot contact and muscle activity, which could be used to calculate transfer functions for the development of an FES control system for gait rehabilitation in SCI. However the preliminary study highlighted the need to repeat the data collection to address the correspondence problem between walking speed and the relationship between foot contact and muscle activity due to the periodicity of the gait cycle. To remove this influence and reduce the variability between subjects, varying walking speed during both treadmill and overground walking modalities should remove the correspondence of walking speed with the recorded data. This strategy should also enable the influence of speed on the EMG and foot contact patterns to be analysed which could be valuable in the development of a control system for generating stepping. This chapter describes the experimental protocol and the equipment used in the data collection.

5.1 Treadmill walking data collection

Following the recommendations of the preliminary study (Chapter 3, Section 3.7.1) the treadmill walking study was repeated using a varying treadmill speed sequence to generate irregular walking patterns and remove the correspondence between the average data and walking speed. Healthy participants were recruited for the study and a 16 channel preamplifier was developed for recording muscle activity and foot contact during ambulation. The effect of the walking speed on the

muscle activity was analysed using event-related averaging.

5.1.1 Ethics statement

The investigation was granted ethical approval by the University of Strathclyde ethics committee. Ten subjects, four males and six females with a mean age of 26.5 years (range 23 - 30 years) were recruited at the Department of Biomedical Engineering, University of Strathclyde and gave full informed written consent before taking part in the study. For demographic information see Table 4.1 in Chapter 4, Section 4.2.3.

5.1.2 EMG and foot contact recording

The data collection involved recording muscle activity and foot contact information during treadmill walking, Fig. 5.1. The muscles recorded were chosen due to their different roles in the gait cycle, two muscles located in the shank (Tibialis Anterior (TA) and Lateral Gastrocnemius (LG)) and two in the thigh (Biceps Femoris (BF) and Rectus Femoris (RF)). These were the same as measured during the preliminary study (Chapter 3). Bipolar surface EMG electrodes were attached parallel to the muscle fibres in the centre of the muscle belly in accordance to the recommendations of SENIAM [179]. Pre-gelled, single use surface electrodes (Blue Sensor N-10-A, Ambu, St. Ives, Cambridgeshire) were used and the skin prepared following standard procedure before electrode attachment [179].

To record muscle activity and foot contact information during the treadmill walking, a purpose designed EMG/FSR amplifier was developed (PCB design files available from <http://www.linux-usb-daq.co.uk/howto2/bio-sigma/>). The device design was based on the EMG and FSR amplifiers used for data recording in the preliminary treadmill walking study, see Chapter 3, Section 3.3. The preliminary study indicated that eight bi-polar channels would be preferable to four for recording EMG from four different leg muscles in both the left and right legs and in addition, the amplifier circuitry for measuring foot contact information should also be integrated into the same device. The complete device was also required to be lightweight and compact so it could be worn by the subject during ambulation. The finished design has eight channels available for recording surface EMG and also incorporates eight inverting op-amp channels for recording from force sensing resistors (FSRs) (Interlink Electronics, Camarillo, CA, USA), measuring foot contact information, Fig. 5.2 and 5.3. The finished constructed device and enclosure is provided in Fig. 5.4. As in the previous EMG preamplifier design,

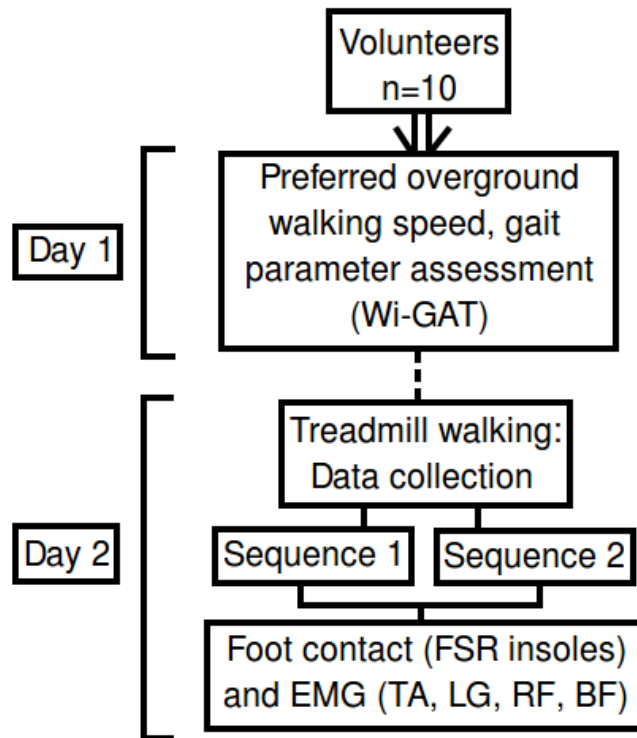


Figure 5.1: **Treadmill walking data collection protocol.**

on each channel there are two-stage amplifiers with a gain of 500. The PCB layout of the EMG/FSR preamplifier and bill of materials (BOM) can be found in Appendix B.

All sixteen of the EMG and FSR channels were recorded simultaneously with a sampling frequency of $f_s = 1$ kHz using the USB-DUX Sigma data acquisition device (Incite Technology Ltd., UK). This device also provides a regulated 5 V power supply to the attached circuitry and electrically isolates the subject from the mains supply. The USB-Dux Sigma Pin diagram is provided in Appendix C. The device connects via USB to a computer running Linux for data acquisition. Comedirecord (open source software available from <http://www.linux-usb-daq.co.uk/software2/comedi-record>) was used to record the walking data and the output saved in a MATLAB compatible ASCII file for further analysis. Fig. 5.5 is a photograph of the finished EMG/FSR preamplifier connected to the USB-DUX Sigma data acquisition device. Direct connection via a D-connector ensures all the equipment is as compact as possible for attaching to the participant during walking.

The FSRs are embedded in standard shoe insoles at four different positions under each of the feet for recording areas of peak pressure distribution during

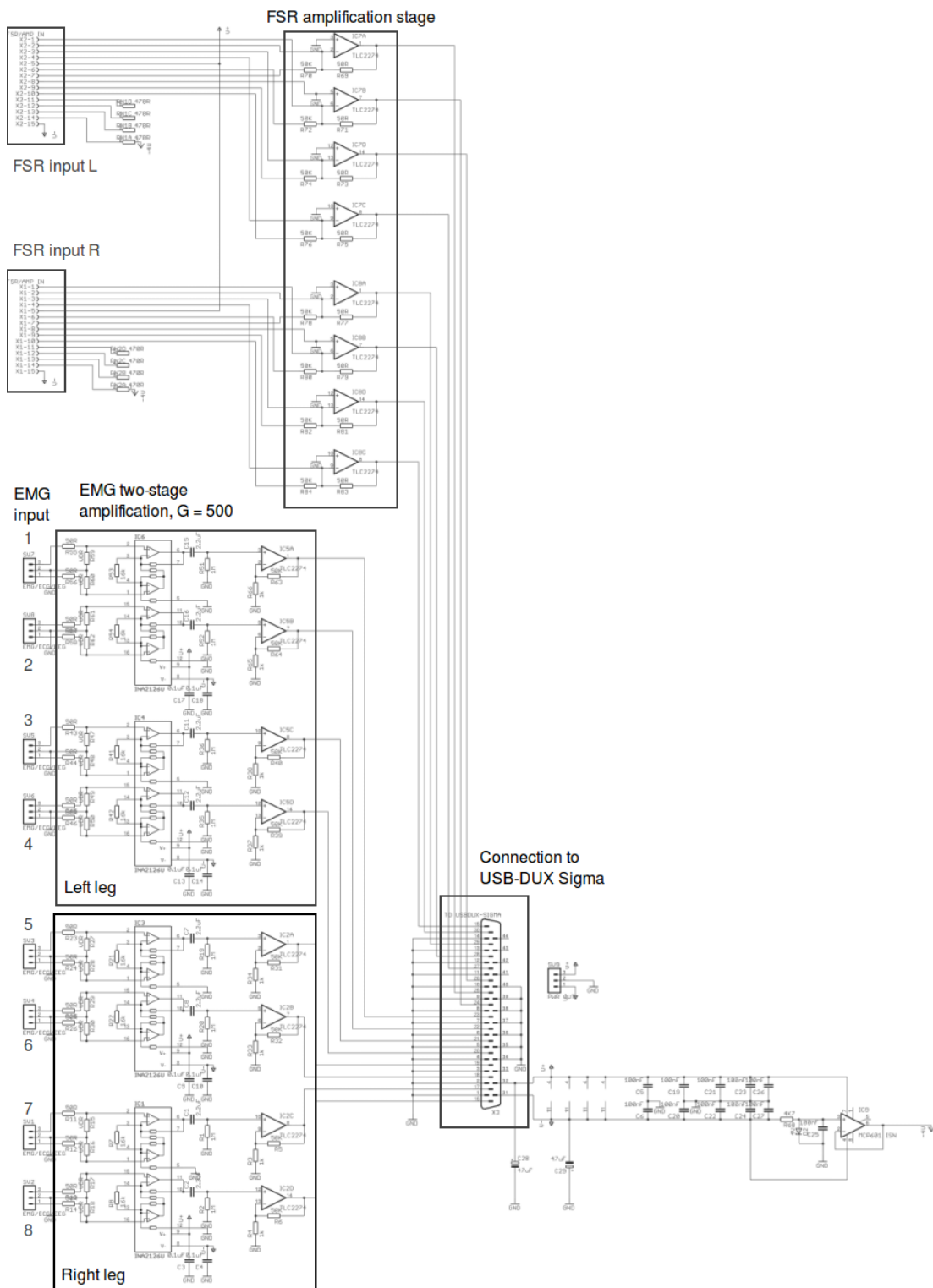


Figure 5.2: Annotated schematic of the EMG/FSR preamplifier.

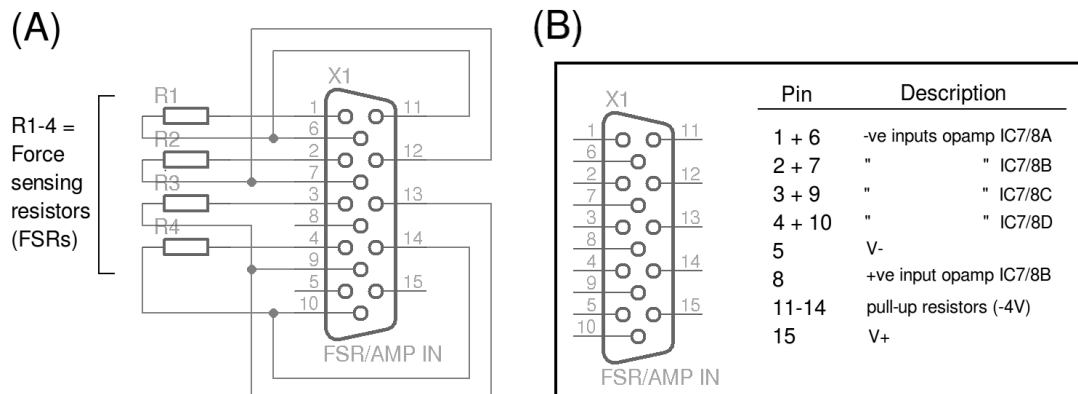


Figure 5.3: **Pin connections for the FSR insoles.** (A) Circuit diagram of the EMG/FSR preamplifier connections the FSR insoles. (B) Pin connections on the EMG/FSR device.

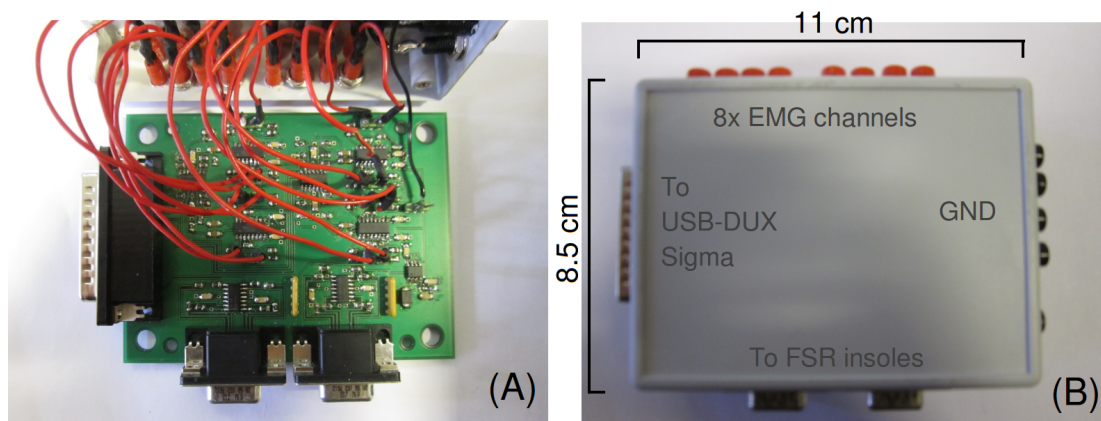


Figure 5.4: **EMG/FSR preamplifier.** (A) The PCB uses SMD components to keep the device as small and light-weight as possible. (B) The EMG/FSR preamplifier fits into a enclosure with dimensions of 11x8.5x3.5 cm. The box connects to the USB-Dux data acquisition device and FSR insoles by D-sub connectors.



Figure 5.5: **EMG/FSR preamplifier connected to the USB-DUX Sigma board.** The preamplifier (white box) connects directly to the USB-DUX Sigma data acquisition device (black box) via a D-connector so the equipment is compact for easy attachment to the participant during walking. The eight bi-polar sockets for connecting to the surface EMG electrodes are visible on the side of the preamplifier box (red).

walking (main weight bearing areas); under the first and fifth metatarsals, big toe and heel, as described by Granat et al. [182]. As the same participants took part in the Wi-GAT validation study and the treadmill walking study, the same insoles made for use with the wi-GAT device (Chapter 4, Section 4.2.1) were also used to record foot contact during the treadmill walking data collection. Images of the experimental setup can be seen in Fig. 5.6.

5.1.3 Treadmill control

A belted treadmill (Quasar Med, h/p/cosmos sports & medical gmbh, Germany) was used during the study. Initially, to ensure its suitability for the study, the treadmill belt speed was analysed for its accuracy to any programmed speed, see Appendix D. To generate an irregular walking pattern, a control program was written in C# (Visual Studio 2008, Microsoft, Washington, USA and MonoDevelop 2.10, <http://monodevelop.com>) to produce a pseudo-random sequence of belt speed settings within a desired range. The program was based on the Coscom V3 interface protocol (available from www.coscom.org) enabling the treadmill to be controlled over a RS232 connection to a computer. The belt speed was transmitted from the treadmill control program via an Ethernet TCP connection so it could be recorded simultaneously to the EMG and FSR data with Comedirecord. This allows the relationship between foot contact and EMG to be compared over the range of walking speeds to identify any speed effect. Synchronisation was achieved by recording in Comedirecord a unit impulse with value of '5555' when the control program start/stop button was pressed. A second impulse was sent

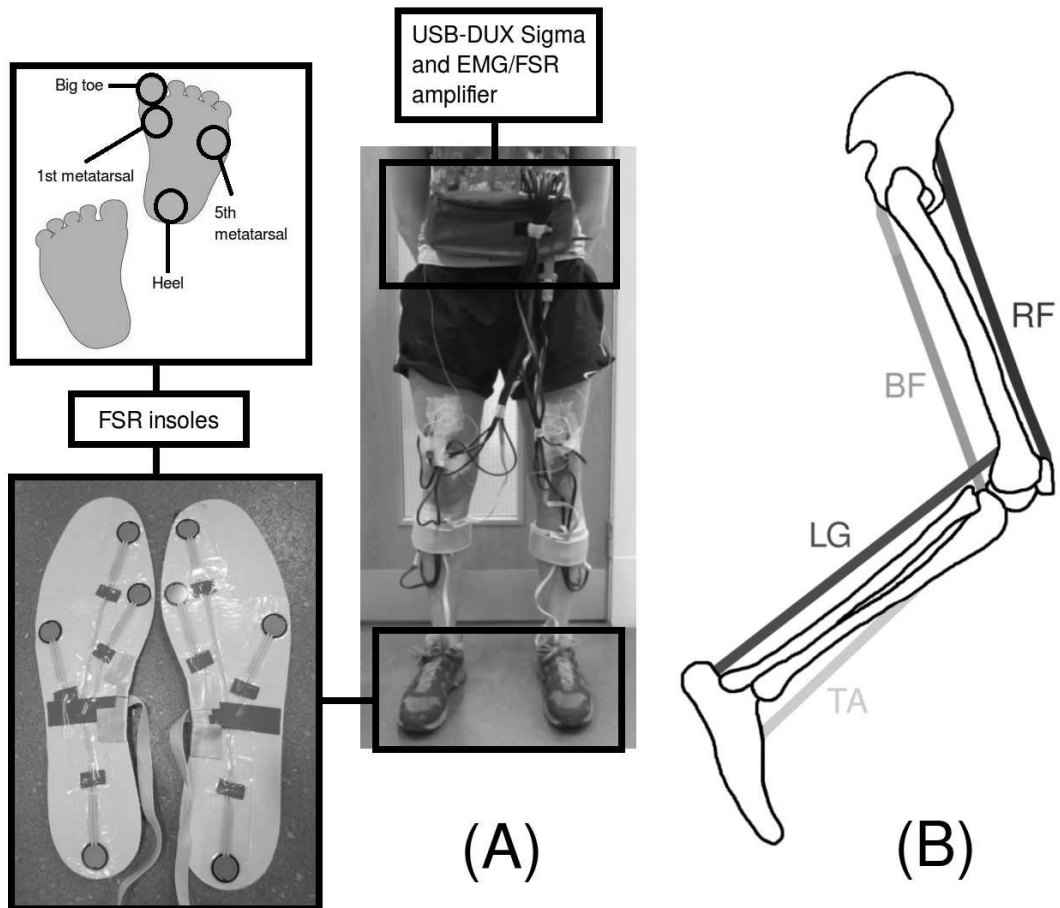


Figure 5.6: **Set-up for the treadmill walking trials.** (A) The USB-DUX Sigma data acquisition device and EMG/FSR amplifier are worn in a waist bag around the subject's waist. FSR insoles in the subject's shoes measure contact signals under different areas of the feet. (B) Position of the recorded muscles on the leg. TA = Tibialis Anterior, LG = Lateral Gastrocnemius, RF = Rectus Femoris and BF = Biceps Femoris.

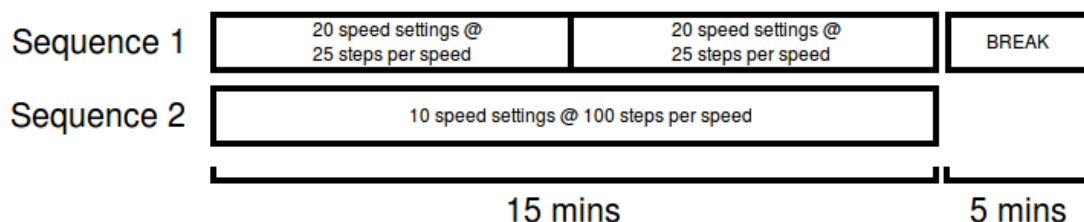


Figure 5.7: **Protocol for the treadmill walking study.**

when the program completed the speed change sequence.

In addition to recording the treadmill belt speed, video of the participant walking on the treadmill was taken for visual analysis of the gait patterns and verify that the measures of foot contact by the FSR insoles corresponded to the actions of the individual. A high definition video (HDV1080i) camcorder (Sony HDR HC1E) was used to record video in the sagittal plane and synchronised to the data collection by the recording of an audio tone emitted by the treadmill control program simultaneously to the ‘5555’ impulse value for syncing the treadmill to Comedirecord. An audio jack cable from the control laptop directly into the video camera ensured this tone was clearly identifiable in the audio recording.

Two treadmill walking speed sequences were generated for each subject to average out the periodicity in the recorded foot contact and EMG, and remove the influence of walking speed. The first generated sequence comprises of 20 speed settings and repeats twice. Each speed setting is programmed to run long enough to generate approximately 25 steps per speed and the complete sequence has a total range of 0.5 m/s. In comparison, the second sequence comprises of 10 speed settings, without a repeat and has a speed range of 0.39 m/s with each speed running for a longer duration to produce approximately 100 steps per speed, Fig. 5.7.

The change in walking speed varied using small increments/decrements to produce speed sequences within the natural walking speed range of each subject. For this purpose, measurements of gait parameters (stride duration (D and stride length (Sl)), were taken prior to the treadmill walking using the wireless gait assessment device (wi-GAT) [177] using the protocol described in Chapter 4, Section 4.2.4. Walking speed (W_s (m/s) and Cadence (C (no. of steps/minute)) can be calculated as follows:

$$W_s = \frac{Sl}{D} \quad (5.1)$$

Table 5.1: **Subject gait parameters.** Once the gait parameters had been calculated using the wi-GAT system, the constant (x_{cons}) could be found.

Subject	Sl (m)	D (s)	W_s (m/s)	C (no. of steps/minute)	x_{cons}
A	1.53	1.23	1.24	97.56	78.68
B	1.34	1.13	1.19	106.19	89.24
C	1.85	1.37	1.35	87.59	64.88
D	1.46	1.12	1.3	107.14	82.42
E	1.47	1.19	1.24	100.84	81.32
F	1.6	1.14	1.4	105.26	75.19
G	1.55	1.25	1.24	96	77.42
H	1.51	1.13	1.34	106.19	79.25
I	1.43	1.10	1.3	109.09	83.92
J	1.42	1.09	1.3	110.09	84.68

$$C = \frac{60}{D/2} \quad (5.2)$$

Where step duration is assumed to be half of the stride duration.

From this data, a constant (x_{cons}) can be calculated to determine the time (t_{ss}) each speed setting needs to run so approximately 100 or 25 steps are recorded per speed setting. Using Eqn. 5.3, the relationship between cadence and walking speed is assumed to be linear [223,224].

$$x_{cons} = \frac{C}{W_s} \quad (5.3)$$

Where C is the subject's cadence (number of steps per minute) and W_s is their average comfortable, walking speed (m/s).

$$t_{ss}(s) = \left(\frac{N}{ss \cdot x_{cons}}\right)/60 \quad (5.4)$$

Here, N is the number of steps required (100 or 25) and ss is the speed setting (m/s).

Using the subject's average walking speed as the initial belt speed, the control program calculates a change in speed chosen using a random-number generator. The change in speed is either an increment or decrement from the previous speed value, in a range between 0.05 and 0.1 m/s, Table 5.2. In order to facilitate a smooth transition from each speed setting to the next, the program calculates the acceleration or deceleration index by taking the present speed and the next speed in the sequence and dividing this by a fixed time interval of 4 s, for the transition. So the acceleration between constant speed values is limited to between 0.0125 and 0.025 ms^{-2} . This prevents periods of fast acceleration/deceleration which

Table 5.2: **Treadmill belt speed sequences listed as a change (+/-) in speed (m/s) from the previous value.** The speed sequence depends on the starting constant speed of the treadmill (the subjects average, comfortable walking speed). In this example, (A) sequence 1 and (B) sequence 2 were calculated for Subject H.

(A)			(B)		
Sequence 1			Sequence 2		
Order	Speed (m/s)	Change in speed (m/s)	Order	Speed (m/s)	Change in speed (m/s)
Start	1.34	-	Start	1.34	-
1	1.27	-0.07	1	1.27	-0.07
2	1.19	-0.08	2	1.19	-0.08
3	1.12	-0.07	3	1.12	-0.07
4	1.03	-0.09	4	1.03	-0.09
5	0.96	-0.07	5	0.96	-0.07
6	1.03	+0.07	6	1.03	+0.07
7	0.97	-0.06	7	0.97	-0.06
8	0.88	-0.09	8	0.88	-0.09
9	0.94	+0.06	9	0.94	+0.06
10	1.01	+0.07	10	1.01	+0.07
11	1.08	+0.07			
12	0.99	-0.09			
13	0.94	-0.05			
14	1.02	+0.08			
15	1.12	+0.1			
16	1.2	+0.08			
17	1.29	+0.09			
18	1.38	+0.09			
19	1.32	-0.06			
20	1.26	-0.06			

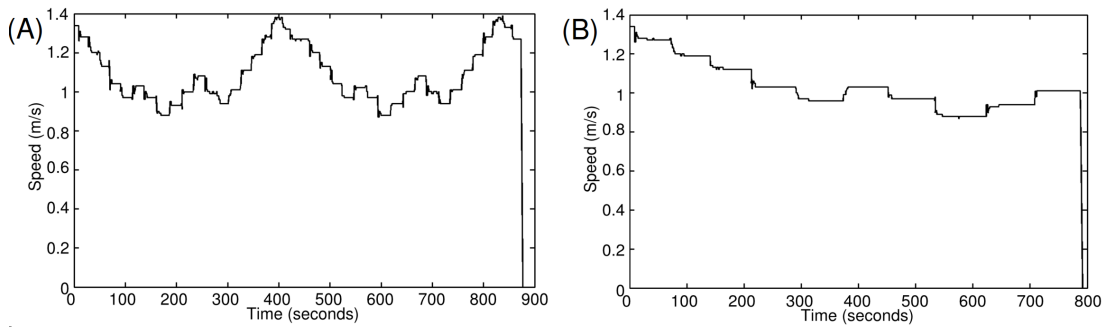


Figure 5.8: **Walking speed sequences for subject H.** (A) 20 different speeds, 25 steps per speed. The whole sequence is repeated twice. (B) 10 different speeds, 100 steps per speed. The whole sequence only runs once. These figures show the treadmill belt speed, recorded during the walking.

may be uncomfortable for the subject or cause stumbling. Using a constant seed value to the random-number generator ensures the program will produce the same sequence of speeds every time it is run, enabling repeatability of the testing protocol.

An example of the treadmill speed sequences calculated by the treadmill control program is provided in Fig. 5.8.

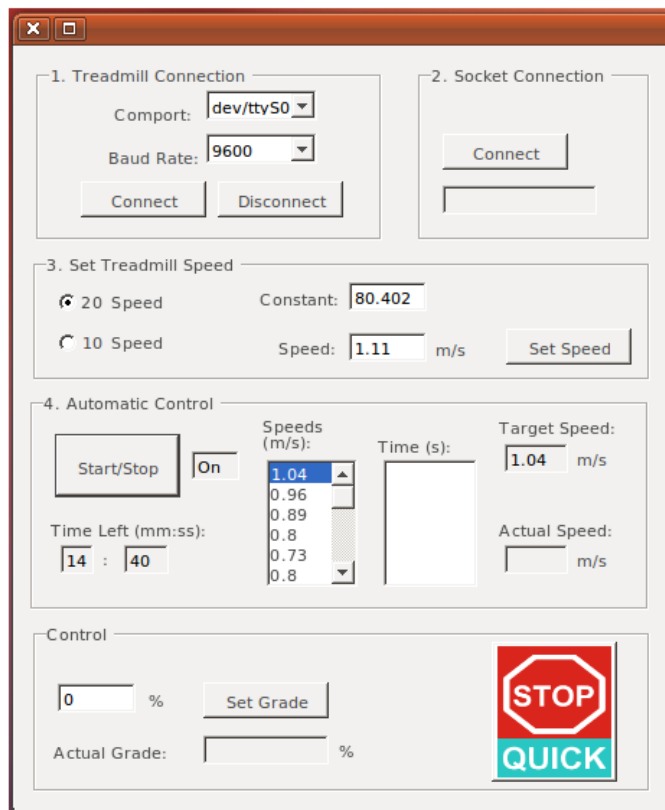
An interface to the program allows for simple control and setup of the treadmill via the laptop which is also running the Comedirecord program, Fig. 5.9.

5.2 Overground walking data collection

Treadmill walking is commonly used for data recording and gait analysis as it provides a controlled environment, with the ability to control speed and incline, and allows the use of wired recording equipment which would limit the distance of overground walking measurement. However treadmill walking may not accurately represent the conditions of overground walking where walking speed may be variable. These differences may affect the ability of transfer functions calculated from treadmill data being transferable into an overground walking behaviour and so it is necessary to compare the walking data collected

To provide a means of comparing foot contact and muscle activity data recorded during treadmill and overground walking, as recommended in the preliminary study (Chapter 3, Section 3.7.1), an overground data collection study was undertaken.

The overground walking data collection was carried out independently and at later date to the treadmill data collection. It should be noted that out of the ten



1. Connection to the h/p/cosmos treadmill through RS232 serial port.
2. Ethernet TCP connection to Comedirecord.
3. Select sequence: 1 = 20 speed settings, 25 steps per speed. 2 = 10 speed settings, 100 steps per speed.

Input constant and starting belt speed and start the treadmill.

4. Start/stop the automatic belt-speed control. The time remaining, list of speeds and time at each speed are displayed alongside the actual belt speed and the target speed.

Control: Change elevation of treadmill (not used) and emergency stop.

Figure 5.9: **User interface for controlling the treadmill.** The program connects over Ethernet to Comedirecord so the actual speed of the treadmill is recorded simultaneously to the EMG and FSR information.

Table 5.3: **Overground walking study participant information.** The subject ID was randomly assigned to the subject after they were recruited to the study.

Subject ID	Gender	Handedness	Age	Height (m)	Shoe size (UK)
OA	F	R	26	1.60	4
OB	M	R	30	1.84	11
OC	F	R	25	1.64	6
OD	M	R	27	1.72	10
OE	F	R	25	1.67	5
OF	F	R	26	1.65	5
OG	M	R	31	1.87	9
OH	M	R	27	1.85	9
OI	M	R	27	1.83	9
OJ	F	R	26	1.66	7
Mean (STD):			27 (2)	1.73 (0.10)	8 (2)

subjects who completed the treadmill based study, seven also took part in the overground walking study. However they were allocated a new subject ID which was randomly assigned after they were recruited for the study.

5.2.1 Ethics statement

The investigation was granted ethical approval by the University of Strathclyde ethics committee. Ten participants, four males and six females with a mean age of 27 years (range 25 - 31 years) were recruited at the Department of Biomedical Engineering, University of Strathclyde and gave full informed written consent before taking part in the study.

Table 5.3 outlines the demographic of the participants who participated in the study.

5.2.2 Experimental setup

The protocol involved each participant walking overground in a figure of eight pathway within a gait laboratory for a total duration of 15 minutes. This was with the aim of recording a smooth walk without any bias towards the right or left leg due to turning in a circle. The figure-of-eight was made of the largest dimensions possible within the gait lab floor space, one circuit equals 25.12 m, Fig. 5.10.

Although the equipment and basic methodology was to be the same as used in the treadmill study, as the subject needed to ambulate without being constrained

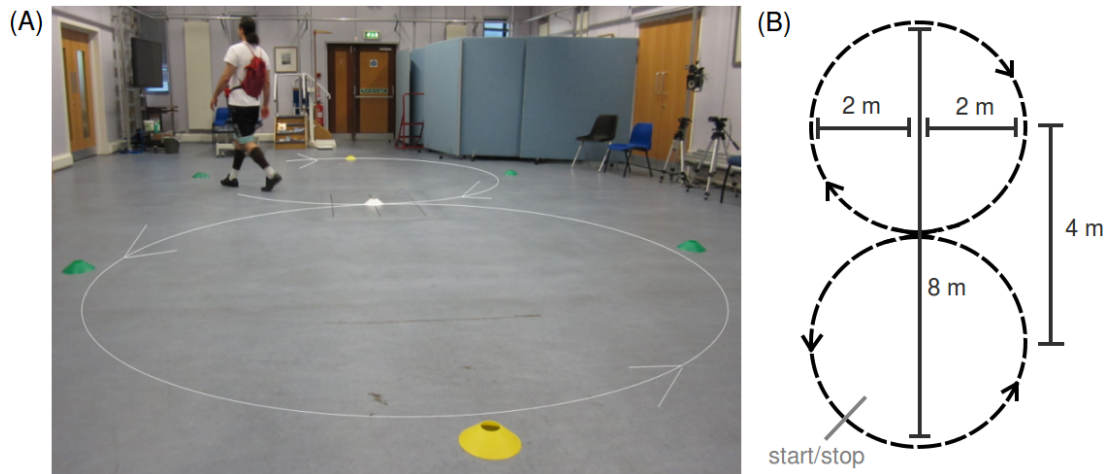


Figure 5.10: **Figure-of-eight walkway used in the overground walking study.** The length of one complete circuit of the walkway was 25.12 m.

by cables for recording the EMG and foot contact information by computer, some adaptation to the protocol was required.

The development of the Wi-GAT device (Chapter 4, Section 4.4.1) suggested Bluetooth wireless communication may not be suitable for use in the recording of EMG and FSR data during overground walking due to restrictions including limited bandwidth and range. Continuing use of USB 2.0 has advantages over Bluetooth as it ensures consistency of the data between the treadmill and the overground data but is limited due to the need for cable connection. The compromise was to use a lightweight netbook laptop running Comedirecord for recording the signals which could be carried in a backpack worn by the participant, allowing them to walk unrestrained. This allows the same EMG/FSR preamplifier and USB-DUX Sigma board used during the treadmill data collection to be used. This device was again worn around the participants waist within a waist bag to not restrict their gait.

To start and stop the data recording and provide a means of monitoring the data, to observe issues such as noise in the signals due to artefacts, a wireless ad-hoc network was created between the laptop in the backpack (comp. A) and a second remote laptop, controlled by the operator. Both laptops ran Linux and the Secure Shell (SSH) protocol was used through the ad-hoc network to provide a connection between the server (comp. A) and the client (comp. B). Through this SSH connection, the Comedirecord program could be controlled and the data monitored and saved post recording on comp. B without physical access to comp. A being required.

As removing the influence of a fixed walking speed was found (in the preliminary study (Chapter 3, Section 3.6)) to be a potential key factor in establishing the relationship between foot contact information and muscle activity, the subjects were instructed to vary their walking speed for every two circuits of the figure-of-eight pathway by responding to vocal commands of ‘slow’, ‘normal’ and ‘fast’. It was left to the individual to choose a comfortable speed from these instructions but they were instructed to remain ‘in walk’. To approximate the average speed of the subject during every chosen speed, a stopwatch recorded the time when they crossed a line marked on the floor with tape and coloured cones every time they completed two circuits of the floor, which was measured to be 50.24 m, Eqn. 5.5. The total time of walking was fifteen minutes without stopping, to correspond with the total time of walking for each sequence within the treadmill walking study. The same investigator controlled the stopwatch during each trial to reduce measurement error between all of the participants.

$$W_s = \frac{50.24}{t} \quad (5.5)$$

5.3 Event-related averaging of the walking data

Generating irregular walking on the treadmill using two different ratios of steps per speed setting had the aim of replicating natural overground walking where the speed can be changing on every step and remove any periodicity in the average. To visualise the relationship between the heel contact and EMG, an event-related average (ERA) was taken in a time period of one stride duration before and after heel contact, normalising the muscle activity to the gait cycle, Fig. 5.12, as described in Chapter 3, Section 3.4. To calculate the ERAs, the time of foot contact during walking needed to be defined in the FSR data using a threshold value. To determine a suitable threshold, the peak and trough voltages in the FSR data were plotted as these points represent the two states: the foot being in contact with the ground and off the ground respectively. The point of foot contact can be defined as the point of change between the baseline (trough value) and the value of the peak, to avoid erroneous contact detection, a value midway between the minimum voltage output of the heel FSR over the entire walk and the maximum was used, where at least 95% of the peak values lay above this value. Example FSR data showing the maximum and minimum voltages recorded over the two treadmill sequences for one subject are provided in Fig. 5.11. The peak voltage values from the FSR appear to follow walking speed (Fig. 5.11A

and B), compare to Fig. 5.8. This demonstrates that the participants walked with higher applied force from the foot with increasing speed. This was seen in the overground walking data. It is well documented that the size of the ground reaction force depends on walking speed (e.g. [225–228]).

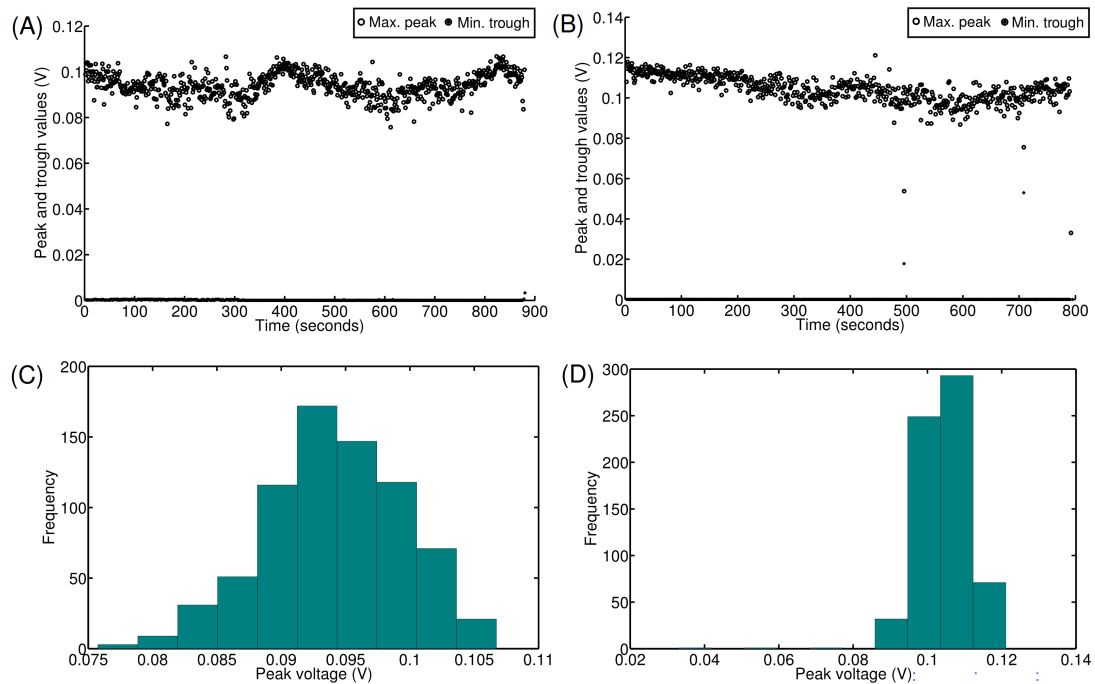


Figure 5.11: **Maximum and minimum peak detection in the FSR voltage recordings from the right heel during treadmill walking (Subject H)** (A) FSR data recorded during treadmill sequence 1 and (B) is FSR data recorded during treadmill sequence 2. (C) and (D) are histograms of the peak voltage output of the heel FSR during the walking. Sequence 1 (C) produced a greater range of voltage output than sequence 2 (D) as it featured a greater range of walking speeds.

Indication of facilitatory or depressed motor neuron pool excitability is related to the troughs or peaks in the ERA of the rectified EMG [186]. Similar to the observation of foot contact force varying with walking speed, EMG activity of the leg muscles also demonstrates an increase in amplitude when walking speed increases. However the patterns of activity remain basically the same (e.g. [189, 199, 229–234]).

5.3.1 Treadmill ERA

By maintaining a treadmill walking speed range within a moderate walking speed range of (0.75 to 1.75 m/s), the effect of speed on the EMG pattern can be viewed as the addition of a speed related gain to a standard pattern [234]. Plotting each

individual's EMG ERAs by walking speed demonstrates the increase in EMG amplitude with increasing walking speed, Fig. 5.12. In addition to the speed related gain, there appears to be phase shifts in the EMG activity envelope with peaks occurring later in the gait cycle as the walking speed increases, Fig. 5.12, Detail (A). In addition, it is evident that the heel is in contact with the ground for a longer duration of the gait cycle with reducing speed, suggesting the ratio of stance to swing duration is not constant over the range of walking speeds. Taking an ERA of the entire sequence (black dashed line in Fig. 5.12) provides an average of the EMG activity over the range of walking speeds with the aim of identifying the base EMG patterns independent of the speed.

5.3.2 Overground ERA

As was identified in the ERAs from the treadmill walking data collection, the effect of walking speed on the muscle activity during overground walking is most distinctly an influence on the amplitude. The faster walking speeds have a greater amplitude than the slower speeds, which again supports the suggestion that walking speed can be seen as the addition of a speed related gain to an underlying base pattern [234], as was observed in the treadmill ERA data (Section 5.3.1). The impression from the graphs is that the ERA over the entire overground walking session (black dashed line in the ERAs) provides an average muscle activity over the gait cycle.

5.3.3 Comparison of overground and treadmill walking EMG ERAs

Comparing the example EMG ERAs from the three different walking modalities it can be seen that they all demonstrate similar features. These include an increase in EMG amplitude with walking speed and an identifiable phase shift in timing of peaks within the gait cycle with increasing speed. In addition, the patterns within the EMG ERAs are similar between modalities with identifiable peaks occurring in the gait cycle. In the example EMG ERAs, the LG muscle ERA appears to have the most variation between the treadmill and overground walking (compare Fig. 5.14 with Fig. 5.12 and 5.13). During treadmill walking the maximum peak in EMG ERA amplitude occurs at heel strike of the contralateral leg (0% of the gait cycle). The LG muscle is involved in plantar flexion of the foot for push off to enter the swing phase which explains the presence of this peak in the LG EMG ERA, Fig. 5.14. However during overground walking the maximum peak in EMG

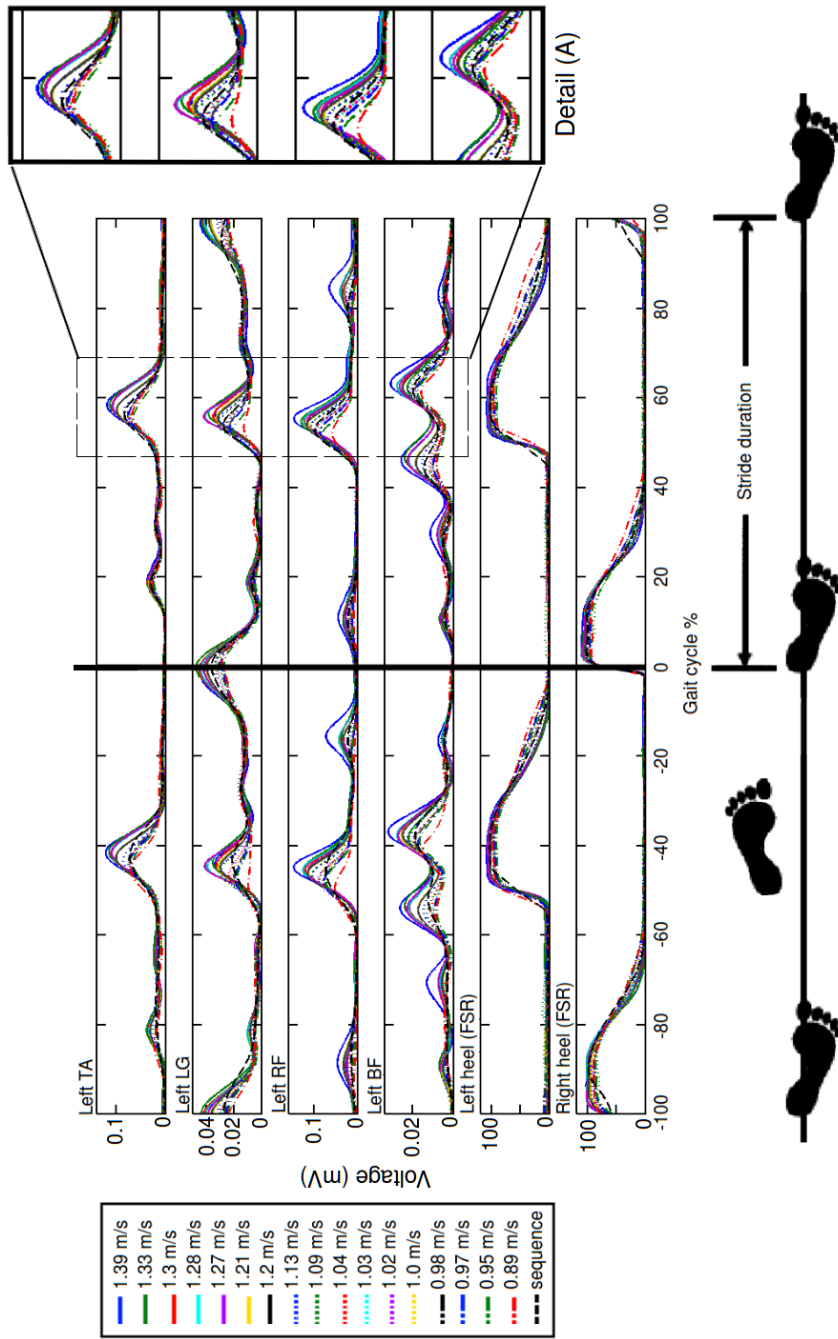


Figure 5.12: **EMG ERAs and FSR foot contact data over a range of treadmill walking speeds (Sequence 1).** The data were separated depending on the walking speed and compared to the activity recorded over the entire sequence (black dashed line in figure). The figure demonstrates the relationship between left leg smoothed and rectified EMG and heel contact information from subject C during walking sequence 1 (25 steps per speed setting). TA = Tibialis Anterior, LG = Lateral Gastrocnemius, RF = Rectus Femoris and BF = Biceps Femoris.

ERA amplitude occurs during stance when the LG muscle is active in support of the knee ($\sim 65\%$ of the gait cycle). This peak is also evident during the treadmill walking, specifically during treadmill belt speed sequence 1 at the higher walking speeds, Fig. 5.12. This is an interesting feature of the LG EMG ERAs of subject C suggesting that for them, the LG muscle was less active during push-off in overground walking compared to during walking on the treadmill. In addition it is evident that as their walking speed increases, the muscle activity related to knee stabilisation also increases. However these were not common features in all of the other participant data, demonstrating the importance of individual characteristics of gait. A comprehensive comparison of treadmill walking data and overground walking data is given in Chapter 8.

5.4 Summary

Following the recommendations of the preliminary study (Chapter 3, Section 3.7.1), the walking data collection was repeated. Leg muscle EMG and foot contact information was recorded using a custom made EMG/FSR pre amplifier. Two sets of ten volunteers participated in different forms of data collection. The first was during walking on a varying speed treadmill which followed two different belt speed sequences: (i) 20 different speed settings, 25 steps per speed and (ii) 10 different speed settings, 100 steps per speed. And the second was during overground walking. By recording the data during the different walking modalities the aim was to analyse the effect on the relationship between muscle activity and foot contact. By comparing the ERAs between the three modalities there are similar characteristics evident. It is clear that increasing the walking speed also increases the amplitude of the muscle activity and adds a shift in phase within the gait cycle. Similar patterns of muscle activations are also identifiable. Recording the data over a range of walking speeds acts to remove the influence of speed in the averaged data, which will allow transfer functions to be calculated between the foot contact information and muscle activity. Calculation of the transfer functions will be discussed in the next chapter (Chapter 6).

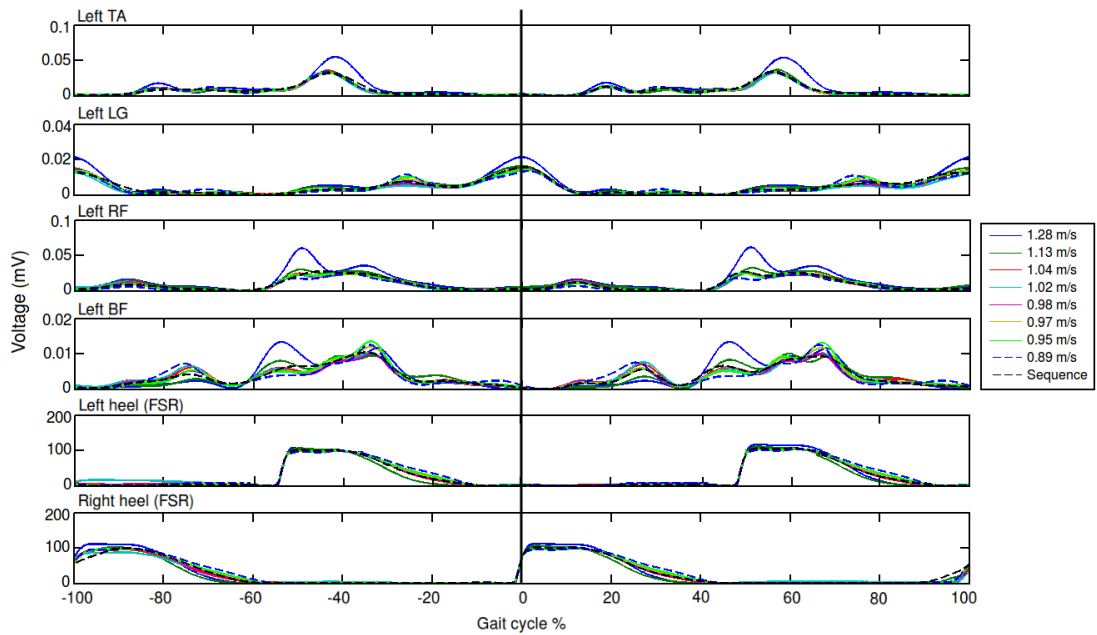


Figure 5.13: **EMG ERAs and FSR foot contact data over a range of treadmill walking speeds (Sequence 2)**. EMG data are an example from the left leg of one of subject C. The trigger is the time of contralateral heel strike (highlighted by black vertical line).

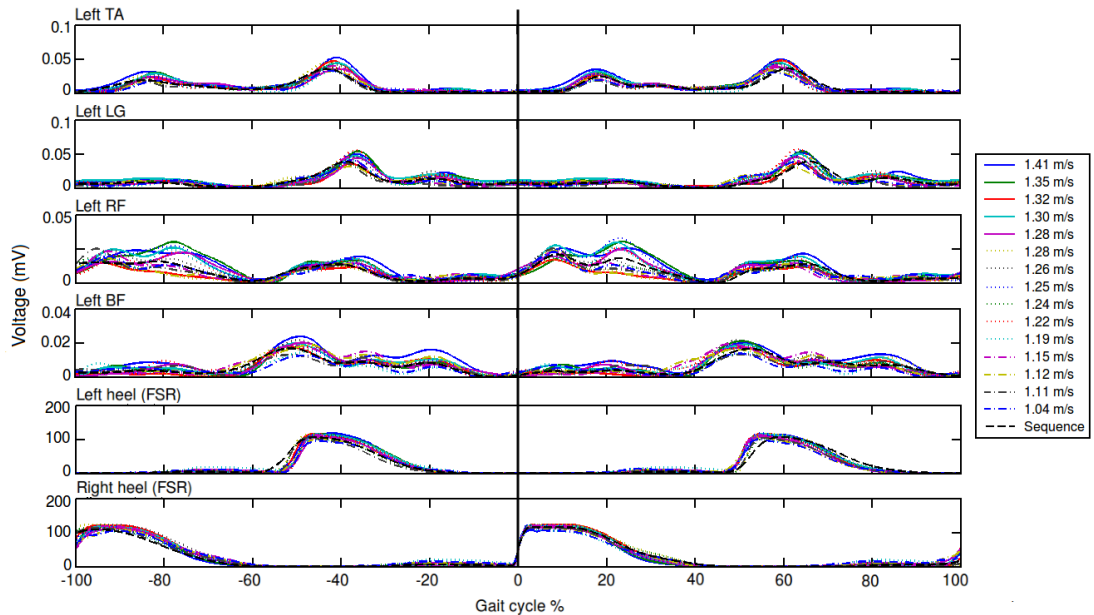


Figure 5.14: **EMG ERAs and FSR foot contact data (overground walking)**. EMG data are an example from the left leg of subject C. The trigger is the time of contralateral heel strike (highlighted by black vertical line).

Chapter 6

Calculation of transfer functions and development of a control system for generating walking

Following the walking data collection, the next stage in the development of a gait control system, which could be used to control FES for SCI gait rehabilitation, is the calculation of transfer functions relating foot contact information and muscle activity during walking. In this chapter, the adaptive filtering process recruited to derive the transfer functions will be described. Following their calculation, details on how the transfer functions can be related to joint actions and integrated into a walking control system will be given. This control system is based on the controller implemented in RunBot II, which is a bipedal robotic walker. For testing the ability of the human transfer functions to generate a stable and efficient gait, they can be applied to RunBot's control system and its gait analysed.

6.1 Adaptive filtering

Adaptive filtering was used to derive the transfer function for each of the recorded muscles and implemented using MATLAB (version 2012a, The MathWorks Inc., Natick, MA). The EMG data for each muscle in the left or right leg, $EMG_{L/R,mus}$ (where mus = TA, LG, RF or BF), was first processed using a band pass filter (h_{BP}) (FIR filter, 20-500 Hz) to remove artefacts, then full-wave rectified and low-pass filtered (h_{LP}) (zero-lag fourth-order IIR Butterworth filter, 6 Hz) to leave the linear envelope of the EMG.

$$\hat{EMG}_{L/R,mus}(t) = |EMG_{L/R,mus}(t) * h_{BP}(t)| * h_{LP}(t) \quad (6.1)$$

Where $\hat{EMG}_{L/R,mus}$ is the smoothed and rectified EMG.

Using the Least Mean Squares (LMS) algorithm, the output signal $EMG_{L/R,est}$ is estimated through convolution of the filter impulse response for each muscle $h_{L/R,mus,CH/IH}$, with the filter input vector $FSR_{CH/IH}$, the FSR contact data from the contralateral (CH) or ipsilateral (IH) heel to the muscle.

$$EMG_{L/R,est}(t) = FSR_{CH/IH}(t) * h_{L/R,mus,CH/IH}(t) \quad (6.2)$$

The error signal $e(n)$ is then calculated as the difference between the desired signal $\hat{EMG}_{L/R,mus}$ and the estimated signal $EMG_{L/R,est}$.

$$e(t) = \hat{EMG}_{L/R,mus}(t) - EMG_{L/R,est}(t) \quad (6.3)$$

The error signal drives the optimisation algorithm which updates the filter coefficients with correction factor h_{opt} at every time instant.

$$h_{opt} = e(t) \cdot FSR_{CH/IH}(t) \cdot \mu \quad (6.4)$$

Where μ is the learning rate of the adaptive filter. The length of the response of the filter was set to the average duration of two strides for each subject and the number of iterations set to 100, where the filter converges. So,

$$h_{L/R,mus,CH/IH}(t+1) = h_{L/R,mus,CH/IH}(t) + h_{opt} \quad (6.5)$$

The transfer function coefficients were calculated using the adaptive filtering method for each of the four leg muscles from each of the ten subjects. A table of the final mean square error (MSE) of the filter coefficients is provided in Appendix F, Table F1. An example of how well the filter output compares to the desired EMG waveform for one muscle from one subject is provided in Fig.6.1.

Applying the coefficients to an FIR filter produces a muscle activation signal when the filter is given an input of a typical FSR heel contact signal. A half Hanning window was convolved with the impulse response of the variable filter to select only the coefficients needed to generate a muscle activation signal one stride duration in length subsequent to the input of a heel contact signal from an FSR. An example of the filter outputs for one subject can be seen in Fig. 6.2 together with corresponding film frames of the subject's gait cycle.

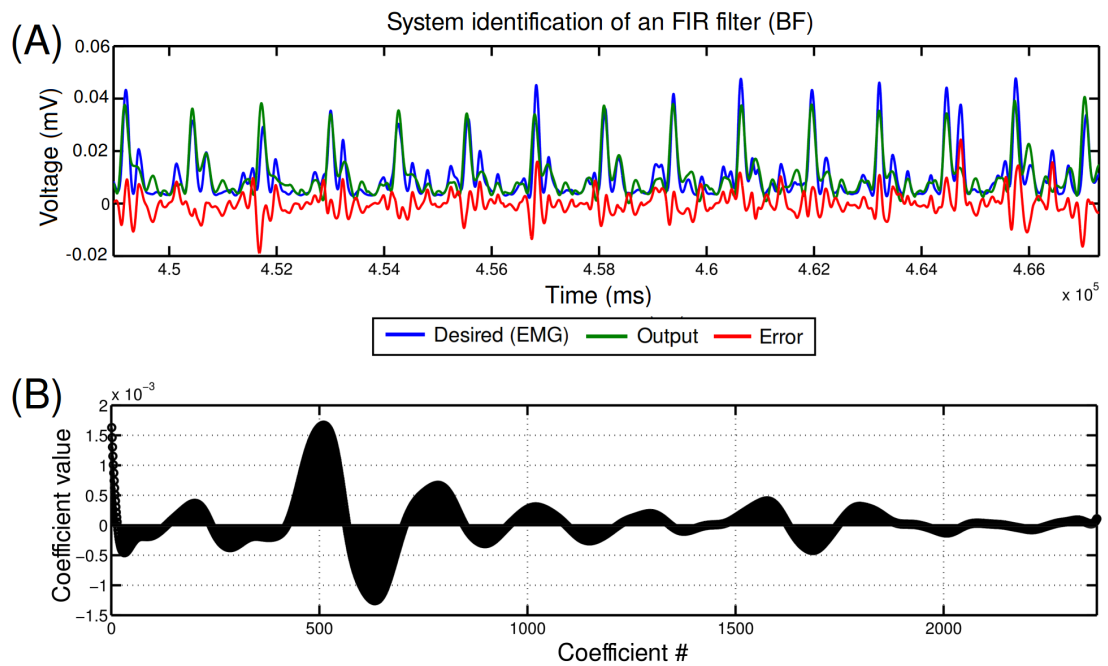


Figure 6.1: **Example results of adaptive filtering of the Biceps Femoris (BF).** (A) Short time window showing the output of the filter (green) compared to the desired EMG waveform (blue) and the final error (red) which is the difference between the desired output and filter output. (B) The resulting filter coefficients. The filter is two stride durations in length.

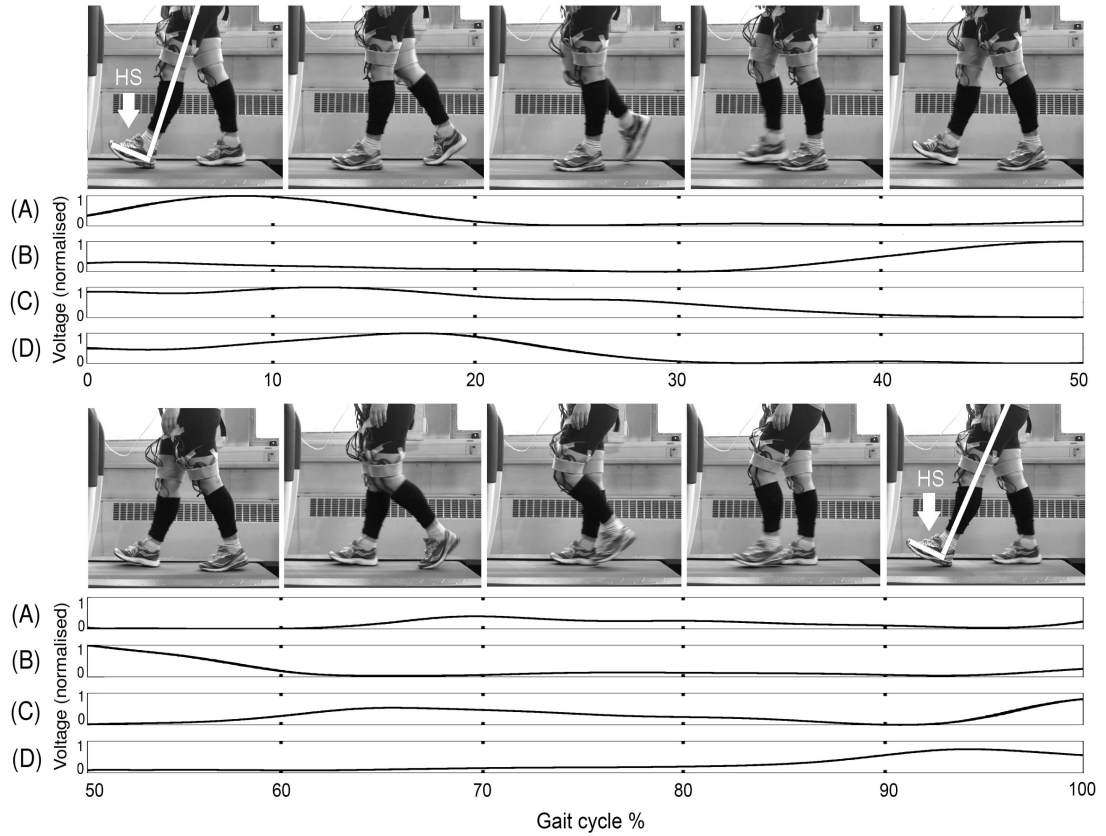


Figure 6.2: **Photograph series representing one stride duration during treadmill walking.** The series of frames corresponds to one stride from heel strike of the left leg (highlighted in white in the first and last frame) to the next heel strike of the same leg. The filter output using the transfer functions for each measured muscle of the left leg corresponding to the heel strike of the ipsilateral leg, found using the adaptive filtering, are shown below the images of one stride duration. (A) = $h_{L,TA,IH}$, (B) = $h_{L,LG,IH}$, (C) = $h_{L,RF,IH}$ and (D) = $h_{L,BF,IH}$, HS = Heel strike.

6.2 RunBot

With the help of the least squares algorithm, causal filter functions were created which relate foot contact information to muscle activation. The next phase, was to develop an adaptive control system based on physiological principles which could be applied to an extrinsic device in order to develop gait cycle modifications to suit the loading conditions.

In order to prove that the transfer functions could actually be used in a closed loop walking scenario the biped robot RunBot II can be used which, if successful, will demonstrate a stable and functional gait pattern. This Robot has been developed by Lin Meng (University of Glasgow) and is the second generation of the bipedal, robotic walker (RunBot I) described by Geng et al. (2006) [3, 4].

Before the transfer functions could be applied to the RunBot robot, the standard operation and basic mechanical structure needed to be understood in terms of how the motors can be controlled by human muscle activation signals.

RunBot I was designed with stiff knees, which had the disadvantage of causing damage to the gearbox of the motor in the joint due to the impact of the leg on the ground at heel strike. To improve the RunBot's knee structure and minimise damage to the joint, the motor was moved up to the thigh and three springs were positioned at the joint. This creates a balanced spring-loaded pulley using a robust bearing at the knee joint. The different springs are dominant either during flexion or extension, similar to muscles in the human leg. Using this configuration of springs, there is still a linear relationship between the motor angle and the knee angle but the knee retains an ability to flex to absorb the impact shock to the joint at heel strike [235–239]. A mechanical stop keeps the knee locked in extension during the stance phase. This stop also prevents hyperextension and damage to the joint at terminal swing.

Further development of RunBot II includes using filter functions to generate a coordinated walking behaviour rather than neuronal processing, which was the original control structure employed in RunBot I.

Filter functions and real-time processing allow fast tuning of few parameters however, like RunBot I, ground contact is still used as the main sensory input to promote joint movement and stepping.

RunBot II has a height of 0.3 m (foot to hip joint axis) and a total weight of approximately 552 g. Motors at RunBot's hip and knee joints are driven by output signals of a reflexive control program written in C++ (running on a Linux PC) with a sampling rate of $f_s = 200$ Hz through a USB-DUX D DA/AD converter board (Incite Technology Ltd., UK). The hips are actuated directly by

DC motors (HS-625MG, Hitec RCD, USA) whereas the knees are actuated by DC motors (HS-85+MG, Hitec RCD, USA), via springs. The four (A/D) input channels of the USB-DUX measure the angles of the joints: at the left and right hip ($\phi_{L/R,H}$) and the left and right knee ($\phi_{L/R,K}$). Two standard micro switches in the feet detect the ground contact: on the left (G_L) and right foot (G_R). Finally, the four analogue outputs (D/A) of the USB-DUX, which have a range of ± 4.096 , are used to drive the four motors on the hip joints $V_{L/R,H}$ and the knee joints $V_{L/R,K}$ following amplification (with a gain of 2.3).

The robot has no ankle joint but features flat feet with serrated soles to increase friction with the ground and prevent slipping, seen in Fig. 6.3. Its feet are scaled to its leg length, typical to the proportions observed in humans and employed in prosthetics for artificial limb design [240]. RunBot is counterweighted in the sagittal plane by a weight and boom. This is connected to the robot by a joint which rotates freely in the forward direction but prevents the robot falling sideways. The boom (total length of approximately 1 m) rotates freely around a central pivot with one end attached to RunBot and the other to a counterweight. With this configuration, the robot is not being suspended or supported in an upright position but its motions are constrained to a circular path. A camera (colour board camera L79AB) is fixed to the boom arm for tracking markers positioned on RunBot's right hip, knee and ankle for gait analysis and calculation of joint kinematics. A photograph of RunBot II is provided in Fig. 6.3.

6.3 Reflexive control system

RunBot's reflexive control system can be explained through description of three important events in the gait cycle:

1. Ground contact
2. Anterior extreme angle (AEA) of the contralateral hip joint
3. Passive dynamic walking phase

(1) Foot contact with the ground triggers the hip and knee of the contralateral leg to begin flexing (swing) and the ipsilateral hip and knee to begin extending (stance), Fig. 6.4i. (2) When the contralateral hip reaches the anterior extreme angle (maximum flexion position) the knee of the same leg is triggered to straighten producing leg extension at terminal swing, Fig. 6.4v. (3) Once the contralateral knee has extended in preparation to contact the ground and the remaining motors have all reached the required positions, the motors are switched

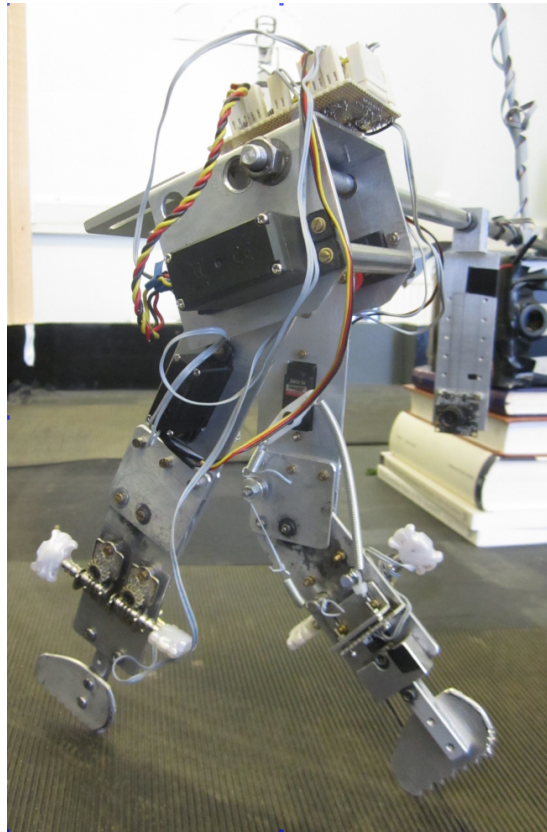


Figure 6.3: **Photograph of the RunBot II robot.** The robot features a serrated flat foot on a fixed ankle with directly actuated hip joints and compliant knee joints actuated by motors via springs. A camera is attached to the boom arm for tracking markers to measure gait parameters.

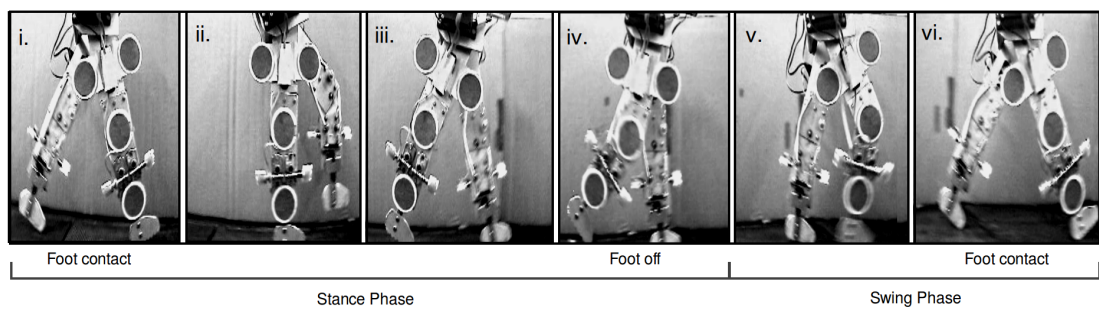


Figure 6.4: **Photographs demonstrating RunBot II's gait cycle.**

off. This causes the centre of gravity of the robot to shift forward of the boom leading to the foot making contact with the ground, which in turn begins the next cycle, Fig. 6.4vi. In RunBot's operation, every motor switches off when the joint reaches the required position so it can be expected that during the gait cycle there may be a period where all of the joint motors are off. During this time RunBot can be termed a passive dynamic walker as the joints are not fixed in an angular position by the motors and are instead driven by the mechanism of natural dynamics acting on the structure.

In mathematical terms, the reflexive model of RunBot is a simple system involving convolution of the summed impulse trigger signals, from the leg joints and the ground contact information from both feet, with transfer functions $H_{L/R,H/K,F/E}$ (left/right leg, hip/knee joint, flexor/extensor). Ground contact switches trigger an impulse signal from the left ($\Theta(G'_L(t))$) and right foot ($\Theta(G'_R(t))$), where $G_{L/R}(t)$ is 1 when the foot contacts the ground and 0 with no contact so $G'_{L/R}(t)$ is the derivative impulse, and are the main inputs to the controller. There is also a local joint control feature for preventing the over-flexion or extension of the joints by calculation of the angle from the motor voltage. The total motor output of each of the four leg motors are defined by $U_{L/R,H/K,F/E}$ and drive the walking behaviour, Eqn. 6.6a, 6.6b, 6.6c and 6.6d.

Shown are the general equations for both legs, with 'I' defining the ipsilateral leg and 'C' the contralateral leg:

$$U_{L/R,H,F}(t) = B_{L/R,H}(t) \cdot H_{L/R,H,F}(t) * \Theta(G'_C(t)) \quad (6.6a)$$

$$U_{L/R,H,E}(t) = B_{L/R,H}(t) \cdot H_{L/R,H,E}(t) * \Theta(G'_I(t)) \quad (6.6b)$$

$$U_{L/R,K,F}(t) = B_{L/R,K}(t) \cdot H_{L/R,K,F}(t) * \Theta(G'_C(t)) \quad (6.6c)$$

$$U_{L/R,K,E}(t) = B_{L/R,K}(t) \cdot H_{L/R,K,E}(t) * (0.3 \cdot \Theta(G'_I(t)) + \Theta(B'_{I,H}(t))) \quad (6.6d)$$

Where $B_{L/R,H/K}$ is a parameter preventing the joints flexing or extending beyond an extreme angle threshold ($\theta_{H/K,F/E} < \phi_{H/K} < \theta_{H/K,E/F}$) by limiting the motor voltages to prevent mechanical damage. $\Theta(B'_{I,H}(t))$ is used as an impulse trigger signal to trigger knee extension of the ipsilateral leg at terminal swing when the anterior extreme angle (AEA) of the hip is detected ($\phi_H = \theta_{H,F}$), Eqn. 6.6d. The values used for the extreme joint angles can be found in Appendix E, Table E1. These values were hand-tuned as described in [3,4].

The final outputs $V_{L/R,H/K}$ to the USB-DUX are found by multiplying $U_{L/R,H/K,F/E}$ with predefined gain coefficients, where $a_{L/R,H/K}$ is the gain of the

motor amplifier (the gain values of the hip and knee motors are provided in Appendix E, Table E2). As with the extreme joint angle values, the gain of the motor amplifier was chosen intuitively in accordance with the method used by [3, 4].

$$\begin{aligned} V_{L/R,H}(t) &= a_{L/R,H} \cdot (U_{L/R,H,F}(t) - U_{L/R,H,E}(t)) \\ V_{L/R,K}(t) &= a_{L/R,K} \cdot (U_{L/R,K,F}(t) - U_{L/R,K,E}(t)) \end{aligned} \quad (6.7)$$

6.3.1 Generating walking using human derived transfer functions

After having established the transfer functions using the human walking data and adaptive filtering ($h_{L/R,mus,CH/IH}$, Eqn. 6.5) which connect the heel contact and muscle activity in the legs, they next need to be translated over to the RunBot. As the hip joint and knee joint controls are separate in RunBot, the features of the human muscle transfer functions needed to be separated according to specific function (e.g hip flexion, hip extension, knee flexion and knee extension). It is also necessary to define the triggers for the transfer function and resample and normalise the functions in accordance with RunBot's control mechanism.

As has been discussed, RunBot has push switches in its feet which generate impulses on contact with the ground ($G'_{R/L}$) to trigger motor switching in the knee and hip joints. However during the human walking data collection, foot contact information was recorded using FSRs positioned under the feet which produce an increasing voltage curve when pressure is applied. To compensate for the difference in foot contact measurement between the two systems, and enable the human derived muscle transfer functions to be applied to the RunBot, the transfer functions calculated using the FSR data ($h_{L/R,mus,CH/IH}$) were convolved with the mean FSR heel contact signal one stride duration in length for each subject, $FSR_{CH/IH}$.

$$H_{L/R,mus,CH/IH}(t) = h_{L/R,mus,CH/IH}(t) * \frac{1}{N} \sum_{k=1}^N FSR_{CH/IH_k}(t) \quad (6.8)$$

Where N is the total number of strides recorded during the treadmill/overground walking.

The effect is that the response of the filter to an impulse becomes equivalent to applying an input of a typical heel contact FSR signal measured during gait and RunBot can still use its original foot contact impulse trigger signal ($\Theta(G'_{L/R}(t))$).

The key is to define the functions $H_{L/R,H,F}$, $H_{L/R,H,E}$, $H_{L/R,K,F}$ and $H_{L/R,K,E}$

Table 6.1: **Relating the muscle transfer function to RunBot’s motor control.**

Transfer Function	RunBot Motor Control
$H_{L/R,LG,CH}$	Knee flexion during swing (CH).
$H_{L/R,RF,CH}$	Knee extension at terminal swing and during the stance phase (CH).
$H_{L/R,RF,CH}$	Hip flexion during swing (CH).
$H_{L/R,BF,CH}$	Knee flexion during the swing phase (CH).
$H_{L/R,BF,IH}$	Hip extension during the stance phase (IH).

which relate to those presented in Eqn. 6.6a, 6.6b, 6.6c and 6.6d.

By examining the muscle activity relating to one stride duration, the peaks and troughs in the data can be analysed and related to knowledge of the muscle actions during the gait cycle and video footage of each subject during the treadmill walking (see Fig. 6.2 and 6.5), to identify the information in the signal which could be used to control RunBot’s hip and knee motors. The action of each muscle on the hip and knee joint motion is summarised in Table 6.1. The trigger for each of these events is either the contralateral heel contact (CH) or the ipsilateral heel contact (IH).

As the ankle joint in the current RunBot II is rigid, the recorded TA activity was not considered relevant as the muscle only has action on the ankle joint in humans. The other three muscles are all bi-functional muscles with action on either the hip or knee joint or both (Table 6.1).

The peaks and troughs visible in the EMG transfer functions, Fig. 6.5, relate to activation and suppression of motor neuron pools. To separate the activity into the transfer functions relating to the joint movement, the data located between the minimum value of the trough preceding the peak to the subsequent trough minimum value was selected.

Using the aforementioned information, how each muscle transfer function is transformed into transfer functions for controlling RunBot’s motors can be discussed.

Rectus Femoris (RF)

RF is responsible for hip flexion (in the swing phase) and knee extension (in the late swing phase and the stance phase). Two separate peaks of activity can be observed in the RF transfer function $H_{L/R,RF,CH}$ (identified by a box in Fig. 6.5B, C and F). As the first peak is during the swing phase, the activity corresponds to hip flexion and the second peak, which coincides with terminal swing, is identified

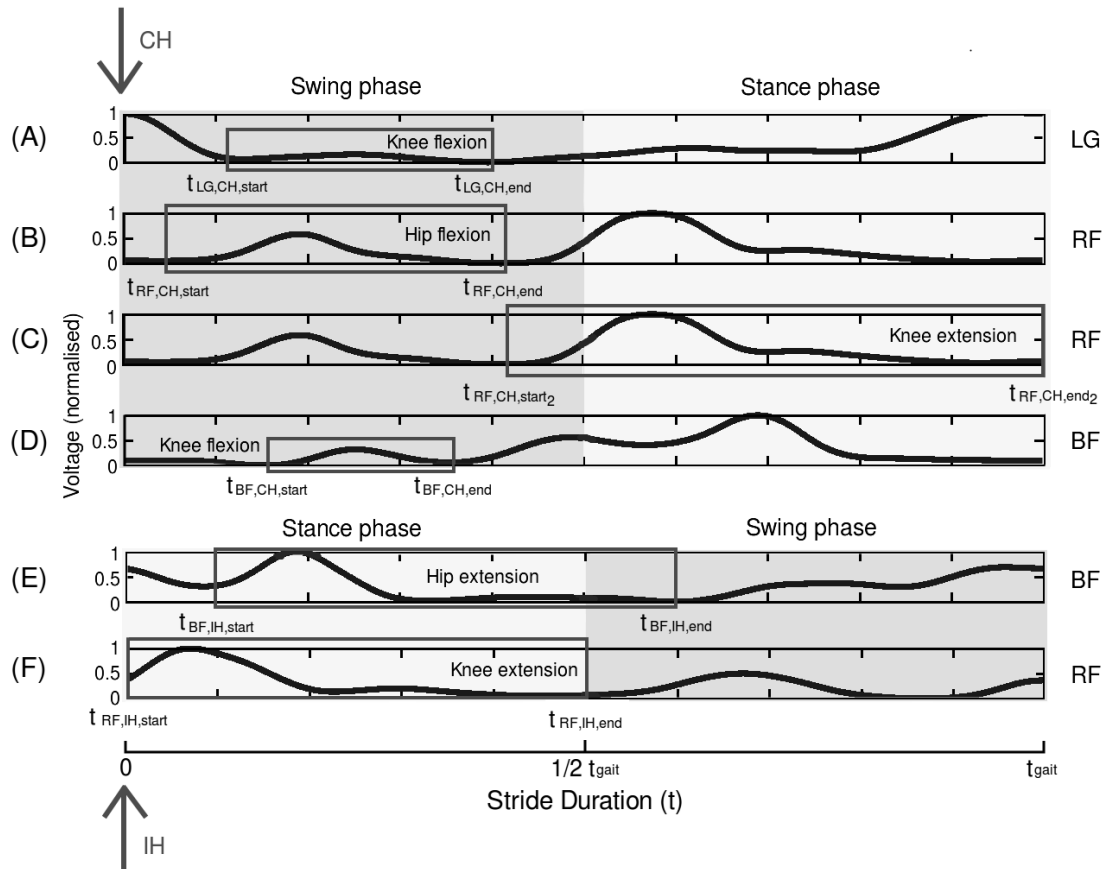


Figure 6.5: **Identifying features of the transfer function coefficients which correspond to muscle activity promoting knee and hip flexion/extension in human walking.** The transfer functions from adaptive filtering heel contact data from the contralateral and ipsilateral foot to the specific leg muscle ((A) $H_{R, LG, CH}$, (B and C) $H_{R, RF, CH}$, (D) $H_{R, BF, CH}$, (E) $H_{R, BF, IH}$ and (F) $H_{R, RF, IH}$) were used to identify the required features. These coefficients were then used in an FIR filter to control motors in RunBot’s hip and knee using the sensory input of the contralateral or ipsilateral heel contact.

as activity related to knee extension.

$$H_{L/R,H,F}(t) = \begin{cases} H_{L/R,RF,CH}(t + t_{RF,CH,start}), & 0 \leq t \leq (t_{RF,CH,end} - t_{RF,CH,start}) \\ 0, & \text{otherwise} \end{cases} \quad (6.9)$$

$$H_{L/R,K,E}(t) = \begin{cases} H_{L/R,RF,CH}(t + t_{RF,CH,start_2}), & 0 \leq t \leq (t_{RF,CH,end_2} - t_{RF,CH,start_2}) \\ 0, & \text{otherwise} \end{cases} \quad (6.10)$$

Where $t_{start/end}$ is the identifiable trough before and after the peak in the data associated with the hip/knee flexion/extension and t_{gait} is the total duration of the gait cycle (i.e $t_{gait} = 100\%$). $H_{L/R,H,F}$ can then be substituted directly into Eqn. 6.6a.

Our aim was to relate muscle activity to foot contact and use this to trigger muscle activation signals with the purpose to attempt to represent the underlying muscle activation dynamics [169]. This theory can be realised when comparing the timing of muscle activity with heel contact information. The only exception where the muscle activity does not follow heel contact is the knee extension at terminal swing which occurs approximately between 40 and 50% of stance before ipsilateral heel contact at 50%, Fig. 6.5C. An alternative, analogous to human walking, involves angular sensory information from the hip or knee joint to trigger the knee extension. This corresponds to the reflexive neuronal control model currently implemented in RunBot II under its normal operation, see Eqn. 6.6d. The Anterior Extreme Angle (AEA) of the hip joint was used as the trigger signal of $H_{L/R,K,E}$, Eqn. 6.10, instead of foot contact. When the hip flexion angle reaches a threshold, the knee motor extends the leg to prepare for foot contact with the ground. For RunBot's reflexive controller Eqn. 6.6d (for the knee extensor) can be replaced with:

$$U_{L/R,K,E}(t) = B_{L/R,K}(t) \cdot H_{L/R,K,E}(t) * \Theta(B'_{I,H}(t)) \quad (6.11)$$

Where, as previously, $\Theta(B'_{I,H}(t))$ is the impulse trigger signal when the ipsilateral hip reaches the AEA.

Biceps Femoris (BF)

BF is responsible for hip extension (in the stance phase) and knee flexion (in the swing phase), two motions in different phases of the gait cycle. By taking the

transfer functions derived from the BF EMG activity and ground contact information from both feet ($H_{L/R,BF,CH}$ and $H_{L/R,BF,IH}$) the peak activity following the contralateral heel contact trigger signal can be identified as the knee flexion transfer function (highlighted by a box in Fig. 6.5D) and the hip extension transfer function (Fig. 6.5E) following ipsilateral heel contact.

$$H_{L/R,H,E}(t) = \begin{cases} H_{L/R,BF,IH}(t + t_{BF,IH,start}), & 0 \leq t \leq (t_{BF,IH,end} - t_{BF,IH,start}) \\ 0, & \text{otherwise} \end{cases} \quad (6.12)$$

$H_{L/R,H,E}$ can be substituted in Eqn. 6.6b and used for hip extension in RunBot's reflexive control system.

$$H_{L/R,K,FBF}(t) = \begin{cases} H_{L/R,BF,CH}(t + t_{BF,CH,start}), & 0 \leq t \leq (t_{BF,CH,end} - t_{BF,CH,start}) \\ 0, & \text{otherwise} \end{cases} \quad (6.13)$$

Lateral Gastrocnemius (LG)

The LG transfer function is responsible for ankle dorsiflexion in the stance phase (body weight supporting in mid-stance phase and heel off motion in terminal stance phase, toe off in pre-swing phase) and knee flexion in pre-swing and initial swing phase. The transfer function relating to contralateral heel contact ($H_{L/R,LG,CH}$) has a peak coinciding with knee flexion following toe off and this feature can be used with RunBot to generate knee flexion triggered by contralateral heel contact (Feature of interest highlighted in Fig. 6.5A).

$$H_{L/R,K,FLG}(t) = \begin{cases} H_{L/R,LG,CH}(t + t_{LG,CH,start}), & 0 \leq t \leq (t_{LG,CH,end} - t_{LG,CH,start}) \\ 0, & \text{otherwise} \end{cases} \quad (6.14)$$

In the case of two of the recorded muscles being responsible for the same action (e.g LG and BF in knee flexion) the sum of the two transfer function coefficients was taken. The sum was then be substituted in Eqn. 6.6c for knee flexion in RunBot's control system:

$$H_{L/R,K,F}(t) = H_{L/R,K,FBF}(t) + H_{L/R,K,FLG}(t) \quad (6.15)$$

The start point for the transfer functions was next defined. It is important to note that the data are cyclic and thus a start and endpoint of the function needs to be decided.

As has already been discussed, the delay between contralateral heel contact and muscle activity related to knee extension at terminal swing ($H_{L/R,K,E}$, Eqn. 6.10) is too large for the heel contact to be deemed a suitable trigger for this action. Using hip AEA as the trigger means that the transfer function start point is taken as the time of the trough minimum ($t_{RF,CH,start}$) which precedes the peak of activity related to knee extension. In this way the filter is triggered immediately when the hip AEA is reached.

The springs used in RunBot's knees produce a latency period due to a delay between the motor turning and the springs reacting which can be viewed as an analogue to the delay between heel strike and toe off of the contralateral foot observed in normal human walking during the double support phase (first 10%) of the gait cycle, see Fig. 6.2.

Unlike the knee, the hip joint motor in RunBot is directly controlled by the motor so there is no spring latency period. The delay in motor activation between heel strike and contralateral toe off in the transfer functions, summed with RunBot's spring latency period produces an extended delay causing knee motion uncoordinated to the hip. For this reason, the delay between the trigger and the onset of knee flexor activity was subtracted from the knee flexion transfer functions. As the hip joint motor is not controlled by springs the delay between trigger and muscle activation for hip joint control was not removed.

6.3.2 Optimisation

The final stage in data processing before applying the transfer functions to RunBot is optimisation by using curve fitting to remove spurious artefacts in the EMG as the assumption is made that a muscle activation signal should be a smooth increase and decrease in voltage with contraction.

The muscle twitch response of muscle has a characteristic shape which closely matches the impulse-response time curve of a damped, linear second-order differential system and models the net result of coupling between the excitation and contraction of the muscle [241]. The second-order model behaves essentially like a low-pass filter producing a delay between the neural excitation and the active state of the muscle [242, 243].

To this purpose the impulse response of a critically damped system has been used to curve fit the muscle excitation of the desired features of the muscle transfer functions using the least mean squares (LMS) algorithm and model optimisation in MATLAB. The resulting transfer functions are ($\hat{H}_{L/R,H/K,F/E}$) which can be applied at RunBot's hip and knee motors (H/K) for flexion or extension (F/E).

$$\hat{H}_{L/R,H/K,F/E}(t) = \begin{cases} \lambda \left(\exp\left(\frac{-(t-\delta)}{\tau_1}\right) - \exp\left(\frac{-(t-\delta)}{\tau_2}\right) \right), & t - \delta \geq 0 \\ 0, & t - \delta < 0 \end{cases} \quad (6.16)$$

Where λ is the amplitude fitted variable. τ_2 and τ_1 are equivalent to the rise and fall time respectively and δ is the delay constant from the trigger signal to the onset of muscle contraction.

Only the positive values of the curve fitted transfer function were taken and normalised to an amplitude range between 0 and 1 V. This enabled the motor voltage to be easily adjusted according to the observed gait pattern stability using Eqn. 6.7.

The transfer functions correspond to one stride duration defined as from foot contact to the next foot contact of the same leg (see Fig. 6.5). The mechanical system mainly dictates how the transfer functions need to be resampled for the RunBot. The transfer functions for the hip and knee motors were sampled at the frequency of the control program ($f_s = 200Hz$ or one second) for one stride duration and the knee motor transfer functions were subsequently halved to a duration of 500 ms, for one step.

6.4 Summary

The full procedure for processing the recorded walking data is summarised in Fig. 6.6.

Adaptive filtering was recruited to find the transfer functions relating foot contact information and muscle activity. In order to be able to relate the transfer functions with hip and knee joint actions for use in a control system for generating stepping, the function features were separated so they could be used to produce hip/knee, flexion/extension. Finally the transfer functions were optimised by curve fitting to produce functions which could then be tested with the RunBot biped robot.

In conclusion the transfer functions $\hat{H}_{L/R,H,F}$, $\hat{H}_{L/R,H,E}$, $\hat{H}_{L/R,K,F}$ and $\hat{H}_{L/R,K,E}$ have been identified, which can be substituted into the equations used within RunBot's reflexive control system, Eqn. 6.6a, 6.6b, 6.6c and 6.11. The other parameters within the control system measuring joint extreme flexion/extension angles ($B_{L/R,H/K}$) remain unchanged in order to prevent damage to RunBot's mechanical structure. The angles utilised to signal AEA of the hip joint (which

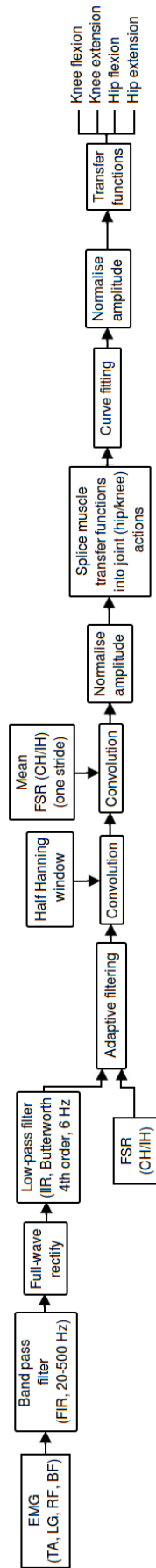


Figure 6.6: **Flow diagram of the signal processing procedure.** The process for determining the transfer functions for hip/knee, flexion/extension was exactly the same for the treadmill walking and overground walking studies.

promotes knee extension of the ipsilateral leg at terminal swing) were also maintained, see Appendix E, Table E1.

The final equations for both legs which define the reflexive control system are as follows:

$$U_{L/R,H,F}(t) = B_{L/R,H}(t) \cdot \hat{H}_{L/R,H,F}(t) * \Theta(G'_C(t)) \quad (6.17a)$$

$$U_{L/R,H,E}(t) = B_{L/R,H}(t) \cdot \hat{H}_{L/R,H,E}(t) * \Theta(G'_I(t)) \quad (6.17b)$$

$$U_{L/R,K,F}(t) = B_{L/R,K}(t) \cdot \hat{H}_{L/R,K,F}(t) * \Theta(G'_C(t)) \quad (6.17c)$$

$$U_{L/R,K,E}(t) = B_{L/R,K}(t) \cdot \hat{H}_{L/R,K,E}(t) * \Theta(B'_{I,H}(t)) \quad (6.17d)$$

Chapter 7

Applying human walking transfer functions to RunBot's reflexive control system

In this chapter the process of calculating the transfer functions from the EMG and foot contact data and the application of the transfer functions to RunBot's reflexive control system will be further discussed. Different sets of transfer functions calculated from the human walking data recorded from three different walking modalities were applied to RunBot's control system to analyse their influence on the produced gait.

7.1 Results: Treadmill walking data

7.1.1 Transfer functions

The final mean square error (MSE) of the coefficients calculated from the adaptive filtering process are provided in Appendix F, Table F1.

As described previously, the final functions after curve fitting were defined as $\hat{H}_{L/R,H,F}$, $\hat{H}_{L/R,H,E}$, $\hat{H}_{L/R,K,F}$ and $\hat{H}_{L/R,K,E}$, and were applied to RunBot using Eqn. 6.17a, 6.17b, 6.17c and 6.17d. To analyse the transfer functions in generating walking with RunBot, 12 different transfer function sets were applied and tested using the reflexive model. This was performed in order to identify the robustness of the employed methodology in defining the transfer functions, and to ascertain whether the two different treadmill walking trials had an effect on the functions, see Table 7.1. Identical transfer functions were applied to the right and left legs as the assumption was made that the activity in both legs was the

Table 7.1: **Different sets of transfer functions applied to RunBot’s control system.** Where A = sequence 1 (25 steps per speed) and B = sequence 2 (100 steps per speed). For example, set 5A is using transfer functions from a single male subject (subject C) from treadmill sequence 1.

Set No.	Description
1A/B	Mean average of all subjects.
2A/B	Mean average of male subjects only.
3A/B	Mean average of female subjects only.
4A/B	Each transfer function is from the subject who had the minimum final MSE value from the adaptive filtering.
5A/B	$\hat{H}_{L/R,H/K,F/E}$ from a single male subject (subject C).
6A/B	$\hat{H}_{L/R,H/K,F/E}$ from a single female subject (subject H).

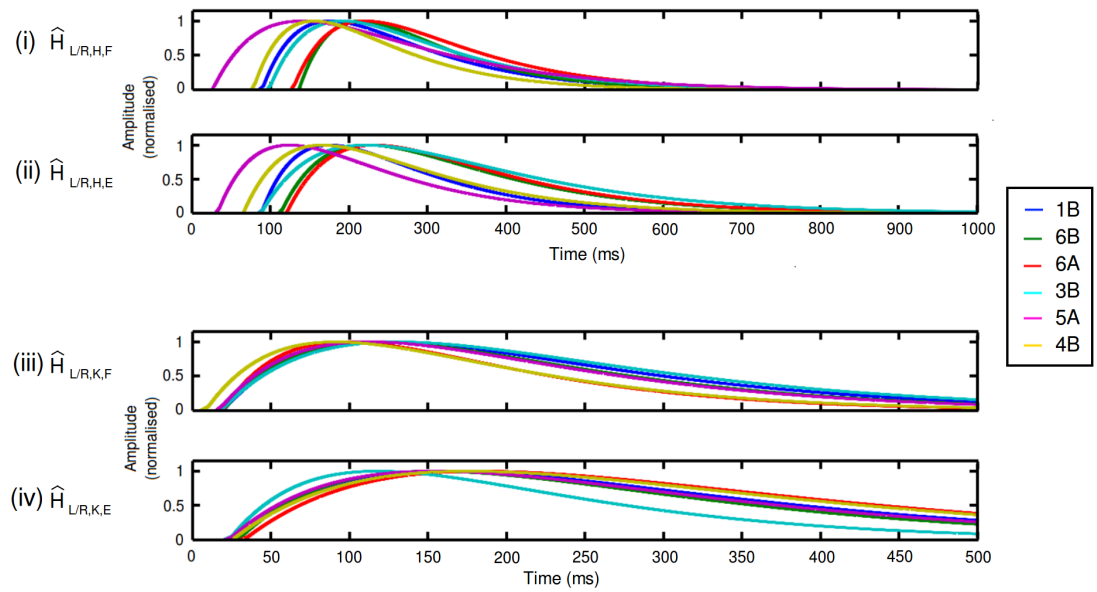
same. The parameter values for the functions calculated from the curve fitting are provided in Table 7.2B and 7.2A. To determine the quality of the curve fitting, goodness-of-fit statistics were calculated for each of the functions related to hip/knee flexion/extension. These are provided in Appendix G, Table G1A and G1B.

7.1.2 RunBot performance

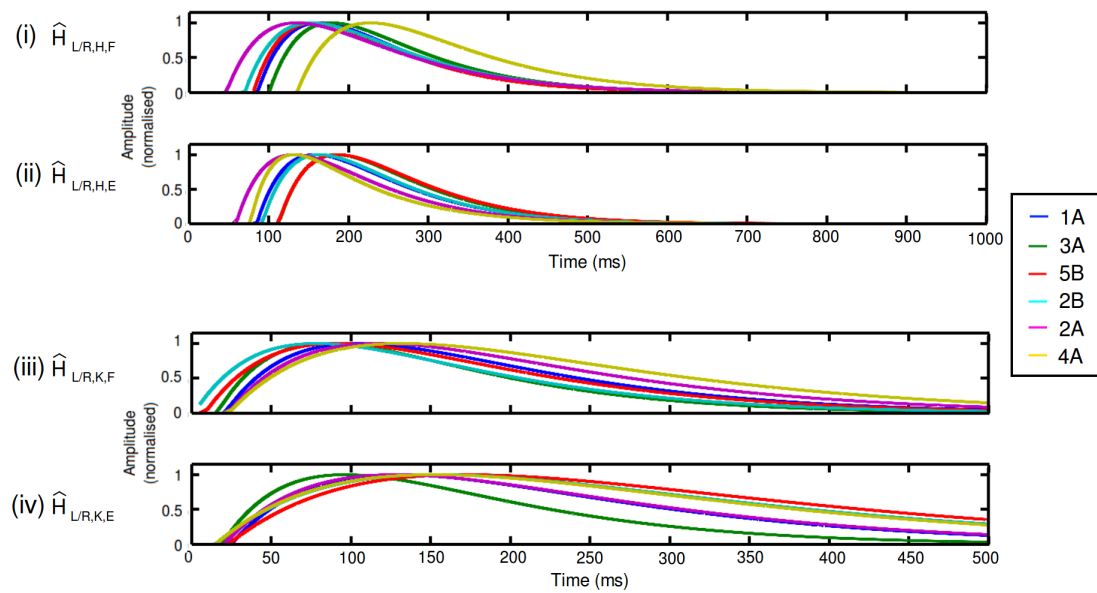
The next stages were to apply the different transfer functions sets to the defined reflexive control system in RunBot, and to analyse the resultant gait.

Videos of RunBot’s gait using each of the applied transfer function sets can be viewed at <https://www.youtube.com/user/reflexwalking>.

Stable walking was defined as a controlled gait cycle with no stumbles or falls for more than 10 rotations of the circular path (approximately 200 steps). Transfer function sets: 1A, 5B, 3A, 2A, 2B and 4A caused RunBot to stumble and fall while the remainder: 1B, 5A, 6A, 6B, 3B and 4B produced a stable gait pattern. Stability performance was evaluated in terms of: i) joint angles, ii) phase plots (dynamic stability) and iii) coordination. Comparison plots of the calculated transfer functions which worked with RunBot can be seen in Fig. 7.1A. On comparing the function characteristics (Table 7.3) an obvious difference was found in the hip extensor transfer functions that produced stable gait compared to those sets which did not. The sets which featured a longer t_d (where t_d is the time period from 50% of the peak amplitude on the rise to 50% of the amplitude on the fall) in the hip extensor function were more likely to produce a stable gait. From this information it can be determined that if t_d is too short, the stance hip cannot extend backwards to the desired angle which will cause the



(A) Plots of the different transfer functions which produced a stable gait in RunBot.



(B) Plots of the different transfer functions tested with RunBot which did not produce a stable gait.

Figure 7.1: **Plots of the different transfer functions applied to RunBot's motors.** The number of samples for the hip motors was set to 200 (1000 ms). Knee flexion/extension was set to 100 samples or 500 ms. (i) Hip flexion of the leg is triggered by the contralateral heel strike. (ii) Hip extension is triggered by the ipsilateral heel strike. (iii) Knee flexion of the leg is triggered by the contralateral heel strike and knee extension (iv) is triggered by the anterior extreme angle (AEA) of the hip to drive knee extension at terminal swing.

Table 7.2: **Results of the curve fitting for hip/knee, flexion/extension.** Values are provided for τ_1 , τ_2 and δ which can be substituted into Eqn. 6.16. As RunBot has a knee structure involving springs, the δ values for the knee joint transfer functions correspond to the delay between the trigger and t_{start} and thus were set to zero.

(A) **Results of the curve fitting for hip flexion/extension.**

Set	$\hat{H}_{L/R,H,F}$			$\hat{H}_{L/R,H,E}$		
	τ_1 (ms)	τ_2 (ms)	δ (ms)	τ_1 (ms)	τ_2 (ms)	δ (ms)
1A	76.97	76.96	75	73.22	73.22	75
1B	86.91	86.91	80	128.24	81.73	85
2A	88.31	88.31	30	72.47	72.47	80
2B	83.80	83.80	60	71.82	71.82	80
3A	78.53	78.52	90	72.31	72.31	100
3B	93.71	93.71	80	133.76	133.76	80
4A	91.96	91.96	125	95.88	34.27	80
4B	77.52	77.52	70	100.46	100.46	50
5A	113.28	113.28	5	91.43	91.43	15
5B	76.18	76.18	75	74.65	74.65	100
6A	93.08	93.08	110	112.16	112.16	100
6B	78.41	78.41	120	110.89	110.89	100

(B) **Results of the curve fitting for knee flexion/extension.**

Set	$\hat{H}_{L/R,K,F}$			$\hat{H}_{L/R,K,E}$		
	τ_1 (ms)	τ_2 (ms)	δ (ms)	τ_1 (ms)	τ_2 (ms)	δ (ms)
1A	83.11	83.11	115	103.84	103.84	425
1B	105.02	105.02	115	134.63	134.59	440
2A	94.47	94.47	110	107.71	107.71	430
2B	76.58	76.58	120	139.47	139.47	435
3A	69.09	69.09	140	77.13	77.12	460
3B	113.76	113.76	125	94.56	94.56	495
4A	108.96	108.96	90	136.61	136.54	450
4B	82.99	82.85	105	150.33	150.33	415
5A	95.95	95.95	110	131.17	131.17	410
5B	82.99	82.85	105	148.99	148.99	420
6A	78.37	78.37	150	151.75	151.75	425
6B	97.24	97.22	130	123.34	123.34	495

foot of the swing leg to scuff the ground and cause a stumble. There was no consistent difference between different knee transfer functions between the sets which worked and those that did not work.

To analyse the effect of the different transfer function coefficients, RunBot's

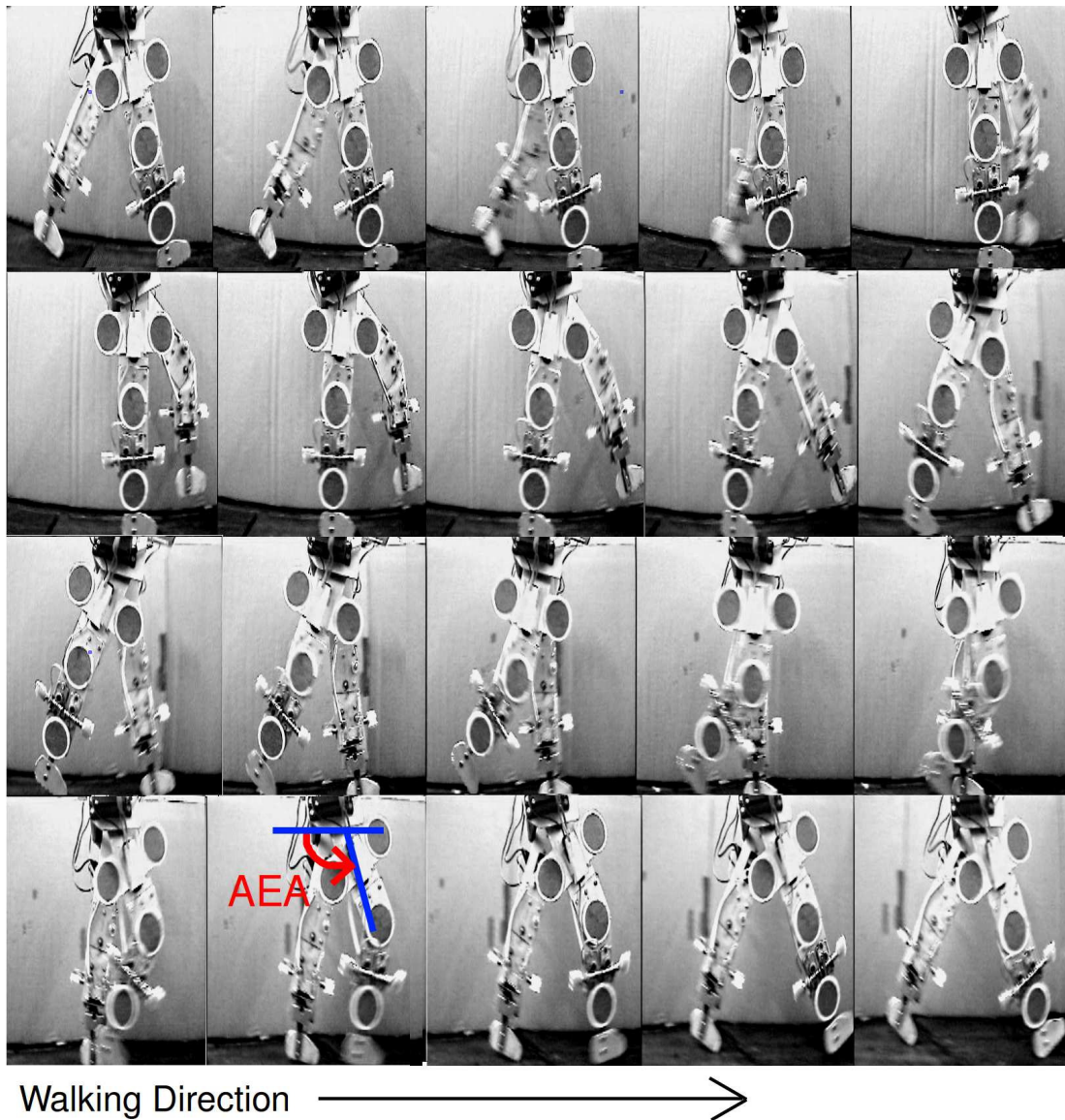


Figure 7.2: **Photographs of one RunBot stride duration.** The series of frames corresponds to one stride recorded after applying transfer functions found from the human study. The time interval between each adjacent frame is 60 ms. Markers were attached to RunBot's right leg for video tracking of the joints for calculation of kinematic data. Heel contact triggers the stance phase of ipsilateral leg and the swing phase of the contralateral leg. Leg extension during terminal swing is triggered by the threshold value for the hip anterior extreme angle (AEA) being reached during hip flexion.

Table 7.3: **Comparison of function characteristics.** The duration (t_d) and peak time (t_p) of the hip transfer functions were compared to determine the influence on whether RunBot’s gait is stable or unstable. $\hat{H}_{L/R,H,E}$ needs to have a longer duration than $\hat{H}_{L/R,H,F}$ to produce a stable gait pattern.

Gait	Set	$\hat{H}_{L/R,H,F}$		$\hat{H}_{L/R,H,E}$	
		t_p (ms)	t_d (ms)	t_p (ms)	t_d (ms)
Stable	1B	175	215	190	255
	3B	190	230	220	330
	4B	155	190	165	245
	5A	140	275	125	225
	6A	220	230	230	275
	6B	215	195	225	270
Unstable	1A	160	190	160	180
	2A	135	215	130	175
	2B	155	205	165	175
	3A	280	195	185	180
	4A	225	225	130	145
	5B	155	185	185	185

gait was analysed using video-tracking of the limbs as the robot walked in a circular path, see Fig. 7.2.

A step is initiated when the stance leg foot makes contact with the ground. The hip of the swing leg then flexes forward and the knee flexes, lifting the foot off the ground. Once the hip reaches the anterior extreme angle (AEA) the knee is triggered into extension until the foot of the swing leg makes contact with the ground. This then triggers the contralateral leg motors and so on.

During joint-tracking, measurements were taken of average walking speed, stride length and the knee joint angle. Fig. 7.3 describes how the walking speed performance of RunBot responds to the different transfer function sets. The speed result was calculated as the circumference of the cycle path ($2\pi 0.5$) divided by the time for completing one circuit. The stride duration was calculated as the time for RunBot to complete a rotation of the circular path, divided by the number of strides recorded.

Flexion/extension angle of the knee was calculated to compare the different transfer function’s effect on RunBot, Fig. 7.4. RunBot II has a knee structure which involves springs to mimic the muscle properties around the human knee joint due to muscle having linear, spring-like properties. Due to the knee mechanics being analogous to humans, the knee angle can be studied during the gait cycle to analyse the difference in transfer function from the different transfer function

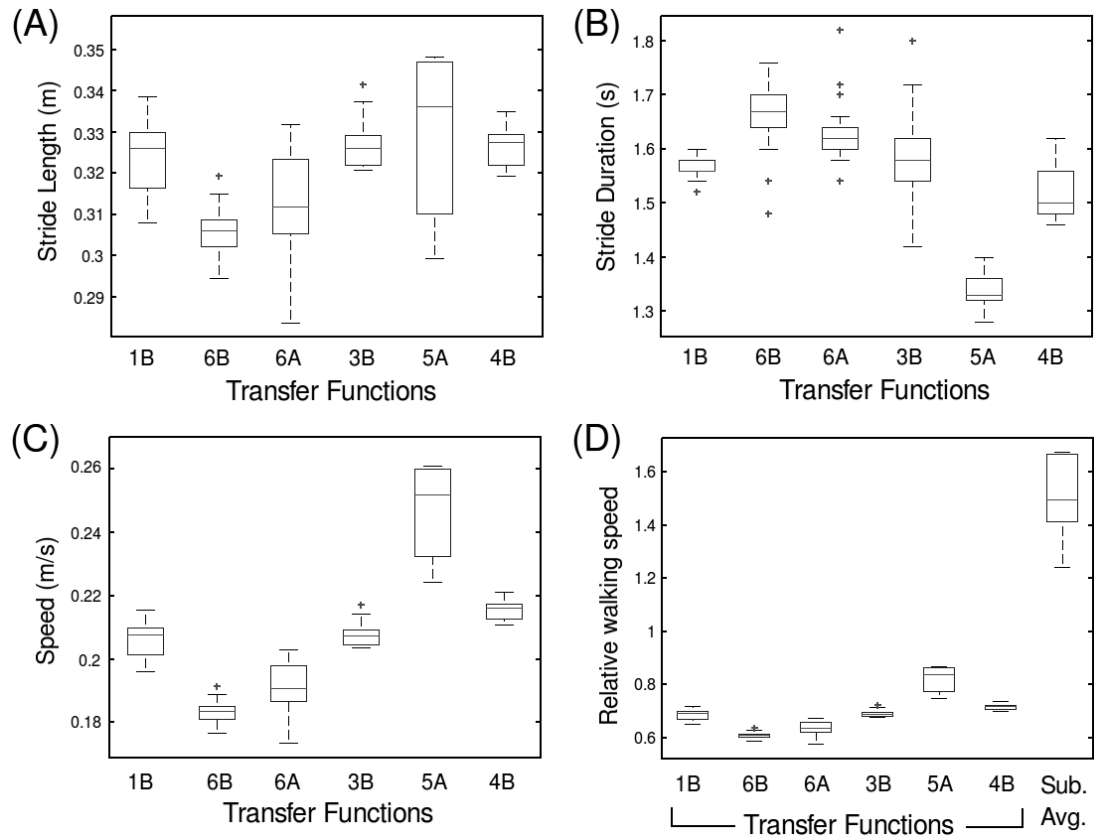


Figure 7.3: **Box plots comparing RunBot's stride length (A), stride duration (B) and walking speed (C).** Using the transfer function sets which produced stable walking ($n = 10$). A box plot comparing the relative walking speed of RunBot using each of the transfer function sets compared to the average relative walking speed of the human test subjects is also provided (D). Relative walking speed of leg-length/s was calculated as the scaled walking speed to leg length where RunBot's leg length is 0.3m

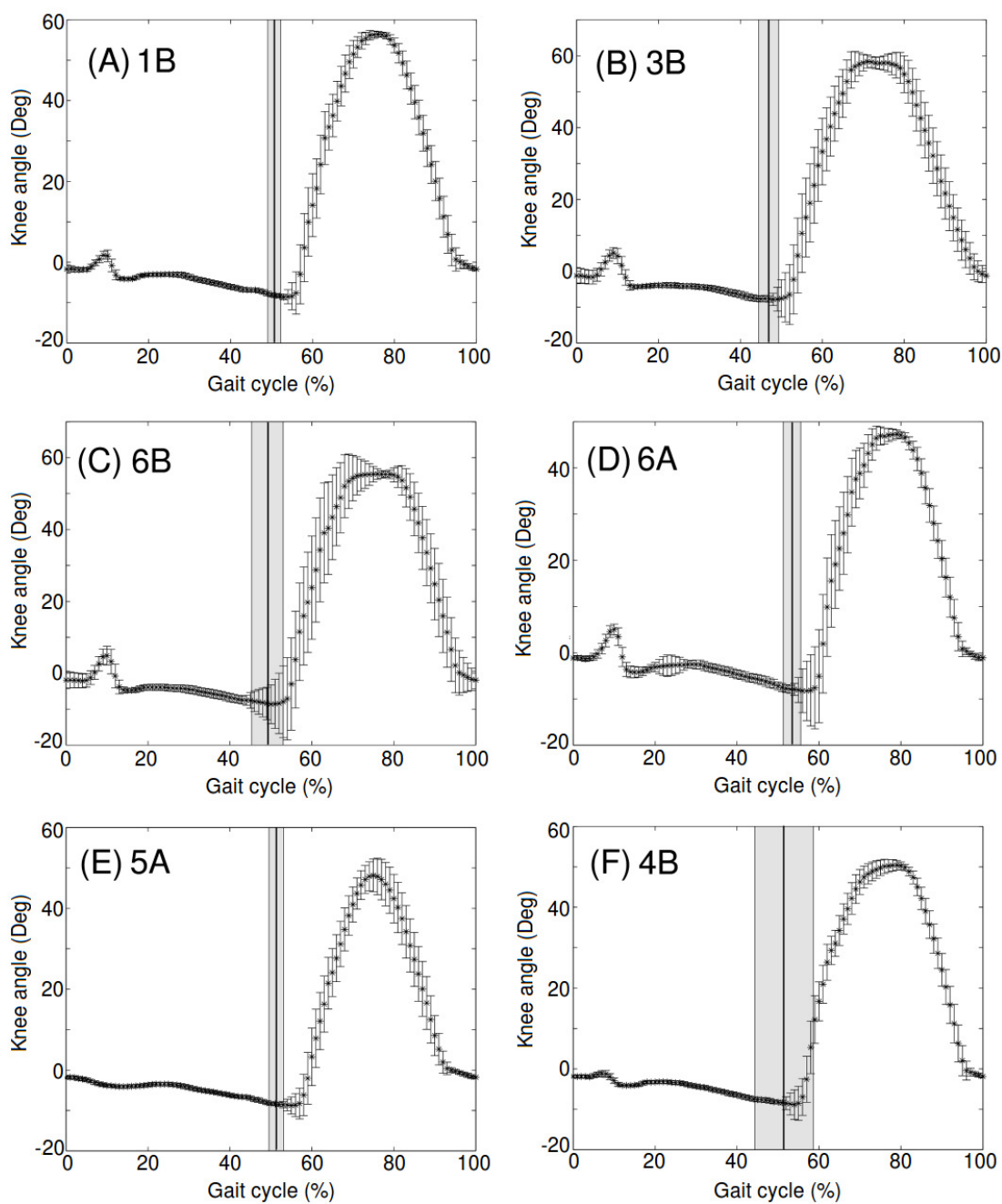


Figure 7.4: Comparison of knee flexion/extension angle of RunBot using transfer function sets which produced a stable gait. The time is normalised to percent of stride, the mean and standard deviation was calculated from the number of strides recorded from the video tracking. The mean percent of stride when the contralateral heel strike was recorded is also shown as a line with the standard deviation highlighted.

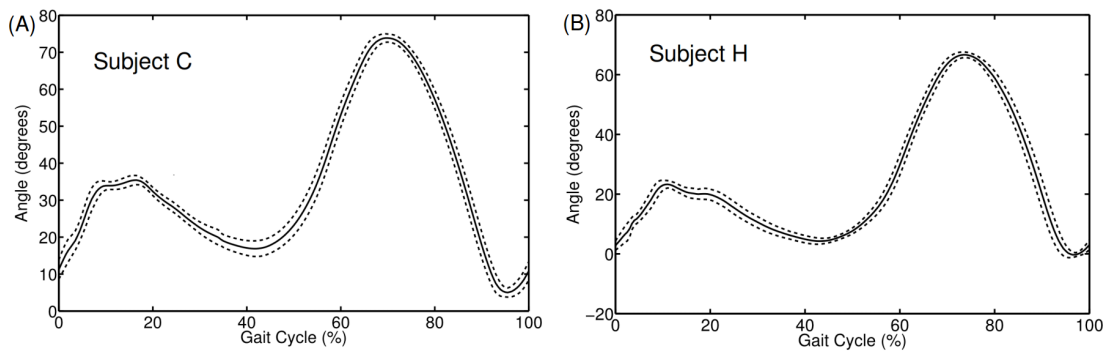


Figure 7.5: **Knee flexion/extension angle of (A) subject C and (B) subject H.** This information was calculated using leg marker coordinate data recorded using the Vicon system. Mean (solid line), standard deviation (dotted line)

sets which produced a stable gait. Comparing the averaged and female and male individual subject transfer function sets, the timing for stance and swing is very similar; the main difference being in the small peak evident during stance when some of the transfer function sets are applied to RunBot. This is due to the knee bending following heel strike because the hip has continued to flex after heel contact and so has pulled the knee into flexion before extension begins.

To allow comparison with the human knee joint action during the gait cycle, the data recorded from the leg by the Vicon system, during the wi-GAT validation study (Chapter 4, Section 4.2.4) was used to visualise the action of the knee joint. Vicon Plug-in-Gait lower limb marker set and model can calculate the joint angles during the gait cycle and these can be saved to ASCII file format for post processing. During the wi-GAT study the participants completed ten overground walks at a self-selected, comfortable walking pace. The generated knee joint angle data can then be averaged over every recorded gait cycle during the ten walks. The knee joint angle plots related to the gait cycle%, from two participants are provided in Fig. 7.5.

Comparing RunBot's knee angle to human knee flexion/extension angle during gait, the plots appear similar, see Fig. 7.4 and 7.5. The major difference is that in humans there is a small flexion peak present during loading in stance before swing begins ($\approx 10-15\%$ of the gait cycle) which is more significant than the small duration peak in RunBot's knee motion. In humans this peak is due to the knee bending following heel strike as the body weight is accepted and transferred onto the leg as the swing phase of the contralateral leg begins. It also acts to absorb the impact of the heel strike by extending the contraction period of the quadriceps muscles.

Another point of interest is in the 3B and 6B knee angle curves, Fig. 7.4B and C. The flat peak during knee flexion in the swing phase is due to the knee flexing to its maximal angle and remaining in this state before the hip reaches the AEA which triggers knee extension. This is in contrast to the other data sets applied to RunBot and the human knee angle example which demonstrate a more fluid movement from knee flexion to knee extension.

To analyse the dynamic stability of RunBot using the different transfer function sets, phase plots of knee angular velocity versus the angular position were used as the movement pattern is cyclic and it is valuable to observe how the performance varies over time, Fig. 7.6. Ideally the phase plots should demonstrate a smooth, repeating pattern with minimum diversion from the path, which would suggest deviations from a stable limit cycle. Although the gait stability is affected by using the different transfer function sets, it can be seen that overall the reflexive control system produces stable limit cycles. This demonstrates that even when there is a disturbance to the gait pattern originating from an unevenness of the ground surface, there is a quick return to the steady-state behaviour. Fig. 7.6E is transfer function set 5A (individual male subject, treadmill sequence 1), this set produced the fastest walking speed with RunBot but the phase plot demonstrates that the limit-cycles are significantly more affected by perturbations than the other sets and so appears less stable.

Again the phase plots generated from RunBot's walking data can be compared to those of the human subjects who participated in the Vicon walking data collection, Fig. 7.7. It can be seen that the human data generates a stable, smooth and regular phase plot with little deviation from a standard path. Although the addition of knee flexion during the loading phase creates a different shape in the phase plot compared to with the RunBot, there is evidence of similar angle and angular velocity being achieved by both at the knee during the gait cycle.

In addition the angle-angle plots of hip angle against knee angle highlight the coordination between RunBot's joints during the gait cycle, Fig. 7.8. These plots demonstrate the trajectories in joint space and how RunBot changes its kinematics with the different applied transfer function sets. Hip joint angle was calculated by analysis of the hip motor voltage, which was recorded simultaneously to the video tracking of the knee angle. Similar to the phase plots, there is a regularity in the angle of the joints throughout the gait cycle and any deviations return to a value, corresponding to a stable limit cycle, within a few steps. However it is evident how the gait kinematics can change notably with the different applied transfer function sets. Again transfer function set 5A (Fig. 7.8E) appears the

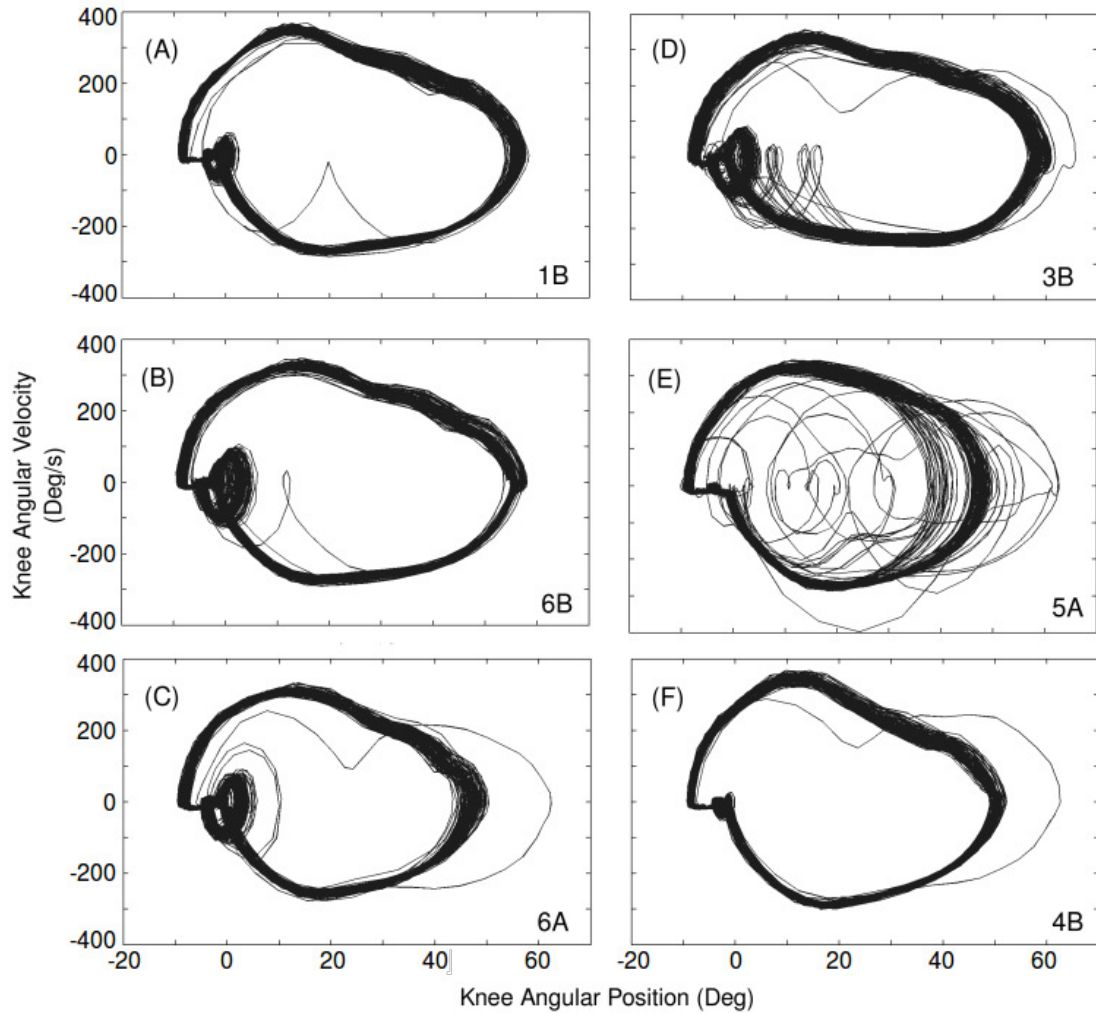


Figure 7.6: **Phase plots of knee angular velocity versus angular position.** The plots show the limit cycles in the phase plane and demonstrate the robustness of the reflexive control system. Even when there is a disturbance to the gait cycle caused by an uneven ground surface, the robot is able to recover and there is a rapid convergence back to the steady-state behaviour in only a few steps.

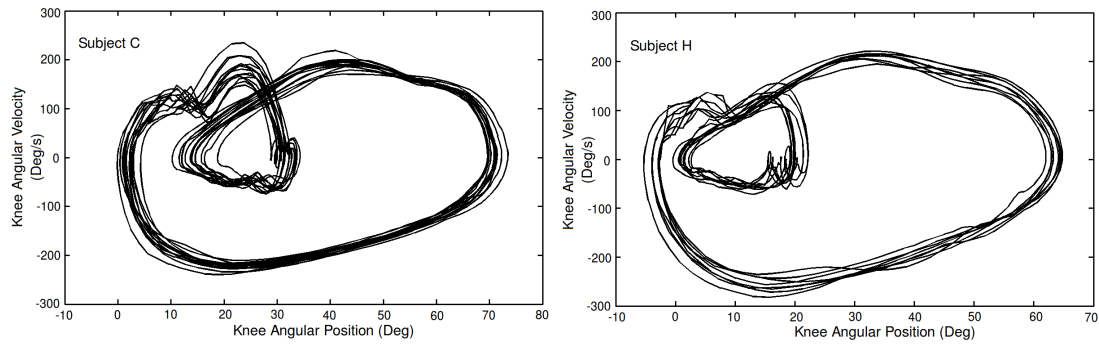


Figure 7.7: **Phase plots of knee angular velocity versus angular position during human walking.** These plots were generated using leg marker coordinate data recorded using the Vicon system.

most variable. Although a clear pattern in the relationship between hip joint angle and knee joint angle can be seen throughout the gait cycle, they appear to have less coordination throughout the entirety of the walk than during the other transfer function sets.

7.1.3 Conclusion

Finally, characteristics of the transfer functions can be identified which worked to produce stable walking in RunBot and explain why other sets did not. In summary:

- Compared to the knee transfer functions, the differences in hip transfer functions have a more significant effect on the walking performance as the hip transfer functions are used to drive the hip motor directly.
- The time delay between the trigger and the hip flexion and between the trigger and the hip extension of the contralateral leg should be very similar or the hip flexion should be longer to produce a stable gait.
- The duration t_d of hip extension (from 50% of the peak amplitude on the rise to 50% on the fall) is significant in establishing a stable gait pattern because the stance leg needs enough torque to support the body weight and extend the leg backward while the swing leg flexes forward.
- The duration of hip extension should be longer than hip flexion to produce a stable gait.

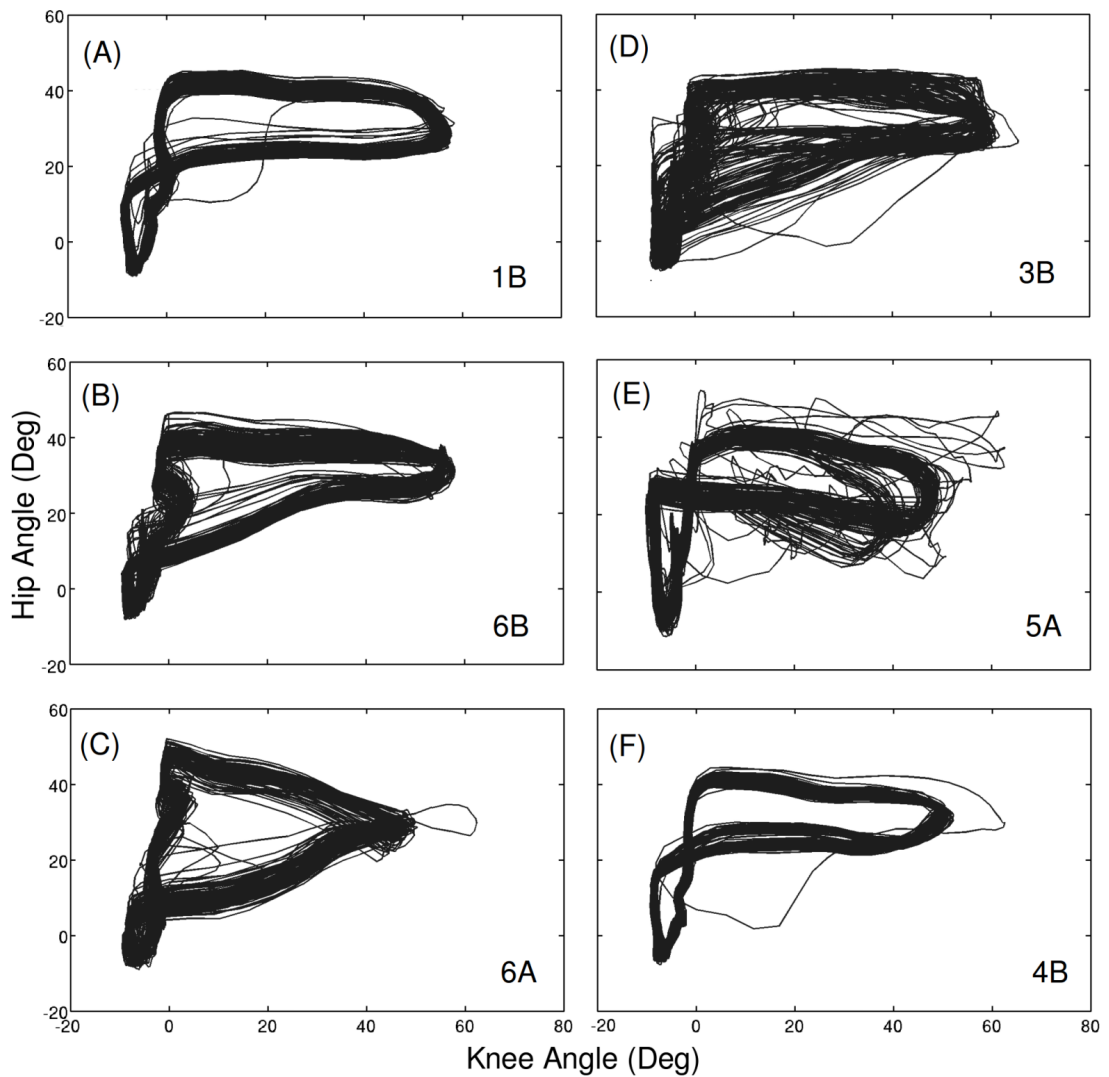


Figure 7.8: **Angle-angle plots of hip angle against knee angle.** These plots demonstrate the coordinated motion of the two joints during the gait cycle. Knee angle was calculated from markers positioned on the knee joint and video camera tracking over ten complete rotations of the circular path. The hip angle was calculated from the voltage of the motor at the hip which was recorded during walking. The plots again demonstrate the robustness of the reflexive control system as even when there is a perturbation there is a rapid convergence to the limit cycle in only a few steps.

7.2 Results: Overground walking data

7.2.1 Transfer functions

The final mean square error (MSE) of the coefficients calculated from the adaptive filtering process are provided in Appendix F, Table F2.

To analyse the transfer functions calculated from the overground walking, in generating walking with RunBot, six different transfer function sets were applied and tested using the reflexive model to identify differences between overground and treadmill walking, see Table 7.4.

These sets were the same as those applied to RunBot in the treadmill walking study, where the transfer functions calculated from individual female and male participants (sets 5 and 6) are the same individuals as chosen previously in the treadmill study. Identical transfer functions were applied to the right and left legs as again the assumption was made that the activity in both legs was the same. The parameter values for the functions calculated from the curve fitting are provided in Table 7.5. Goodness-of-fit statistics for the curve fitting are provided in Appendix G, Table G2A and G2B.

7.2.2 RunBot performance

The different transfer functions sets were applied to the defined reflexive control system in RunBot and the resultant gait analysed. Each of the sets of functions failed to produce a stable gait in RunBot. Where a stable gait was defined as RunBot being able to complete at least ten complete circuits of the circular pathway without falling or stopping. Some sets of functions were able to produce

Table 7.4: **The different sets of transfer functions applied in RunBot's control system.** Different sets of transfer functions were applied to RunBot's control system to establish whether a stable gait pattern can be produced by combining transfer functions from the range of participants or by just using functions from individual participants.

Set No.	Description
1	Mean average of all participants.
2	Mean average of male participants only.
3	Mean average of female participants only.
4	Each transfer function is from the participant who had the minimum final MSE value from the adaptive filtering.
5	$\hat{H}_{L/R,H/K,F/E}$ from a single male participant (participant B).
6	$\hat{H}_{L/R,H/K,F/E}$ from a single female participant (participant J).

Table 7.5: **Results of the curve fitting for hip/knee, flexion/extension.** Values are provided for τ_1 , τ_2 and δ which can be substituted into Eqn. 6.16. As RunBot has a knee structure involving springs, the δ values for the knee joint transfer functions, corresponding to the delay between trigger and t_{start} , were set to zero.

(A) **Results of the curve fitting for hip flexion/extension.**

Set	$\hat{H}_{L/R,H,F}$			$\hat{H}_{L/R,H,E}$		
	τ_1 (ms)	τ_2 (ms)	δ (ms)	τ_1 (ms)	τ_2 (ms)	δ (ms)
1	109.35	109.35	75	41.65	41.65	125
2	106.70	106.70	60	40.60	40.60	125
3	127.35	127.40	30	52.75	52.75	135
4	57.15	57.15	125	42.15	42.15	100
5	68.55	68.55	45	45.50	45.50	95
6	55.20	55.20	125	31.00	31.00	130

(B) **Results of the curve fitting for knee flexion/extension.**

Set	$\hat{H}_{L/R,K,F}$			$\hat{H}_{L/R,K,E}$		
	τ_1 (ms)	τ_2 (ms)	δ (ms)	τ_1 (ms)	τ_2 (ms)	δ (ms)
1	84.55	84.55	130	105.05	105.00	550
2	122.00	122.00	45	132.05	132.05	550
3	71.70	71.70	170	93.10	93.10	550
4	55.05	55.50	125	71.65	71.65	500
5	67.10	67.10	75	63.35	65.35	650
6	59.30	59.30	70	70.10	70.10	500

a series of steps but none could establish a stable and controlled gait. To analyse why the sets of functions calculated from overground walking failed in comparison to the sets which were successful from the treadmill walking data collection, the characteristics of the functions can be studied, Fig. 7.9 and Table 7.6.

On plotting the transfer functions for controlling Hip extension ($\hat{H}_{L/R,H,E}$) from the different sets it is clear that this function is significantly shorter than those calculated from the treadmill walking. This function is calculated from the muscle activity in the BF muscle which has action related to hip extension during walking. It could be implied from the results that the BF muscle may behave differently during overground walking in comparison to treadmill walking.

7.2.3 Conclusion

Observations were made in Section 7.1.3, which explained why some of the transfer function sets could produce a stable gait and others could not. These conclu-

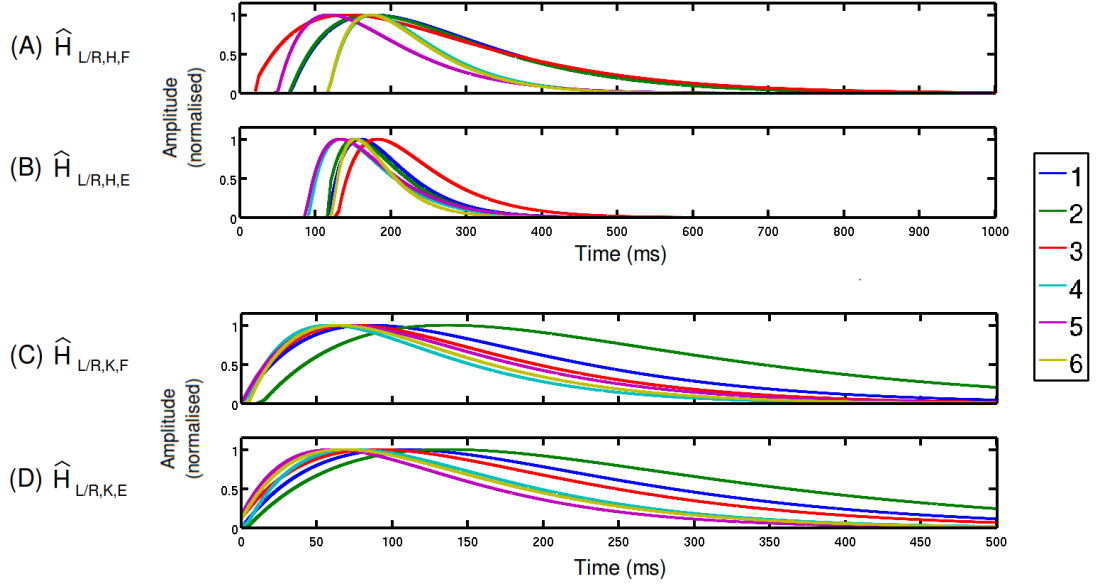


Figure 7.9: **Plots of the different transfer functions tested with RunBot** The number of samples for the hip motors was set to 200 (1000 ms). This is the same frequency used during the normal operation of RunBot II. Knee flexion/extension was set to 100 samples or 500 ms. (A) Is the transfer function coefficients from the double exponential curve fitting for the hip flexion. Hip flexion of the leg is triggered by the contralateral heel strike. (B) Hip extension is triggered by the ipsilateral heel strike. (C) Knee flexion of the leg is triggered by the contralateral heel strike and knee extension (D) is triggered by AEA (anterior extreme angle) of the hip to drive knee extension at terminal swing.

Table 7.6: **Function characteristics.** The duration (t_d) and peak time (t_p) of the hip transfer functions were studied to compare with the hip functions calculated from the treadmill walking data collection. Here, it was inferred that $\hat{H}_{L/R,H,E}$ needs to have a longer duration than $\hat{H}_{L/R,H,F}$ to produce a stable gait pattern.

Set	$\hat{H}_{L/R,H,F}$		$\hat{H}_{L/R,H,E}$	
	t_p (ms)	t_d (ms)	t_p (ms)	t_d (ms)
1	176	262	161	95
2	171	257	151	95
3	141	307	181	120
4	176	135	136	95
5	121	161	131	105
6	171	130	151	70

sions also explain why RunBot was not able to walk with a stable gait cycle using the transfer functions calculated from the overground walking data. As variation in hip transfer function characteristics have been found to have more of a significant effect on walking stability than the knee functions functions, the short duration of hip extension means the stance leg is not producing enough torque to support the body weight while the contralateral limb flexes during swing. In addition the hip extension delay was longer than hip flexion in all of the sets apart from set 6 where it was exactly the same delay value. This means that the contralateral hip is starting to flex before the ipsilateral hip begins to extend meaning the legs can potential get locked in phase causing RunBot to stumble and fall due to gravity.

7.3 Summary

It is clear that overground and treadmill walking produce a variation in gait parameters. It is thus important to further understand the differences and how they may effect the usefulness of the calculated transfer functions in generating gait in RunBot and most importantly be used in the development of a an FES control system for use in retraining functional walking in individuals with SCI. Ideally the transfer functions calculated from treadmill walking will be able to translate into functional walking of the individual overground.

Chapter 8

Comparison of treadmill and overground walking

The results of applying human walking transfer functions to the RunBot II robot suggested that the functions calculated from treadmill walking data were more likely to produce a stable gait in the robot compared to functions calculated from overground walking data. It is thus of interest to examine what effect the different walking modalities have on gait parameters and muscle activity in an attempt to understand why this result was found in the robot, and how this could impact the use of the control system to generate a functional gait pattern in human gait rehabilitation.

Many studies have aimed to provide a thorough comparison of temporal gait parameters [244–248] and muscle activation patterns [244, 246, 248, 249] between overground and treadmill walking. However, as was highlighted by Lee and Hidler (2008), the literature contains conflicting evidence, which is overall inconclusive [248]. Statistical differences in temporal gait parameters were not found between overground and treadmill walking by Murray et al. (1985) but they did observe that participants produced shorter step lengths, higher cadences, shorter swing phases, and longer double-limb support during treadmill walking [244]. A statistical difference in muscle activity in quadriceps EMG activity was also found, whereas Arsenault et al. (1986) found elevated activity in the Biceps Femoris (BF) with lower variability in muscle firing patterns during treadmill than in overground walking [249]. Lee and Hidler’s (2008) study also found differences in muscle activity between the two walking environments but most obviously in the TA muscle throughout stance, and in the hamstrings during swing [248].

The advantage of the protocol discussed in this thesis compared to previous studies [244, 246, 248, 249] analysing treadmill and overground walking, is the

use of FSR insoles for recording foot contact information during walking. Using the same equipment for data collection during each modality eliminates any experimental bias introduced by using different experimental setups. And FSRs are advantageous over force plates or pressure sensitive mats, used extensively in previous studies, as they can record foot contact over an unlimited distance, compared to a limited capture area of only a few steps.

To study and attempt to quantify the differences between the three different walking modalities used in this thesis for data collection ((1) treadmill sequence 1: 20 speeds, \approx 25 steps per speed, (2) treadmill sequence 2: 10 speeds, \approx 100 steps per speed and (3) overground walking) temporal gait parameters and event-related averages (ERA) of the muscle activity were examined.

8.1 Analysis

8.1.1 Temporal gait parameters

Temporal gait parameters were estimated for the treadmill and overground walking conditions in relation to walking speed. Measures include stance duration, swing duration, stride time and the relationship between stance and swing duration. Walking speed and stride, swing and stance duration were normalised into dimensionless measures using the procedures described by Hof (1996) [190] to account for individuals of various heights. This strategy also allows comparison between the three walking modalities, which were not conducted using the same walking speed range.

Dimensionless time (\hat{t}) can be defined as the time in seconds divided by the square-root of leg-length (l), measured from the anterior superior iliac spine (ASIS) to the medial malleolus (true leg length), divided by acceleration due to gravity (g), where $g = 9.8 \text{ ms}^{-2}$.

$$\hat{t} = \frac{t}{\sqrt{l/g}} \quad (8.1)$$

Similarly, dimensionless velocity \hat{v} can be defined:

$$\hat{v} = \frac{v}{\sqrt{g \cdot l}} \quad (8.2)$$

\hat{v} is also known as the Froude number (Fr) and is the ratio of a body's (in this case limb's) inertia to gravitational forces. These scaling methods originate from the condition that inertial and gravitational forces should scale proportionally to

each other [190].

For each walking speed recorded for each participant, the average stride, swing and stance durations were calculated using the FSR insoles worn for recording foot contact information during the walking modalities. Stride was calculated as the time between subsequent heel strikes of both the right and left feet measured using the FSR positioned under the heel. Stance was measured as the time from heel contact to toe off, measured using the FSR positioned under the first metatarsal (FM). Swing was calculated as the time from toe off to the next heel contact of the same foot.

Stride duration (s)

$$D_{L/R} = \frac{1}{N} \sum_{k=1}^N t_{L/R,FSR,heel_{k+1}} - t_{L/R,FSR,heel_k} \quad (8.3)$$

Where $t_{L/R,FSR,heel}$ is the time of heel contact in seconds.

Stance duration (s)

$$St_{L/R} = \frac{1}{N} \sum_{k=1}^N t_{L/R,FSR,FM_k} - t_{L/R,FSR,heel_k} \quad (8.4)$$

Where $t_{L/R,FSR,FM}$ is the time when the toe leaves the ground, indicating a toe off gait event, in seconds.

Swing duration (s)

$$Sw_{L/R} = \frac{1}{N} \sum_{k=1}^N t_{L/R,FSR,heel_k} - t_{L/R,FSR,FM_k} \quad (8.5)$$

8.1.2 Muscle activity

To study the relationship between foot contact and muscle activity, and compare the inter-subject variability during walking overground and on the treadmill, the average waveform for each muscle in the right leg during two strides (before and after a heel contact FSR event) was analysed. The population mean ($M_{ER\hat{A},mus,CH/IH}$) and standard deviation ($STD_{ER\hat{A},mus,CH/IH}$) of the ERAs were found from the data collected from each of the two treadmill walking sequences and the overground walking. Where *mus* is the muscle in which the EMG was recorded and CH/IH is the heel contact event recorded from the FSR under the

contralateral (CH) or ipsilateral (IH) heel.

The coefficient of variation ($CV_{ER\hat{A},mus,CH/IH}$) was used as a statistical method to measure the overall variability between subjects of the averaged ERAs. Where $CV_{ER\hat{A},mus,CH/IH}$ is described as the ratio of the standard deviation to the mean. The process for calculating the ERA and CV was the same as described in Chapter 3, Section 3.4.

In addition, peaks in the ERA of the muscle activity related to joint actions (hip/knee, flexion/extension), as identified in the muscle transfer functions (Chapter 6, Section 6.3.1), were compared to determine whether the different walking modalities affects the timing of this activity. Paired t-tests with a Bonferroni correction were used to compare the timing of the identified peaks in the ERAs from the three walking methods ({tread 1 - tread 2}, {tread 1 - overgnd}, {tread 2 - overgnd}). The Bonferroni correction is used to reduce the chances of obtaining false-positive results (type I errors) when multiple pair-wise tests are performed on the data sets. The critical p value ($\alpha=0.05$) is divided by the by the number of comparisons being made, in this case 3, so now $\alpha = 0.0167$.

The statistical tests were run using SPSS (version 20.0, IBM Corp., Armonk, NY). As only seven of the participants took part in both the overground and the treadmill walking sessions, only the data from these seven people was included in the statistical analysis to compare the methods.

8.2 Results

8.2.1 Temporal gait parameters

Each of the seven subject's walks (treadmill (sequence 1 and sequence 2) and overground) were plotted on the same graphs so trends in the recorded data could be identified and compared, Fig. 8.1, 8.2 and 8.3.

All of the graphs demonstrate that the different walking modalities produce stride, swing and stance durations which all have a general linear relationship with walking speed over the participant population. Examining the graphs, visually there is a distinct difference between the gait parameters calculated from the overground and treadmill walking. The overground walking gait parameters, stride and stance duration, (Fig. 8.1A, B, C and D) are more variable with a greater distribution from the regression line than is seen in the treadmill walking gait parameters (Fig. 8.2A, B, C and D, and 8.3A, B, C and D). For example, stride duration (Fig. 8.1A and B): $R^2 = 0.30$ (left leg) and $R^2 = 0.31$ (right leg), compared to the treadmill walking sequence 1 (Fig. 8.2A and B): $R^2 = 0.77$ (left

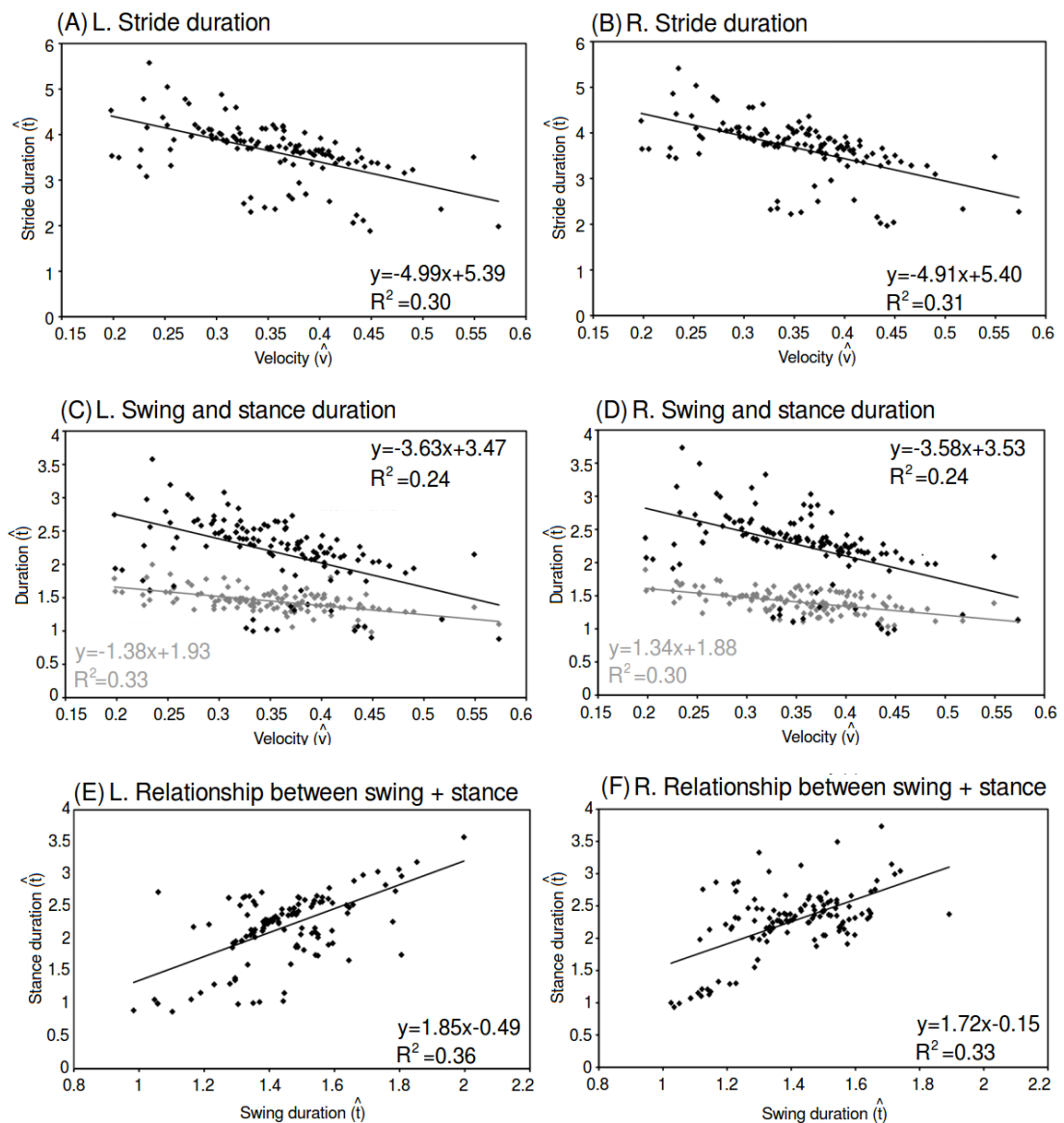


Figure 8.1: **Temporal gait parameters - overground walking.** (A), (C) and (E) are the gait parameters calculated for the left leg and (B), (D) and (F) are calculated for the right. In plots (C) and (D), swing is shown in grey, stance in black. In all parameter linear regression analysis, changes in predictor's value (walking speed and swing duration) are related to changes in the response variable. The null hypothesis that predictor variables have no effect on the response variables can be rejected ($P < 0.05$).

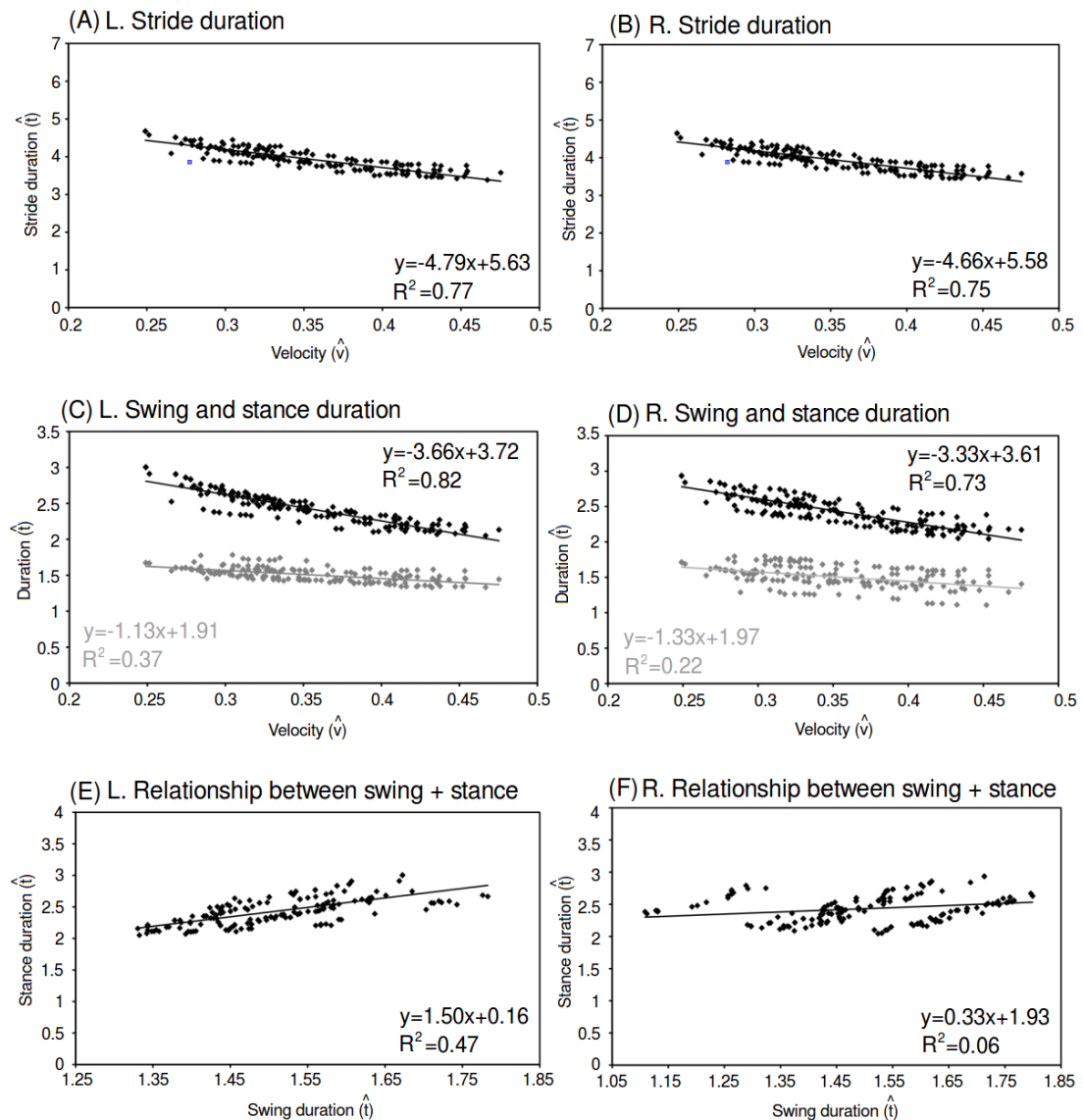


Figure 8.2: **Temporal gait parameters - treadmill walking (sequence 1).** (A), (C) and (E) are the gait parameters calculated for the left leg and (B), (D) and (F) are calculated for the right. In plots (C) and (D), swing is shown in grey, stance in black. In all parameter linear regression analysis, changes in predictor's value (walking speed and swing duration) are related to changes in the response variable. The null hypothesis that predictor variables have no effect on the response variables can be rejected ($P < 0.05$).

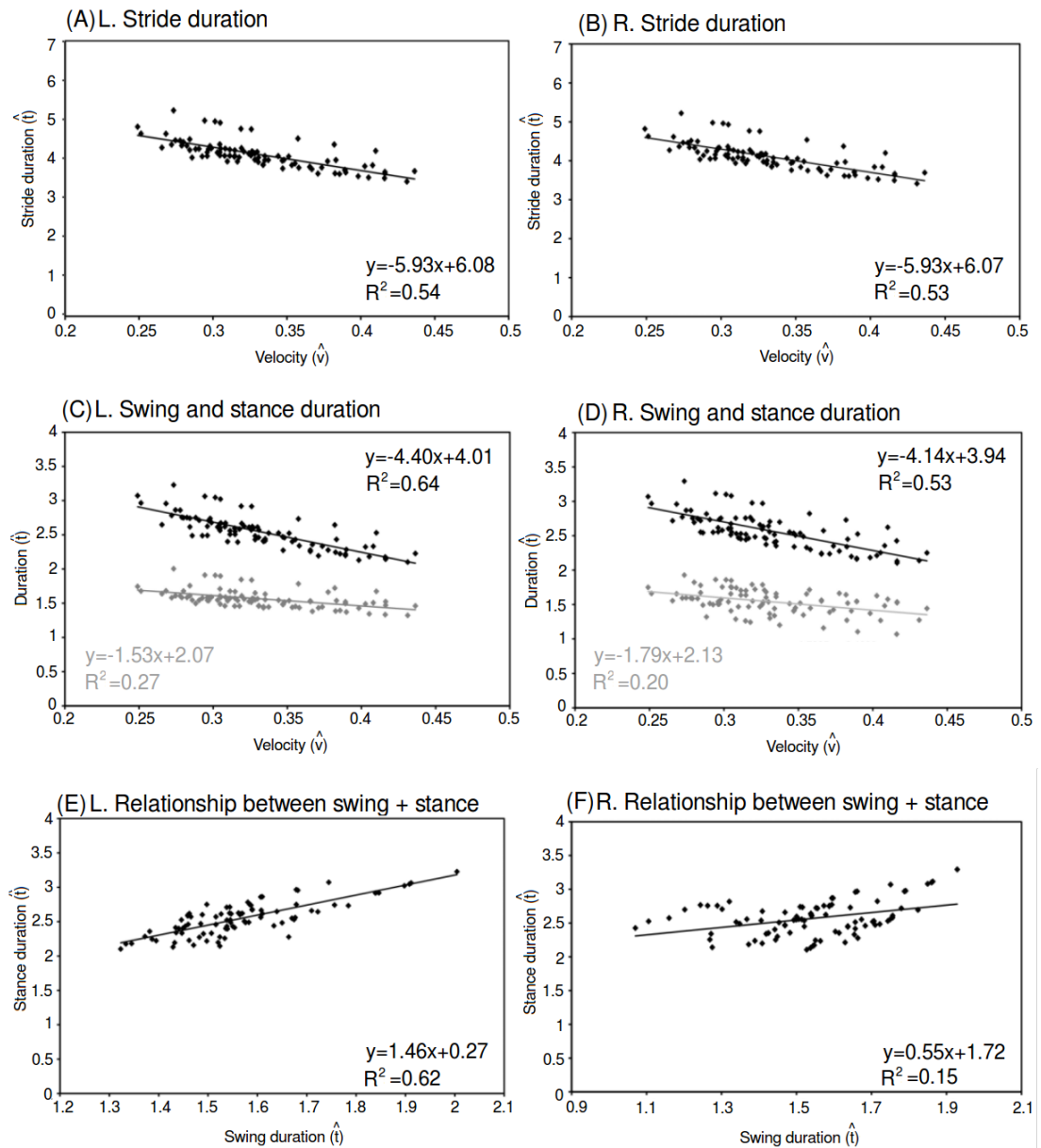


Figure 8.3: **Temporal gait parameters - treadmill walking (sequence 2)**. (A), (C) and (E) are the gait parameters calculated for the left leg and (B), (D) and (F) are calculated for the right. In plots (C) and (D), swing is shown in grey, stance in black. In all parameter linear regression analysis, changes in predictor's value (walking speed and swing duration) are related to changes in the response variable. The null hypothesis that predictor variables have no effect on the response variables can be rejected ($P < 0.05$).

Table 8.1: **Difference in gait parameter values between legs. Provided as both a mean difference value and percent error.** The difference values showed normal distribution over the range of walking speeds.

Modality	Stride duration (\hat{t})		Swing duration (\hat{t})		Stance duration (\hat{t})	
	Difference (Left-Right)	Error (%)	Difference (Left-Right)	Error (%)	Difference (Left-Right)	Error (%)
Overground	-0.03	-0.91	0.04	2.99	-0.07	-3.28
Treadmill seq. 1	-0.87×10^{-3}	-0.02	3.00×10^{-3}	0.20	-3.90×10^{-3}	-0.16
Treadmill seq. 2	1.60×10^{-3}	0.04	0.03	1.61	-0.02	-0.90

leg) and $R^2 = 0.75$ (right leg) and sequence 2 (Fig. 8.3A and B): $R^2 = 0.54$ (left leg) and $R^2 = 0.53$ (right leg)).

The symmetry between the left and right legs can also be compared by looking at the difference and % error values calculated during the different walking modalities, Table 8.1.

The largest difference in gait parameter values between the right and left legs is in the overground walking data. However, overall there is a close relationship between the trends in the gait parameters of the right and left legs suggesting a prediction of symmetry is valid (maximum error of 3% between legs in stance duration during overground walking). It is however interesting to note that the graphs demonstrating the largest degree of difference between legs during both of the treadmill walking sequences, were those showing the relationship between swing and stance (Fig. 8.2E and F, and Fig. 8.3E and F). This is in contrast to the overground walking, where both legs demonstrated a similar swing/stance relationship (Fig. 8.1E and F). This appears to be due to shorter swing durations being recorded in the right leg compared to the left, during treadmill walking, Table 8.1. This may be due to leg preference while walking on the treadmill promoting an asymmetry in the swing phase of the gait cycle.

8.2.2 Muscle activity

Graphs of the population average ERAs are provided in Fig. 8.4, 8.5 and 8.6.

It can be observed in the ERA graphs that the standard deviation is not uniform across the stride and fluctuates according to amplitude changes in the muscle activity during the different phases of the gait cycle. This was also a finding of the preliminary study where the EMG was recorded at only one walking speed (Chapter 3, Section 3.5.2). However, unlike the preliminary study, the varying walking speed produced during both of the treadmill sequences and overground

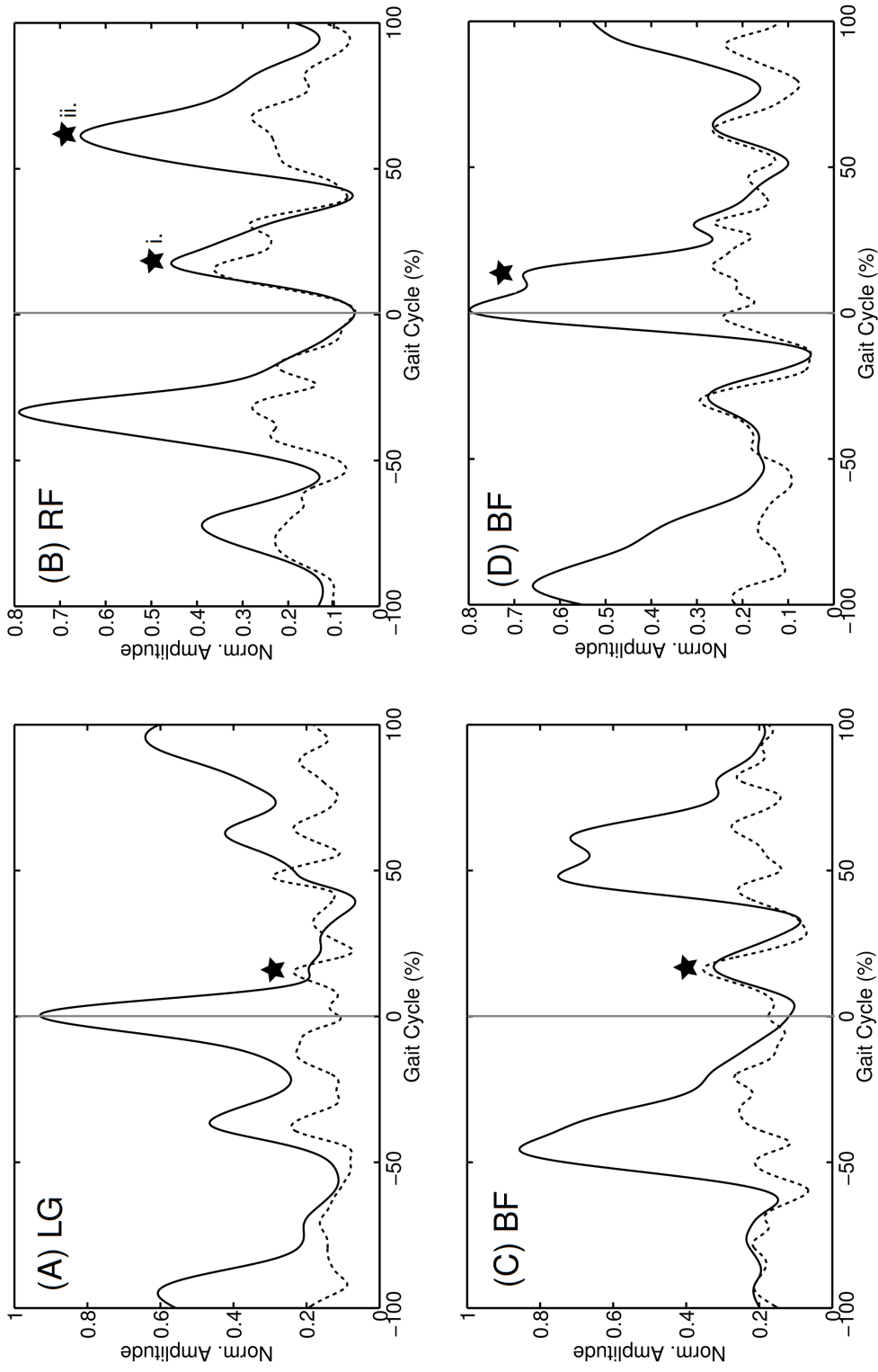


Figure 8.4: **Mean ERA - overground walking.** (-) = $M_{ER\dot{A},mus,CH/IH}$, (- -) = $STD_{ER\dot{A},mus,CH/IH}$, (-) = time of heel contact $t_{FSR,CH/IH}$ and the star highlights the peak associated with hip/knee joint flexion/extension. (A) $M_{ER\dot{A},LG,CH}$ and $STD_{ER\dot{A},LG,CH}$. (B) $M_{ER\dot{A},RF,CH}$ and $STD_{ER\dot{A},RF,CH}$. (C) $M_{ER\dot{A},BF,CH}$ and $STD_{ER\dot{A},BF,CH}$. (D) $M_{ER\dot{A},BF,IH}$ and $STD_{ER\dot{A},BF,IH}$.

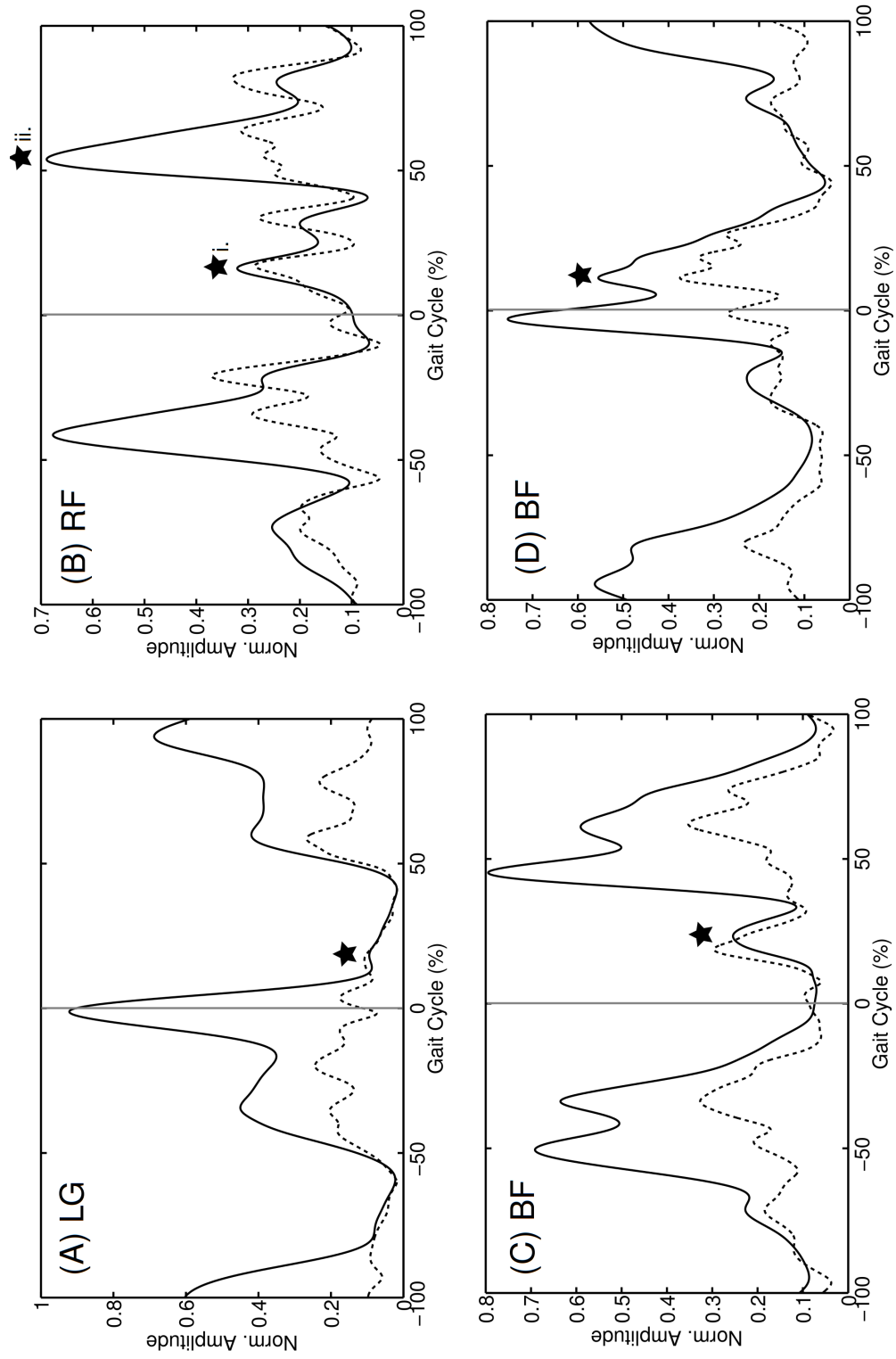


Figure 8.5: Mean ERA - treadmill walking, sequence 1. (-) = $M_{\dot{E}RA,mus,CH/IH}$, (- -) = $STD_{\dot{E}RA,mus,CH/IH}$, (-) = time of heel contact $t_{FSR,CH/IH}$ and the star highlights the peak associated with hip/knee joint, flexion/extension. (A) $M_{\dot{E}RA,RF,CH}$ and $STD_{\dot{E}RA,RF,CH}$. (B) $M_{\dot{E}RA,BF,CH}$ and $STD_{\dot{E}RA,BF,CH}$. (C) $M_{\dot{E}RA,BF,CH}$ and $STD_{\dot{E}RA,BF,CH}$. (D) $M_{\dot{E}RA,BF,IH}$ and $STD_{\dot{E}RA,BF,IH}$.

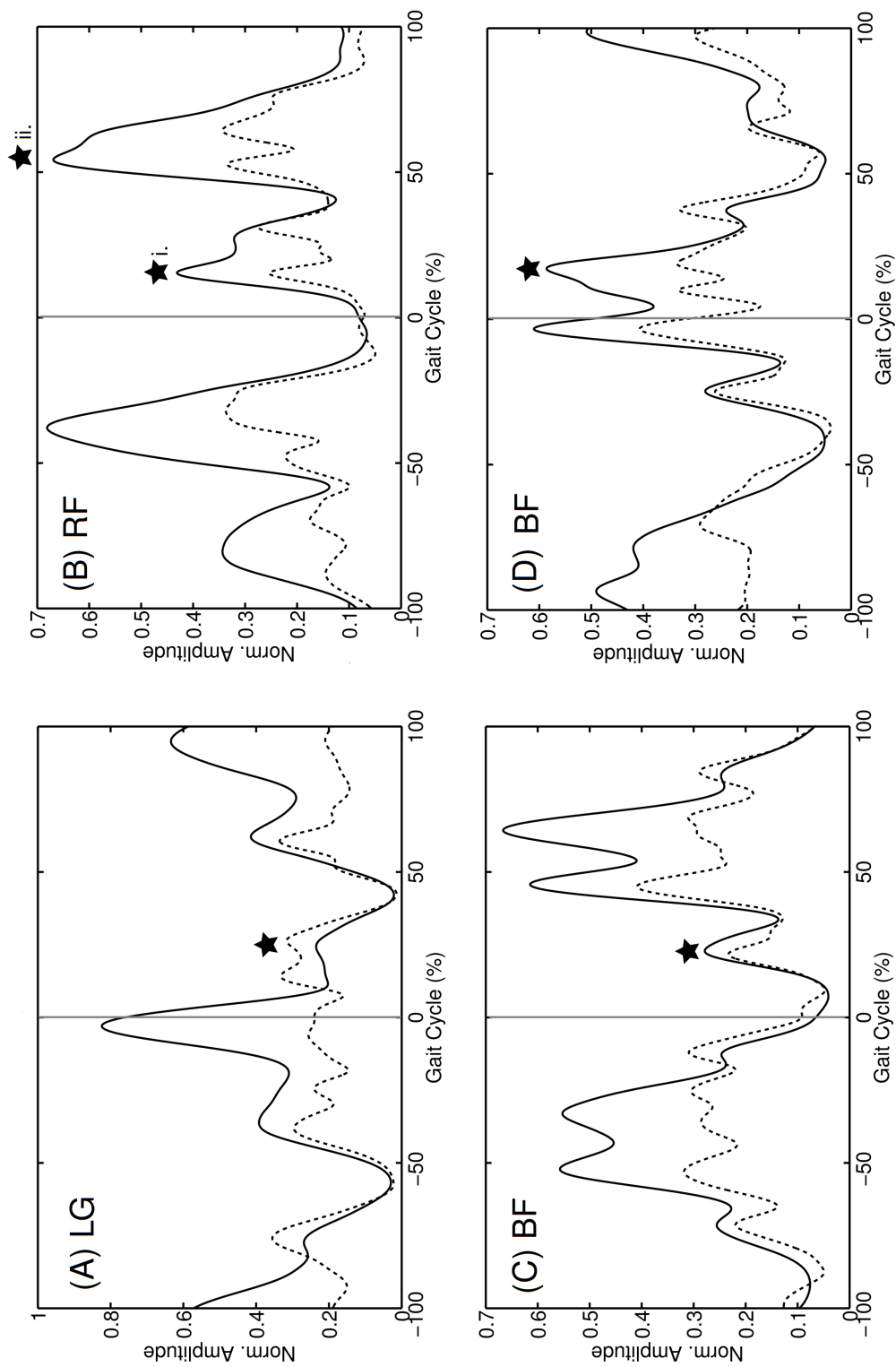


Figure 8.6: Mean ERA - treadmill walking, sequence 2. ((-) = $M_{\hat{E}RA, mus, CH/IH}$, (- -) = $STD_{\hat{E}RA, mus, CH/IH}$, (-) = time of heel contact $t_{FSR, CH/IH}$ and the star highlights the peak associated with hip/knee joint flexion/extension. (A) $M_{\hat{E}RA, LG, CH}$ and $STD_{\hat{E}RA, LG, CH}$. (B) $M_{\hat{E}RA, RF, CH}$ and $STD_{\hat{E}RA, RF, CH}$. (C) $M_{\hat{E}RA, BF, IH}$ and $STD_{\hat{E}RA, BF, IH}$. (D) $M_{\hat{E}RA, BF, IH}$ and $STD_{\hat{E}RA, BF, IH}$.

Table 8.2: Coefficient of variation (CV).

Muscle,CH/IH	Overground	Treadmill seq. 1	Treadmill seq. 2
LG,CH	0.46	0.38	0.63
RF,CH	0.59	0.72	0.58
BF,CH	0.54	0.51	0.70
BF,IH	0.52	0.52	0.72

walking has reduced the variability of the duration of phases of muscle activity in the standard deviation (compare Fig. 8.4, 8.5 and 8.6 with Fig. 3.16 and 3.17). This is most obvious in the reduction of variability in the ERA of the LG muscle (Fig. 8.4A, 8.5A and 8.6A). This suggests that the method of varying the treadmill belt speed during the data collection was successful in removing the influence of walking speed in the ERA and is a closer representation of the variability seen in overground walking than walking on a treadmill with one constant average speed.

The CVs calculated from the three walking methods are provided in Table 8.2 and demonstrate what percentage of the mean the standard deviation represents. Variation between subjects was greatest in the RF muscle during treadmill sequence 2 (72% of the mean value) whereas it was lowest in the LG muscle during treadmill sequence 1 (38% of the mean). All of the CV values calculated from the three walks are large values, which was also a finding in the preliminary study as well (Chapter 3, Section 3.5.2). This data reiterates that averaging muscle activity data over a population produces a significant amount of variability, which makes the average less useful in the analysis of muscle function during walking. It was identified that the variability appears to come from variation in amplitude of the EMG rather than from the duration of different phases of activity. However, the large CV values suggest that averaging may not produce a representative muscle activity waveform containing characteristics featured in an individuals data, which may be important for function.

The timing of peaks in the EMG are important to consider as these peaks were associated with joint motion in the development of a control system for generating walking. Any variation may influence whether the walker is able to coordinate joint motion and produce functional stepping. The ERAs from the three walking methods were plotted on the same graph to visualise the differences in the average muscle activity, Fig. 8.7. The timing of the peaks in the gait cycle were compared to define whether there was any significant difference between the three walking methods, Table 8.3. The timing of the peaks were recorded as a % of the gait cycle

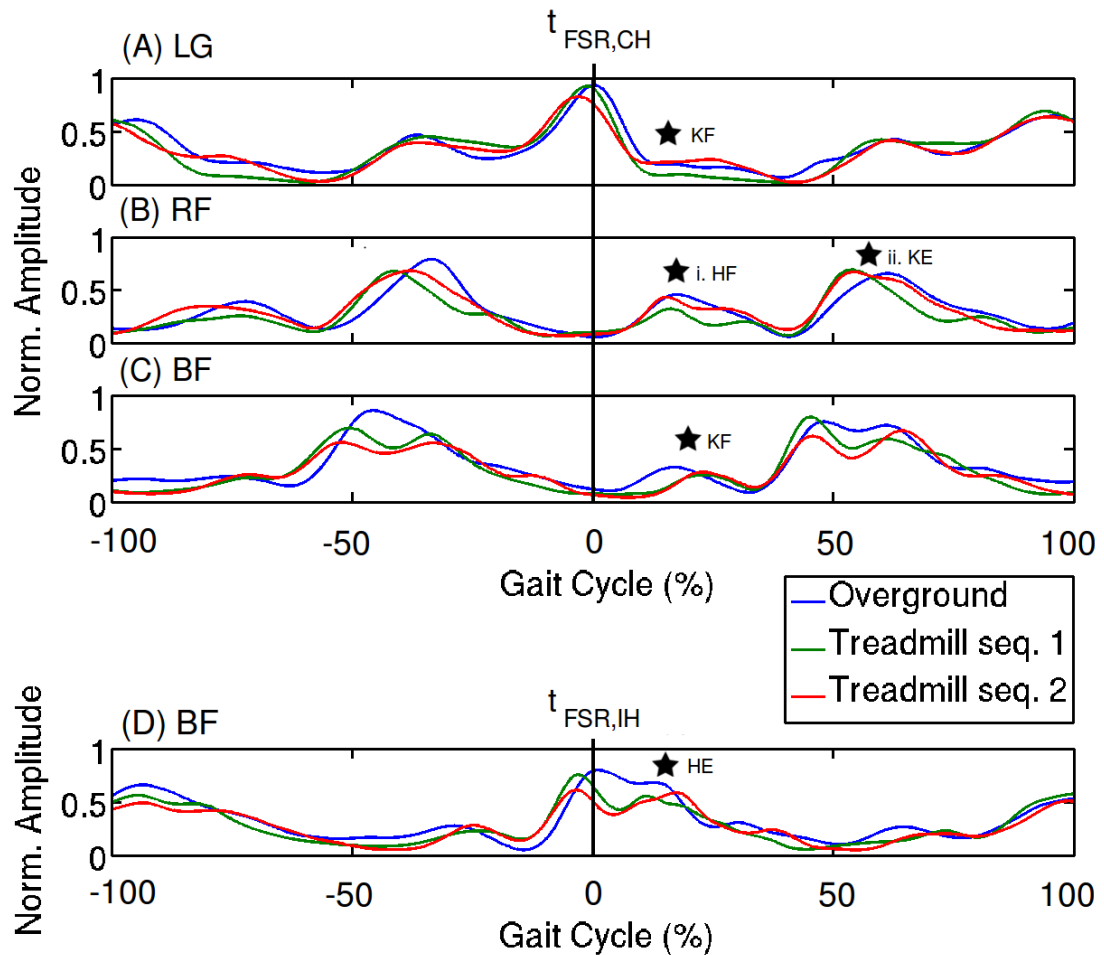


Figure 8.7: **Mean ERAs from the three different walking modalities.** The black line represents the time of the heel contact event ($t_{FSR,CH/IH}$). The stars identify the peaks in the ERA which were related to hip/knee joint actions in the walking control system used with the RunBot robot (KF = Knee flexion, KE = knee extension, HF = hip flexion, HE = hip extension).

and in dimensionless time to account for the different heights and leg lengths of the participants. The data suggests that there is not enough evidence to reject the null hypothesis of equal means between the three walking modalities in the timing of the peaks in activity associated with joint flexion/extension ($P > 0.0167$ using the Bonferroni correction), see Table 8.4. There is however a visual difference in the group ERA plots, with the peak related to knee extension at terminal swing occurring later in the gait cycle (average of 59%) in the overground walking than in the treadmill walking sequences 1 and 2 (55.35% and 56.46% respectively), Fig. 8.7ii and Table 8.3.

Table 8.3: **Time of peaks in muscle ERA.** This average value was recorded as a % of stride. Values are provided as a mean and standard deviation (STD)

Muscle,CH/IH	Overground t_{peak} (%) (STD)	Treadmill seq. 1 t_{peak} (%) (STD)	Treadmill seq. 2 t_{peak} (%) (STD)
LG,CH	21.72 (4.89)	22.50 (5.47)	21.77 (5.63)
RF,CH (i)	18.57 (5.96)	16.85 (5.55)	17.84 (4.42)
RF,CH (ii)	59.81 (5.79)	55.35 (4.79)	56.46 (6.23)
BF,CH	17.80 (4.02)	17.74 (6.52)	19.60 (5.08)
BF,IH	15.64 (7.40)	16.65 (6.02)	17.50 (6.44)

Table 8.4: **Results of the paired t-tests between the three walking modalities.** Three paired t-tests compared the time of peaks in muscle ERA during two different treadmill walking speed sequences and overground walking. Not enough evidence was found to reject the null hypothesis of equal means ($p > 0.0167$).

Muscle,CH/IH	tread 1 - tread 2	tread 1 - overgnd	tread 2 - overgnd
LG,CH	0.900	0.519	0.437
RF,CH (i)	0.817	0.710	0.858
RF,CH (ii)	0.089	0.176	0.502
BF,CH	0.307	0.934	0.240
BF,IH	0.787	0.570	0.628

8.3 Discussion

In comparing the three different walking modalities, overground and treadmill sequence 1 and 2, it is evident that the temporal gait parameters all follow a general trend with increasing walking speed. However, it can be observed that all of the gait parameters are more variable during overground walking compared to during treadmill walking, Fig. 8.1, 8.2 and 8.3. This suggests that treadmill walking is able to control the walking environment and limit external influences, which may produce spurious artefacts within the calculated gait parameters. These include, stumbles, uneven ground surface, obstacles, leg preference and periods of acceleration and deceleration. With use of a treadmill it is also easier to control and monitor the walking speed of the walker. During overground walking, speed was recorded by measuring the time taken for the participant to complete two laps of a figure-of-eight pathway while changes in speed were communicated by verbal commands, as described in Chapter 5, Section 5.2. This means that fluctuations in walking speed throughout the two laps of the circuit are not recorded and could explain the variability seen in the gait parameters.

Although the gait parameters and walking speed were normalised to the participant's leg length, there is distinct grouping seen within the stance duration

versus swing plots during treadmill walking, Fig. 8.2 and 8.3. As expected, the change in stance phase with walking speed is greater than for swing duration. Although both parameters exhibit a decrease in duration with increasing walking speed. It was expected that the relationship between stance duration and swing duration would thus be linear, however the grouping in the plots suggests the relationship between stance duration and swing duration may be dependent on an additional factor. This could be due to individual gait characteristics of the participants which was not compensated for by normalisation. It is interesting to note that this grouping of values was not seen in the overground data, although the variability in the data could be masking it.

The timing of the peaks of activity in the individual subject muscle ERAs were not found to be statistically different between the three walking modalities. However, it is evident in the group ERAs (Fig. 8.7) that the rise time of the peak in the RF at terminal swing (Fig. 8.7Bii) is slower during the overground walking than both of the treadmill walking sequences. It also appears as that the onset of activity related to knee flexion in the BF muscle (Fig. 8.7C) occurs earlier in the gait cycle during overground walking compared to during treadmill walking.

It was clear from the experiments applying the muscle transfer functions to the RunBot robot that the functions associated with hip flexion/extension had the most effect on the gait stability of the robot. Comparing $M_{ERA,BF,IH}$, i.e. Fig. 8.4D with 8.5D and 8.6D in Fig. 8.7D, it is clear that the peak in the BF muscle, which is associated with hip extension, is less distinguishable from the prior peak of activity during overground walking than during treadmill walking, highlighted in Fig. 8.8D. The peak is most well defined in treadmill sequence 2 when the subjects walked for approximately 100 steps at 10 different speed settings. As the knee extends at terminal swing, the BF muscle is lengthening, Fig. 8.8Ai. It is known that the BF muscle has action at terminal swing to decelerate the leg through eccentric contraction [13], which explains the presence of the peak identified in Fig. 8.8C. The observation that the rise time of the peak in the RF at terminal swing is slower during the overground walking will influence the relative eccentric contraction of the BF muscle as it is acting as an antagonist to the action of the RF, Fig. 8.8B and C. It seems logical that the differences seen in treadmill walking are due to the belt movement under the feet counter to the direction of walking. As soon as the leg touches the belt at heel strike, the belt is acting to extend the leg behind the body reinforcing the action of the muscle. This observation may also explain why the fall time of the BF muscle activity peak (Fig. 8.8C) is faster in treadmill walking than

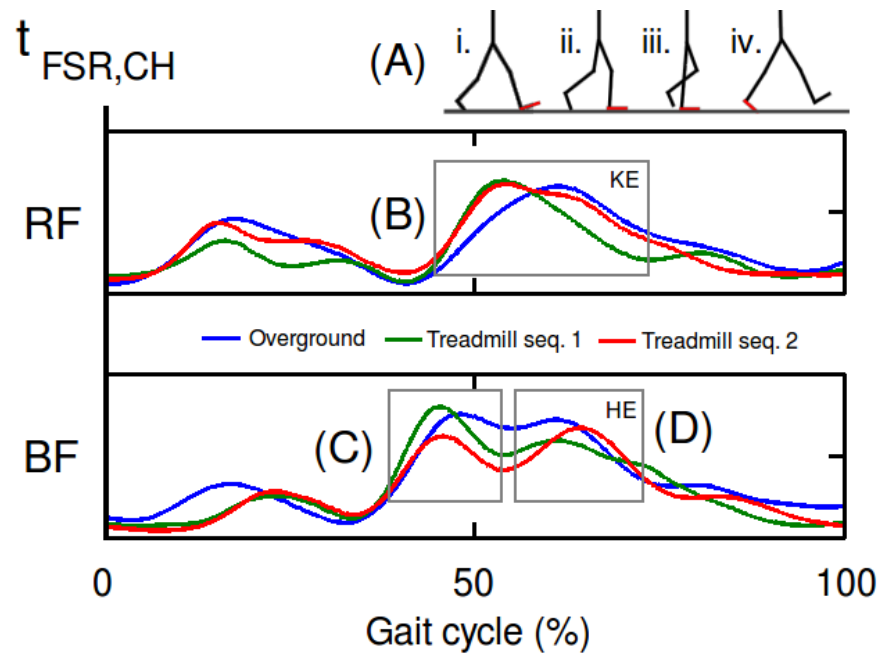


Figure 8.8: **Further detail in the mean ERAs (RF and BF) from the three different walking modalities.** (A) The ipsilateral leg movement related to be muscle activity. (B) The peak in RF muscle activity ERA related to knee extension (KE) at terminal swing. (C) Eccentric contraction of the BF muscle, acting as antagonist to the RF muscle. (D) The peak in BF muscle activity ERA related to hip extension (HE).

during overground walking, as it is related to the movement of the belt rather than forward propulsion of the body. It could also be inferred however, that the participants may be walking with longer step lengths during overground walking compared to during the treadmill walking sequences. Longer step lengths require greater hip flexion during the swing phase. This would also increase the muscle activity in the BF muscle, as antagonist to this action, prior to contraction related to hip extension. The result is a peak in the BF muscle activity related to hip extension that is less distinguishable from the prior period of eccentric contraction in the muscle, Fig. 8.8D. This would relate well to the findings of Murray et al. (1985) who found participants produced shorter step lengths during treadmill walking [244].

The study by Murray et al. (1985) found a statistical difference in quadriceps muscle activity between overground and treadmill walking which differs from the findings of this study [244]. However, it should be noted that previous studies measured statistical difference in the integral of the EMG (defined as the area under the curve of the rectified EMG signal). Using this technique, the amplitude of the EMG will affect the result. In this comparison study, the difference in peak timing was of interest and not amplitude and so the results are not directly

comparable to previous studies.

The results of Lee and Hidler (2008) found that during treadmill walking, participants modified their muscle activation patterns, joint powers and moments while maintaining relatively constant limb kinematics and spatiotemporal gait parameters [248]. Their conclusion was that reduced optic flow during treadmill walking compared to overground walking resulted in altering the participants balance and stability or perception of the position of the body on the treadmill or speed of ambulation.

This is an interesting theory but highlights the adaptability of the human body to compensate for loss, reduction or change of sensory input. What is important is that treadmill walking provides a walking environment which is able to produce a similar gait pattern to overground walking while providing a controlled and safe walking environment, making it a suitable technique for data recording and gait rehabilitation strategies. It is clear that in the BF muscle during overground walking it is difficult to separate the activity at terminal swing and beginning of stance to classify the function as specific to joint action. The treadmill data features a clear trough following heel strike which allows activity related to hip extension to be defined. For this reason the treadmill data are suited to the data analysis used to define the transfer functions for generating stepping compared to overground walking.

Relating muscle activity to foot contact information is key in this thesis study to replace sensory input which is missing or lacking in an individual with spinal cord injury (SCI). It can be seen that although the onset of the activity in the BF relating to hip extension is less well defined in the overground walking data compared to the treadmill data, the timing of the peak in activity is not statistically different.

An ideal control system for generating walking in individuals with SCI needs to be simple and minimal to not override residual function. It can be concluded from this comparison of the different walking modalities that the treadmill walking data provides transfer functions which relate foot contact information and muscle activity with similar gait parameters and properties to overground walking and should produce a functional gait in humans.

8.4 Summary

EMG activity and foot contact information recorded during treadmill and overground walking were compared with the aim of gaining insight into why RunBot

was able to walk using transfer functions calculated from the treadmill data but not from the overground data. Previous studies have indicated minor differences in gait parameters and EMG between the two modalities but to a large extent the reports have been inconclusive. Comparing the data recorded during this investigation, it was clear that a treadmill can provide a stable walking platform producing controllable features such as speed and direction of walking which are difficult to control and monitor overground. Treadmill walking does result in some changes to the muscle activity related to hip extensors, due to the belt actively pushing the foot backwards rather than as a response to forward momentum during overground. However, it can be concluded that a treadmill provides a useful strategy for recording gait data which can then be used to calculate transfer functions for generating stepping.

Chapter 9

Ankle control

Although RunBot II does not feature an actuated ankle it is still valuable to calculate these transfer functions for potential use in the development of a control system for functional electrical stimulation (FES).

The ankle has motion of either dorsiflexion or plantar flexion of the foot during the gait cycle. Using the coordinate data recorded from the leg by the Vicon system, during the wi-GAT validation study (Chapter 4, Section 4.2.4), the motion of the ankle can be visualised. Vicon Plug-in-Gait lower limb marker set and model can be used to calculate the joint angles during the gait cycle and save the data to ASCII file format for post processing. During the wi-GAT study the participants completed ten overground walks at a self-selected, comfortable walking pace. The generated ankle joint angle data were averaged over every recorded gait cycle during the ten walks. The ankle joint motion plots from two participants are provided in Fig. 9.1. From this information a pictorial diagram demonstrating the joint motion during the gait cycle can be generated, Fig. 9.2.

Following heel strike (HS) at the start of the gait cycle, loading of the leg from HS to foot flat (FF) moves the ankle into a neutral position, Dorsiflexion increases during stance as the hip extends the leg behind the body before heel off (HO). Plantar flexion at terminal stance helps push the toe off (TO) the ground and accelerate the leg at the onset of swing. Dorsiflexion during mid-swing works for foot clearance of the ground until HS.

Of the muscles recorded during the treadmill and overground walking studies, the Tibialis Anterior (TA) and Lateral Gastrocnemius (LG) both have action on the ankle joint. By knowledge of the function of these muscles on the ankle joint and whether the muscle action is concentric or eccentric during the gait cycle (Fig. 1.5 in Chapter 1, Section 1.3), the EMG can be analysed for peaks which can be related to joint action using the same procedure as outlined in Chap-

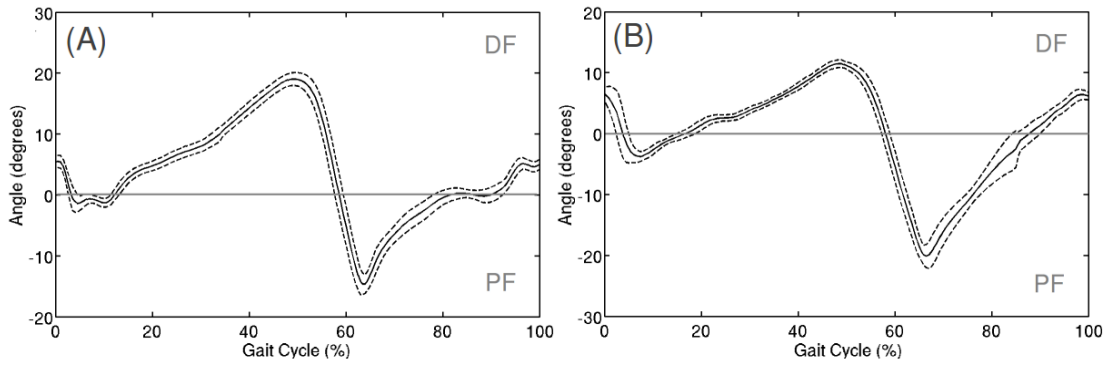


Figure 9.1: **Ankle joint dorsiflexion/planter flexion during human walking.** These plots of the joint motion were calculated using the leg coordinate data recorded over ten moderate speed walks, using the Vicon system. A positive angle denotes dorsiflexion (DF) of the foot, whereas a negative angle is planter flexion (PF). (A) Shows the mean (solid line) and standard deviation (dotted line) from subject C. (B) Subject H.

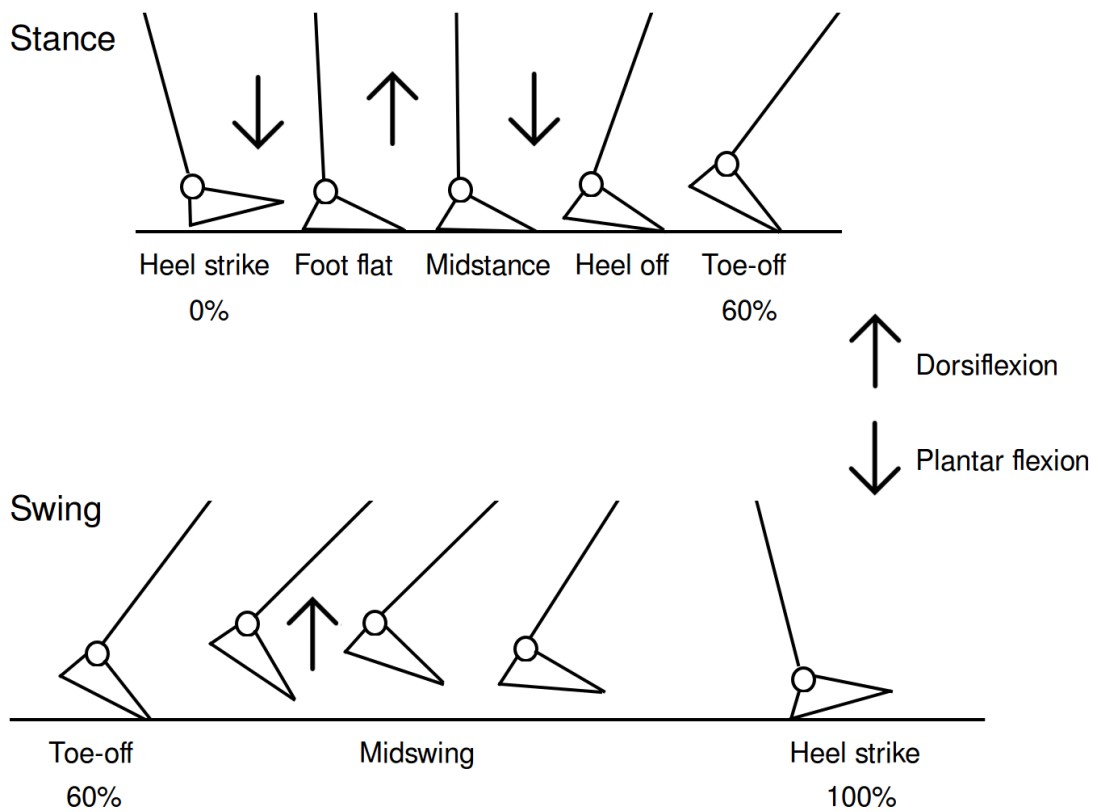


Figure 9.2: **Ankle joint motion during walking.** The joint dorsiflexes and planter flexes the foot during the gait cycle.

Table 9.1: **Relating ankle joint motion with muscle transfer function.**

	Event	Ankle motion	Transfer function
1	HS-FF	Plantar flexion	TA muscle (AEA)
2	FF-HO	Plantar flexion	Eccentric contraction of LG caused by knee extension and counteraction to dorsiflexion to decelerate mass (IH).
3	HO-TO	Plantar flexion	LG muscle (PEA)
4	TO-HS	Dorsiflexion	TA muscle (IT)

ter 6, Section 6.3.1. Before deciding what transfer functions may be necessary for controlling ankle joint motion, the TA and LG activity needs to be analysed in relation to the foot contact recorded from the FSRs during gait. Specifically the FSR under the ipsilateral (I) or contralateral (C) heel $FSR_{CH/IH}$, where output corresponds to foot contact with the ground, and the FSR under the first metatarsal $FSR_{CT/IT}$, where toe-off can be observed as a descending waveform in the output. It should be noted that the FSR under the first metatarsal was chosen to define toe-off rather than the FSR positioned under the subject's big toe. The first metatarsal proved to be more reliable for recording signals compared to the toe, which did not consistently record regular patterns of output during walking. This may have been due to the participant's shoes moving the insole under the foot during walking or the FSR not being accurately positioned under the big toe.

As can be seen from Fig. 9.3, observing a relationship between foot contact and muscle activity for ankle joint motion is not as obvious as for the hip and knee. Using the available information, how each muscle transfer function could be transformed into transfer functions for controlling a potential ankle joint motor in a future generation of RunBot can be discussed, Table 9.1.

As well as the transfer functions relating heel contact information to muscle activity as defined previously, transfer functions relating toe-off information to muscle activity in the TA are also required.

As has been used previously, the EMG activity averaged in relation to a foot contact event (ERAs) can be produced to visualise the relationship between toe-off and muscle activity, and the dependency on walking speed (See Chapter 5, Sections 5.3.1 and 5.3.2). ERAs were produced for the three different walking modalities in which, walking data were recorded: (i) treadmill sequence 1 (Fig. 9.4A), (ii) treadmill sequence 2 (Fig. 9.4B) and (iii) overground walking (Fig. 9.4C).

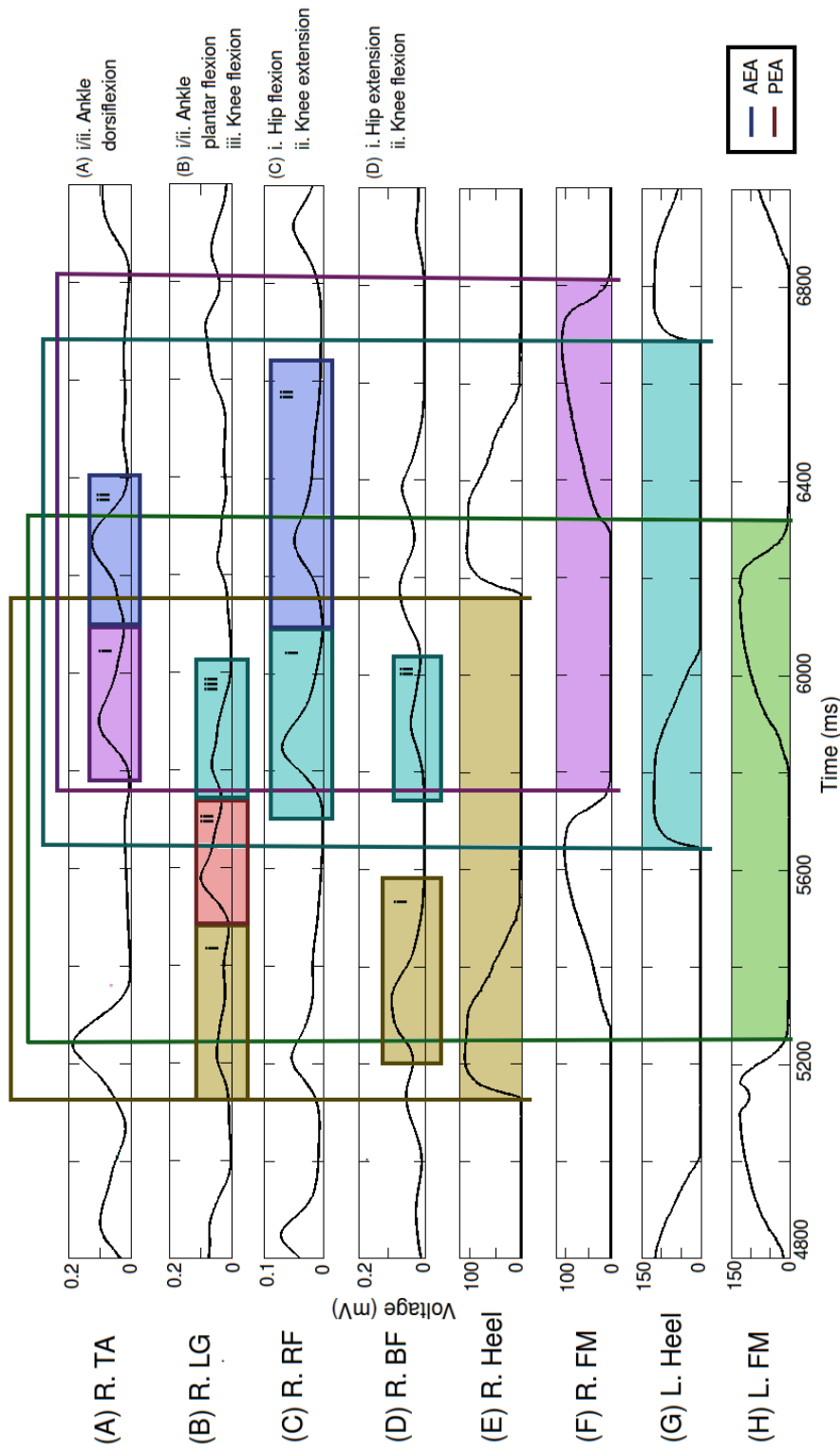
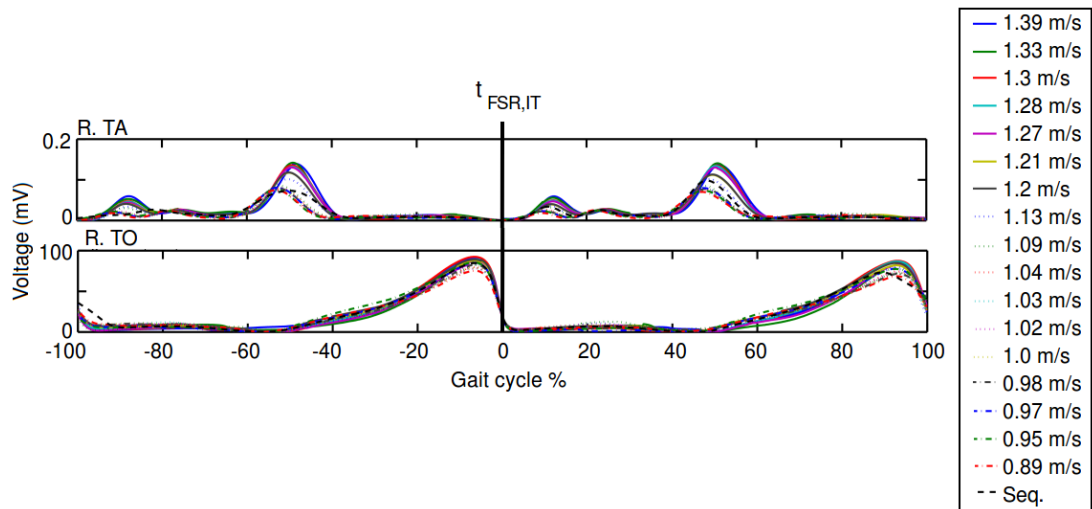
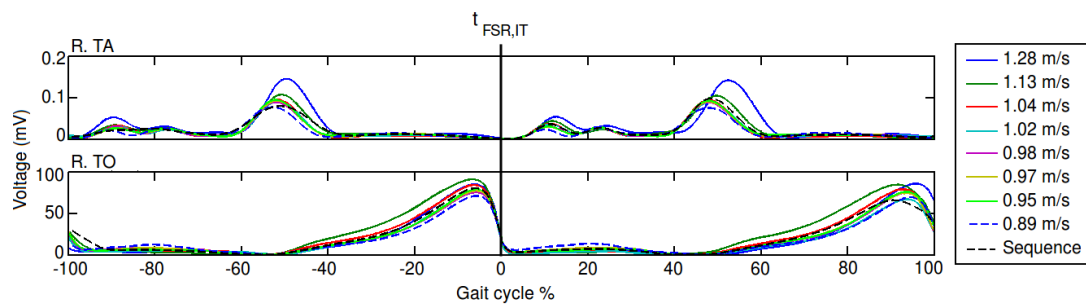


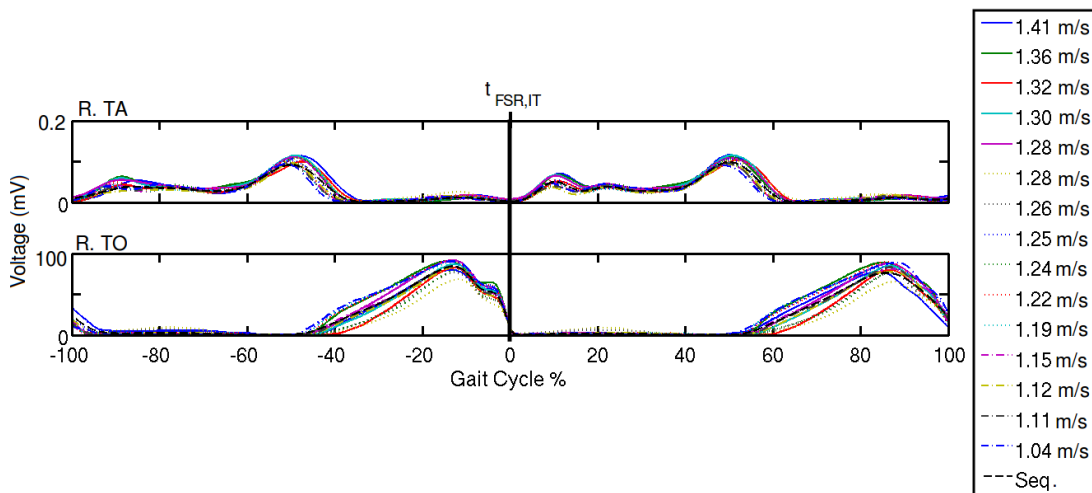
Figure 9.3: **Relationship between foot contact information and muscle activity.** rectified and filter EMG and FSR data for one subject during a short time period of treadmill walking. The relationships between foot contact and muscle activity found for the hip and knee joint transfer functions is also summarised. The diagram indicates how the muscle activation signals are triggered and how they relate to each other. The different colours demonstrate which trigger is used for each peak of activity, i.e. the contralateral heel contact (blue) relates to hip flexion (RF muscle), knee flexion (BF and LG muscles). Similarly ipsilateral toe-off (FM) (pink) is related to ankle dorsiflexion (TA) during swing. AEA (purple) and PEA (red). AEA = anterior extreme angle of the hip, PEA = posterior extreme angle.



(A) Treadmill walking data collection (Sequence 1).



(B) Treadmill walking data collection (Sequence 2).



(C) Overground walking data collection.

Figure 9.4: **Event-related averages of the TA muscle using the ipsilateral toe-off as the trigger.** Graphs taken from one subject as an example. The event is taken as the time of the ipsilateral toe-off (TO). (A) and (B) Data recorded during the treadmill walking study. Where (A) is data recorded during treadmill belt speed sequence 1 and (B) during sequence 2. (C) Data recorded during the overground walking study.

As was observed from the ERAs related to heel contact information (Chapter 5, Sections 5.3.1 and 5.3.2), the amplitude of the ERA EMG related to toe-off increases with walking speed, Fig. 9.4. A phase shift can also be seen with increasing speed, with peaks in the ERA EMG occurring later in the gait cycle with increasing speed. The ERAs from the three different walking modalities appear visually similar, however the shape of the averaged FSR output from under the first metatarsal during overground walking (Fig. 9.4C) is different to that seen during walking treadmill (Fig. 9.4A and 9.4B) with a less sharp drop off at the time of toe-off at the stance to swing transition. It could be inferred from this observation that a more smooth roll of the foot (from the metatarsal making contact with the ground to it lifting off) is seen during overground walking compared to during walking on the treadmill, where the foot is propelled backwards by the moving belt.

The ERA over the entire walking session (black dashed line in Fig. 9.4) demonstrates that recording over a range of walking speeds produces an average in the data removing the dependency on walking speed.

9.1 Calculating transfer functions

The process for calculating the ankle transfer functions was the same as used for the hip and knee, outlined in Fig. 6.6 in Chapter 6, Section 6.3.

The EMG data for the TA muscle in the left or right leg, $EMG_{L/R,TA}$, was first processed using a band pass filter (h_{BP}) (FIR filter, 20-500 Hz) to remove artefacts, then full-wave rectified and low-pass filtered (zero-lag fourth-order IIR Butterworth filter, 6 Hz) to leave the linear envelope of the EMG.

The transfer function coefficients were calculated using the adaptive filtering method for the TA muscle from each of the ten subjects. Adaptive filtering was implemented using MATLAB (version 2012a, The MathWorks Inc., Natick, MA). The functions were calculated from both the treadmill and the overground walking data. Tables of the final mean square error (MSE) of the filter coefficients is provided in Appendix F, Table F3 and F4.

After having found the transfer functions using the human walking data and adaptive filtering ($h_{L/R,TA,IT}$) which connects the ipsilateral toe-off information to the TA activity in the legs, they next need to be processed for use with the RunBot model using the same procedure outlined for the hip and knee joints. As previously, to compensate for the difference in foot contact measurement between the two foot contact measurement systems (foot switches in RunBot and the

FSRs used to measure foot contact during the human walking)¹, and enable the human derived muscle transfer functions to be applied to the RunBot, the transfer functions calculated using the first metatarsal FSR data $h_{L/R,TA,IT}$ were convolved with the mean FSR signal (toe-off to subsequent toe-off) taken from the first metatarsal, one stride duration in length for each subject, FSR_{IT} .

$$H_{L/R,TA,IT}(t) = h_{L/R,TA,IT}(t) * \frac{1}{N} \sum_{k=1}^N FSR_{IT_k}(t) \quad (9.1)$$

Where N is the total number of strides (stride = toe-off to subsequent toe-off) recorded during the treadmill walking.

The impulse response of the filter becomes equivalent to applying an FSR toe-off signal and RunBot can use foot contact impulse trigger signals from the forefoot ($\Theta(G'_{L/R,T}(t))$). These signals would have to be triggered at the start of toe off, so when the contact switches go from 1 to 0. Transfer functions relating to ankle joint motion can now be defined as in Table 9.1.

9.1.1 Tibialis Anterior (TA)

The TA acts to dorsiflex the foot during swing and at terminal swing to stabilise the ankle at HS. Following toe off of the ipsilateral leg (identified using the FSR data from under the first metatarsal), there is a peak in activity related to dorsiflexion of the ankle during swing to provide foot clearance of the ground. The transfer function ($H_{L/R,A,D}$) relating the TA to dorsiflexion during swing (D_S) of the ankle (A) and be defined as:

$$H_{L/R,A,D_S}(t) = \begin{cases} H_{L/R,TA,IT}(t + t_{TA,IT,start}), & 0 \leq t \leq (t_{TA,IA,end} - t_{TA,IA,start}) \\ 0, & \text{otherwise} \end{cases} \quad (9.2)$$

Where $t_{start/end}$ is the identifiable trough before and after the peak in the data associated with the ankle dorsiflexion and t_{gait} is the total duration of the gait cycle (i.e $t_{gait} = 100\%$). The transfer function could be applied to a control system for the ankle as follows,

$$U_{L/R,A,D_S}(t) = B_{L/R,A}(t) \cdot H_{L/R,H,F}(t) * \Theta(G'_{I,T}(t)) \quad (9.3)$$

Where, $B_{L/R,A}$ would define a parameter for preventing the ankle joints dor-

¹It is assumed that a RunBot with an actuated ankle joint would feature two contact switches in the feet, one at the forefoot for signalling toe-off and one at the heel for measuring heel contact.

siflexing or plantar flexing beyond an extreme angle threshold ($\theta_{A,D/P} < \phi_A < \theta_{A,P/D}$) by limiting the motor voltages to prevent mechanical damage. This is the same idea as described for the general hip and knee control of RunBot II, see Eqn. 6.6a, 6.6b, 6.6c and 6.6d in Chapter 6, Section 6.3.

When the knee extends at terminal swing triggered by the hip reaching its anterior extreme angle (AEA) there is also simultaneously an increased dorsiflexion of the foot to stabilise the ankle in preparation for HS. From HS to FF the TA muscle de-contracts from this dorsiflexed position causing the fore foot to make contact with the ground to allow loading of the leg during stance.

Similar to the peak in the RF muscle relating to knee extension at terminal swing, the peak in the TA relating to dorsiflexion of the foot at terminal swing does not relate well to contact information from the foot. As the onset of activity corresponds well to the onset of activity in the RF, it would be logical to use the same trigger for both joint motion actions.

The angular sensory information from the hip was used to trigger the knee extension. The Anterior Extreme Angle (AEA) of the hip joint was used as the trigger signal for $H_{L/R,K,E}$, Eqn. 6.10, instead of foot contact. When the hip flexion angle reaches a threshold, the knee motor extends the leg to prepare for foot contact with the ground. For the ankle dorsiflexion at terminal swing (D_{TS}), the AEA can also be used so it starts at the same time as knee extension to prepare the foot for heel strike. Like the for knee extension at terminal swing, dorsiflexion of the foot at terminal swing can be described from the transfer functions relating to the contralateral heel and then defined for an ankle control system using the AEA as the trigger.

$$H_{L/R,A,D_{TS}}(t) = \begin{cases} H_{L/R,TA,CH}(t + t_{TA,CH,start}), & 0 \leq t \leq (t_{LG,IH,end} - t_{LG,IH,start}) \\ 0, & \text{otherwise} \end{cases} \quad (9.4)$$

$$U_{L/R,A,D_{TS}}(t) = B_{L/R,A}(t) \cdot H_{L/R,A,D_{TS}}(t) * \Theta(B'_{I,H}(t)) \quad (9.5)$$

Where, $\Theta(B'_{I,H}(t))$ is the impulse trigger signal when the ipsilateral hip reaches the AEA.

9.1.2 Lateral Gastrocnemius (LG)

The LG muscle plantar flexes the foot at terminal stance to push the foot off the ground at TO to begin swing. Observing the muscle activity in relation to the

foot contact information recorded from the FSRs, there is no obvious correlation, which suggests foot contact is not the cause of plantar flexion. As has been discussed for the TA for dorsiflexion and the RF for knee extension at terminal swing, hip angle is a suitable alternative to foot contact information for triggering plantar flexion at terminal stance. As the hip is fully extended behind the body before toe-off it would be logical to assume a relationship between the posterior extreme angle (PEA) and plantar flexion of the foot. RunBot already has the ability to measure PEA in the same way it measures AEA. The transfer function $H_{L/R,A,P}$ for plantar flexion at terminal stance can be described from the transfer functions relating to the ipsilateral heel and then defined for RunBot's control system using the PEA as the trigger.

$$H_{L/R,A,P}(t) = \begin{cases} H_{L/R,LG,IH}(t + t_{LG,IH,start_2}), & 0 \leq t \leq (t_{LG,IH,end_2} - t_{LG,IH,start_2}) \\ 0, & \text{otherwise} \end{cases} \quad (9.6)$$

$$U_{L/R,A,P}(t) = B_{L/R,A}(t) \cdot H_{L/R,A,P}(t) * \Theta(B'_{I,H,P}(t)) \quad (9.7)$$

Where, $\Theta(B'_{I,H,P}(t))$ is the impulse trigger signal when the ipsilateral hip reaches the PEA. Here, $(\phi_H = \theta_{H,E})$. The values used for the extreme joint angles can be found in Appendix E, Table E1.

Although there is evidence of the LG contracting, producing plantar flexion of the ankle during stance, this is due to eccentric contraction due to the extension of the knee and hip and the muscle having action to counteract the dorsiflexion of the foot and decelerate the leg during stance. Thus its action can be seen as the muscles mechanical response to other primary activity within the leg and not valuable to add to the control system creating a functional ankle for RunBot.

9.2 Ankle transfer functions

Finally, curve fitting of the functions using the impulse response of a critically damped system, as described in Chapter 6, Section 6.3.2, produces the final transfer functions which could be used to produce a functional ankle for RunBot ($\hat{H}_{L/R,A,D_S}$, $\hat{H}_{L/R,A,D_{TS}}$ and $\hat{H}_{L/R,A,P}$).

The final equations for both legs which define a control system for an actuated ankle are as follows:

$$U_{L/R,A,D_S}(t) = B_{L/R,A}(t) \cdot \hat{H}_{L/R,A,D_S}(t) * \Theta(G'_{I,T}(t)) \quad (9.8a)$$

$$U_{L/R,A,D_{TS}}(t) = B_{L/R,A}(t) \cdot \hat{H}_{L/R,A,D_{TS}}(t) * \Theta(B'_{I,H}(t)) \quad (9.8b)$$

$$U_{L/R,A,P}(t) = B_{L/R,A}(t) \cdot \hat{H}_{L/R,A,P}(t) * \Theta(B'_{I,H,P}(t)) \quad (9.8c)$$

9.3 RunBot ankle transfer functions

Comparing RunBot's motor control with human muscle activity has shown that it is possible to use human muscle transfer functions to control RunBot's motors. The difficulty with using the transfer functions defined for ankle control (Eqn. 9.8a, 9.8b and 9.8c) can be seen in using the TA muscle to plantar flex the foot between HS and FF. In the human this action is due to the TA dorsiflexing the foot in preparation for heel strike and then at HS the TA muscle relaxes causing the foot to return (plantar flex) to a neutral position. In the robot, when a leg motor has completed the action of flexion/extension it remains in the final angular position until counteracted by a function relating to extension/flexion. For this purpose, instead of using Eqn. 9.8b to dorsiflex the foot at terminal swing, as RunBot's foot will already be in a dorsiflexed position due to Eqn. 9.8a at TO, this function can instead be used to plantar flex the foot to FF. This would however have the effect of the robot plantar flexing it's feet prior to foot contact, which may give the appearance of it pointing its toes in a similar style to the gait of a dancer. Thus using the ipsilateral heel contact as a trigger may provide be a suitable solution for providing the correct joint action with timing in the gait cycle to match the typical human gait cycle.

The resulting function (Eqn. 9.9) can thus replace Eqn. 9.8b for applying to the control system.

$$U_{L/R,A,P_{TS}}(t) = B_{L/R,A}(t) \cdot \hat{H}_{L/R,A,P_{TS}}(t) * \Theta(G'_{I,H}(t)) \quad (9.9)$$

9.4 RunBot testing

For future testing of the functions for ankle control with RunBot in relation to the previously calculated functions for the hip and knee joints, the same sets of functions calculated for the hip and knee joints would be used, see Table 7.1 and 7.4. It would be logical to first test the addition of ankle functions to the transfer function sets which already produce stable walking in RunBot, i.e set

1B, 3B, 4B, 5A, 6A and 6B. As none of the overground transfer function sets produced a stable gait in RunBot it would be interesting to investigate whether the addition of an actuated ankle joint actually resulted in producing an overall stable system. For this reason, all sets should be tested again, i.e set 1, 2, 3, 4, 5 and 6. The parameter values for these functions calculated from the curve fitting are provided in Table 9.2 and 9.3. Goodness-of-fit statistics for the curve fitting are provided in Appendix G, Table G4 and G4.

Table 9.2: **Results of the curve fitting for ankle dorsiflexion/plantar flexion - treadmill.**

Set	$\hat{H}_{L/R,A,P}$			$\hat{H}_{L/R,A,D_S}$			$\hat{H}_{L/R,A,P_{TS}}$		
	τ_1 (ms)	τ_2 (ms)	δ (ms)	τ_1 (ms)	τ_2 (ms)	δ (ms)	τ_1 (ms)	τ_2 (ms)	δ (ms)
1B	107.50	107.50	300	84.90	84.90	0	117.40	117.40	300
3B	114.50	114.50	270	88.45	88.45	0	116.05	116.00	305
4B	62.05	62.05	415	64.75	64.75	0	147.65	147.65	305
5A	112.25	112.25	345	93.75	93.75	0	75.25	75.25	370
6A	79.55	79.55	475	103.30	103.25	0	93.65	93.65	335
6B	85.35	85.35	495	98.10	98.10	0	112.85	112.80	340

Table 9.3: **Results of the curve fitting for ankle dorsiflexion/plantar flexion - overground.**

Set	$\hat{H}_{L/R,A,P}$			$\hat{H}_{L/R,A,D_S}$			$\hat{H}_{L/R,A,P_{TS}}$		
	τ_1 (ms)	τ_2 (ms)	δ (ms)	τ_1 (ms)	τ_2 (ms)	δ (ms)	τ_1 (ms)	τ_2 (ms)	δ (ms)
1	81.20	81.10	375	67.95	67.95	0	88.25	88.25	325
2	102.05	102.05	415	62.95	62.95	0	108.55	108.55	290
3	92.25	92.25	435	67.60	67.60	0	107.90	107.90	265
4	75.45	75.45	425	61.50	61.50	0	66.20	66.20	355
5	57.10	57.10	430	107.95	107.95	0	64.45	64.45	485
6	87.85	87.85	450	67.80	67.80	0	72.25	72.25	335

9.5 Summary

This chapter describes the addition of ankle control to the reflexive control system for walking. The transfer functions related to dorsiflexion and plantar flexion of the foot were calculated using the same process outlined for hip and knee flexion/extension, with the addition of toe-off information being used for causal

control of foot dorsiflexion during swing. Although the calculated transfer functions and control cannot be tested on RunBot II at present, due to the robot not featuring an actuated ankle joint, the functions and control could be integrated with the system described for the hip and knee to create a full system for walking generation. This has potential use in future development of the robot and in developing a controller for FES with application in gait rehabilitation in individuals with SCI.

Chapter 10

Discussion

The development of a reflexive control system based on filter functions calculated from human walking data, aimed to demonstrate that using sensory feedback can be a successful method to generate stable and coordinated limit cycle stepping. The research outlined in this thesis has shown that there is a positive correlation between foot contact information and muscle activity during human walking. This relationship allowed causal filter functions to be calculated which reproduce the activations of the relevant muscles after foot contact. The reflexive controller was applied to the RunBot II robot as a proof of concept. The control mechanism exploits the natural dynamics of the robot for motion generation without the requirement of central pattern generators, trajectory planning or tracking control.

10.1 Interpretation of results

Foot contact is commonly recorded for use in gait analysis as a method of determining spatial and temporal parameters such as stride length, cadence and predicting the onset and timing of gait cycle events. This information can be used alongside EMG data for analysis of muscle function to classify normal and identify pathological gait [208]. For this purpose, the generalised muscle activity patterns in relation to a normalised gait phase (0 to 100%) have been long documented [195]. In addition, different strategies for generating control based on muscle activity and foot contact information have been studied by others for use in research on human motor control and in rehabilitation engineering. These include simulated systems based on human data and control derived directly from biosignals, an area of research commonly known as brain-computer interfaces (BCI), for review [159]. However, to the author's knowledge, the transfer functions which directly relate foot contact and muscle activity within humans,

either averaged from a population or from an individual, have not been calculated to create a minimalistic, linear, analogue control system for applications in gait control.

The relationship between muscle activity and walking speed is of interest as it influences how foot contact information could be used as a trigger for muscle activation for applications in gait rehabilitation and robotic biped walking design. In human studies it has been documented that the stance phase of gait decreases as speed increases [250]. And it has been shown that the timing of certain gait phases occurs earlier in relative stride time as speed increases, particularly in the TA, LG, and RF muscles. The EMG patterns also tend to become more consistent with an increase in walking speed, with slow speeds causing an EMG pattern dependent on the muscle characteristics and motion of the specific individual [189]. By varying the speed of the treadmill and recording over over-ground walking, the aim was to remove the correspondence between the patterns in muscle activity and walking speed. However, changes to the gait phase timing of muscle activity during ramp acceleration and deceleration is less well understood with the majority of studies focusing on EMG analysis at constant walking speeds. This is a valuable consideration since each of the data collection modalities included periods of acceleration and deceleration between constant walking speeds which were included in the calculation of the muscle transfer functions. It could be considered that a reason for treadmill sequence 1 (25 steps per speed) being less successful in producing a functional and stable gait pattern in RunBot, compared to treadmill sequence 2, is due to the influence of the larger number of acceleration/deceleration periods and reduced constant walking speed duration. The second sequence provides a higher number of complete gait cycles at every steady-state speed which produced an average which was less skewed by the periods of acceleration and deceleration. The effect of acceleration and deceleration on the muscle activity may be interesting for further study and demonstrate whether the muscles demonstrate a specific adaptive pattern of activity related to these actions. In addition, it could be argued that walking when the speed is changing rapidly (every 25 steps) is challenging and demands more of a conscious awareness and effort to constantly adapt the stepping to maintain balance of the body and stability of the gait pattern. It has been shown that adaptation of gait to the changing walking conditions is faster with conscious control compared to during normal walking conditions on a split-belt treadmill [251,252]. Specifically this was seen in spatial elements of walking (i.e. the centre of oscillation of the limbs and stepping distance). If conscious effort was indeed more prevalent as

subjects walked during treadmill sequence 1, it would then be prudent to assume that this could translate into differences in transfer functions related to the average of the entire walk.

However, another simple reason for the variation in results between the treadmill sequences could be due to the range of treadmill belt speeds used in the second sequence. This range was 0.11 m/s smaller than the first, which may have produced a stride average more compatible with the RunBot's mechanical structure. As RunBot's design is not a scale representation of human leg length and mass ratios, the faster walking speeds used in the first sequence may have produced stance to swing ratios which were incompatible with RunBot's design and construction.

10.1.1 RunBot walking results

Treadmill walking data

Application of the human transfer functions to the RunBot II robot showed that a functional and stable gait pattern could be generated. This demonstrates that a simple mechanical system can walk using causal transfer functions calculated from human data. However, there were observed differences between the gait generated using the different sets of transfer functions. Different sets were used in an attempt to identify whether there are differences between averaged data and data from individual participants.

The findings were that transfer functions from individual participants were more likely to produce functional walking in RunBot compared to averaged data or a set of transfer functions from different subjects combined. It can be concluded that individual data are more likely to produce a coordinated joint motion enabling a functional gait pattern to be generated. This finding suggests that variations in the transfer functions observed between the individual participants are due to natural variation in physiology and gait characteristics which, when averaged, lose the coordinated action on the joints required for a functional gait. This makes these functions less appropriate for use in SCI rehabilitation.

Although averaged gait data from a healthy population has been used in the design of gait rehabilitation devices including the Lokomat [253], these devices may require gait pattern adaptations to suit the individual walker and promote recovery of a functional gait. Where the device simply 'replays' a standard gait pattern as accurately as possible, the patient remains passive and the kinematic variability is minimal. This is undesirable as both active participation and vari-

ation in kinematics are considered as vital in the promotion of motor learning in rehabilitation [254–256]. The current Lokomat uses position control to realise a physiologic-like gait-pattern that was recorded from a single healthy subject walking in an unactuated Lokomat [23]. It does this by using path control strategies to ensure that the spatial kinematics of the legs stay within definable desired limits [256, 257] while integrating automatic gait pattern adaptation algorithms to improve in the functionality of the gait, by introducing a degree of voluntary locomotor capability [258]. The idea behind the reflexive control system for gait is that the movements are minimally imposed on the walker and are not based on a fixed gait pattern or joint trajectories. Using this strategy the natural dynamics of the walker influence the walking and so the mechanism should reinforce residual movement ability of individuals with SCI to promote functional stepping. This system reinforces the crucial role of kinematic variability during motor learning, expressed by Bernstein as “repetition without repetition” which he based on practical experiences and theoretical consideration [254].

Comparing the walking speeds achieved using each of the different transfer function sets, set 5A produced the fastest average speed which was from a single male subject. However when scaled to leg length (Fig. 7.3 in Chapter 7, Section 7.1.2), RunBot’s walking speed is approximately half of what the human subjects achieved walking at a constant average speed. This could be attributed to reduced energy efficiency in the robot’s mechanical design by lack of an actuated ankle joint which would provide the addition of a push off force from the foot at pre-swing. Currently the knee motor has to lift the weight of the lower leg without major contribution from a ground reaction force. It would be interesting to examine whether the addition of an actuated ankle joint in RunBot II, controlled using human muscle transfer functions as in the hip and knee motors, increased the relative walking speed of the robot significantly.

Overground walking data

The transfer functions calculated from overground walking were found to not produce functional gait in the RunBot II robot. The short duration of the function related to hip extension was found to be a factor in understanding the differences between the transfer functions generated from the treadmill and overground walking modalities. This was suggested as being influenced by participants taking shorter step lengths on the treadmill compared to during the overground walking, producing a loss of definition of when the BF muscle is eccentrically contracted due to stretch and concentrically contracted to promote hip exten-

sion. This provides a problem in applying the transfer functions to the robot as it does not feature the properties of human muscle in the control of its hip joint but in using the calculated transfer functions with humans it may be found that these functions can produce a functional and coordinated hip movement. This remains to be seen. However, what is evident from comparing muscle activity and gait parameters recorded over the different walking modalities is that treadmill walking can replicate similar gait parameters and muscle activity to that seen during overground walking with the advantage of controlling walking speed and simplifying data collection setup making it suitable for the recording of EMG and FSR data in this research study.

10.1.2 Limitations

There are some limitations to the present study which need to be considered. Although using a robot to test elements of a control system for walking provides a simple and controlled method of experimentation, its mechanical structure is not an accurate scale representation of the human body and with anthropomorphic differences and lack of trunk rotation the effect of applying the control system to humans cannot be conclusively deduced. Its lack of trunk and arms may also affect the stability due to the robot needing to keep its centre of mass forward to ensure a stable gait. The robot is a planar robot (supported in the sagittal plane) and so cannot demonstrate lateral movements which will be an important consideration in successful gait rehabilitation. However, the robot does allow the theory of the reflexive control system using transfer functions calculated from human data to be tested on a basic and simple mechanical model, without the complexity of the human body. This enables conclusions to be made on the suitability of the approach before the development of a rehabilitation strategy for use with humans.

During the experimentation with RunBot II, only transfer functions from two individual participants were applied to the robot. As these transfer function sets were found to be the most successful in producing a functional gait in the robot it would have been interesting to apply the transfer functions from each of the ten participants to further support this conclusion. This technique would also allow comparison between the functions from the female and male subjects to analyse the effect on RunBot's gait. This is of interest as there are gender differences in anatomy and sagittal plane joint mechanics which may affect the resulting gait function [259].

One observation of RunBot's gait was that the robot was able to return to

a stable limit cycle when a disturbance originating from an unevenness of the ground surface was encountered. This behaviour was not studied further but it would be interesting to analyse the gait stability when perturbations are introduced to the robot. This will demonstrate the robustness of the system to adapt to the loading conditions.

Hip anterior extreme angle (AEA) was used in the final control system for causal control of knee extension at terminal swing. Although this technique proved to successfully produce functional gait it was a limitation of the study as this control mechanism was not based on data recorded from the healthy subjects during the treadmill and overground walking data collection. Instead, the transfer functions were calculated from those related to contralateral heel strike so may not demonstrate the actual transfer functions which relate the hip angle and muscle activity. It would thus be prudent to repeat the data collection to include the recording of hip angle information during gait to further study this relationship. This would also be beneficial in calculating the hip AEA value for applying these transfer functions in a human model.

Throughout this research, the assumption was made that the leg joints are simple joints with one axis of rotation. In the case of RunBot this is true, but in humans the leg joints provide multiple degrees of freedom and this is something which may warrant further development and understanding as a potential limitation to the proposed control system. This may be a particular issue with the ankle joint which has had its actions considerably simplified in the control system and may prove difficult to control in an individual with limited voluntary control. This will influence the stability and efficiency of the generated gait cycle. As heel contact is the main sensory input within the control system, correct foot placement is a vital consideration in generating functional stepping. One strategy for use of the system with patients could be the addition of an articulating ankle orthosis to restrict the ankle rotation planes and support correct foot placement during ground contact.

10.2 Human walking

In human walking, several studies have indicated that ground reaction forces influence the locomotor activity of the leg [120–122] and the action of plantar pressure signals from the foot sole have been implicated in the reflex regulation of locomotion [123–125]. Research involving spinalised and decerebrated animals has suggested that afferents from the foot sole interact with the neuronal cir-

uits involved in stepping. Sensory afferents in the sole of the foot signal spinal interneuronal circuits which can delay or suppress the initiation of swing, encouraging the stance phase as well as contribute to the correct placement of the foot during stepping [82, 84, 124, 126]. Load receptors can also act to signal unloading of the limb following heel strike of the contralateral leg and contribute to the termination of stance [39]. There is a significant amount of afferent activity originating from the skin of the foot after ground contact [128], which suggests there is potential that this information could be used to reinforce the ongoing muscle activations during stance. In addition, research studying electrical stimulation of nerves that supply the skin of the foot suggests that strong reflex activations in various leg muscles can be triggered during human gait [127].

It can be considered that sensory feedback from the foot sole may be of major significance in the control of human walking. The reflexive controller described in this thesis uses heel contact as a sensory input trigger to activate muscles relating to flexion/extension of the hip or knee joints. The only exception to the rule is employing the hip AEA to determine the moment for knee extension at terminal swing because, for this event, there is no causal relationship between heel contact and muscle activity. A stable transition from swing to stance is dependent on the swing leg becoming sufficiently protracted before ground contact. For this reason position of the hip is a suitable candidate for producing an afferent signal regulating swing-to-stance transition [196]. A direct connection between joint angle and motor output is inspired by reflexes found in different animals [196, 197] and also in humans [6]. When the limb of an animal reaches an extreme position, joint and muscle stretch receptors signal the controller to reset the phase of the limbs [172]. The role of hip position in regulating the stance-to-swing transition has been well documented within animal models [76, 77] and in human infant stepping [111, 260]. Hip angle contribution to swing-to-stance transition during the swing phase of walking is indicated as the position of the hip closely reflects the forward motion of the leg. Studies involving decerebrate cats found that assisting flexion movements of the hip joint shortened the burst duration of activity within the Iliopsoas hip flexor muscles and promoted early onset of activity in the Medial Gastrocnemius producing ankle extension. This is significant as burst activity in ankle and knee extensors occurs at the swing-to-stance transition just prior to ground contact [196]. There is also evidence that feedback from stretch receptors is vital for maintaining the frequency and duration of regular locomotive movements in some insects [261]. The reflexive controller demonstrates that feedback of hip extreme flexion angle is a suitable

and effective means of triggering knee extension at terminal swing, initiating the swing-to-stance transition and ensuring stability of the walker while protecting the mechanical hip joint from overflexion.

10.3 Control system

Many different control strategies have been used within robotics, not only to produce bipeds with a stable and efficient gait pattern, but also for studying biological models and gaining insight into walking control systems that may be present in humans. This allows simplification and analysis individual components of a complex system to study their role in generating functional locomotion.

Classical control strategies employed in bipedal robotics, which have a biomechanic inspired design, include passive dynamic walkers, that are simple and can remain stable while walking down slopes [166]. Robots featuring this design have demonstrated gait, which appears visually human-like, however they cannot adapt and/or change their speed or walk on a level or inclined surface without the addition of actuators and controllers. Conversely, other robotic walkers, such as the well publicised bipedal walker ASIMO [168], have moved towards highly complex systems such as precise joint-angle control and trajectory-based methods (including Zero-Moment Point (ZMP) based [262] and Virtual Model control [263]). However the need for precision in the actuators and frequency response of these systems cannot be easily related to the human model which uses the less precise musculoskeletal system integrating muscles, tendons and joints under neuronal control [169]. Central pattern generator (CPG) methodology has also been investigated for creating humanoid bipedal robot walkers, which can be partially autonomous using local oscillators to generate limb motion patterns and limited sensory information as feedback (for review see [264]). Although this technique has proved successful in producing gait in a range of robotic walkers, including bipeds [170, 265, 266], and uses a biological approach conclusively described in animal locomotion, there remains debate over the importance of this strategy in human walking control. This has promoted development of biped locomotion controllers based on reflexes rather than on CPGs [3, 167, 267].

Compared to these robots, the reflexive control system described in this thesis is based on actual human walking data, creating a closed loop system based on the idea of a causal relationship between the foot contact information and the muscle activation signals (in humans). And when applied to the RunBot, translates to motor activation for movement of the the limbs. The result is so-called limit

cycle walking which is defined by Hobbelen and Wisse (2007) as a nominally periodic sequence of steps which although not locally stable at every instant in time, is stable as a whole [171]. Limit cycle walking allows a walker to adapt its gait to the changing natural dynamics producing a convergence to a desired motion following any deviation from the desired trajectory, using only zero or low feedback gains. As can be expected this is more energy efficient than using high feedback gain to force the walker to remain on an intended path, which is a constant fight against natural deviations [171]. The control strategy detailed in this thesis demonstrates limit cycle walking in RunBot as the motion is able to return naturally to the desired trajectory following a perturbation, after only a short time and without CPGs or trajectory control.

10.3.1 Comparison to human control

The precise function of load dependent reflexes and the extent to which reflex responses generated by sensory input from peripheral receptors contribute to human bipedal gait in comparison to other mammals is not thoroughly understood. It is still unclear how significant spinal networks are in the generation of human walking and whether the functional effect of load receptors and reflexes play a similar role in human muscle activation as in the animal models.

Neurophysiological studies have revealed in different animal species that during locomotion (including walking, flying, swimming etc.), motor neurons are being driven by CPGs. These central networks have been observed to work independent of sensory or descending inputs carrying specific timing information and generate the rhythm and pattern of the locomotor bursts of the motor neurons [50, 268]. Thomas Graham Brown, demonstrated through experimentation on spinal and decerebrate cats in 1911 that a basic stepping pattern can be produced by the spinal cord without the need of descending control from the brain [53]. More recently, evidence of CPGs was successfully demonstrated in the oscillatory output of the deafferented locust wing in response to non-rhythmic stimulation of the nerve cord which was maintained in the complete absence of sensory input [269–271]. CPGs have been identified and documented in mammals such as the cat but for humans they have yet to be conclusively described as the experimental procedures used cannot be replicated (for review see [272]). However, even in animals where CPGs are most studied, it should be remembered that the evolving views of the control of locomotion is that sensory feedback activity through the CPG provides the ability of the gait to adapt to the environment. The significant amount of evidence for locomotor CPGs in various different ani-

mals suggests it would be very unusual if a similar system was completely absent in humans. However humans are unique among mammals as habitual bipeds making comparison to an animal model difficult. The lack of evidence could be due to other mechanisms being of primary importance such as contribution from reflexive and supraspinal controls. One significant observation highlighting differences between potential human CPGs and those found in other species is that following a complete spinal cord injury, humans become completely paralysed below the level of injury and locomotor activity is typically not evident for many years [63], whereas rhythmic stepping can be evoked in a cat after complete spinal transection (for review see [50]). Direct evidence of locomotor CPGs may be limited in humans but there has been some indication that initiation of movement could be due to the activation of neurons of a locomotor CPG by a train of stimuli to the spinal cord. It was concluded, in a study involving individuals with complete SCI using epidural spinal cord stimulation, that both patterned and non-patterned stimulus generated locomotor-like activity [273]. This led to suggestion that a difference exists between peripheral and central input to the CPG, but once activated, the result is a coordinated movement in the lower limbs. However, cases of ‘spinal stepping’ in neurologically complete humans is hard to confirm as occurring in complete isolation from any residual descending control. A study of patients with spinal cord injuries (SCI) by Dietz et al. (2002) describes a limited coordination between the legs suggesting the coupling between any potential CPGs is weak when the input from supraspinal structures is reduced [96]. Similarly, an extensive study on Macaque monkeys with transected spinal cords failed to produce hind leg stepping using procedures similar to those used on cats, which raises doubt over the existence of locomotor CPGs in primates. However, rhythmic alternating activity could be generated if part of the spinal cord was left intact and more successfully when locomotor centres in the brain stem were stimulated in decerebrate animals with an intact spinal cord [24, 63, 95]. The conclusion from primate studies is that if a CPG is present in primates then it may involve pathways that include supraspinal centres [63].

A reflex is often defined as a local motor response to a local sensory input. In the locomotion of human and animals, multiple reflexes act together to control the limbs and their integration contributes to the regulation of the locomotor gait cycle [46]. The concepts that have emerged from walking studies are that reflexes are dependent on task, phase and context and they require modulation using sensory feedback from peripheral afferents in order to function effectively in locomotion where the initial conditions are changing on every step [42, 46, 69,

274, 275].

Within a human model, feedback on the current status of the walking process is fed back from different sensory organs located locally in muscles, tendons, joints and from the vestibular and visual systems. At high walking speeds, coordination between the sensory input and motor output needs to act quickly with efficiency and these high dynamic walking demands are currently not possible using existing artificial robotic control systems [5, 167, 170]

This controller demonstrates that complex behavioural patterns can result from a simple model for locomotion and gait control based on simple reflexes. An achievement where much of the biological complexity within the true human motor control system has been omitted.

In the future it would be exciting to adapt this simple reflexive control system employed by RunBot into an FES controller for gait rehabilitation, which could assist stepping and promote limit cycle walking in patients with spinal cord injuries or stroke.

10.4 Implications

A reflexive controller based on human data has implications for locomotor training and the development of assistive technologies for patients with spinal cord injury. Producing coordinated stepping with muscle activation timing observed in normal gait should generate an appropriate afferent input to the spinal cord to influence mechanisms of neuroplasticity [20].

Functional electrical stimulation (FES) is commonly used as a rehabilitation strategy for SCI to exercise and strengthen weakened muscles as well as artificially replace muscle activation that is missing or lacking (for review see [25]). FES uses small electrical currents to directly stimulate peripheral motor nerves, to cause muscle contraction. For gait rehabilitation, FES is applied to nerves which innervate leg muscles with particular motor functions during the swing and stance gait phases, activating them (artificially) with timing consistent with a normal walking gait cycle [26–31]. Research within the last decade has suggested walking function is vastly improved in individuals with incomplete SCI undergoing functional electrical stimulation (FES) therapy [32].

Sophisticated FES devices have been designed to enable patients with SCI to stand, walk and sit but the most common form of commercial stimulator systems available are primarily for correcting drop-foot and for generating standing (for review see [148]). The most simple method of control used by stimulator

systems, including the Parastep I (Sigmedics, Inc., Fairborn, OH) [149, 150], is open-loop control to provide stimulation pulses to assist in standing or walking by coordinating the activation of muscles. Open-loop involves no direct feedback back to the controller about the actual state of the system and so there are complications in generating accurate control of movement generation using these systems due to difficulty in predicting the correct timing of stimulus, non-linearity of the neuromuscular-skeletal system and inability for modulation during deviations from an ideal gait cycle [25]. Providing sensory feedback from the patient to the FES device should allow improvement in control of the generated movement and produce walking which is more normal than seen with open-loop systems, improving speed and efficiency [158]. Feedback allows a modulation of the stepping by the walking, adapting the gait in compensation for changes within the terrain or environment.

Closed-loop control has been studied using two different forms of sensory feedback; biological signals generated by the individual (EMG, ENG or EEG) and signals derived from artificial sensors. Research involving gait event detection have traditionally been based on a single type or an integration of different body-worn sensors typically positioned on the thigh, shank or foot to measure ambulation and have included accelerometers [163, 164], gyroscopes and FSRs [162], and accelerometers and FSRs [161]. Many closed-loop control strategies for FES applications in SCI individuals have been reported in the literature. These fall into categories which include dynamic controllers, finite state controllers and artificial networks (for full review of FES control see [160]). Similar to controllers developed for bipedal robotic walkers, the different controllers applied to FES have issues with computational power. These issues include: (i) high gain requirements for error correction, (ii) complicated algorithms for trajectory control, and (iii) difficulties in implementing the control strategy on a human model (with complications such as latency, muscle spasticity, voluntary control and fatigue). None of these control methods have managed to produce an adaptive gait pattern based on self-stabilising dynamic processes as observed in natural walking, which may explain why open-loop controllers remain the most common in commercial FES systems.

The main difference between the previously discussed control schemes and the one presented here, is that this approach uses linear transfer/filter functions which do not require any thresholding. Although bipedal robots featuring finite-state machines can exhibit a stable limit cycle [276], it is well known from behaviour based robotics [277] that systems acting without any thresholds or states are

very robust. In contrast Kojovic et al. (2009) [161] used computer learning to map sensory information to the EMG activity, requiring thresholds to be set for the accelerometer and FSR inputs to switch the stimulation on and off. The controller outlined in this thesis uses a filter which translates linearly the input of the heel contact and translates this input into a muscle stimulation signal. The only threshold which had to be employed was on the hip anterior extreme angle (AEA) to determine the trigger time for knee extension at terminal swing; however this threshold is not critical and could probably be replaced by a soft threshold.

As this is an analogue linear system using foot contact as the main source of feedback, the system has high reliability where the output is dependent on there being an input. This means that the system can never enter any unknown or unpredictable state as it is not a finite state machine and uses no threshold on the input to determine the output state. If there was a loss of feedback information relating to foot contact, there would be no output from the system. We never experienced a loss of foot contact feedback in using this system with the RunBot robot or during the data collection with human participants, although a failure of the foot contact sensors could occur with potential dangerous consequences for the biped locomotion. The FSRs used in the study have a typical operation beyond 1,000,000 actuations [181], making them suitable for use in the detection of foot contact, for which they have been used previously [177, 182, 200]. Future development of the system to improve robustness and fault tolerance could involve integration of internal forward models with efference copy. As walking is a cyclic and repetitive process, the system could calculate a prediction (forward model) of the output and if the actual and predicted outputs differed the system would halt, bringing the walker to a standing stop.

10.5 Significance and future work

The work outlined in this thesis demonstrates an initial stage in the development of a rehabilitation device for use with individuals with iSCI for improving in their gait ability. Although a limitation of the study is that the developed control strategy was not applied within a rehabilitation context in the experimentation which would demonstrate clearly a contribution to this community, the process of taking the idea to the level of patient testing needs to be approached carefully and iteratively. Initially it was necessary to test how aspects of locomotion depend on the interaction with the environment and the natural dynamics of the walker and

so it was logical to apply the control strategy and transfer functions back to the RunBot robot, whose function was the inspiration behind the whole project. This provides both a proof of concept and safe means of testing without endangering individuals with SCI or the additional complexity of compensating for individual challenges due to the extent and level of injury and limitations imposed by issues including muscle spasticity and muscle fatigue. Using the robot has provided useful information necessary in a preliminary experimentation, i.e. which transfer functions were most successful in producing a stable gait cycle (transfer functions from individual subjects), which was not (transfer functions calculated from averaged data across the subject population and from overground walking).

It was found in creating a suitable control system for applying the human transfer functions to RunBot that foot contact information could be causally used to trigger flexion or extension of all the joints except knee extension at terminal swing and in plantar flexion during late stance. To apply these functions with correct timings in humans requires a means of calculating when the hip reaches an anterior/posterior extreme angle (AEA and PEA) as used in RunBot. This could be achieved using goniometers to measure the angle or potentially accelerometers. It was found during the preliminary treadmill data collection study (Chapter 3) that peak acceleration of the hip in the vertical axis during the gait cycle related to muscle activity during mid-stance which may be suitable for triggering plantar flexion of the foot in a causal system. In addition, there was a second smaller peak observed in the hip acceleration during swing which has potential to be used to trigger knee extension. However, clearly distinguishing the hip reaching the AEA or PEA may require some further work and would require further data collection from healthy subjects during variable speed walking to properly establish the suitability, biomechanically, of this approach.

The next stage would be to apply the control strategy and transfer functions to a hybrid FES system and conduct a study with individuals with iSCI. This would involve integration of the control system with a commercially available multichannel muscle stimulator. The individual would wear FSR insoles in their shoes to trigger stimulation of selected muscles (potentially TA, LG, RF and BF muscles) using feedback from the heel contact and toe-off information. These muscles are typically used in FES for generating walking and standing so this strategy should be suitable for generating stepping with the proposed system. Some considerations of FES control which will need to be considered include:

- Ensuring correct foot contact during the gait cycle.
- Body-weight support of the trunk using a harness or use of a walker or

sticks may be necessary.

- Control of lateral hip movement.
- Initiation of gait with the FES system.
- Amplitude of stimulation required, this was not studied during the preliminary experiments.
- Fault tolerance to ensure patient safety.

Chapter 11

Conclusions

11.1 Relevance to the research hypothesis

The research hypothesis of the thesis was that foot contact information could be used to causally control leg muscle activity during human walking. This theory was tested muscle by muscle to identify whether this mechanism was feasible and whether a coordinated stepping response could be generated this way. This theorised control strategy was categorised as a closed-loop analogue Class D system (Fig. 11.1B).

The results of the study demonstrate that it is possible to use foot contact information in a causal system to control joint actions at the hip and knee and generate a functional and stable gait in the RunBot II robot.

The study has provided a complete recipe for recording foot contact information and muscle activity from ten subjects, both during treadmill walking and overground walking, and processing the data to produce transfer functions which relate the foot contact information with muscle activation signals for controlling joint movements. Testing muscle by muscle to relate muscle function related to joint movement found that hip/knee flexion/extension could be controlled causally by ipsilateral or contralateral heel contact apart from knee extension at terminal swing. This finding indicated that a purely analogue system was not possible as hypothesised (Class D control system (Fig. 11.1B)), due to the need for setting a threshold in defining hip AEA for triggering knee extension at terminal swing. However this threshold value was not critical to the operation of the system, suggesting the complete control system can be classified somewhere between Class C and Class D (Fig. 11.1). Although not purely analogue, it can be defined as a minimal, linear, reflexive control system which will be supportive to the user and will not override any residual function, working with the natural

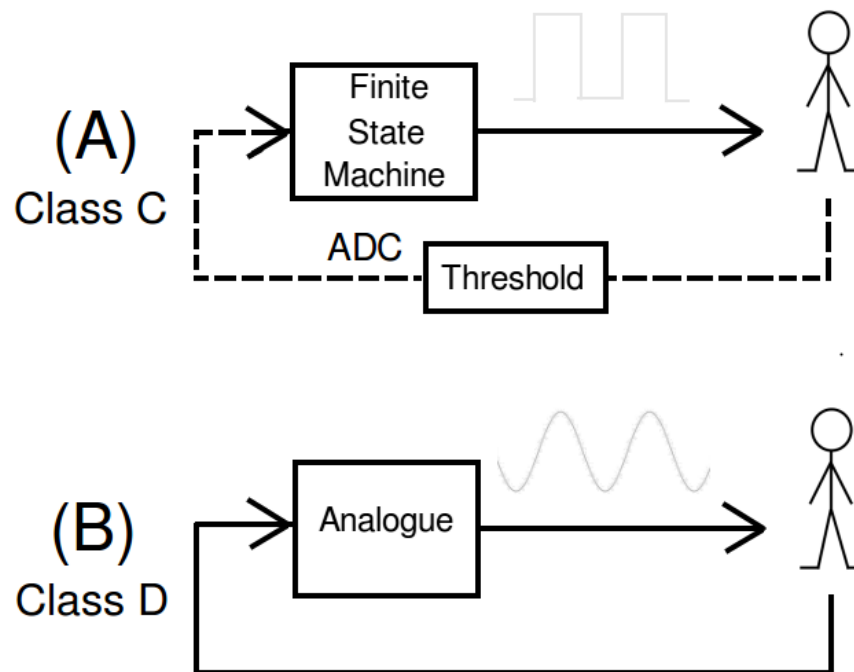


Figure 11.1: **Control systems for walking.** (A) Finite state controller, feedback controls the output state of the system. Thresholding acts like an ADC to determine the input state, converting the feedback signals from analogue to digital. (B) A completely analogue system was the hypothesis of this thesis. Feedback controls the output of the system.

dynamics of the body. These are important characteristics of a controller for use in rehabilitation of walking.

11.2 Summary of thesis conclusions

The key outcomes of the thesis studies are:

- Development of an eight channel EMG preamplifier and eight channel FSR amplifier for recording data during ambulation.
- Development and validation of a wireless gait analysis device for measuring gait parameters during overground walking.
 - The spatio-temporal gait parameters: walking speed, stride length, stride duration, stance duration and cadence showed excellent agreement with the values estimated by the Vicon 3D motion analysis system (ICC values between 0.99 and 0.94).
 - Spatio-temporal parameters, swing duration and double support time, showed lesser levels of agreement between the wi-GAT and the Vicon 3D motion analysis system (ICC values between 0.84 and 0.49).
 - Although successful in the wi-GAT's design, Bluetooth is not suitable for the 16 channel EMG/FSR preamplifier design due to low bandwidth and limited distance capabilities.
- Identifying a relationship between foot contact information and muscle activity during treadmill and overground walking by removing the influence of walking speed.
- Calculating transfer functions which relate foot contact information and muscle activity during walking in a causal system.
- A strategy for splicing the muscle transfer functions to relate to joint actions at the hip, knee and ankle.
- Description of a minimal, reflexive control system for walking using human transfer functions, based on the controller used in RunBot II.
- Application of the human transfer functions to the RunBot II robot and analysis of its gait ability.

- During treadmill walking features of the transfer functions determined whether RunBot’s gait was stable or not:
 1. Compared to the knee transfer functions, the differences in hip transfer functions have a more significant affect on the walking performance as the hip transfer functions are used to drive the hip motor directly.
 2. RunBot’s walking is more likely to be stable when the time delay between the trigger and the hip flexion and between the trigger and the hip extension of the contralateral leg are very similar or the hip flexion is longer.
 3. The duration t_d of hip extension (from 50% of the peak amplitude on the rise to 50% on the fall) is significant in establishing a stable gait pattern because the stance leg needs enough torque to support the body weight and extend the leg backward while the swing leg flexes forward.
 4. Gait is more likely to be stable if the duration of hip extension is longer than hip flexion.
 5. RunBot’s Gait was more likely to be stable if all the transfer functions applied to the control system were from an individual participant rather than averaged or from different subjects. This may be due to the necessity for coordination between the joints, which is dependent on individual characteristics.
 6. RunBot’s Gait was more likely to be stable using transfer functions calculated from treadmill walking sequence 2 (10 different speeds, 100 steps per speed).
 - RunBot could not walk with a stable gait using any of the transfer functions calculated from data recorded during overground walking due to features of the transfer functions as defined above.
- Analysis of the differences between muscle activity and temporal gait parameters during overground and treadmill walking.
 - Description of a prospective controller for the ankle joint (based on the same mechanism as described for the hip and knee).
 - Calculation of transfer functions related to ankle plantar flexion/dorsiflexion from the treadmill and overground human walking data.

In conclusion, the study indicates that it is possible to calculate transfer functions relating foot contact information and muscle activity during human walking and use the functions in a minimal, reflexive control system to generate a functional and stable gait in the bipedal robot, RunBot II. Indication that this simple control mechanism has great potential in the development of gait rehabilitation strategies. In particular in combination with FES for individuals with spinal cord injuries to support and retrain in their gait capability, producing functional gait cycle modifications to suit the loading conditions.

Appendix A

EMG preamplifier PCB layout and BOM

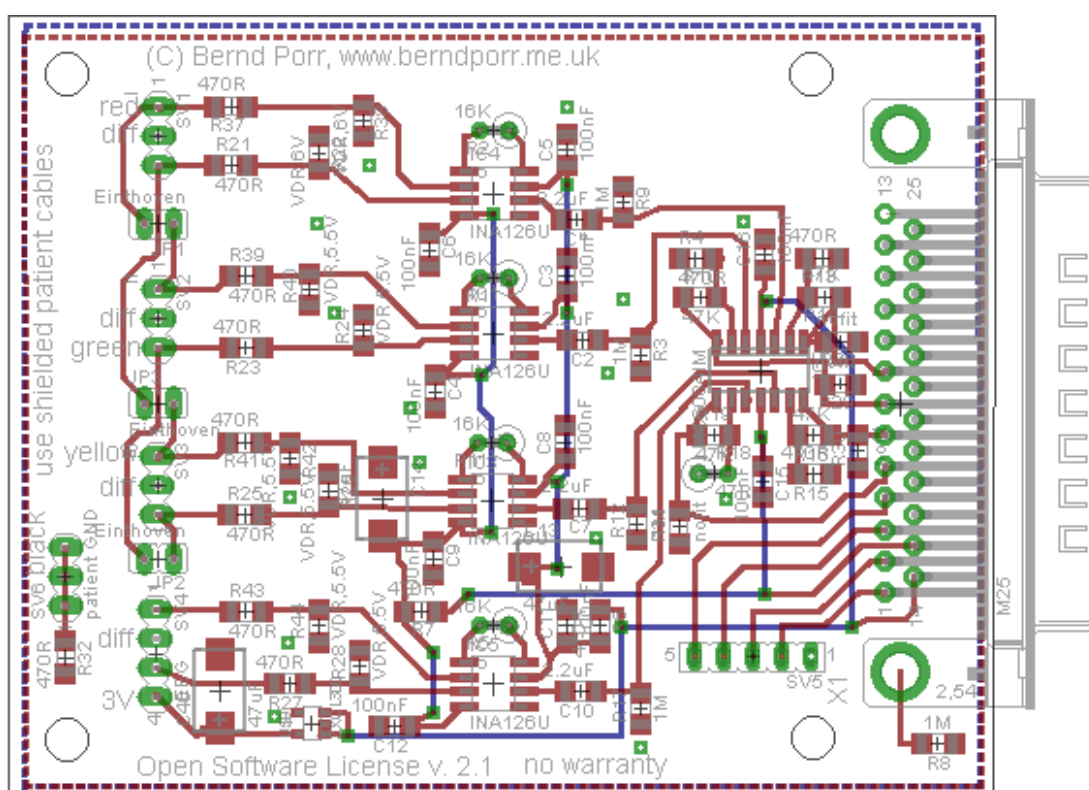


Figure A1: **PCB design of the four channel EMG preamplifier.** The PCB uses SMD components to keep the device as small and portable as possible. The EMG design was adapted from an ECG amplifier (Eagle files available from <http://www.linux-usb-daq.co.uk/howto2/ecg/>).

Table A1: Bill of materials (BOM) for the four channel EMG preamplifier.

Qty	Value	Device	Parts	Farnell
1		FE05-1	SV5	1248143
1		M25HP	X1	1099291
5	1M	R-EU_R1206	R3, R8, R9, R12, R17	9241124
4	2.2uF	C-EUC1206	C1, C2, C7, C10	9406565
4	47K	R-EU_R1206	R10, R14, R16, R19, R32	9241043
3	47uF	CPOL-EUCT7343	C13, C14, C40	1135205
10	100nF	C-EUC1206	C3, C4, C5, C6, C8, C9, C11, C12, C15, C16	499390
1	47R	R-EU_0309/2V	R18	9343288
14	470R	R-EU_R1206	R4, R6, R7, R13, R15, R21, R23, R25, R27, R37, R39, R41, R43	9240926
3	Eindhoven	JP1E	JP1, JP2, JP3	1248140
1	I	MA03-1	SV1	1248141
1	II	MA03-1	SV2	1248141
1	III	MA03-1	SV3	1248141
4	INA126U	INA126U	IC1, IC3, IC4, IC5	1212409
1	AD8609ARZ	4AMP_P4+11ID	IC9	8454078
8	VDR,5.5V	R-EU_R1206	R22, R24, R26, R28, R38, R40, R42, R44	8832552
1	ZXCL300	ZXCL300	U\$9	1132755
4	16K	R-EU_0309/2V	R1, R2, R5, R11	9342699
4	nofit	R-EU_R1206	R20, R29, R30, R31	
1	patient GND	MA03-1	SV6	1248141
1	pressure	MA04-1	SV4	1248141
1	black banana socket			1854580
1	red banana socket			1854581
1	yellow banana socket			1854583
1	green banana socket			1854584
1	BIM 7003/13	Polystyrene Enc		1171635

Appendix B

EMG/FSR preamplifier and BOM

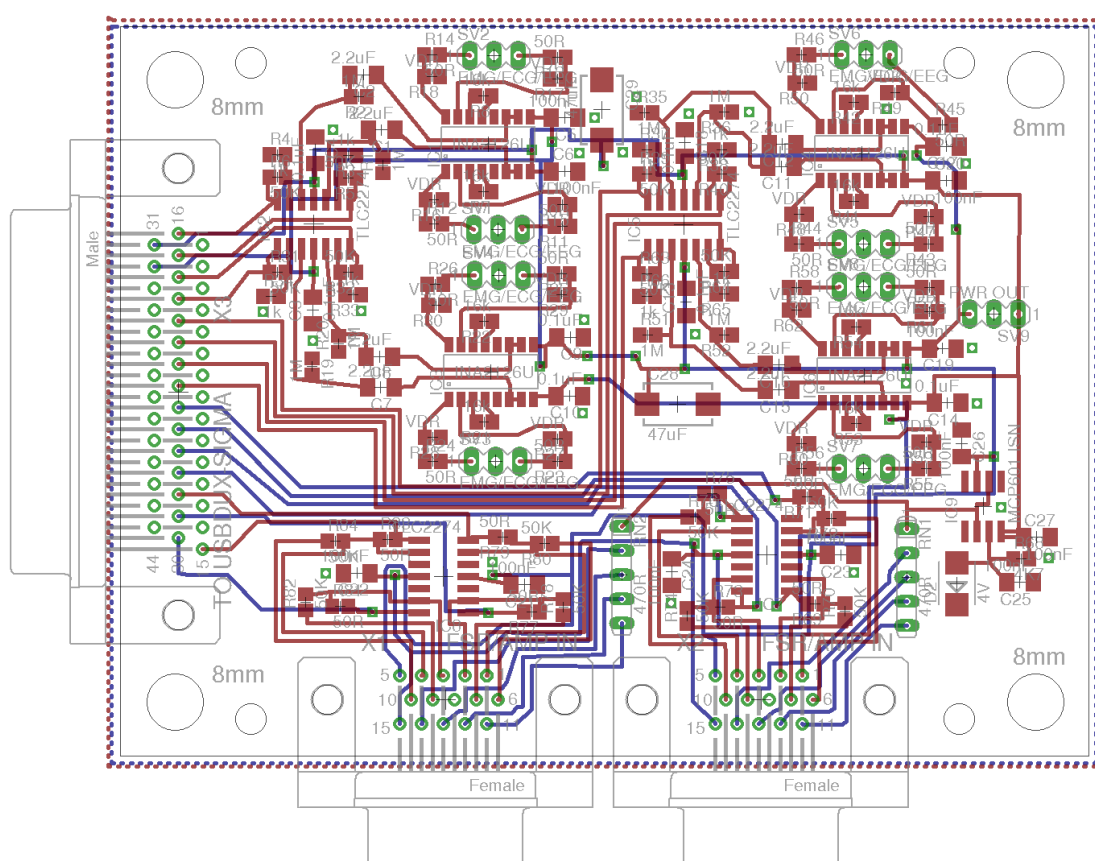


Figure B1: PCB design for the EMG/FSR preamplifier. The board uses SMD components to keep the device as small and portable as possible. There are eight channels for EMG and two D-connectors for amplifying signals from the FSR insoles with four channels per insole (eight in total). The EMG/FSR preamp connects via D-connector to the USB-DUX Sigma board for data acquisition and power supply. Eagle files available from <http://www.linux-usb-daq.co.uk/howto2/bio-sigma/>.

Table B1: Bill of materials (BOM) for the EMG/FSR preamplifier.

Qty	Value	Device	Parts	Farnell	RS
8	2.2uF	C-EUC1206	C1, C2, C7, C8, C11, C12, C15, C16	9406565	
19	100nF	C-EUC1206	C3, C4, C9, C10, C13, C14, C17, C18, C5, C6, C19, C20, C21, C22, C23, C24, C25, C26, C27	499390	
1	3.9V Zener Diode	ZENER-DIODESMB	D2	1431157RL	
4	INA2126U	INA2126U SO16	IC1, IC3, IC4, IC6	1459464	
4	TLC2274	TLC2274 SO14	IC2, IC5, IC7, IC8	1470385	
1	MCP601-I/SN - OP AMP	MCP601 ISN SO08	IC9	9758623	
8	1M	R-EU_R0805	R1, R2, R19, R20, R35, R36, R51, R52	1099823	
8	1K	R-EU_R0805	R3, R4, R33, R34, R37, R38, R65, R66	9332383	
16	51K	R-EU_R0805	R5, R6, R31, R32, R39, R40, R63, R64, R70, R72, R74, R76, R78, R80, R82, R84	9333339RL	
8	16K	R-EU_R0805	R7, R8, R21, R22, R41, R42, R53, R54	9332677	
24	51R	R-EU_R0805	R11, R12, R13, R14, R23, R24, R25, R26, R43, R44, R45, R46, R55, R56, R57, R58, R69, R71, R73, R75, R77, R79, R81, R83	1469944	
16	VDR	R-EU_R0805	R15, R16, R17, R18, R27, R28, R29, R30, R47, R48, R49, R50, R59, R60, R61, R62	8832463	
1	4K7	R-EU_R0805	R68	1469923	
2	470R	GE04R SIL5	RN1, RN2	1612539	
8	EMG/ECG	MA03-1	SV1, SV2, SV3, SV4, SV5, SV6, SV7, SV8	1248141	
1	PWR OUT	MA03-1	SV9	1248141	
2	FSR/AMP IN	F15HDHS SUB-D	X1, X2		740-7212
1	TO USB-SIGMA	HM44H SUB-D	X3		736-1529
1	BOX ENCLOSURE			1171635	

Appendix C

USB-DUX Sigma pin diagram

USB-DUX-SIGMA Pinouts

Analogue I/O

The analogue I/O have a 44 pin D connector (f). All signals and the supply output are electrically isolated from the USB and the digital I/O.

Pin	Direction	Function
1-14	GND	GND
15	I	A/D channel 15
16	I	A/D channel 0
17	I	A/D channel 1
18	I	A/D channel 2
19	I	A/D channel 3
20	I	A/D channel 4
21	I	A/D channel 5
22	I	A/D channel 6
23	I	A/D channel 7
24	I	A/D channel 8
25	I	A/D channel 9
26	I	A/D channel 10
27	I	A/D channel 11
28	I	A/D channel 12
29	I	A/D channel 13
30	I	A/D channel 14
31	O (!)	-5V
32	O (!)	+5V
33	N/C	N/C
34-40	GND	
41	O	D/A channel 0, unipol
42	O	D/A channel 1, unipol
43	O	D/A channel 2, unipol
44	O	D/A channel 3, unipol

Pins 31 and 32 are outputs (!) which can provide about 20mA of supply current for external circuitry such as amplifiers. It is advised to add 10 μ F decoupling capacitors because the voltage is unregulated and the internal DC/DC converter generates high frequency noise. The supply is provided through 51 Ω resistors so that there will be a voltage drop when the current increases. Rail to rail amplifiers are recommended.

Figure C1: **USB-DUX Sigma pin diagram.** Information from <http://www.linux-usb-daq.co.uk/dev2/>.

Appendix D

Treadmill belt speed accuracy

The treadmill has a digital display for setting the belt speed and displaying the actual current speed. During the treadmill walking data collection study the current treadmill belt speed was recorded every time it changed to enable muscle activity and foot contact information be analysed in relation to walking speed. The accuracy of the programmed belt speed compared to the actual speed was thus necessary to establish before starting the data collection. The treadmill was professionally serviced by h/p/cosmos prior to the study beginning and all calibration methods were in accordance with the manufacturers handbook.

A simple test was performed to compare the treadmill belt speed to the display. The belt of the treadmill was marked with coloured tape and a corresponding piece of tape was positioned parallel on the treadmill's static frame. The treadmill was then set to run at four different speeds covering the full range used in the treadmill walking study. After allowing the treadmill to ramp up to each speed, the time for 15 rotations of the treadmill belt was measured using a stopwatch. This procedure was then repeated three times so the mean time could be calculated (t_{avg}). The average reaction time of the person controlling the stopwatch was measured to be 0.30 s and was subtracted from the recorded time for 15 belt rotations.

The belt of the treadmill was measured to have a length of 3.74 m ($L = 3.74$) so the belt speed (S) could be calculated using Equation D.1.

$$S = \frac{(15L)}{t_{avg}} \quad (\text{D.1})$$

A table of the results for each speed setting is provided in Table D1.

It can be concluded that the treadmill speed settings have a mean error of approximately +0.041 km/h (+0.011 m/s) or 1.35%, which is small but should

Table D1: **Treadmill belt speed error, without load.** The error was calculated as the difference between the measured belt speed and the programmed speed on the treadmill's digital display.

Speed setting (km/h)	Mean time for 15 rotations (s)	Actual belt speed (km/h)	Error (actual - set)	% Error
1	198.8	1.015	0.015	1.5
2.5	79.2	2.550	0.050	2.0
4	49.9	4.032	0.032	0.8
6	33.3	6.065	0.065	1.1
Mean:			0.041	1.35

be considered when programming the walking speeds used in the treadmill study and analysing the results.

Appendix E

Supplementary tables for RunBot

Table E1: **Values for the extreme angle of each joint ($\theta_{L/R,H/K}$).** RunBot II features an elastic knee structure so real-time tracking of the knee joint angle is not possible. Instead, the motor position voltage (V) is used to predict the knee joints reaching the joint angle threshold. The hip angles differ from left to right leg due to the effect of RunBot being constrained to a circular walking path and are different values than those documented from humans due to the mechanical structure and the need of RunBot to keep its centre of mass forward.

	$\theta_{L,H}(Deg)$	$\theta_{R,H}(Deg)$	$\theta_{L,K}(V)$	$\theta_{R,K}(V)$
Extensor	91	88	3.50	3.50
Flexor	126	119	0.80	0.80

Table E2: **The gain of the motor amplifier ($a_{L/R,H/K}$).**

$a_{L/R,H}$	$a_{L/R,K}$
1.50	3.00

Appendix F

Adaptive filtering - MSE

Table F1: **The final mean square error result for each subject for each muscle transfer function from the adaptive filtering.** The transfer functions were calculated using the EMG activity recorded from the subject's right leg with heel contact information from both the right and left foot. Transfer functions related to the Lateral Gastrocnemius (LG), Rectus Femoris (RF) and Biceps Femoris (BF) are given, contralateral heel contact are labelled (CH) and ipsilateral heel contact (IH).

Treadmill Sequence	Subject	Mean Square Error (MSE)			
		$H_{LG,CH}$	$H_{RF,CH}$	$H_{BF,CH}$	$H_{BF,IH}$
25 steps per speed	A	9.39e-06	4.17e-05	1.56e-05	1.64e-05
	B	4.27e-05	3.63e-07	9.60e-04	9.77e-04
	C	9.09e-06	2.46e-05	2.47e-04	2.48e-04
	D	1.01e-04	1.28e-04	7.12e-06	7.88e-06
	E	2.20e-05	2.47e-04	1.54e-04	1.49e-04
	F	9.21e-05	2.42e-05	4.39e-05	4.02e-05
	G	4.18e-05	7.51e-05	6.44e-05	5.72e-05
	H	1.31e-04	2.59e-05	6.74e-05	7.22e-05
	I	3.67e-05	3.05e-04	1.66e-03	1.70e-03
	J	4.27e-05	1.27e-06	9.20e-06	1.14e-05
100 steps per speed	A	9.69e-06	5.85e-05	1.40e-05	1.45e-05
	B	3.24e-05	3.53e-07	2.34e-06	2.33e-06
	C	5.21e-05	4.7e-05	3.33e-04	6.91e-05
	D	3.06e-04	2.1e-04	7.43e-06	7.95e-06
	E	2.56e-05	2.21e-04	2.16e-04	1.77e-04
	F	7.60e-05	3.50e-05	4.83e-05	5.14e-05
	G	2.34e-05	2.45e-06	5.04e-05	3.97e-05
	H	3.17e-04	3.14e-05	4.86e-05	5.25e-05
	I	2.82e-05	9.02e-03	8.78e-05	8.45e-05
	J	4.61e-05	1.69e-06	8.52e-06	1.02e-05

Table F2: **The final mean square error result for each subject for each muscle transfer function from the adaptive filtering (overground walking).** The transfer functions were calculated in the same way as for the treadmill walking, see Table F1.

Subject	Mean Square Error (MSE)			
	$H_{LG,CH}$	$H_{RF,CH}$	$H_{BF,CH}$	$H_{BF,IH}$
OA	4.23E-04	3.03E-06	2.61E-05	2.23E-05
OB	1.06E-04	6.57E-05	1.00E-04	9.29E-05
OC	1.82E-05	1.95E-06	8.38E-06	8.74E-06
OD	3.33E-05	5.25E-06	1.77E-05	1.69E-05
OE	8.97E-05	5.89E-04	4.98E-04	4.49E-04
OF	1.41E-04	4.24E-04	3.03E-05	3.05E-05
OG	5.33E-05	2.73E-06	5.55E-05	5.64E-05
OH	4.79E-05	1.63E-04	1.90E-05	1.85E-05
OI	5.64E-05	2.65E-06	4.74E-06	4.88E-06
OJ	4.24E-04	6.39E-06	7.63E-06	7.91E-06

Table F3: **The final mean square error result for each subject for each muscle transfer function from the adaptive filtering (treadmill walking).** The transfer function $H_{TA,IT}$ was calculated between fore-foot contact information and the TA muscle activity, where fore-foot contact information was measured using an FSR positioned under the first metatarsal. In addition heel contact information was used to calculate the transfer functions $H_{TA,CH}$ and $H_{LG,IH}$ using the same methodology as described for Table F1 and F2.

Treadmill Sequence	Subject	Mean Square Error (MSE)		
		$H_{TA,CH}$	$H_{LG,IH}$	$H_{TA,IT}$
25 steps per speed	A	4.94E-05	1.11E-05	4.47E-05
	B	1.41E-04	4.16E-05	1.06E-04
	C	7.04E-05	9.13E-06	4.85E-05
	D	8.30E-04	9.69E-05	7.77E-04
	E	5.24E-05	2.37E-05	5.54E-05
	F	8.38E-05	9.35E-05	6.39E-05
	G	1.66E-04	4.83E-05	1.90E-04
	H	6.52E-05	1.11E-04	5.02E-05
	I	9.95E-05	3.49E-05	9.22E-05
	J	5.94E-05	4.15E-05	5.13E-05
100 steps per speed	A	5.19E-05	1.15E-05	4.53E-05
	B	1.30E-04	3.47E-05	1.02E-04
	C	2.27E-04	8.34E-06	6.45E-05
	D	7.19E-04	2.96E-04	6.24E-04
	E	3.05E-05	2.72E-05	3.32E-05
	F	7.92E-05	7.77E-05	5.86E-05
	G	6.88E-05	2.54E-05	6.87E-05
	H	6.72E-05	2.35E-04	5.06E-05
	I	8.58E-05	2.76E-05	7.62E-05
	J	6.53E-05	4.35E-05	5.80E-05

Table F4: **The final mean square error result for each subject for each muscle transfer function from the adaptive filtering (overground walking).** The transfer functions $H_{TA,CH}$, $H_{LG,IH}$ and $H_{TA,IT}$ were calculated using the same methodology as used for Table F3.

Subject	Mean Square Error (MSE)		
	$H_{TA,CH}$	$H_{LG,IH}$	$H_{TA,IT}$
OA	1.19E-04	4.03E-04	1.44E-04
OB	8.57E-05	8.62E-05	1.32E-04
OC	8.60E-05	1.91E-05	1.03E-04
OD	8.26E-05	3.68E-05	6.73E-05
OE	3.32E-05	8.48E-05	1.48E-04
OF	5.23E-05	1.36E-04	2.80E-05
OG	1.15E-04	4.86E-05	4.51E-05
OH	1.38E-05	4.72E-05	1.18E-04
OI	8.77E-05	5.66E-05	9.46E-05
OJ	7.85E-05	4.19E-04	1.12E-04

Appendix G

Curve fitting - goodness-of-fit

Goodness-of-fit statistics were used to define how well the curve fit matched the transfer functions for flexion/extension of the joint. The statistics chosen are the standard reported in the literature.

- The sum of squares due to error (SSE)
- R-square
- Root mean squared error (RMSE)

Sum of squares due to error (SSE)

The SSE is a measure of the total deviation of the values of the transfer function to the fitted curve. An SSE value which is closer to zero is an indication that the fitted curve contains a small amount of random error. This suggests that the fit is more suitable for prediction than a model with a large SSE.

R-square

R-square measures how successfully the fit explains the variation of the data. R-square is defined as the square of the correlation between the response values and the predicted response values. The R-square value lies between 0 and 1, where a value closer to 1 indicates that the model is able to account for a large proportion of variance.

Root mean squared error (RMSE)

RMSE is an estimate of the standard deviation of the random component in the data.

Table G1: **Goodness-of-fit statistics - hip/knee (treadmill)**. These statistics define how well the second exponential fitted the transfer functions calculated from the treadmill walking data for hip/knee flexion/extension.

(A) **Goodness-of-fit statistics - hip.**

Set	$\hat{H}_{L/R,H,F}$			$\hat{H}_{L/R,H,E}$		
	SSE	R-square	RMSE (V)	SSE	R-square	RMSE (V)
1A	2.32	0.82	0.11	2.19	0.83	0.11
1B	1.74	0.89	0.10	1.27	0.92	0.08
2A	3.32	3.32	0.13	1.24	0.91	0.08
2B	2.28	0.83	0.11	1.39	0.88	0.09
3A	2.72	0.83	0.12	2.80	0.77	0.13
3B	3.35	0.79	0.14	2.85	0.85	0.13
4A	2.42	0.88	0.12	1.13	0.94	0.08
4B	0.91	0.94	0.07	1.34	0.92	0.08
5A	3.73	0.81	0.14	4.37	0.69	0.15
5B	0.75	0.95	0.06	1.71	0.85	0.10
6A	3.14	0.81	0.13	5.83	0.74	0.18
6B	2.97	0.79	0.13	2.60	0.88	0.12

(B) **Goodness-of-fit statistics - knee.**

Set	$\hat{H}_{L/R,K,F}$			$\hat{H}_{L/R,K,E}$		
	SSE	R-square	RMSE (V)	SSE	R-square	RMSE (V)
1A	3.88	0.71	0.15	3.00	0.83	0.12
1B	2.71	0.88	0.12	2.99	0.85	0.12
2A	4.44	0.78	0.16	1.68	0.91	0.09
2B	0.57	0.97	0.06	1.78	0.94	0.10
3A	2.30	0.84	0.12	2.61	0.81	0.12
3B	2.72	0.87	0.13	3.55	0.80	0.13
4A	5.16	0.75	0.17	5.11	0.76	0.16
4B	0.52	0.97	0.05	3.53	0.84	0.13
5A	2.61	0.82	0.12	2.01	0.92	0.10
5B	0.52	0.97	0.05	3.30	0.85	0.13
6A	3.30	0.78	0.14	7.12	0.64	0.19
6B	3.08	0.82	0.13	4.44	0.76	0.15

Table G2: **Goodness-of-fit statistics - hip/knee (overground)**. These statistics define how well the second exponential fitted the transfer functions calculated from the overground walking data for hip flexion/extension.

(A) **Goodness-of-fit statistics - Hip**

Set	$\hat{H}_{L/R,H,F}$			$\hat{H}_{L/R,H,E}$		
	SSE	R-square	RMSE (V)	SSE	R-square	RMSE (V)
1	0.32	0.94	0.04	0.24	0.94	0.04
2	0.69	0.85	0.06	0.21	0.94	0.04
3	0.53	0.91	0.05	0.26	0.95	0.04
4	0.96	0.94	0.07	1.45	0.88	0.09
5	2.50	0.87	0.11	1.70	0.87	0.10
6	0.88	0.94	0.07	0.35	0.97	0.04

(B) **Goodness-of-fit statistics - knee.**

Set	$\hat{H}_{L/R,K,F}$			$\hat{H}_{L/R,K,E}$		
	SSE	R-square	RMSE (V)	SSE	R-square	RMSE (V)
1	3.74	0.85	0.15	3.04	0.84	0.12
2	3.82	0.83	0.14	2.34	0.90	0.11
3	2.99	0.87	0.13	2.15	0.86	0.10
4	1.19	0.93	0.08	1.99	0.89	0.10
5	1.27	0.91	0.08	0.77	0.96	0.06
6	3.92	0.80	0.15	1.54	0.92	0.09

Table G3: **Goodness-of-fit statistics - ankle (treadmill)**. These statistics define how well the second exponential fitted the transfer functions calculated from the treadmill walking data for ankle dorsiflexion/plantar flexion.

Set	$\hat{H}_{L/R,A,P}$			$\hat{H}_{L/R,A,D_S}$			$\hat{H}_{L/R,A,P_{TS}}$		
	SSE	R-square	RMSE (V)	SSE	R-square	RMSE (V)	SSE	R-square	RMSE (V)
1B	1.62	0.93	0.09	0.77	0.86	0.11	2.45	0.85	0.11
3B	4.65	0.80	0.15	0.58	0.87	0.11	2.94	0.82	0.12
4B	0.61	0.92	0.06	0.35	0.96	0.06	2.98	0.83	0.12
5A	3.75	0.82	0.14	0.38	0.87	0.09	2.12	0.86	0.10
6A	0.50	0.91	0.10	0.83	0.82	0.14	3.58	0.77	0.13
6B	0.60	0.90	0.13	0.74	0.82	0.14	2.56	0.84	0.11

Table G4: **Goodness-of-fit statistics - ankle (overground)**. These statistics define how well the second exponential fitted the transfer functions calculated from the overground walking data for ankle dorsiflexion/plantar flexion.

Set	$\hat{H}_{L/R,A,P}$			$\hat{H}_{L/R,A,D_S}$			$\hat{H}_{L/R,A,P_{TS}}$		
	SSE	R-square	RMSE (V)	SSE	R-square	RMSE (V)	SSE	R-square	RMSE (V)
1	0.94	0.95	0.07	1.80	0.85	0.13	0.77	0.96	0.06
2	1.80	0.92	0.10	1.62	0.90	0.11	1.32	0.94	0.08
3	1.44	0.94	0.09	1.81	0.81	0.14	1.73	0.92	0.09
4	1.57	0.92	0.09	0.90	0.81	0.15	0.55	0.97	0.05
5	1.00	0.90	0.07	0.40	0.89	0.09	1.32	0.93	0.08
6	2.72	0.86	0.12	0.25	0.95	0.07	1.93	0.89	0.10

Bibliography

1. Neptune RR, Kautz SA, Zajac FE (2001) Contributions of the individual ankle plantar flexors to support, forward progression and swing initiation during walking. *J Biomech* 34: 1387-1398.
2. Duysens J (2002) Human gait as a step in evolution. *Brain* 125: 2589-2590.
3. Geng T, Porr B, Worgotter F (2006) Fast Biped Walking with A Sensor-driven Neuronal Controller and Real-time Online Learning. *Int J Robot Res* 25: 243-259.
4. Geng T, Porr B, Worgotter F (2006) Advances in Neural Information Processing Systems 18, Cambridge, MA: MIT Press, chapter Fast biped walking with a reflexive controller and real-time policy searching. pp. 243-259.
5. Manoonpong P, Geng T, Kulvicius T, Porr B, Worgotter F (2007) Adaptive, Fast Walking in a Biped Robot under Neuronal Control and Learning. *PLoS Comput Biol* 3: e134.
6. Nielson JB (2002) Reflex excitation of muscles during human walking. *Adv Exp Med Biol* 508: 369-375.
7. Mehrholz J, Kugler J, Pohl M (2012) Locomotor training for walking after spinal cord injury (Review). *Cochrane Database of Systematic Reviews* 11.
8. Waters RL, Adkins RH, Yakura J, Sie I (1993) Motor and sensory recovery following complete tetraplegia. *Arch Phys Med Rehabil* 74: 242-247.
9. Wirz M, Zemon D, Rupp R, Scheel A, Colombo G, Dietz V, Hornby T (2005) Effectiveness of automated locomotor training in patients with chronic incomplete spinal cord injury: a multicenter trial. *Arch Phys Med Rehabil* 86: 672-680.

10. Kirshblum S, Burns S, Biering-Sorensen F, Donovan W, Graves D, Jha A, Johansen M, Jones L, Krassioukov A, Mulcahey M, Schmidt-Read M, Waring W (2011) International standards for neurological classification of spinal cord injury (Revised 2011). *J Spinal Cord Med* 34: 535-546.
11. Marino R, Barros T, Biering-Sorensen F, Burns S, Donovan W, Graves D, Haak M, Hudson L, Priebe M (2003) International standards for neurological classification of spinal cord injury. *J Spinal Cord Med* 26: 50-56.
12. Taghva A, Hoh D, Laurysen C (2012) Elsevier, volume 109 (3rd series), chapter Advances in the management of spinal cord and spinal column injuries. pp. 105-126.
13. Moore K, Dalley A (2006) *Clinically Oriented Anatomy*. Philadelphia, USA: Lippincott Williams & Wilkins, fifth edition.
14. Hulsebosch C (2002) Recent Advances In Pathophysiology and Treatment of Spinal Cord Injury. *Adv Physiol Ed* 26: 238-255.
15. Sekhon LHS, Fehlings MG (2001) Epidemiology, Demographics, and Pathophysiology of Acute Spinal Cord Injury. *Spine* 26: S2-S12.
16. McDonald J, Sadowsky C (2002) Spinal-cord injury. *The Lancet* 359: 417-424.
17. Barbeau H, Fung J, Leroux A, Ladouceur M (2002) A review of the adaptability and recovery of locomotion after spinal cord injury. *Prog Brain Res* 137: 9-25.
18. Barbeau H, Nadeau S, Garneau C (2006) Physical determinants, emerging concepts, and training approaches in gait of individuals with spinal cord injury. *J Neurotrauma* 23: 571-585.
19. Dietz V, Fouad K (2013) Restoration of sensorimotor functions after spinal cord injury. *Brain* 137: 654-667.
20. Dobkin B, Apple D, Barbeau H, Basso M, Behrman A, Deforge D, Di-tunno J, Dudley G, Elashoff R, Fugate L, Harkema S, Saulino M, Scott M (2003) Methods for a Randomized Trial of Weight-Supported Treadmill Training Versus Conventional Training for Walking During Inpatient Rehabilitation after Incomplete Traumatic Spinal Cord Injury. *Neurorehabil Neural Repair* 17: 153-167.

21. Harkema SJ (2001) Neural Plasticity after Human Spinal Cord Injury: Application of Locomotor Training to the Rehabilitation of Walking. *Neuroscientist* 7: 455-468.
22. Dietz V, Colombo G, Jensen L, Baumgartner L (1995) Locomotor capacity of spinal cord in paraplegic patients. *Ann Neurol* 37: 574-582.
23. Jezernik S, Colombo G, Keller T, Frueh H, Morari M (2003) Robotic orthosis lokomat: A rehabilitation and research tool. *Neuromodulation* 6: 108-115.
24. Fouad K, Pearson K (2004) Restoring walking after spinal cord injury. *Prog in Neurobiol* 73: 107-126.
25. Ragnarsson KT (2008) Functional electrical stimulation after spinal cord injury: current use, therapeutic effects and future directions. *Spinal Cord* 46: 255-274.
26. Kralj A, Bajd T (1989) *Functional Electrical Stimulation, Standing and Walking after Spinal Cord Injury*. Boca Raton, Florida: CRC Press.
27. Bajd T, Kralj A, Turk R, Segal J (1983) The use of a four-channel electrical stimulator as an ambulatory aid for paraplegic patients. *Phys Ther* 63: 1116-1120.
28. Kobetic R, Triolo RJ, Marsolais EB (1997) Muscle selection and walking performance of multichannel FES systems for ambulation in paraplegia. *IEEE Trans Rehabil Eng* 5: 23-29.
29. Marsolais EB, Kobetic R (1987) Functional electrical stimulation for walking in paraplegia. *J Bone Joint Surg* 69A: 728-733.
30. Hardin E, Kobetic R, Murray L, Corado-Ahmed M, Pinault G, Sakai J, Bailey SN, Ho C, Triolo RJ (2007) Walking after incomplete spinal cord injury using an implanted FES system: a case report. *J Rehabil Res Dev* 44: 33-46.
31. Granat MH, Heller BW, Nicol DJ, Baxendale RH, Andrews BJ (1993) Improving limb flexion in FES gait using the flexion withdrawal response for the spinal cord injured person. *J Biomed Eng* 15: 51-56.

32. Thrasher TA, Flett HM, Popovic MR (2006) Gait training regimen for incomplete spinal cord injury using functional electrical stimulation. *Spinal Cord* 44: 357-361.
33. Nielson JB (2003) How we walk: central control of muscle activity during human walking. *Neuroscientist* 9: 195-204.
34. Barthelemy D, Willerslev-Olsen M, Lundell H, Conway BA, Knudsen H, Biering-Sorensen, Nielsen JB (2010) Impaired Transmission in the Corticospinal Tract and Gait Disability in Spinal Cord Injured Persons. *J Neurophysiol* 104: 1167-1176.
35. Oxford English Dictionary (2002) Oxford: Oxford University Press, fifth edition.
36. Sherrington CS (1906) *The Integrative Action of the Nervous System*. Oxford: Oxford University Press.
37. Rose J, Gamble JG (2006) *Human Walking*, 3rd ed . Philadelphia, USA: Lippincott Williams & Wilkins.
38. Uustal H, Baerga E (2004) *Physical Medicine and Rehabilitation Board Review*, New York, USA: Demos Medical Publishing, chapter Gait Analysis.
39. Duysens J, Clarac F, Cruse H (2000) Load-Regulating Mechanisms in Gait and Posture: Comparative Aspects. *Physiol Rev* 80: 83-133.
40. Grillner S (1981) *Handbook of Physiology Section 1 The Nervous System, Motor control*, Bethesda, MD: Am Physiol Soc, volume 2, pt 2, chapter Control of locomotion in bipeds, tetrapods, and fish. pp. 1179-1236.
41. McCrea DA (2001) Spinal circuitry of sensorimotor control of locomotion. *J Physiol* 533: 41-50.
42. Pearson KG (2003) Generating the walking gait: role of sensory feedback. *Prog Brain Res* 143: 123-129.
43. Dietz V, Duysens J (2000) Significance of load receptor input during locomotion: a review. *Gait Posture* 11: 102-110.
44. Duysens J, Van de Crommert HWAA (1998) Neural control of locomotion; Part 1: The central pattern generator from cats to humans [Review Paper]. *Gait and Posture* 7: 131-141.

45. Pearson KG (1995) Proprioceptive regulation of locomotion. *Curr Opin Neurobiol* 5: 786-791.
46. Zehr EP, Stein RB (1999) What Functions Do Reflexes Serve During Human Locomotion? *Prog Neurobiol* 58: 185-205.
47. Courtine G, Gerasimenko Y, van den Brand R, Yew A, Musienko P, Zhong H, Song Y B, Ao, Ichiyama R, Lavrov I, Roy R, Sofroniew M, Edgerton V (2009) Transformation of nonfunctional spinal circuits into functional states after the loss of brain input. *Nature Neuroscience* 12: 1333-1342.
48. Dietz V (1992) Human neuronal control of automatic functional movements: interaction between central programs and afferent input. *Physiol Rev* 72: 33-69.
49. Dietz V (1993) *Progress in Brain Research*, Amsterdam: Elsevier, volume 97, chapter Gating of reflexes in ankle muscles during human stance and gait. pp. 181-188.
50. Grillner S, Wallen P (1975) Central pattern generators for locomotion, with special reference to vertebrates. *Annu Rev Neurosci* 8: 233-261.
51. Grillner S (1985) Neurobiological bases of rhythmic motor acts in vertebrates. *Science* 228: 143-149.
52. Brown TG (1914) On the nature of the fundamental activity of the nervous centres; together with an analysis of the conditioning of rhythmic activity in progression, and a theory of the evolution of function in the nervous system. *J Physiol* 48: 18-46.
53. Brown TG (1911) The intrinsic factors in the act of progression in the mammal. *Proc R Soc Lond* 84: 308-319.
54. Grillner S, Zangger P (1979) On the central generation of locomotion in the low spinal cat. *Exp Brain Res* 34: 241-261.
55. Bem T, Orsal D, Cabelguen JM (1993) Fictive locomotion in the adult thalamic rat. *Exp Brain Res* 97: 301-304.
56. Pearson K (2000) Review: Motor systems. *Current Opinion in Neurobiology* 10: 649-654.

57. Shik ML, Severin FV, Orlovsky GN (1966) Control of walking and running by means of electrical stimulation of the mid-brain. *Biophysics* 11: 756-765.
58. Grillner S (1973) *Control of Posture and Locomotion*, N Y: Plenum Press, chapter Locomotion in the spinal cat. pp. 515-535.
59. Pearson KG, Duysens J (1976) *Neural Control of Locomotion*, Plenum, New York: *Advances in Behavioural Biology*, volume 18, chapter Function of Segmental Reflexes in the Control of Stepping in Cockroaches and Cats. pp. 519-537.
60. Clarac F, Chrachri A (1988) *Stance and Motion: Facts and concepts*, New York: Plenum, chapter The stance phase and its control by sensory information during walking in crustacea. pp. 93-106.
61. Schmitz J, Hassfeld G (1989) The treading-on-tarsus reflex in stick insects: phase-dependence and modifications of the motor output during walking. *J Exp Biol* 143: 373-388.
62. Pearson KG (1993) Common principles of motor control in vertebrates and invertebrates. *Ann Rev Neurosci* 16: 265-297.
63. Hultborn H, Nielsen JB (2007) Spinal control of locomotion - from cat to man. *Acta Physiol* 189: 111-121.
64. Armstrong DM (1988) The supraspinal control of mammalian locomotion. *J Physiol* 405: 1-37.
65. Grey MJ, Nielson JB, Mazzaro N, Sinkjaer T (2007) Positive force feedback in human walking. *J Physiol* 581: 99-105.
66. Brooks VB (1986) *The Neural Basis of Motor Control*. Oxford: Oxford University Press.
67. Rossignol S, Dubuc R, Gossard JP (2006) Dynamic Sensorimotor Interactions in Locomotion. *Physiol Rev* 86: 89-154.
68. Grillner S (1972) The role of muscle stiffness in meeting the changing postural and locomotor requirements for force development by the ankle extensors. *Acta Physiol Scand* 86: 92-108.

69. Donelan JM, Pearson KG (2004) Contribution of sensory feedback to ongoing ankle extensor activity during the stance phase of walking. *Can J Physiol Pharmacol* 82: 589-598.
70. Duysens J, Pearson KG (1980) Inhibition of flexor burst generation by loading ankle extensor muscles in walking cats. *Brain Res* 187: 321-332.
71. Stein RB, Misiaszek JE, Pearson KG (2000) Functional role of muscle reflexes for force generation in the decerebrate walking cat. *J Physiol* 525: 781-791.
72. Hiebert GW, Pearson KG (1999) Contribution of sensory feedback to the generation of extensor activity during walking in the decerebrate cat. *J Neurophysiol* 81: 758-770.
73. Hultborn H (2006) Spinal reflexes, mechanisms and concepts: From Eccles to Lundberg and beyond. *Prog Neurobiol* 78: 215-232.
74. Schomburg ED, Petersen N, Barajon I, Hultborn H (1998) Flexor reflex afferents reset the step cycle during fictive locomotion in the cat. *Exp Brain Res* 122: 339-350.
75. Conway BA, Hultborn H, Kiehn O (1987) Proprioceptive input resets central locomotion in the spinal cat. *Exp Brain Res* 68: 643-656.
76. Grillner S, Rossignol S (1978) On the initiation of the swing phase of locomotion in chronic spinal cats. *Brain Res* 146: 269-277.
77. Hiebert GW, Whelan PJ, Prochazka A, Pearson KG (1996) Contribution of hind limb flexor muscle afferents to the timing of phase transitions in the cat step cycle. *J Neurophysiol* 75: 1126-1137.
78. Kriellaars DJ, Brownstone RM, Noga BR, Jordan LM (1994) Mechanical entrainment of fictive locomotion in the decerebrate cat. *J Neurophysiol* 71: 2074-2086.
79. Whelan PJ, Hiebert GW, Pearson KG (1995) Stimulation of the group I extensor afferents prolongs the stance phase in walking cats. *Exp Brain Res* 103: 20-30.
80. Forsberg H (1979) Stumbling corrective reaction: a phase-dependent compensatory reaction during locomotion. *J Neurophysiol* 42: 936-953.

81. Sherrington CS (1939) Selected Writings of Sir Charles Sherrington, A Testimonial Presented by the Neurologists Forming the Guarantors of the Journal Brain. London: Hamish Hamilton Medical Books.
82. Duysens J, Pearson KG (1976) The role of cutaneous afferents from the distal hindlimb in the regulation of the step cycle of treadmill walking thalamic cats. *Exp Brain Res* 24: 245-255.
83. Bouyer LJ, Rossignol S (2003) Contribution of cutaneous inputs from the hindpaw to the control of locomotion I Intact cats. *J Neurophysiol* 90: 3625-3639.
84. Bouyer LJ, Rossignol S (2003) Contribution of cutaneous inputs from the hindpaw to the control of locomotion II Spinal cats. *J Neurophysiol* 90: 3640-3653.
85. Duysens J, Stein RB (1978) Reflexes induced by nerve stimulation in walking cats with implanted cuff electrodes. *Exp Brain Res* 32: 213-224.
86. Loeb GE, Bak MJ, Duysens J (1977) Long-term unit recording from somatosensory neurons in the spinal ganglia of the freely walking cat. *Science* 197: 1192-1194.
87. Loeb GE, Hoffer JA, Marks WB (1987) Cat hindlimb motoneurons during locomotion IV Participation in cutaneous reflexes. *J Neurophysiol* 57: 563-573.
88. Lacquaniti F (1992) Automatic control of limb movement and posture. *Curr Opin Neurobiol* 2: 807-814.
89. Nashner LM, Woolacott M, Tuma G (1979) Organisation of rapid responses to postural and locomotor-like perturbations of standing man. *Exp Brain Res* 36: 463-476.
90. Illis LS (1995) Is there a central pattern generator in man? *Paraplegia* 33: 239-240.
91. Vilensky JA, O'Connor BL (1997) Stepping in humans with complete spinal cord transection: a phylogenetic evaluation. *Motor Control* 1 : 284-292.
92. Pierrot-Deseilligny E, Burke D (2005) The Circuitry of the Human Spinal Cord, Cambridge, UK: Cambridge University Press.

93. Yang JF, Stephans MJ, Vishram R (1998) Infant stepping: a method to study the sensory control of human walking. *J Physiol* 507: 927-937.
94. Crenna P, Frigo C (1991) A motor programme for the initiation of forward-orientated movements in humans. *J Physiol (Lond)* 437: 635-653.
95. Eidelberg E, Walden JG, Nguyen LH (1981) Locomotor control in macaque monkeys. *Brain* 104: 647-663.
96. Dietz V, Muller R, Columbo G (2002) Locomotor activity in spinal man: significance of afferent input from joint and load receptors. *Brain* 125: 2626-2534.
97. Fedirchuk B, Nielsen J, Petersen N, Hultborn H (1998) Pharmacologically evoked fictive motor patterns in the acutely spinalised marmoset monkey (*Callithrix jacchus*). *Exp Brain Res* 122: 351-361.
98. Calancie B, Needham-Shropshire B, Jacobs P, Willer K, Zych G, Green B (1994) Involuntary stepping after chronic spinal cord injury: evidence for a central rhythm generator for locomotion in man. *Brain* 117: 1143-1159.
99. Dietz V, Gollhofer A, Kleiber M, Trippel M (1992) Regulation of bipedal stance: dependency on "load" receptors. *Exp Brain Res* 89: 299-231.
100. Stein JF, Stoodley CJ (2006) *Neuroscience An Introduction*. England: John Wiley & Sons Ltd.
101. Dietz V, Schmidtbleicher D, Noth J (1979) Neuronal mechanisms of human locomotion. *J Neurophysiol* 42: 1212-1222.
102. Dietz V, Quintern J, Sillem M (1987) Stumbling reactions in man: significance of proprioceptive and pre-programmed mechanisms. *J Physiol (Lond)* 386: 149-163.
103. Gollhofer A, Horstmann BA, Berger W, Dietz V (1989) Compensation of translational and rotational perturbations in human posture: stabilisation of the centre of gravity. *Neurosci Lett* 105: 73-78.
104. Hansen PD, Woollacott MH, Debu B (1988) Postural responses to changing task conditions. *Exp Brain Res* 73: 627-636.
105. Dietz V (1998) Evidence for a load receptor contribution to the control of posture and locomotion. *Neurosci Biobehav Rev* 22: 495-499.

106. Yang JF, Stein RB, James KB (1991) Contribution of peripheral afferents to the activation of the soleus muscle during walking in humans. *Exp Brain Res* 87: 679-687.
107. Andersen JB, Sinkjaer T (1995) An actuator system for investigating electrophysiological and biomechanical features around the human ankle joint during gait. *IEEE Trans Rehab Eng* 3: 299-306.
108. Sinkjaer T, Andersen JB, Larsen B (1996) Soleus stretch reflex modulation during gait in humans. *J Neurophysiol* 76: 1112-1120.
109. Sinkjaer T, Anderson JB, Ladouceur M, Christensen LOD, Nielson JB (2000) Major role for sensory feedback in soleus EMG activity in the stance phase of walking in man. *J Physiol* 523: 817-827.
110. Lamb T, Yang JF (2000) Could different directions of infant stepping be controlled by the same locomotor central pattern generator? *J Neurophysiol* 83: 2814-2824.
111. Pang MY, Yang JF (2000) The initiation of the swing phase in human infant stepping: importance of hip position and leg loading. *J Neurophysiol* 528: 389-404.
112. Pang MY, Yang JF (2002) Sensory gating for the initiation of the swing phase in different directions of human infant stepping. *J Neurosci* 22: 5734-5740.
113. Dietz V, Horstmann GA, Trippel M, Gollhofer A (1989) Human postural reflexes and gravity - an under water simulation. *Neurosci Lett* 106: 350-355.
114. Dietz V, Colombo G (1996) Effects of body immersion on postural adjustments to voluntary arm movements in humans: role of load receptor input. *J Physiol* 497: 849-856.
115. Pearson KG, Collins DF (1993) Reversal of the influence of group Ib afferents from plantaris on activity in medial gastrocnemius muscle during locomotor activity. *J Neurophysiol* 70: 1009-1017.
116. Berger W, Dietz V, Quintern J (1984) Corrective reactions to stumbling in man: neuronal coordination of bilateral leg muscle activity during gait. *J Physiol (Lond)* 357: 109-125.

117. Dietz V, Horstmann GA, Berger W (1989) Interlimb coordination of leg-muscle activation during perturbation of stance in humans. *J Neurophysiol* 62: 680-693.
118. Gruner JA, Altman J (1980) Swimming in the rat: analysis of locomotor performance in comparison of stepping. *Exp Brain Res* 40: 374-382.
119. Jensen L, Prokop T, Dietz V (1998) Adaptional effects during human split-belt walking: influence of afferent input. *Exp Brain Res* 118: 126-130.
120. Faist M, Hofer C, Hodapp M, Dietz V, Berger W, Duysens J (2006) In humans Ib facilitation depends on locomotion while suppression of Ib inhibition requires loading. *Brain Res* 1076: 87-92.
121. Harkema SJ, Hurley SL, Patel UK, Requejo PS, Dobkin BH, Edgerton VR (1997) Human Lumbosacral Spinal Cord Interprets Loading During Stepping. *J Neurophysiol* 77: 797-811.
122. Stephans MJ, Yang JF (1999) Loading during the stance phase of walking in humans increases the extensor EMG amplitude but does not change the duration of the step cycle. *Exp Brain Res* 124: 363-370.
123. Aniss AM, Gandevia SC, Burke D (1992) Reflex responses in active muscles elicited by stimulation of low-threshold afferents from the human foot. *J Neurophysiol* 67: 1375-1384.
124. Conway BA, Scott DT, Riddell JS (1995) Alpha and gamma motor systems, New York, USA: Springer US, chapter The effects of plantar nerve stimulation on long latency flexion reflexes in the acute spinal cat. pp. 593-595.
125. Conway BA, Knikou M (2008) The action of plantar pressure on flexion reflex pathways in the isolated human spinal cord. *Clinical Neurophysiol* 119: 892-896.
126. Duysens J (1977) Reflex control of locomotion as revealed by stimulation of cutaneous afferents in spontaneously walking preammillary cats. *J Neurophysiol* 40: 737-751.
127. Yang J, Stein R (1990) Phase-dependent reflex reversal in human leg muscles during walking. *J Neurophysiol* 63: 1109-1117.

128. Sinkjaer T, Haugland M, Haase J (1994) Natural neural sensing and artificial muscle control in man. *Exp Brain Res* 98: 542-545.
129. Patla AE (1986) Effects of walking on various inclines on EMG patterns of lower limb muscles in humans. *Hum Mov Sci* 5: 345-357.
130. Burke D, Dickson HG, Skuse NF (1991) Task-dependent changes in the responses to low-threshold cutaneous afferent volleys in the human lower limb. *J Physiol* 432: 445-458.
131. DeSerres SJ, Yang JF, Patrick SK (1995) Mechanism for reflex reversal during walking in human tibialis anterior muscle revealed by single motor unit recording. *J Physiol* 488: 249-258.
132. Stein RB (1991) Adaptability of human gait: implications for the control of locomotion, Amsterdam: Elsevier Science, chapter Reflex modulation during locomotion: functional significance.
133. Zehr EP, Komiyama T, Stein RB (1997) Cutaneous Reflexes During Human Gait: Electromyographic and kinematic Responses to Electrical Stimulation. *J Neurophysiol* 77: 3311-3325.
134. Zehr EP, Stein RB, Komiyama T (1998) Function of sural nerve reflexes during human walking. *J Physiol* 507: 305-314.
135. Gossard JP, Brownstone RM, Barajon I, Hultborn H (1994) Transmission in a locomotor-related group Ib pathway from hind-limb extensor muscles in the cat. *Exp Brain Res* 98: 213-228.
136. McCrea DA (1998) Neuronal basis of afferent-evoked enhancement of locomotor activity. *Ann N Y Acad Sci* 860: 216-225.
137. Pearson K, Ramirez J, Jiang W (1992) Entrainment of the locomotor rhythm by group Ib afferents from ankle extensor muscles in spinal cats. *Exp Brain Res* 90: 557-566.
138. Whelan PJ (1996) Control of locomotion in the decerebrate cat. *Prog Neurobiol* 49: 481-515.
139. Komiyama T, Zehr E, Stein R (2000) Absence of nerve-specificity in human cutaneous reflexes during standing. *Exp Brain Res* 133: 267-272.

140. Duysens J, Tax A, Trippel M, Dietz V (1993) Increased amplitude of cutaneous reflexes during human running as compared to standing. *Brain Res* 613: 230-238.
141. Duysens J, Trippel M, Horstmann G, Dietz V (1990) Gating and reversal of reflexes in ankle muscles during human walking. *Exp Brain Res* 82: 351-358.
142. Bastiaanse CM, Duysens J, Dietz V (2000) Modulation of cutaneous reflexes by load receptor input during human walking. *Exp Brain Res* 135: 189-198.
143. Brooke J, Cheng J, Collins D, McIlroy W, Misiaszek J, Staines W (1997) Sensori-sensory afferent conditioning with leg movement: gain control in spinal reflex and ascending paths. *Prog Neurobiol* 51: 393-421.
144. Clement G, Gurfinkel V, Lestienne F, Lipshits M, Popov K (1984) Adaptation of postural control to weightlessness. *Exp Brain Res* 57: 61-72.
145. Dietz V (2010). International encyclopedia of rehabilitation. URL http://cirrie.buffalo.edu/encyclopedia/en/pdf/rehabilitation_of_locomotor_function_after_a_central_motor_lesion.pdf/.
146. Beaumont E, Guevara E, Dubeau S, Lesage F, Nagai M, Popovic M (2014) Functional electrical stimulation post-spinal cord injury improves locomotion and increases afferent input into the central nervous system in rats. *J Spinal Cord Med* 37: 93-100.
147. Dean JC, Yates LM, Collins DF (1995) Turning on the central contribution to contractions evoked by neuromuscular electrical stimulation. *J Appl Physiol* 103: 170-176.
148. Lyons GM, Sinkjaer T, Burridge JH, Wilcox DJ (2002) Review of portable FES-Based neural orthoses for the correction of drop foot. *IEEE Trans Neur Syst Rehab Eng (TNSRE)* 10: 260-279.
149. Graupe D, Kohn KH (1994) *Functional Electrical Stimulation for Ambulation by Paraplegics*. Malabar, FA: Krieger Publishing.
150. Graupe D, Kohn KH (1997) Transcutaneous functional neuromuscular stimulation of certain traumatic complete thoracic paraplegics for independent short-distance ambulation. *Neurol Res* 19: 323-333.

151. Riener R (1999) Model-based development of neuroprostheses for paraplegic patients. *Philos Trans R Soc Lond* 354: 877-894.
152. Chizeck HJ, Kobetic R, Marsolais EB, Abbas JJ, Donner IH, Simon E (1988) Control of functional neuromuscular stimulation systems for standing and locomotion in paraplegics. *Proc IEEE* 76: 1155-1165.
153. Fuhr T, Quintern J, Riener R, Schimidt G (2001) Walk! - experiments with a cooperative neuroprosthetic system for the restoration of gait. In: Triolo RJ, editor, *Proceedings of the IFESS 2001: the 6th annual conference of the International Functional Electrical Stimulation Society*. Cleveland, USA: Case Western Reserve University Press, volume 97, pp. 1-3.
154. Mulder AJ, Veltink PH, Boom HB (1992) On/off control in FES-induced standing up: a model study and experiments. *Med Biol Eng Comput* 30: 205-212.
155. Mulder AJ, Boom HB, Hermens HJ, Zilvold G (1990) Artificial-reflex stimulation for FES-induced standing with minimum quadriceps force. *Med Biol Eng Comput* 28: 483-488.
156. Ladouceur M, Barbeau H (2000) Functional electrical stimulation-assisted walking for persons with incomplete spinal injuries: changes in kinematics and physiological cost of over-ground walking. *Scand J Rehabil Med* 32: 72-79.
157. Popovic DB, Popovic MB, Schwirtlich L, Grey M, Mazzaro N, Sinkjaer T (2005) Functional electrical therapy of walking: pilot study. In: *Proc 10th Ann Conf Intern IFFES Society*. pp. 86-88.
158. Popovic D, Radulovic M, Schwirtlich L, Jaukovic N (2003) Automatic vs hand-controlled walking of paraplegics. *Med Eng Phys* 23: 63-73.
159. Sinkjaer T, Haugland M, Inmann A, Hansen M, Nielsen K (2003) Biopotentials as command and feedback signals in functional electrical stimulation systems. *Med Eng Phys* 25: 29-40.
160. Braz GP, Russold M, Davis GM (2009) Functional Electrical Stimulation Control of Standing and Stepping After Spinal Cord Injury: A Review of Technical Characteristics. *Neuromodulation* 12: 180-190.

161. Kojovic J, Djuric-Jovicic M, Dosen S, Popovic MB, Popovic DB (2009) Sensor-driven four-channel stimulation of paretic leg: Functional electrical walking therapy. *J Neurosci Meth* 181: 100-105.
162. Pappas IP, Popovic MR, Keller T, Dietz V, Morari M (2001) A reliable gait phase detection system. *IEEE Trans Neural Syst Rehabil Eng* 9: 113-125.
163. Willemsen AT, Bloemhof F, Boom HB (1990) Automatic stance-swing phase detection from accelerometer data for peroneal nerve stimulation. *IEEE Trans Biomed Eng* 37: 1201-1208.
164. Williamson R, Andrews BJ (2000) Gait event detection for FES using accelerometers and supervised machine learning. *IEEE Trans Rehabil Eng* 8: 312-319.
165. Esquenazi A, Talaty M, Packel A, Saulino M (2012) The reWalk powered exoskeleton to restore ambulatory function to individuals with thoracic-level motor-complete spinal cord injury. *Am J Phys Med Rehabil* 91: 911-921.
166. McGeer T (1990) Passive dynamic walking. *Int J Robot Res* 9: 62-82.
167. Collins SH, Ruina A, Tedrake R, Wisse M (2005) Efficient bipedal robots based on passive dynamic walkers. *Science* 307: 1082-1085.
168. Sakagami Y, Watanabe R, Aoyama C, Matsunaga S, Higaki N, Fujimura K (2002) The intelligent ASIMO: System overview and integration. In: *Proceedings of the IEEE/RSJ International Conference on Intelligent Robots and Systems*. Lausanne, Switzerland, pp. 2478-2483.
169. Zajac FE (1989) Muscle and tendon properties, models, scaling and application to biomechanics and motor control. *Crit Rev Biomed Eng* 17: 359-411.
170. Endo G, Morimoto J, Matsubara T, Nakanishi J, Cheng G (2005) Learning CPG sensory feedback with policy gradient for biped locomotion for a full body humanoid. In: *Proceedings of the Twentieth National Conference on Artificial Intelligence*. pp. 1267-1273.
171. Hobbelen DGE, Wisse M (2007) Humanoid Robots: Human-like Machines, Vienna, Austria: InTech, chapter Limit Cycle Walking. pp. 277-294.

172. Cruse H, Kindermann T, Schumm M, Dean J, Schmitz J (1998) Walknet- A biologically inspired network to control six-legged walking. *Neural Networks* 11: 1435-1447.
173. Pratt J (2000) Exploiting inherent robustness and natural dynamics in the control of bipedal walking robots. Ph.D. thesis, Cambridge, Massachusetts.
174. Chevallereau C, Abba G, Aoustin Y, Plestan F, Westervelt E, Canudas-de Wit C, Grizzle J (2003) Rabbit: A testbed for advanced control theory. *IEEE Control Systems Magazine* 23: 57-79.
175. Sreenath K, Park H, Poulakakis I, Grizzle J (2011) A Compliant Hybrid Zero Dynamics Controller for Stable, Efficient and Fast Bipedal Walking on MABEL. *Int J Robot Res* 30: 1170-1193.
176. Dietz V, Colombo G, Jensen L (1994) Locomotor activity in spinal man. *Lancet* 344: 1260-1263.
177. Macleod CA, Conway BA, Allan DB, Galen SS (2014) Development and validation of a low-cost, portable and wireless gait assessment tool. *Med Eng Phys* 36: 541-546.
178. Shewman T, Konrad P (2008). Clinical semg electrode sites. URL <http://www.noraxon.com/training-tools>.
179. Hermens HJ, Freriks B, Merletti R, Stegeman D, Blok J, Rau G, Disselhorst-Klug C, Hagg G (1999) SENIAM 8: European Recommendations for Surface ElectroMyoGraphy. Enschede, the Netherlands: Roessingh Research and Development.
180. Chu-Andrews J, Johnson R (1986) *Electrodiagnosis: An anatomical and clinical approach*. Philadelphia, USA: J.B. Lippincott Company.
181. Interlink Electronics (2013) Interlink Electronics FSR Force Sensing Resistors: FSR Integration Guide. URL <http://www.interlinkelectronics.com/prodinfo.php>. EIG-10000 Rev. B.
182. Granat MH, Maxwell DJ, Bosch CJ, Ferguson ACB, Lees KR, Barbenel JC (1995) A body-worn gait analysis system for evaluating hemiplegic gait. *Med Eng Phys* 17: 390-394.

183. Galen SS, Wiggins L, McWilliam R, Granat M (2012) A combination of Botulinum Toxin A therapy and Functional Electrical Stimulation in children with cerebral palsy - a pilot study. *Technol Health Care* 20: 1-9.
184. STMicroelectronics (2005) LIS2L02AS4, MEMS INERTIAL SENSOR: 2-Axis - $\pm 2g/\pm 6g$ LINEAR ACCELEROMETER. Rev. 2.
185. Verplaetse C (1996) Inertial proprioceptive devices: Self-motion-sensing toys and tools. *IBM Syst J* 35: 639-650.
186. Davidson A, O'Dell R, Chan V, Schieber M (2007) Comparing effects in spike-triggered averages of rectified EMG across different behaviours. *J Neurosci Meth* 163: 283-294.
187. Yang J, Winter D (1984) Electromyographic amplitude normalization methods: improving their sensitivity as diagnostic tools in gait analysis. *Arch Phys Med Rehab* 65: 517-521.
188. Shiavi R, Green N (1983) Ensemble averaging of locomotor electromyographic patterns using interpolation. *Med & Biol Eng & Comput* 21: 573-578.
189. Shiavi R, Bugle HJ, Limbird T (1987) Electromyographic gait assessment, Part 1: Adult EMG profiles and walking speed. *J Rehabil Res Dev* 24: 13-23.
190. Hof AL (1996) Scaling gait data to body size. *Gait Posture* 4: 222-223.
191. Paninski L (2003) Convergence properties of some spike-triggered analysis techniques. *Network-Comp Neural* 14: 437-464.
192. Hof AL, Elzinga H, Grimmius W, Halbertsma JP (2005) Detection of non-standard EMG profiles in walking. *Gait Posture* : 171-177.
193. Farina D, Cescon C, Merletti R (2002) Influence of anatomical, physical, and detection-system parameters on surface EMG. *Biol Cybernet* 86: 445-456.
194. Shiavi R (1985) Electromyographic patterns in adult locomotion: A comprehensive review. *J Rehabil Res Dev* 22: 85-98.
195. Winter DA, Yack HJ (1987) Emg profiles during normal human walking: stride-to-stride and inter-subject variability. *Electroen Clin Neuro* 67: 402-411.

196. McVea DA, Donelan JM, Tachibana A, Pearson KG (2005) A Role for Hip Position in Initiating the Swing-to-Stance Transition in Walking Cats. *J Neurophysiol* 94: 3497-3500.
197. Beer RD, Quinn RD, Chiel HJ, Ritzmann RE (1997) Biologically inspired approaches to robotics: What can we learn from insects? *Commun ACM* 40: 30-38.
198. Konrad P (2005) *The ABC of EMG: A practical guide to kinesiological Electromyography*. Arizona, USA: Noraxon USA., Inc.
199. Winter DA (1983) Biomechanical motor patterns in normal walking. *J Motor Behav* 3: 302-330.
200. Galen SS, Clarke CJ, Allan DB, Conway BA (2011) A portable gait assessment tool to record temporal gait parameters in SCI. *Med Eng Phys* 33: 626-632.
201. Caty GD, Detrembleur C, Bleyenheuft C, Lejeune TM (2009) Reliability of lower limb kinematics, mechanics and energetics during gait in patients after stroke. *Rehabil Med* 41: 588-590.
202. Kinsella S, Moran K (2008) Gait pattern categorization of stroke participants with equinus deformity of the foot. *Gait Posture* 27: 144-151.
203. Piccinini L, Cimolin V, D'Angelo MG, Turconi AC, Crivellini M, Galli M (2011) 3D gait analysis in patients with hereditary spastic paraparesis and spastic diplegia: a kinematic, kinetic and EMG comparison. *Eur J Paediatr Neurol* 15: 38-45.
204. Gil-Agudo A, Perez-Rizo E, Del Ama-Espinosa A, Crespo-Ruiz B, Perez-Nombela S, Sanchez-Ramos A (2009) Comparative biomechanical gait analysis of patients with central cord syndrome walking with one crutch and two crutches. *Clin Biomech (Bristol, Avon)* 24: 551-557.
205. Barak Y, Wagenaar RC, Holt KG (2006) Gait characteristics of elderly people with a history of falls: a dynamic approach. *Phys Ther* 86: 1501-1510.
206. Toro B, Nester CJ, Farren PC (2003) The status of gait assessment among physiotherapists in the United Kingdom. *Arch Phys Med Rehabil* 84: 1878-1884.

207. Simon SR (2004) Quantification of human motion: gait analysis-benefits and limitations to its application to clinical problems. *J Biomech* 37: 1869-1880.
208. Williams G, Galna B, Morris ME, Oliver J (2010) Spatiotemporal deficits and kinematic classification of gait following a traumatic brain injury: a systematic review. *J Head Trauma Rehabil* 25: 366-374.
209. Bilney B, Morris M, Webster K (2003) Concurrent related validity of the GAITRite walkway system for quantification of the spatial and temporal parameters of gait. *Gait Posture* 17: 68-74.
210. Greene BR, Foran TG, McGrath D, Doheny EP, Burns A, Caulfield B (2012) A Comparison of Algorithms for Body-Worn Sensor-Based Spatiotemporal Gait Parameters to the GAITRite Electronic Walkway. *J Appl Biomech* 28: 349-355.
211. Webster KE, Wittwer JE, Feller JA (2005) Validity of the GAITRite walkway system for the measurement of averaged and individual step parameters of gait. *Gait Posture* 22: 317-321.
212. Davis RB, Ounpuu S, Tyburski D, Gage JR (1991) A gait analysis data collection and reduction technique. *Hum Mov Sci* 10: 575-587.
213. Kadaba MP, Ramakrishnan HK, Wootten ME (1990) Measurement of lower extremity kinematics during level walking. *J Orthop Res* 8: 383-392.
214. Shrout PE, Fleiss JL (1979) Intraclass correlations: Uses in assessing rater reliability. *Psychol Bull* 86: 420-428.
215. Bland JM, Altman DG (1986) Statistical methods for assessing agreement between two methods of clinical measurement. *Lancet* i: 307-310.
216. Bland JM, Altman DG (1999) Measuring agreement in method comparison studies. *Stat Methods Med Res* 8: 135-160.
217. Kyriazis V, Rigas C, Xenakis T (2001) A portable system for the measurement of the temporal parameters of gait. *Prosthet Orthot Int* 25: 96-101.

218. Huitema RB, Hof AL, Postema K (2002) Ultrasonic motion analysis system-measurement of temporal and spatial gait parameters. *J Biomech* 35: 837-842.
219. Lienhard K, Schneider D, Maffioletti NA (2012) Validity of the Optogait photoelectric system for the assessment of spatiotemporal gait parameters. *Med Eng Phys* 35: 500-504.
220. Greene BR, McGrath D, O'Donovan KJ, O'Neill R, Burns A, Caulfield B (2010) Adaptive estimation of temporal gait parameters using body-worn gyroscopes. *Conf Proc IEEE Eng Med Biol Soc*, 2010 : 1296-1299.
221. Merletti R (1999) Standards for Reporting EMG data. *J Electromyogr Kinesiol* 9: III-IV.
222. Macleod CA, Meng L, Conway BA, Porr B (2014) Reflex control of robotic gait using human walking data. *PLoS ONE* 9: e109959.
223. Zijlstra W, Rutgers A, Hof A, Van Weerden T (1995) Voluntary and involuntary adaptation of walking to temporal and spatial constraints. *Gait Posture* 3: 13-18.
224. Egerton T, Danoudis M, Huxham F, Ianssek R (2011) Central gait control mechanisms and the stride length - cadence relationship. *Gait & Posture* 34: 178182.
225. Andriacchi TP, Ogle JA, Galante JO (1977) Walking speed as a basis for normal and abnormal gait measurements. *J Biomech* 10: 261-268.
226. Vaughan CL, Du Toit LL, Roffey M (1987) *Biomechanics X-A*, Umea, Sweden: National Board of Occupational Safety and Health, chapter Speed of walking and forces acting on the feet. pp. 349-353.
227. Nilsson J, Thorstensson A (1989) Ground reaction forces at different speeds of human walking and running. *Acta Physiol Scand* 136: 217-227.
228. Winter DA (1991) *The biomechanics and motor control of human gait: Normal, elderly and pathological*. Waterloo, Canada: University of Waterloo Press, second edition.
229. Miyashita M, Matsui H, Miura M (1970) The relation between electrical activity in muscle and speed of walking and running. *Res Bull* 14: 41-49.

230. Milner M, Basmajian JV, Quanbury AO (1971) Multifactorial analysis of walking by electromyography and computer. *Am J Phys Med* 50: 235-258.
231. Brandell BR (1977) Functional roles of the calf and vastus muscles in locomotion. *Am J Phys Med* 56: 59-74.
232. Murray MP, Mollinger LA, Gardner GM, Sepic SB (1984) Kinematic and EMG patterns during slow, free and fast walking. *J Orthop Res* 2: 272-280.
233. Nilsson J, Thorstensson A, Halbertsma J (1985) Changes in leg movements and muscle activity with speed of locomotion and mode of progression in humans. *Acta Physiol Scand* 123: 457-475.
234. Hof A, Elzinga H, Grimmius W, Halbertsma JP (2002) Speed dependence of averaged EMG profiles in walking. *Gait Posture* 16: 78-86.
235. Iida F, Rummel J, Seyfarth A (2008) Bipedal walking and running with spring-like biarticular muscles. *J Biomech* 41: 656-667.
236. Seyfarth A, Iida F, Tausch R, Stelzer M, von Stryk O, Karguth A (2009) Towards Bipedal Jogging as a Natural Result of Optimizing Walking Speed for Passively Compliant Three-Segmented Legs. *Int J Robot Res* 28: 257-265.
237. Rummel J, Blum Y, Maus HM, Rode C, Seyfarth A (2010) Stable and robust walking with compliant legs. In: *IEEE International Conference on Robotics and Automation (ICRA)*. Anchorage, Alaska, pp. 5250-5255.
238. Owaki D, Koyama M, Yamaguchi S, Kubo S, Ishiguro A (2011) A 2-D passive-dynamic-running biped with elastic elements. *IEEE Trans Robot* 27: 156-162.
239. Park HW, Sreenath K, Ramezani A, Grizzle JW (2012) Switching control design for accommodating large step-down disturbances in bipedal robot walking. In: *IEEE International Conference on Robotics and Automation (ICRA)*. Saint Paul, MN, pp. 45-50.
240. Ray T, Porten L (1980) Technical Note: Proportions of the Human Body Segments for Use in Design of Artificial Limbs. *Orthotics and Prosthetics* 34: 36-37.

241. Milner-Brown HS, Stein RB, Yemm R (1973) The contractile properties of human motor units during voluntary isometric contractions. *J Physiol* 228: 285-306.
242. Petiot E, Barres C, Chapius B, Julien C (2001) Frequency response of renal sympathetic nervous activity to aortic depressor nerve stimulation in the anaesthetized rat. *J Physiol* 537: 949-959.
243. Reeve RE, Webb BH (2003) New neural circuits for robot phototaxis. *Philosophical Transactions of the Royal Society of London , Series A: Mathematical, Physical and Engineering Sciences* 361: 2245-2266.
244. Murray M, Spurr G, Sepic S, Gardner G, Mollinger L (1985) Treadmill vs floor walking: kinematics, electromyogram, and heart rate. *J Appl Physiol* 59: 87-91.
245. Alton F, Baldey L, Caplan S, Morrissey M (1998) A kinematic comparison of overground and treadmill walking. *Clin Biomech* 13: 434-440.
246. Nymark J, Balmer S, Melis E, Lemair E, Millar S (2005) Electromyographic and kinematic nondisabled gait differences at extremely slow overground and treadmill walking speeds. *J Rehabil Res Dev* 42: 523-534.
247. Riley P, Paolini G, Croce U, Paylo K, Kerrigan D (2007) A Kinematic and kinetic comparison of overground and treadmill walking in healthy subjects. *Gait Posture* 26: 17-24.
248. Lee S, Hidler J (2007) Biomechanics of overground vs. treadmill walking in healthy individuals. *J Appl Physiol* 104: 747755.
249. Arsenault A, Winter D, Marteniuk R (1986) Treadmill versus walkway locomotion in humans: an EMG study. *Ergonomics* 29: 665-676.
250. Shiavi R, Bugle HJ, Limbird T (1981) Variability of electromyographic patterns for level surface walking through a range of self-selected speeds. *Bull Prosthet Res* 18: 5-14.
251. Malone LA, Bastian AJ (2010) Thinking about walking: Effects of conscious correction versus distraction on locomotor adaptation. *J Neurophysiol* 103: 1954-1962.
252. Torres-Oviedo G, Vasudevan E, Malone L, J BA (2011) Locomotor adaptation. *Prog Brain Res* 191: 65-74.

253. Colombo G, Joerg M, Schreier R, Dietz V (2000) Treadmill training of paraplegic patients using a robotic orthosis. *J Rehabil Res Dev* 37: 693-700.
254. Bernstein NA (1967) *The Co-ordination and regulation of movements*. Oxford, NY, USA: Pergamon Press Ltd.
255. Lotze M, Braun C, Birbaumer N, Anders S, Cohen LG (2003) Motor learning elicited by voluntary drive. *Brain* 126: 866872.
256. Duschau-Wicke A, Caprez A, Riener R (2010) Patient-cooperative control increases active participation of individuals with SCI during robot-aided gait training. *J Neuroeng Rehabil* 7: doi:10.1186/1743-0003-7-43.
257. Duschau-Wicke A, von Zitzewitz J, Caprez A, Lunenburger L, Riener R (2010) Path control: a method for patient-cooperative robot-aided gait rehabilitation. *IEEE Trans Neural Syst Rehabil Eng* 18: 38-48.
258. Jezernik S, Colombo G, Morari M (2004) Automatic Gait-Pattern Adaptation Algorithms for Rehabilitation With a 4-DOF Robotic Orthosis. *IEEE Trans Robot Autom* 20: 574-582.
259. Kerrigan D, Todd M, Della Croce U (1998) Gender differences in joint biomechanics during walking: normative study in young adults. *Am J Phys Med Rehabil* 77: 2-7.
260. Pang MY, Yang JF (2001) Interlimb co-ordination in human infant stepping. *J Physiol* 533: 617-625.
261. Chiel H, Beer RD (1997) The brain has a body: Adaptive behavior emerges from interactions of nervous system, body, and environment . *Trends Neurosci* 20: 553-557.
262. Vukobratović M, Borovac B (2004) Zero-moment point - thirty five years of its life. *Int J Human Robot* 1: 157-173.
263. Pratt J, Chew CM, Torres A, Dilworth P, Pratt G (2001) Virtual model control: An intuitive approach for bipedal locomotion. *Int J Robot Res* 20: 129-143.
264. Ijspeert AJ (2008) Central pattern generators for locomotion control in animals and robots: A review. *Neural Networks* 21: 642-653.

265. Nakanishi J, Morimoto J, Endo G, Cheng G, Schaal S, Kawato M (2004) Learning from demonstration and adaptation of biped locomotion. *Robot Auton Syst* 47: 79-91.
266. Endo G, Morimoto J, Matsubara T, Nakanishi J, Cheng G (2008) Learning CPG-based Biped Locomotion with a Policy Gradient Method: Application to a Humanoid Robot. *Int J Robot Res* 27: 213-228.
267. Geyer H, Seyfarth A, Blickhan R (2003) Positive force feedback in bouncing gaits? In: *Proc R Soc Lond B*. volume 270, pp. 2173-2183.
268. Grillner S (1975) Neurobiological bases on rhythmic motor acts in vertebrates. *Science* 228: 143-149.
269. Wilson D (1961) The central nervous control of locust flight. *J Exp Biol* 38: 471-490.
270. Wilson DM, Wyman RJ (1965) Motor output patterns during random and rhythmic stimulation of locust thoracic ganglia. *Biophys J* 5: 121-145.
271. Wilson DM (1966) Central nervous mechanisms for the generation of rhythmic behaviour in arthropods. *Symp Soc Exp Biol* 20: 199-228.
272. Duysens J, Van de Crommert HWAA, Smits-Engelsman BCM, Van der Helm FCT (2002) A walking robot called human: lessons to be learned from neural control of locomotion. *J Biomech* 35: 447-453.
273. Dimitrijevic MR, Gerasimenko Y, Pinter MM (1998) Evidence for a Spinal Central Pattern Generator in Humans. *Ann N Y Acad Sci* 860: 360-376.
274. Marchand-Pauvert V, Nielson JB (2002) Modulation of heteronymous reflexes from ankle dorsiflexors to hamstring muscles during human walking. *Exp Brain Res* 142: 402-408.
275. Marchand-Pauvert V, Nielson JB (2002) Modulation of non-monosynaptic excitation from ankle dorsiflexor afferents to quadriceps motoneurons during human walking. *J Physiol* 538: 647-657.
276. Geng T (2014) Online regulation of the walking speed of a planar limit cycle walker via model predictive control. *IEEE Trans Ind Electron* 61: 2326-2333.
277. Braitenberg V (1984) *Vehicles-Experiments in Synthetic Psychology*. Cambridge, MA: The MIT Press.